HYDROGEL MEMBRANES FOR BIO-SEPARATIONS

A THESIS

SUBMITTED TO THE

UNIVERSITY OF PUNE

FOR THE DEGREE OF

DOCTOR OF PHILOSOPHY

(IN CHEMISTRY)

By

SHUBHANGI G. GHOLAP

POLYMER SCIENCE & ENGINEERING DIVISION

NATIONAL CHEMICAL LABORATORY (NCL)

PUNE – 411008, INDIA

APRIL, 2005

CERTIFICATE

Certified that the work incorporated in the thesis entitled **"Hydrogel membranes for bio-separations"** submitted by Ms. Shubhangi G. Gholap, was carried out under my supervision. Such material as has been obtained from sources has been duly acknowledged in the thesis.

Date:15/04/05

National Chemical Laboratory

Pune 411008

Dr. M. V. Badiger

(Research Guide)

DECLARATION

I hereby declare that the work presented in the thesis entitled **"Hydrogel membranes for bio-separations"** submitted for Ph.D. degree to the University of Pune, has been carried out by me at the National Chemical Laboratory, Pune, under the supervision of Dr. M. V. Badiger. The work is original and has not been submitted in part or full by me for any degree or diploma to this or any other university.

Date:15/04/05 (**Shubhangi G. Gholap**)

National Chemical Laboratory
Pune-411008.

Dedicated to my family

Acknowledgement

I would like to express my deep gratitude and sincere thanks to my research guide, Dr. M. V. Badiger, for his invaluable guidance and constant encouragement throughout the research work. He taught me useful skills of research, technical writing and understanding the core of subject and advised throughout the course of this doctoral research. It would have been impossible without his freehand given to me to explore the work of interest.

The valuable guidance given by Dr. P. P. Wadgaonkar was very precious in my work, I am grateful for the same. I am also deeply indebted to Dr. S. S. Kulkarni, Dr. D. A. Musale and Dr. S. K. Karode for introducing me to the area of membranes and their provoking discussions as well as moral support, which gave me stimulus to work with such a new subject in that instance.

I take this opportunity to thank Mr. Mahendra Jagtap for all kind of timely help in the duration of this work especially for technical part. Without his help it would have been difficult to carry out all permeation experiments.

I am very much thankful to Dr. C. S. Gopinath for guidance during the experimental part of my research work. The discussion with him gave me a new altitude regarding the subject, which will guide me in my future. I also thank Dr. J. P. Jog for her encouragement and proper suggestions in my tenure.

It gives me honour to express my gratitude towards Dr. M. G. Kulkarni, Head of PSE Division for his moral support shown towards me. He took special effort for building up a right approach to present our views through series of seminars.

It is my pleasure to acknowledge Dr. S. Sivaram, Director, NCL for permitting me to present this work in the form of thesis.

I would like to acknowledge the financial support received from CSIR in the form of Senior Research Fellowship.

My sincere thanks go to Dr. B. D. Kulkarni, Head of CE Division, Dr. A. K. Lele, Mr. M. J. Thakar, Dr. S. B. Umbarkar and Dr. G. V. N. Rathna for the support given to me in my work.

It was a great pleasure to work with my colleagues who always kept me in the lively working environment and make each and every moment cheerful. No words can express my feeling for my friends who shared all the moments in my life. It is really difficult to thank them in words for their unconditional support.

The achievement made in my life was a dream of my parents, which came true. I am thankful to my parents and my family for being always with me and giving me the right direction in my life. I am really inspired by my father for his hard work and my mother who actually strengthened my goals and taught me to stand in all types of situation in the life.

Shubhangi G. Gholap

CONTENTS

Page No.

CHAPTER 1

Literature Survey

CHAPTER 2

Objective and scope of work

CHAPTER 3

Synthesis and Characterization of Polyamphoteric Hydrogel Membrane based on Chitosan

CHAPTER 4

Synthesis and Characterization of Hydrophobically Modified Poly(Vinyl Alcohol) Hydrogel Membrane

CHAPTER 5

Nanocomposite Hydrogel Membranes Based on PVA: Synthesis and Characterization

CHAPTER 6

Molecular Origins of Wettability of Hydrophobic Poly(vinylidene fluoride) Microporous Membranes on Poly(vinyl alcohol) Adsorption: Surface and Interface Analysis by XPS

CHAPTER 7

Conclusions and Direction for future work

List of Figures

CHAPTER 3

CHAPTER 4

CHAPTER 5

CHAPTER 6

List of Tables

CHAPTER 5

Abbreviations

π	Osmotic pressure
ν	Volume fraction of network
χ	Flory Polymer-solvent interaction parameter
V_1	Molar volume of the solvent
ϕ	Functionality of the junctions
X_c	Number of repeat unit of the network chain
$\in$	cycle rank of the network
J	Permeation rate
n	Number of pores per cm^2
P	Applied pressure
r	Pore radius
η	Viscosity of flowing liquid
d	Thickness of the membrane
M_c	Molecular weight between crosslinks
M_n	Number of average molecular weight
M_r	Molecular weight of repeat unit
ξ	Mesh size
γ_0	End-to-end distance in the unperturbed state
C_n	Characteristic ratio of polymer
γ_f	End to end distance in the freely jointed chain
λ	Number links per repeat unit
I	Ionic Strength
q	Swelling ratio
C_t	Solute concentration in the receptor cell
C_0	Initial solute concentration in the donor cell
V	Volume of each half cell
A	Effective permeation area

P	Permeability coefficient
t	Time
δ	Thickness of the membrane
η	intrinsic viscosity
θ	Contact angle

ABSTRACT

Introduction

Recently, major attention has been focused towards developing stimuli sensitive hydrogels and membranes for selective separations.[1-4] Membranes are semipermeable barrier materials, which are the main components of a separation process. The separation through porous membranes is mainly due to sieving mechanism of membranes and therefore, the efficiency of selective separation depends upon the size of the pores, chemical nature of membrane and the interaction between membrane and the permeate. Because of the unique properties, membranes have found large number of applications in bio-separation processes. Hydrogels are hydrophilic polymers and have three-dimensional network structures. These hydrogels are insoluble in water but exhibit swelling/shrinking depending on various external stimuli such as temperature, pH, electric field, magnetic field, light, etc. Therefore, they have been termed as stimuli responsive gels. The combination of hydrogels and membranes provide hydrogel membranes with synergistic properties of membranes and hydrogels with a good mechanical strength. Furthermore, these membranes mimic the biological tissues and exhibit excellent biocompatibility. The swelling and shrinking property of hydrogels can be used to adjust the pore size/mesh size of membranes.[5,6] Hydrogel membranes are generally characterized by swelling properties as well as the molecular weights between crosslinks(mesh size/crosslinking density). Permeation through hydrogel membranes not only depends on the molecular structure but also on the external conditions. Such membranes have applications in bio-separation, controlled drug delivery, bio-hybrid artificial organs and multi-component separations and also used as sensors and chemical valves.[7-11] Hydrogel membranes can be synthesized either by chemical crosslinking wherein, the covalent bonds are present between different polymer chains or by physical crosslinking, wherein the dissolution of polymer is prevented by physical interactions between polymer chains. In this work, we have applied both the methods for the synthesis of novel hydrogel membranes. We have selected chitosan [CS] and poly(vinyl alcohol) [PVA] due to their hydrophilic nature, biocompatibility and excellent film forming properties. The membranes, which show discontinuous volume transition in

water as a function of temperature, have potential applications in drug delivery system. So the work was undertaken to design and develop the thermosensitive membranes, which exhibit discontinuous volume transition in water as a function of temperature. Poly(N-isopropylacrylamide) [PNIPAm], is the most commonly used thermosensitive polymer exhibiting the lower critical solution temperature [LCST] in the range of 31-33°C.[12] Thermo- and pH- sensitive hydrogel membranes were synthesized based on chitosan and PNIPAm. It is well established that, the appropriate balance between hydrophilic and hydrophobic interactions lead to discontinuous phase separations. Therefore, the study was undertaken to synthesize thermosensitive hydrogel membranes whose homopolymers do not show LCST at an observable temperature range. In order to develop such thermosensitive hydrogel membranes without chemical crosslinker, N-tertiary butyl acrylamide [NTBA] monomer was grafted onto PVA. Moreover, post crosslinking of PVA film can be easily done by simple techniques like heat treatment/annealing of membranes at high temperature. In order to improve the mechanical strength of these membranes, water swellable nano-clay was incorporated and properties of the membranes were studied. It is well established that the presence of nano-clay in polymer system increases the mechanical property of the system.[13] The irreversible adsorption of PVA onto hydrophobic membranes such as polyvinylidene fluoride [PVDF] has been studied using XPS, water contact angle, etc. The molecular origin of the wettability of PVDF surface by hydrophilic PVA has been deduced by XPS and EDAX measurements.

The major emphasis is given on the synthesis and characterization of hydrogel membranes by different techniques. The swelling properties of these hydrogel membranes were carried out as a function of pH and temperature. Permeation studies through hydrogel membranes were undertaken using biomacromoles. The incorporation of nano fillers into hydrogels was performed to obtain nanocomposite hydrogel membranes with varying properties. The entire work is presented in seven chapters and the outline of each chapter is given in the foregoing.

Chapter 1: Literature Survey

The introductory chapter describes the background and the overview of membranes, hydrogels, stimuli sensitive membranes, different stimuli, applications and permeation studies. This chapter also includes the recent literature on nanocomposite gels, clays and salient features of nanocomposite hydrogel membranes. The details of techniques such as X-ray photoelectron spectroscopy, dynamic mechanical analysis [DMA] and contact angle measurements, which are used for characterization of membranes, are also discussed.

Chapter 2: Objective and scope of the work

The major focus of this work is to design and develop hydrogel membranes whose properties can be controlled by external conditions. This chapter highlights the objectives of the present work such as different strategies for synthesis of hydrogel membranes, nanocomposite gel membranes, adsorption of hydrophilic polymers onto hydrophobic membranes and characterization in terms of swelling, permeability, etc. The chapter also explains the scope of the present work.

Chapter 3: Synthesis and characterization of polyamphoteric hydrogel membrane based on chitosan

This part describes the synthesis and characterization of polyamphoteric chitosan [CS] hydrogel membrane. Grafting of N-isopropylacrylamide [NIPAm] and 2-acrylamido-2-methyl propane sulfonic acid [AMPS] monomers onto chitosan was carried out by free radical polymerization. Incorporation of NIPAm and AMPS was confirmed by FTIR spectroscopy. The swelling behaviour of these polyamphoteric hydrogel membranes was studied as a function of pH, temperature and ionic strength of the external solution. The influence of polyelectrolyte complex formation between CS and PAMPS on the swelling behaviour as well as LCST was studied in these membranes. Permeation of solutes with different sizes was carried out through these membranes. The

permeabilties of solutes through these membranes were strongly dependent on the size of solutes, solution temperature and hydrophilicity of the membranes.

Chapter 4: Synthesis and characterization of hydrophobically modified poly(vinyl alcohol) hydrogel membrane

This chapter deals with the details of synthesis of hydrophobically modified poly(vinyl alcohol), [PVA] by graft copolymerization of N-tertiary butyl acrylamide [NTBA] onto PVA by free radical polymerization. The incorporation of NTBA onto PVA chains was confirmed by IR and NMR spectroscopy method and contact angle measurements. Swelling behaviour and permeation of membranes were investigated as a function of NTBA content and temperature. The graft copolymeric membranes with low content of NTBA showed discontinuous transition with respect to temperature whereas, the presence of higher amounts of NTBA showed decreased swelling ratios with very little influence of temperature on the swelling. Effect of annealing at high temperature on the crystallinity and mechanical properties of membranes were investigated by DSC, DMA and XRD. It was found that the permeabilities of solutes through these membranes were strongly dependent on the size of the solute, solution temperature and hydrophobicity of the membrane.

Chapter 5: Nanocomposite hydrogel membranes based on PVA: synthesis and characterization

Nanocomposite hydrogels, composed of specific polymers and water-swellable inorganic clay have attracted increasing attention lately because of their enhanced mechanical properties. The novel nanocomposite hydrogels can overcome some of the limitations in the conventional hydrogels.

This chapter reports on the study of laponite (inorganic clay) incorporated PVA-NTBA hydrogel. The swelling and mechanical properties of the nanocomposite hydrogels were studied as a function of laponite content. It was observed that the content

of laponite in the membrane has a strong influence on the swelling and mechanical properties. The permeability of membranes with different solutes was studied and correlated.

Chapter 6: Molecular origins of wettability of hydrophobic poly(vinylidene fluoride) membranes upon poly(vinyl alcohol) adsorption: surface and interface analysis by XPS

This chapter deals with the study of irreversible adsorption of poly(vinyl alcohol) [PVA] onto porous hydrophobic poly(vinylidene fluoride) [PVDF] membranes. Although most of the synthetic water-soluble polymers do not adsorb onto hydrophobic surfaces, PVA spontaneously adsorbs irreversibly onto hydrophobic substrates. The underlying mechanism of irreversible adsorption is yet to be fully understood. Therefore, in order to understand the molecular origin of the adsorption, these membranes were subjected to intense physico-chemical analysis with X-ray photoelectron spectroscopy [XPS]. Membrane texture properties were studied by using mercury porosimetry analysis. XPS and energy dispersive analysis of X-ray [EDAX] measurements confirmed the adsorption of PVA onto PVDF membranes and explained the molecular origins of wettability. The driving force for adsorption is an irreversible electronic interaction between PVA and PVDF possibly through the charge transfer between the polymers as observed by XPS results. Improved wettability and water permeation was found after PVA adsorption onto porous hydrophobic PVDF membranes. XPS and water permeation studies indicated that there is a threshold coverage of PVA onto porous PVDF membranes that is at 4% PVA concentration. This can be a very simple technique to hydrophilize the hydrophobic membranes.

Chapter 7: Conclusions and direction for the future work

The important conclusions of the work are summarized in this chapter. Polyamphoteric hydrogel membranes based on chitosan showed duel sensitivity towards pH and temperature. These membranes also showed the important role of polyelectrolyte complex formation on swelling properties. With a critical balance between hydrophilic and hydrophobic interactions in PVA and PNTBA, the discontinuous volume transition was observed. This can have significance in the design of smart membranes for separation processes. Novel nanocomposite hydrogel membranes based on PVA and water swellable laponite clay were synthesized. The swelling and mechanical properties of the nanocomposite gels were found to depend on the clay content in the gel membranes. It was demonstrated that PVA irreversibly adsorbed onto hydrophobic PVDF membrane. Further insight into the molecular origin of irreversible adsorption has been gathered using XPS and EDAX. This chapter also explains the future scope of the work.

References

1. Hoffman, A.S. Advanced Drug Delivery Reviews **2002**, *54*, 3.
2. Park, Y. S.; Ito, Y.; Imanishi, Y. Langmuir **1998**, *14*, 910.
3. Liang, L.; Shi, M.; Viswanathan, V. V.; Peurrung, L. M.; Young, J. S. J. Membr. Sci., **2000**, *177*, 97.
4. Jiang, W.; Childs, R. F.; Mika, A. M.; Dickson, J. M. Desalination **2003**, *159*, 253.
5. Liang, L.; Feng, X.; Peurrung, L.; Viswanathan, V. J. Membr. Sci., **1999**, *162*, 235.
6. Bell, C. L.; Peppas, N. A. J. Controlled Release **1996**, *39*, 201.
7. Okano, T.; Bae, Y.H.; Jacobs, H.; Kim, S.W. J. Controlled Release **1990**, *11*, 255.
8. Burczak, K.; Gamian, E.; Kochman, A. Biomaterials **1996**, *17*, 2351.
9. Feil, H.; Bae, Y. H.; Feijen, J.; Kim, S. W. J. Membr. Sci. **1991**, *64*, 283.
10. Mika, A. M.; Childs, R. F.; Dickson, J. M. J. Membr. Sci. **1999**, *153*, 45.
11. Kermis, H. R.; Rao, G.; Barbari, T. A. J. Membr. Sci. **2003**, *212*, 75.

12. Heskins, M.; Guillet, J. E. J. Macromol. Sci. Chem. A2 **1968**, *8*, 1441.

13. Giannelis, E. P. Adv. Mater. **1996**, *8*, 29.

CHAPTER 1

Literature Survey

1.1 Introduction

Hydrogel is a three dimensional polymeric network that is insoluble in water at physiological pH, temperature and ionic strength. The existence of hydrogel dates back to 1960, when, Wichterle and Lim first proposed the use of hydrophilic networks of (2-hydroxyethyl methacrylate) [PHEMA] in contact lens applications.[1] Since then, the use of hydrogels has been extended to various biomedical and pharmaceutical applications.[2-4] Hydrogels resemble living tissues very closely in their physical properties because of their relatively high water content and soft and rubbery nature. There are large number of natural and man-made hydrogels. For example, the vitreous humor that fills the interior of the eye and the synovial fluid that lubricates the joints of the skeleton are natural gels. These hydrogels consist of two components, a polymer network and a liquid. The network provides a structural framework and holds the liquid in space. Depending on the chemical compositions and various other factors, hydrogels vary in consistency from viscous fluid to fairly rigid solids, but typically, they are soft and resilient, like jelly. They are viscoelastic in nature i.e. they have properties of a viscous solution and of an elastic solid. Routinely, the terms 'gel' and 'hydrogel' are used interchangeably. This could be a misinterpretation because although, as polymer networks, both gels and hydrogels might be similar chemically, but they are physically distinct. Hydrogels are generally described as gels swollen in water. Whereas, gel need not contain any solvent and could be a flexible/hard matter, for example, rubbery silicon gel or polystyrene gel, etc. Therefore, Dorothy Jordon Lloyd, a chemist, aptly said that "It is easier to recognize a gel than to define it".

1.2 Classification of Hydrogels

There are two types of hydrogels

1. Naturally occurring hydrogels and
2. Synthetic hydrogels

1.2.1 Naturally Occurring Hydrogels

These are polysaccharides, carrageenans, gum arabic, agarose, cuprophan, dextran, collagens, etc. They have applications in pulp and paper production, artificial silk and cellulosic membrane production. However, they have limitations due to their poor mechanical properties, low temperature tolerance and poor resistance to microbial attack.

1.2.2 Synthetic Hydrogels

Synthetic hydrogels have mostly been prepared from monomers and polymers such as hydroxyethyl methacrylate (HEMA), polyethyleneglycol methacrylate (PEGMA), acrylamide (AAm), methoxy-terminated PEG derivative (MPEGMA), N-vinyl pyrrolidone (NVP), polyethylene oxide (PEO), acrylic acid (AA), poly(vinyl alcohol) etc. These gels have been prepared mostly in the form of membranes, beads, rods, strips, etc. Synthetic hydrogels demonstrate better mechanical properties, good temperature tolerance and resistance to microbial attack. Some of these hydrogels do not exhibit significant sensitivity to the external changes and termed as conventional hydrogels. Whereas, others show varying degree of responses to different stimuli such as temperature, pH, electric field etc. and are popularly known as “stimuli-responsive” hydrogels.[5,6]

1.3 Synthesis of Hydrogels

Hydrogel is formed by crosslinking of polymer chains and the crosslinking can be provided by covalent bonds, hydrogen bonding, van der Waals interactions or physical entanglements. Different crosslinking methods, including physical and chemical crosslinking have been explored and used for the synthesis of hydrogel.[7] In chemically crosslinked hydrogels, covalent bonds are present between the polymer chains and generally include the chemical crosslinker in the structure whereas, in physically crosslinked gels the network is formed by the physical interactions between

polymer chains. The chemical and physical crosslinking methods are summarized in **Table 1.1**.

Table 1.1: Different crosslinking methods for the synthesis of hydrogels

Chemical Crosslinking	**Reference**
1. Radical polymerization	8, 9
2. Chemical reaction with complementary groups	
a. Crosslinking of alcohol, amine and hydrazide groups with aldehyde	10, 11
b. Crosslinking by addition reaction	12, 13
c. Crosslinking by condensation reaction	14
3. High energy irradiation	15-18
4. Crosslinking using enzymes	19, 20
Physical Crosslinking	
1. Ionic interactions	21, 22
2. Crosslinking by crystallization	
a. Crystallization in homopolymer	23, 24
b. Crosslinking by stereocomplex formation	25
3. Amphiphilic block and graft copolymers	26, 27
4. Hydrogen bonds	28
5. Protein interactions	29

1.4 Swelling of Hydrogel

The most remarkable feature of hydrogels is their property of swelling and deswelling in a aqueous medium. The theory of swelling of non-ionic, crosslinked polymeric network was first proposed by Flory in 1950s[30], who subsequently modified his theory to take into account the effects of ionic substituents. Flory proposed an analogy between swelling equilibrium and an osmotic equilibrium. The total osmotic pressure (π) acting on the gel comprises of the forces arising from polymer-polymer affinity (mixing), rubber elasticity and hydrogen ion pressure and is given by,

$$\pi = \Delta\mu_1 = \mu_1 - \mu_1^0 = (\Delta\mu_1)_{mix} + (\Delta\mu_1)_{el} + (\Delta\mu_1)_i \qquad (1.1)$$

where,

$$\left(\Delta\tilde{\mu}_1\right)_{mix} = \ln(1-v_2) + v_2 + \chi v_2^2 \qquad (1.2)$$

v_2 = volume fraction of the network

χ = polymer-solvent interaction parameter.

$$\left(\Delta\tilde{\mu}_1\right)_{el} = \frac{\beta}{\lambda}\left[1 + \frac{\mu}{\in} k(\lambda)\right] \qquad (1.3)$$

$$\beta = \frac{V_1}{RT}\frac{\in kT}{v_0} = \frac{v_{2c}}{X_C}\left(1 - \frac{2}{\phi}\right) \qquad (1.4)$$

$V_1 =$ molar volume of the solvent

$\phi =$ functionality of the junctions

$X_C =$ number of repeat units of the network chain

$\in =$ cycle rank of the network

$$\lambda = \left(\frac{v}{v_0} \right)^{\frac{1}{3}} \text{ and}$$

$$\left(\Delta \bar{\mu}_1 \right)_i = \frac{-iv_2}{X_C} \tag{1.5}$$

$i =$ number of ionic centers in the polymer

$$\Delta \bar{\mu}_1 = \ln(1 - v_2) + v_2 + \chi v_2^2 + \frac{\beta}{\lambda}\left[1 + \frac{\mu}{\in} k(\lambda)\right] - \frac{iv_2}{X_C} \tag{1.6}$$

When the gel is immersed in solvent, it swells by taking up solvent until equilibrium is reached between entropic forces that encourage the solvent molecules to mix into the network, and the elastic forces of the stretched chains, which tend to prevent further swelling. At conditions of equilibrium, the activity a_1 of the solvent equates to unity and the solvent chemical potential equals to zero. The solution of equation (1.6) for ν_2 then gives the equilibrium degree of swelling of the network.

Various thermodynamic models have been extensively used to explain the swelling of specific hydrogels.[31,32] An equilibrium model has been developed to predict the swelling kinetics of hydrogel at a given pH and salt concentrations by De *et. al.*[33] **Table 1.2** highlights the different factors which influence the swelling of hydrogels.

Table 1.2: Different factors which influence the swelling of hydrogels

Favourable to swelling	Inhibit swelling
• Osmotic pressure • Strong interactions (H-bonding) with water • High free volume • Chain flexibility • Low crosslinking density	• Weak interactions with water • Low free volume • Low chain flexibility • High crosslinking density

1.5 Stimuli-Responsive Hydrogels

Various terms have been coined to hydrogels such as 'intelligent gels' or 'smart hydrogels' or 'stimuli-responsive' hydrogels. The smartness of these materials is a key to their ability to receive, transmit or process a stimulus, and respond by producing a useful effect. These polymer hydrogels are known to exist in two distinct phases, swollen and collapsed. These transitions particularly the discontinuous ones, can be induced by using the trigger of an external stimuli such as temperature, pH, light, solvent composition, electric field, etc.[6,34] Interestingly, their stimuli responses are smartly and intelligently manifested in changes in shapes, phases, optics, mechanics, surface energies, permeation, etc. Therefore, these gels have shown promising applications[35,36] in gel-based actuators,[37,38] valves,[39] molecular sensors,[40] artificial muscles,[41,42] robotics, controlled release systems,[43,44] optical shutters and molecular separation systems.[45-47] In view of the emerging practical applications in various fields, these hydrogels have been considered as the materials of 21st century.

There are many possible molecular mechanisms, which can cause such sharp and discontinuous transitions in hydrogels and they are listed in **Table 1.3**.

The four fundamental interactions which govern the volume phase transitions in hydrogels are van der Waal's interactions, hydrophobic interactions, H-bonding and electrostatic interactions.[48]

Table 1.3: Molecular mechanisms of sharp phase transition

Ø Ionization or neutralization
Ø Ion-exchange
Ø Ion-ion repulsion or attraction
Ø Release or formation of hydrophobically bound water
Ø Coil-globule transition
Ø Onset or inhibition of chain motion
Ø Crystallization or melting
Ø Isomerization between hydrophilic and hydrophobic forms
Ø Counter-ion movement in an electric field
Ø Electron transfer redox reactions

1.5.1 Temperature Sensitive Hydrogels

Amongst the various stimuli mentioned earlier, temperature is the most widely studied stimulus in 'stimuli-responsive' hydrogels. These hydrogels are called as "thermosensitive or thermoreversible hydrogels." The property of thermoreversibility arises from the fact that, these polymers exhibit the thermodynamic lower critical solution temperature (LCST) and show inverse solubility behaviour with an increase in temperature. The classical example is the solution of poly (N-isopropylacrylamide) [PNIPAm] in water, which shows an LCST in the range of 31-33 °C.[49,50] The crosslinked hydrogels obtained from such thermosensitive polymers undergo a first order volume transition at LCST and are highly swollen below LCST and completely

collapsed or shrunk above LCST. **Figure 1.1** gives the schematic representation of the phase transition in thermosensitive polymers.

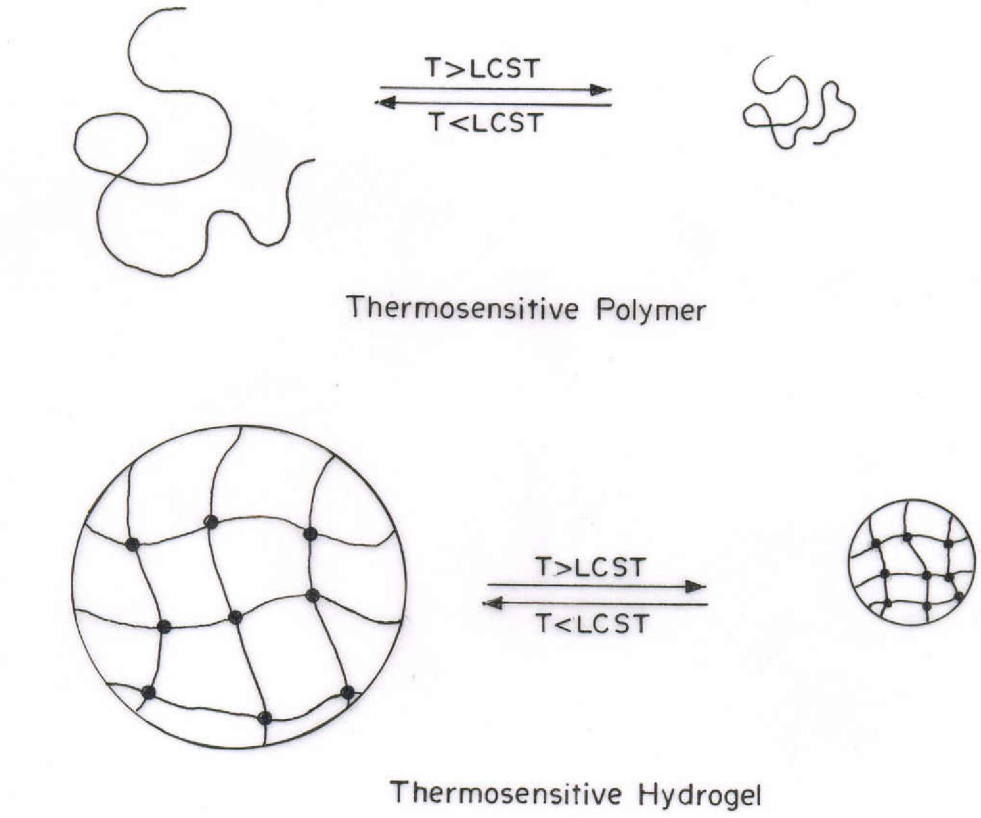

Figure 1.1: Schematics of the phase transition in thermosensitive polymer and hydrogel.

These volume transitions are attributed to the hydrophobic interactions and polymer-polymer/polymer-solvent H-bonding interactions. These hydrogels are made up of polymer chains that either possesses moderately hydrophobic groups or a mixture of hydrophilic and hydrophobic segments. Thermosensitive hydrogels have been usually synthesized from N-substituted acrylamides, monomer containing ether groups such as vinyl methyl ether (VME), monomers containing alcohol groups such as hydroxypropyl acrylate, hydroxypropyl methyl cellulose, methyl cellulose, polyvinyl alcohol and their derivatives. Certain types of block copolymers made up of

poly(ethylene oxide) (PEO) and poly(propylene oxide) (PPO) chains exhibit LCST behaviour in aqueous solutions. Important water-soluble, non-ionic polymers, which form thermosensitive polymers with a wide range of LCSTs are based on N-alkyl acrylamide homopolymers and copolymers. Transition temperatures of poly(N-alkylacrylamide) derivatives are summarized in **Table 1.4**.[51]

Table 1.4: Transition temperatures of poly(N-alkylacrylamide) derivatives

Polymer	Transition temperature/°C
Poly(N-ethylacrylamide)	72.0
Poly(N-ethylmethacrylamide)	50.0
Poly(N-n-propylacrylamide)	21.0
Poly(N-n-propylmethacrylamide)	28.0
Poly(N-isopropylacrylamide)	30.9
Poly(N-isopropylmethacrylamide)	44.0
Poly(N-cyclopropylacrylamide)	45.5
Poly(N-cyclopropylmethacrylamide)	59.0
Poly(N-methyl-N-ethylacrylamide)	56.0
Poly(N,N-diethylacrylamide)	32.0
Poly(N- methyl-N-isopropylacrylamide)	22.3
Poly(N- methyl-N-n-propylacrylamide)	19.8
Poly(N-acryloylpyrrolidine)	56.0
Poly(N-acryloylpiperidine)	5.5

It can be realized that, below LCST, the hydrogel swells as a result of H-bonding between hydrophilic groups of polymer and water. However, above LCST, this H-bonding interaction breaks/weakens and the hydrophobic interactions dominate resulting into shrinking of the gels. Therefore, the balance of hydrophilic and hydrophobic groups on the polymer chain plays a crucial role in the determining LCST of the polymer. Nevertheless, the LCST of the polymer can be changed/designed to a desired value by proper balance of hydrophobic/hydrophilic content in the polymer. In general, the LCST of the polymer/copolymer increases with an increase in the hydrophilic content and decrease with an increase in the

hydrophobic content. Different factors, for example, hydrophobic,[52] hydrophilic modification,[53] solvent,[54,55] additives[56] influence the LCST of polymer.

Thermosensitive hydrogels have been explored in different applications such as drug delivery,[57,58] bioseparations,[59] tissue culture, etc.[60]

1.5.2 pH Sensitive Hydrogels

pH sensitive hydrogels contain ionic groups in their chain and are also called as polyelectrolyte hydrogels. pH-sensitive hydrogels usually contain pendant acidic (e.g. carboxylic and sulfonic acids) or basic (e.g. ammonium salts) groups, which either accept or release protons (i.e. undergo ionization) in response to changes in environmental pH resulting into introduction of charges in the hydrogel. **Table 1.5** lists ionizable cationic and anionic monomers used in the synthesis of pH-sensitive hydrogels. pH sensitive hydrogels often show high degree of swelling than non ionic or neutral hydrogels. Hydrogels containing acidic groups ionize and swell more (due to electrostatic repulsion between charges present on the polymer chains) in the weakly alkaline medium but collapse in acid medium due to charge neutralization. On the contrary, hydrogels with basic groups protonate and swell more in the acidic medium and collapse at highly basic medium. **Figure 1.2** shows the swelling behaviour of anionic and cationic hydrogels as a function of pH.

Equillibrium degree of swelling depends on the charge on the monomer, pKa of the ionizable groups, degree of ionization, the concentration of ionic monomer in the polymer system, degree of the crosslinking, hydrophilicity of polymer, pH and ionic strength of the medium.[61] The electrostatic repulsion along the polymer chains contributes to increase in swelling of pH-sensitive hydrogels. However, the addition of small amount of electrolytes such as NaCl leads to a Debye-Huckel shielding effect and the polymer chains undergo conformational transitions adopting a smaller, more entropically favoured conformation as shown in **Figure 1.3**.

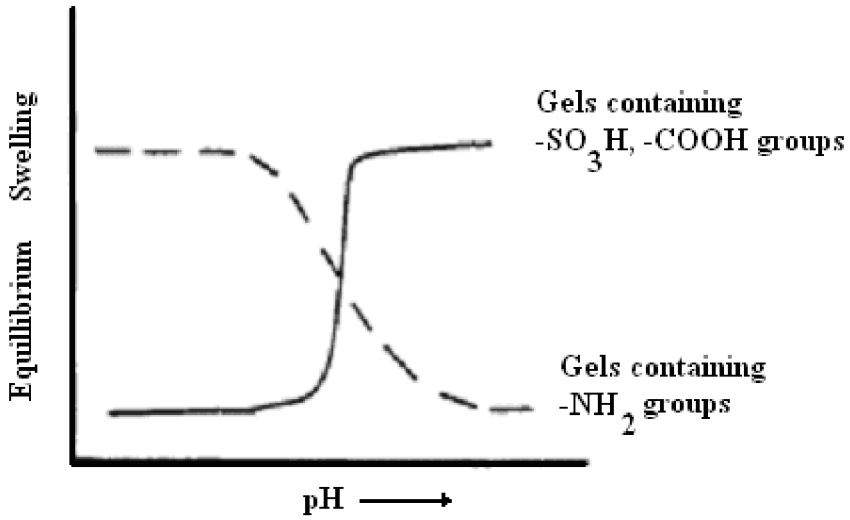

Figure 1.2: Swelling behaviour of anionic and cationic hydrogels as a function of pH

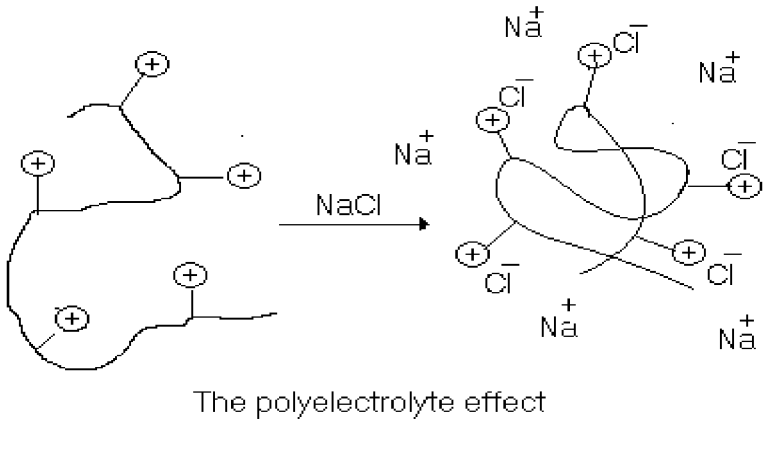

Figure 1.3: Polyelectrolyte effect due to addition of ions

Table 1.5: Important ionic monomer/polymer and respective pK value of corresponding homopolymers

Type	Monomer	pH-sensitive group	pK_a	Reference
Acidic	Acrylic acid	-COOH	4.7	62
	Methacrylic acid	-COOH	6.15/6.35	63
	Sodium styrene sulfonate	$-SO_3^-Na^+$	<1	64
	2-acrylamido-2-methyl-1- propane sulphonic acid	$-SO_3H$	2.86	65
Basic	N, N-Dimethylaminoethyl methacrylate	$-N(CH_3)_2$	6.6	66
	N, N-Diethylaminoethyl methacrylate	$-N(CH_2CH_3)_2$	6.9	66
	2-/4-Vinyl pyridine	Pyridine ring	5	67
	Chitosan	$-NH_2$	6.3	68

The pH in stomach (<3) is quite different from the neutral pH in the intestine. Therefore, pH-sensitive hydrogels have been most frequently used to develop controlled release formulations for oral administration because of pH variation throughout the gastro-intestinal tract.[69,70] Furthermore, anionic hydrogels made up of poly(acrylic acid) (PAA) or poly(methacrylic acid) (PMA) can be used to develop formulations that release drugs in a neutral pH environment. The degree of swelling increases as the hydrogel passes down the intestinal tract due to increase in pH leading to ionization of the carboxylic groups.[71,72]

1.5.3 Electric-Field Sensitive Hydrogels

Electric current can be used as one of the stimuli to induce volume transitions in hydrogels. Electro-sensitive hydrogels usually consist of polyelectrolytes and undergo volume transition in the presence of an electric field.[73] Under the influence of a dc electric field, three types of deformations such as shrinking, swelling and bending of hydrogels can be observed. For example, swollen acrylic acid-acrylamide copolymer gels undergo volume transition under the influence of an electric field.[74] They also made a prototype of robot's hand having soft fingers and an artificial fish having a soft tail, both of them showed the electrically driven motality. Electro-sensitive hydrogels also have applications in drug delivery.[75]

1.5.4 Light-Sensitive Hydrogels

Light-sensitive gels have been developed by incorporating photosensitive molecules such as bis(4-(dimethylamino) phenyl)(4-vinyl phenyl) methyl leucocyanide, into the PNIPAm gels.[76] A discontinuous volume phase transition was observed in these gels of N-isopropylacrylamide when exposed to ultraviolet irradiation. The phenomena were caused by osmotic pressure of cyanide ions created by ultraviolet irradiation which photodissociates the leucocynide groups. Visible light-sensitive hydrogels were prepared by introducing a light-sensitive chromophore (e.g. trisodium salt of copper chlorophyllin) into poly(*N*-isopropylacrylamide) hydrogels.[77]

Other stimuli sensitive hydrogels include magnetic field sensitive[78], pressure sensitive[79], biochemically sensitive hydrogels[80] have been studied and reported.

However, weak mechanical strength of these stimuli sensitive hydrogels limit their applications in certain areas. Therefore, in order to improve the mechanical strength of hydrogels, synthesis of hydrogels in confined geometry such as pores of microfiltration/ultrafiltration membranes or nanocomposite hydrogels have been developed.

We describe briefly the membranes, properties and their applications in the following section.

1.6 Membranes

Membranes are semi-permeable barrier between two phases, which restrict the movement of one or more components of one or both fluids across the barrier. A membrane process allows selective and controlled transfer of one species from one bulk phase to another bulk phase separated by the membrane. **Figure 1.4** shows the schematic of separation process through membrane.

Membranes are made from different materials like organic and inorganic, and can be in the form of sheets or tubes. The movement of any species across the membrane is caused by one or more driving forces, which arise, from the gradient of chemical potential or electrical potential. A gradient in chemical potential may be due to a concentration or pressure gradient or it can be both.

1.6.1 Classification of Membranes

In this thesis, we have focused on the polymeric membranes used for liquid separations. Generally membrane separation process is driven by concentration, pressure and electrical gradients. The classification of membranes by driving forces is given in **Table 1.6**.

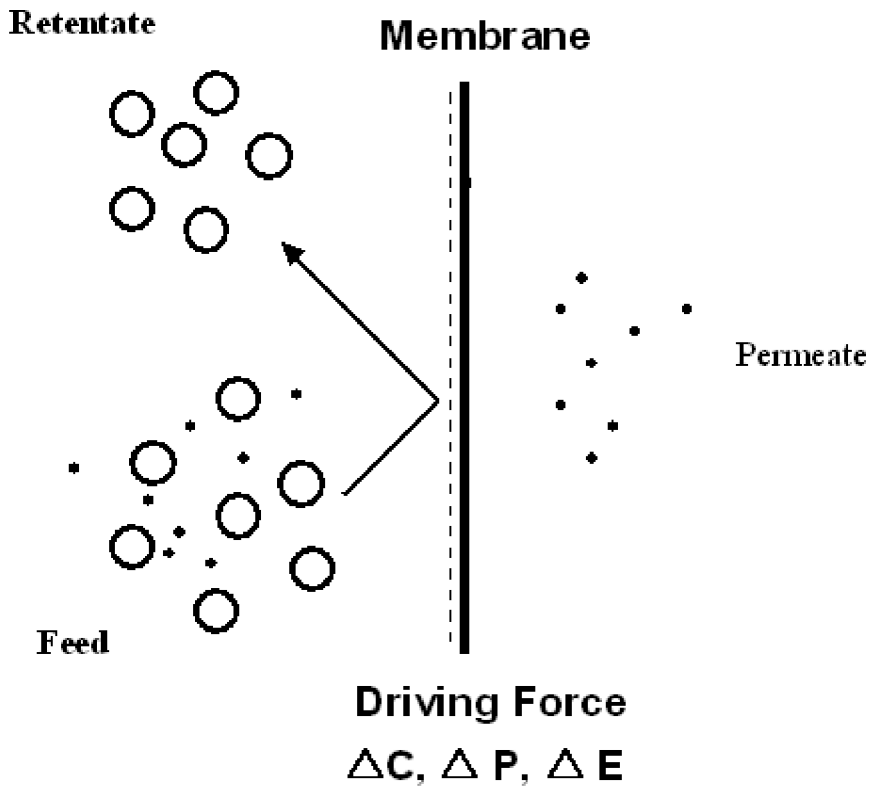

Figure 1.4: Schematic of membrane separation process.

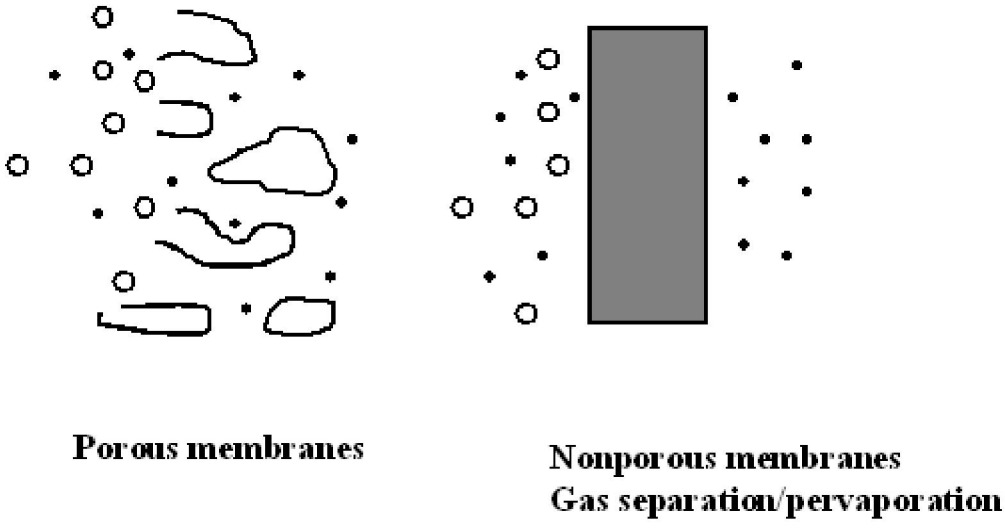

Figure 1.5: Separation of solutes through porous and nonporous membranes.

Table 1.6: Classification of Membranes

Driving Force	Process	Mechanism	Membrane type	Nature of species retained (size)
Pressure	Microfiltration	Sieving	Porous with clarification pores	0.1 to 10μm
Pressure	Ultrafiltration	Sieving	Porous with 1-100 nm	10 to 200Å
Pressure	Reverse osmosis	Solution-diffusion	Dense skin asymmetric	1 to 10 Å
Concentration	Dialysis	Diffusion	Microporous	>0.02μm retained, >0.005μm retained in haemodialysis
Concentration (pressure + temperature assisted)	Gas	Solution-diffusion	Dense skin asymmetric	Larger species retained unless highly soluble
Concentration (pressure + temperature assisted)	Pervaporation	Solution-diffusion	Dense skin asymmetric	Larger species retained unless highly soluble
Electrical	Electrodialysis	Charge and size of particle	Ion-exchange	Coions, macroions macromolecules with charge and water

Membranes are broadly classified into porous and nonporous membranes. Sieving mechanism plays a vital role in separation of solutes through porous membranes. However, diffusion and solution mechanism becomes important when the sizes of both pores and solutes decrease as shown in **Figure 1.5**. Porous membranes are further classified into microfiltration, ultrafiltration, nanofiltration and reverse osmosis membranes depending on the pore size of the membranes. However, in nonporous membranes permanent or fixed pores are absent but on molecular level dynamic molecular pores are present which allow the transport. The existence of these dynamic molecular pores can be adequately described in terms of free volume.

Microfiltration membranes contain macropores in the range of 0.05-5 μm, which are typically used in separation of suspended matter (in the size range from 0.1 to 10 μm) in liquids and gases. In the microfiltration membranes, the pore size and permeate flux are larger than ultrafiltration and reverse osmosis membranes.[81]

Ultrafiltration membranes contain mesopores and typically have pore sizes in the range of 10-1000Å. They can reject macromolecular solutes, which have molecular weight in the range of 300 to 500,000 daltons. Ultrafiltration is mainly used for clarification, concentration and fractionation of macromolecules.[82]

Nanofiltration and reverse osmosis membranes contain micropores, which are in the size below 2 nm. They are able to reject microsolutes in the range of 200-1000 daltons. Commercial reverse osmosis membranes are either asymmetric or thin film composite membranes. Applications of these membranes include sea-water and brackish water desalination, treatment of water and hazardous wastes, separation processes in the food, beverage, pulp and paper industries and recovery of organic and inorganic materials from chemical processes.[83]

Separation through porous membranes is considered to be size exclusion based pressure driven process. The membranes are generally characterized in terms of their molecular weight cut-off value (MWCO), which is defined as the smallest molecular weight of the species for which the membrane has more than 90% rejection.

1.6.2 Fouling of Membranes

The major limitation in the ultra or microfiltration process is the membrane fouling and concentration polarization that occurs due to the rejection of solute molecules at the membrane surface. Concentration polarization can be controlled by changing module design and system hydrodynamics. However, fouling is mainly dependent on the various solute-membrane interactions, membrane morphology and solute-solute interactions. The adsorption of solutes depends on the solute-membrane interactions[84] such as hydrogen bonding, dipole interactions, van der Waals interactions and electrostatic interactions.[85-87]

1.6.3 Different Techniques used to increase the Hydrophilicity of the Membranes and reduce the Fouling

Different techniques such as plasma polymerization, UV polymerization, coating and chemical methods have been used to increase the hydrophilicity of the membranes, which are discussed below.

1.6.3.1 Chemical method (chemical/UV irradiation)

Hydrophobic surfaces can be chemically modified by introducing charges or hydrophilic groups such as carboxylic, amino, hydroxyl, sulfonic, quaternary ammonium on the surface.[88-92]

1.6.3.2 Plasma treatment

Plasma treatment is a versatile technique to improve the surface hydrophilicity of membranes by inducing polar functional groups at the surface. The modification of hydrophobic membranes with variety of plasma treatment using carbondioxide,[93] nitrogen,[94] argon,[95] oxygen,[96] have been reported.

1.6.3.1 Coating

Surface coating is one of the methods of imparting the hydrophilic properties to the membrane and reduce the fouling of the membrane.[97,98] Li and Barbari[98] have reported poly (vinyl alcohol) (PVA) thin-gel composite ultrafiltration membrane by spin coating of PVA hydrogel onto cellulose membranes. The effects of hydrogel thickness and the degree of crosslinking on the pure water flux and ultrafiltration flux were studied and their resistance to the fouling was investigated.

1.6.4 Stimuli-Sensitive Porous Membranes

Stimuli-sensitive membranes are those whose permeability is very sensitive to the external stimuli. Stimuli-sensitive membranes have been extensively studied and reported in the recent past. The commonly used stimuli are pH, ionic strength and temperature. Due to change in conformations of stimuli-sensitive polymers as a function of external medium, the effective pore size and consequently the permeation through these membranes is controlled by stimuli as shown in the **Figure 1.6**. These membranes enlarge and contract pores reversibly resulting in a controlled permeability and improved performance in separation of macromolecular solutes. The importance of pore size on the permeability is given by Hagen-Poiseuille's equation.

$$J = \frac{n\pi r^4 AP}{8\eta d} \qquad (1.7)$$

Where,

J = Permeation rate

n = Number of pores per cm^2

A = Surface area of the membrane

r = Pore radius

P = Applied pressure

η = Viscosity of flowing liquid

d = Thickness of the membrane

Some of the stimuli responsive polymer systems with their method of synthesis, monomer/polymer and various stimuli are given in **Table 1.7**.

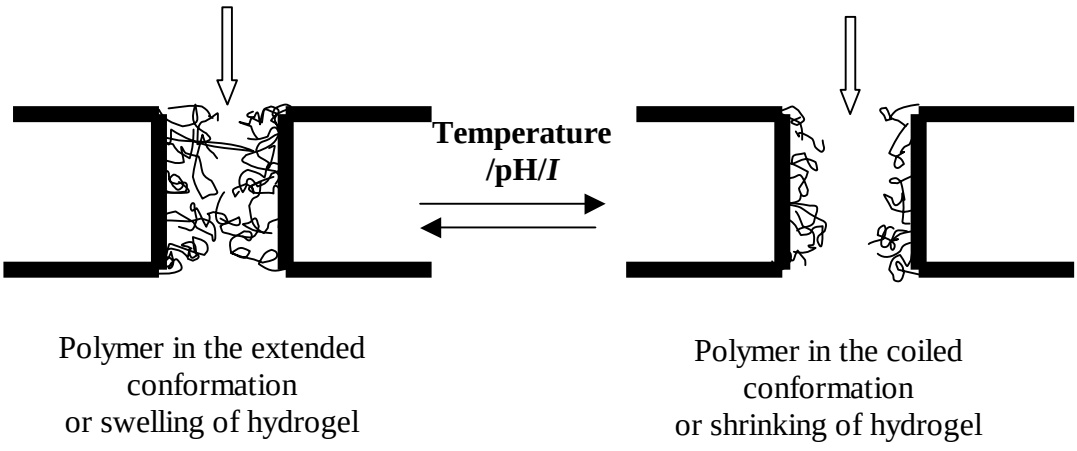

Figure 1.6: Effect of conformational changes of polymer/hydrogel on the pore size of membrane

Table 1.7: Stimuli-Sensitive Membranes System

Stimuli	Monomer/ Polymer	Membrane	Method of Grafting	Ref.
pH/Ionic strength./ metal ions	MMA	PVA	Plasma initiated	99
pH	MMA	PC	Glow discharge	100
pH	4-VP	PP	Photo initiation	101
pH	4-VP	PP/PE	Photo initiation	102
pH	AA / AA - co- VA	PVDF	Plasma	103
Ionic strength	AMPS	Nylon	Chemical	104
pH/ Ionic strength	AAc/MAA/EAA	PC	Glow discharge	105
pH	AAc	PVDF	radiation	106
pH	AAc	PC	Glow discharge	107
pH	MAA	PC	Glow discharge	108
pH	PVP	PP	Photoinitiated	109
pH, Temperature	AA, MAA	Polyamide	Plasma treatment, uv irradiation	110
Temperature	NIPAm	PP	Plasma	111
Temperature	NIPAm	PC	photoimmobilization	112
Temperature	NIPAm, NIPAm-co-AAm, NIPAm-co-BMA	PVDF	Plasma treatment	113
Temperature	NIPAm	Nylon capsule	Chemical	114
Temperature	NIPAm	PE	UV irradiation	115
photo	SPMMA/AAm	PTFE	Glow discharge	116

AMPS: 2-acrylamido-2-methyl-1-propane sulfonic acid
AAm: Acrylamide
AAc: Acrylic acid
MAA: Methacrylic acid
NIPAm: N-isopropylacrylamide
PC: polycarbonate
PE: polyethylene
PP: polypropylene
PVA: poly(vinyl alcohol)
PVDF: poly(vinylidenedifluoride)
PTFE : Polytetrafluoroethylene
SPMMA: Spiropyran containing methacrylate
VA: Vinylamine
VP: Vinyl pyridine

Major attention has been focused on developing hydrophilic membranes because of their low fouling tendency. The combination of hydrogels and membranes can provide synergistic properties of both hydrogels and membranes. In the following, we provide some literature on stimuli responsive hydrogel membranes, gel filled membranes and nanocomposite membranes.

1.7 Hydrogel Membranes

Hydrogel membranes are macroscopically nonporous but microscopically they constitute of a network of macromolecular chains connected through chemical or physical crosslinks, which form a mesh like structure. Due to this network they are capable of swelling the fluid medium and could be in the form of symmetric and asymmetric membranes. These membranes are highly hydrophilic in nature and consequently have advantages in membrane separations since they exhibit low fouling tendency. It is well established that permeation through hydrogel membranes not only depends on the molecular structure of the solute but also on the external conditions, which influence swelling and shrinking properties of hydrogels.

1.7.1 Important Parameters to Evaluate Membrane Properties

Hydrogel membranes are generally characterized by the swelling properties of the membranes. Different factors such as crosslinking density 'ρ', molecular weight between crosslink points 'M_c' and mesh size 'ξ' influence the swelling ratio of the membranes. The presence of crystallinity in the polymer system can act as physical crosslinks in the network.[117-122] It was observed that the degree of swelling decreases with increase in crystallinity.[123]

1.7.1.1 Mesh size and M_c of Hydrogel

Mesh size (ξ) is a space that is not occupied by the polymer, which is an effective area available for diffusion as shown in **Figure 1.7**. However, in the case of semi-crystalline hydrogel membranes, the mesh size is considered to be the space volume between the crystalline regions (see **Figure 1.8)**. 'M_c' and 'ξ' can be determined by knowing the equilibrium swelling ratio of hydrogels. The equilibrium-swelling ratio (q), is the weight ratio of the swollen to the dry gel.

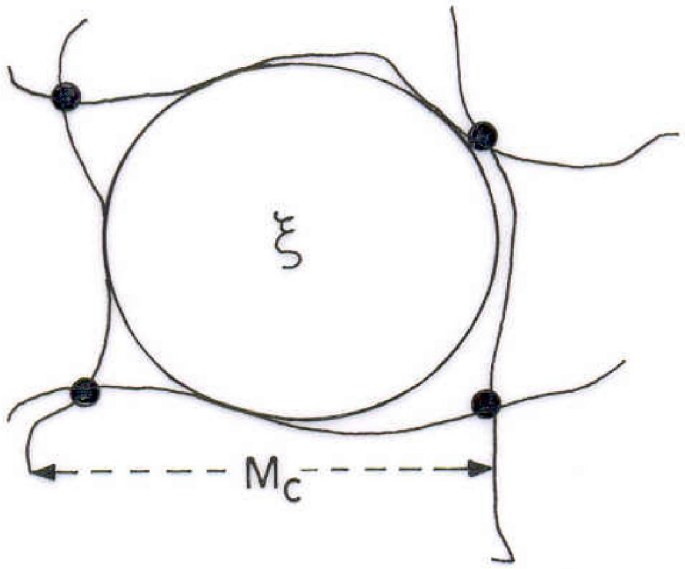

Figure 1.7: Mesh size and molecular weight between crosslinks of hydrogel membrane

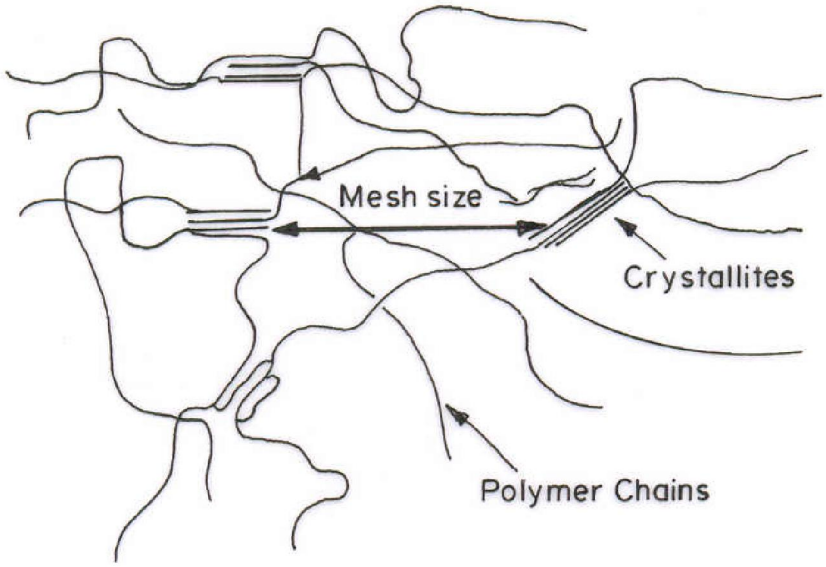

Figure1.8: Physical network in semi-crystalline hydrogel membrane

1.7.1.2 Swelling Ratio

Swelling ratio is a very important parameter since it determines the equilibrium amount of water the hydrogel can absorb. It is a function of network structure, crosslink density, hydrophilicity and ionization of functional groups. Swelling ratios are calculated from swelling studies and can be used to determine the molecular weight between crosslinks M_c and the mesh size ξ of the membrane. As the crosslink density of the hydrogel increases the M_c and ξ decreases and vice versa.[124,125] Therefore, by adjusting the degree of crosslinking one can tailor make hydrogels with required M_c and ξ values. Several studies have been reported on the determination of M_c and ξ.[125-129]

We describe in the following, the procedure for determining 'M_c' and 'ξ'.

Using the Flory's theory of swelling, at equilibrium $\pi=0$ and with some rearrangements of the Flory's equations the average molecular weight between crosslinks, M_c can be calculated as follows,

$$\frac{1}{M_c} = \frac{2}{M_n} - \frac{\frac{\bar{v}}{V_1}\left[\ln\left(1-2v_{2,s}\right)+v_{2,s}+\chi v^{2}{}_{2,s}\right]}{\left(v_{2,s}{}^{\frac{1}{3}} - \frac{v_{2,s}}{2}\right)} \tag{1.8}$$

Where,

$M_n =$ number of average molecular weight of polymer without the crosslinking

$M_c =$ Molecular weight between crosslinks

$\bar{v} =$ specific volume of the polymer

$V_1 =$ molar volume of the swelling agent

$v_{2,s} =$ volume fraction of the network

$\chi =$ Flory's polymer-solvent interaction parameter

The mesh size 'ξ' of the network is related to the ability of the network to 'sieve' different sizes of molecules through it. The mesh size is given by,

$$\xi = v_{2,s}{}^{-1/3}\gamma_0 \tag{1.9}$$

where γ_0 denotes the end-to-end distance in the unperturbed state and is given by

$$\gamma_0 = C_n\gamma_f^2 \tag{1.10}$$

where

$$\gamma_f = \lambda\sqrt{N} \tag{1.11}$$

and

$$N = \frac{\lambda M_c}{M_r} \tag{1.12}$$

In the above equation, γ_f is the end-to-end distance in the freely jointed chain, λ is the C-C bond length (1.54Å), C_n is the characteristic ratio of polymer, λ is the number of links per repeat unit, M_r is the molecular weight of the structural repeat unit.

1.7.2 Diffusion Mechanisms Through Hydrogel Membranes

Solute transport through polymeric membranes is generally described by two mechanisms; pore mechanism and solution-diffusion or partition mechanism.[130,131]

In the pore mechanism, solutes are presumed to permeate the membrane by diffusion through micro-channels or pores within membrane structure. Primarily the pore size of the membrane and the molecular volume of the solute (solute size) control the rate at which solutes permeate the membrane.

In solution-diffusion or partition mechanism, solute transverses the membrane by process of solute dissolution in the membrane followed by solute diffusion along and between the polymer segments that make up the membrane structure. For any nonporous gel membrane, permeation probably occurs by both mechanisms however, one of the two dominates depending on the nature of membrane, water content of the membrane and solubility of the solute.[132] Wisniewski *et. al.*[133] indicated that the crosslinked poly(2-hydroxyethylmethacrylate) hydrogel membrane may provide both pore (at low crosslinking density) as well as partition mechanism (high crosslinking concentration) of solute transport depending on the crosslinker concentration.

1.7.2.1 Important Parameters Influencing the Membrane Diffusion

From the free volume theory of diffusion in swollen hydrogels, it can be expected that the permeation of solutes through the hydrogel membrane is dependent on the degree of swelling of the membrane.[134-137] Highly swollen hydrogel membrane exhibits the size exclusion phenomenon i.e. solute with smaller hydrodynamic radii diffuse faster than the solutes with larger hydrodynamic radii.

Influence of different parameters of hydrogel membranes such as crosslinking density, molecular weight between crosslinks and mesh size on the solute diffusion have been studied earlier.[117,134,138-141] The crosslinked structure of polymer acts as a molecular screen for diffusion of large solutes. Further, these studies indicate that with an increase in crosslinking density, M_c and mesh size decreases resulting into decrease in diffusion. By varying crosslinking density or mesh size of hydrogel membranes, small solute permeability and exclusion of large solutes may be possible.

1.7.2.2 Transport Studies Through Stimuli Sensitive Hydrogel Membrane

Swelling and thus, resulting mesh size of the stimuli-responsive hydrogel membranes reversibly change with external conditions such as pH [62,125] temperature, etc. These reversible changes in mesh size allow the permeation of solutes or release of drugs. Permeation through such membranes were studied and reported as a function of stimuli.[142-145]

Bell and Peppas[146] demonstrated the drug permeation through interpolymer complexed pH sensitive hydrogels based on poly(methacrylic acid-g-ethylene glycol)copolymers. They reported the higher solute diffusivity in uncomplexed system at high pH than in complexed P(MAA-g-EG) membranes at low pH.

Thermosensitive hydrogel membranes whose swelling and permeation properties depend on the temperature of environment were extensively studied. [147-149] Grassi *et. al.*[150]developed the mathematical model to understand the solute transport through the temperature sensitive poly(N,N-dimethylaminoethylmethacrylate-co-acrylamide) (DMAEMA/AAm) hydrogel membrane. Phase transition of PNIPAm as a function of temperature was used to control the permeation of membranes by adjusting the temperature of surrounding. The swelling and shrinking of PNIPAm hydrogel was considered to change the mesh size of the network and used for drug delivery as a function of temperature.

PNIPAm hydrogel has been extensively studied due to its excellent thermosensitive nature. Hydrogel membranes based on these polymers have shown enhanced permeation at lower temperature (below LCST) and decreased permeation at higher temperature (above LCST).[147] The combination of PVA and PNIPAm have been used to design hydrogel membranes with synergestic properties, wherein PVA gives good mechanical strength and PNIPAAm gives the thermosensitive nature.[151-156] Some new strategies have been used to design thermosensitive hydrogel membranes, where the permeabilities are higher at higher temperatures.[157-159] The hydrogel membranes based on poly(acrylic acid) grafted oligo-PNIPAm give PAA network

with grafted with PNIPAm chains. The schematic of this polymer is shown in **Figure 1.9**.

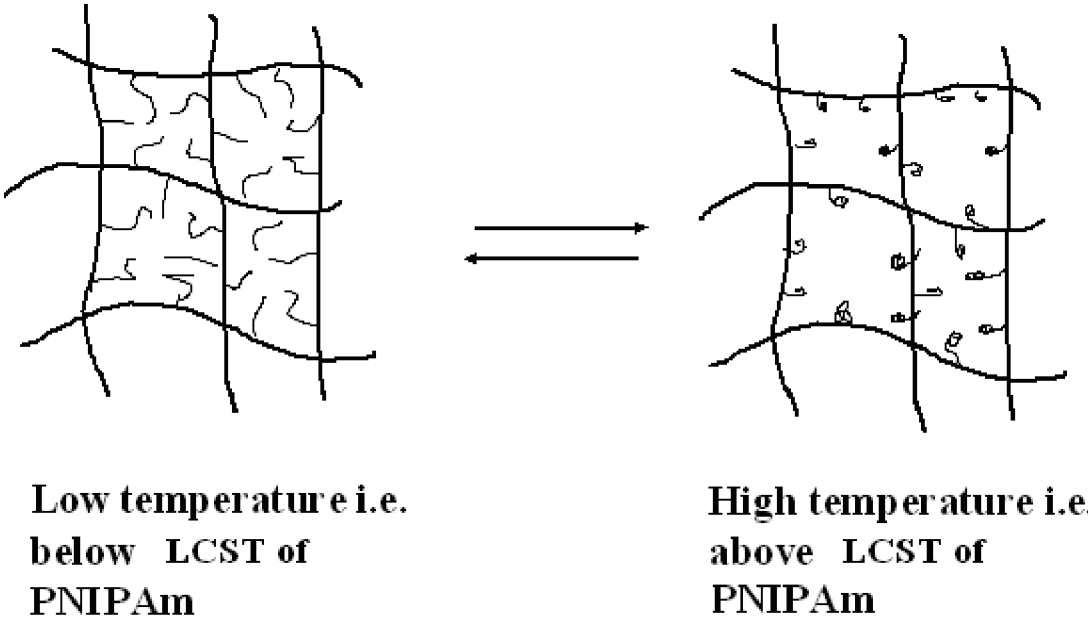

Figure 1.9: Different conformations of PNIPAm in thermosensitive membrane as a function of temperature

Above LCST, the PNIPAm chains are in the collapsed state to give compact conformations and gave more space, which was considered as opening of valve for the permeating solute molecules as shown in **Figure 1.9** or increase the pore volume facilitating the permeation. However, below LCST the PNIPAm chains are in the expanded state, which fills the channels and subsequently reduces the permeation rates. Therefore, the grafted oligoPNIPA chains in crosslinked PAA network dehydrate rapidly to give compact conformation at high temperature and open the channels for solutes resulting into higher permeation.

1.8 Gel-Filled Membranes

Recently, gel-filled porous membranes have been designed and used in the area of ion exchange membranes[160,161], water softening[162,163], nanofiltration and reverse osmosis[164] and diffusion/dialysis of acid/salt solutions.[165] Gel-filled membranes are novel membranes made up of gel anchored within the pores of a microporous membrane either physically or chemically. The combination of hydrogels and membranes provide hydrogel membranes with synergistic properties of membranes and hydrogels with a good mechanical strength. In gel filled membranes, gel properties determine the permeability and selectivity whereas, the host membranes provide the mechanical support to the gel. Due to the stimuli sensitive nature of gels the effective pore size of membranes can be adjusted by changing external stimuli and thus, making membranes more selective in nature. These gel/pore filled membranes are characterized in terms of gel concentration in the pores, volume fraction of water in the membrane, degree of ionization and charge density in case of pH sensitive ionic hydrogels and the thickness. In the gel filled membranes the permeability is a function of pore volume fraction[166] and substrate porosity and pore tortuosity.[167] Poly(4-vinylpyridine) (PVP) is a pH dependent cationic polymer, which undergoes volume transitions as a function of pH. Gel filled membranes based on this polymer have been synthesized and studied extensively in ion exchange membranes. Mika and coworkers have examined the effect of pH on the permeability of poly(4-vinyl pyridine) filled polyethylene membranes.[168,169] Gel-filled membranes based on neutral poly(acrylamide) have been reported earlier by Kapur and coworkers[167] and the rate of diffusion of ribonuclease A (RNAse) and bovin serum albumin (BSA) were demonstrated as a function of gel volume. They concluded that the gel-filled porous membrane with excellent selectivity can be fabricated.[170] The impregnation of PVA hydrogel with mesh size asymmetry within the pores of microfiltration membrane provide the gel-filled membrane with higher selectivity and mechanical stability than homogeneous membrane.[171,172]

The non-selective PVDF microfiltration membranes were made selective by impregnating (in-situ crosslinking of PVA) the pores with a crosslinked PVA and then

chemical activation with Cu (II), which was able to facilitate the histidine transport and the PVDF membrane provides the mechanical stability to the gel.[173]

The temperature sensitive hydrogel such as PNIPAm have been filled in the pores of the membranes.[174] The permeation characteristics were controlled by using temperature.[175,176] The permeability through these membranes generally increase with an increase in temperature above the LCST of N-isopropyl acrylamide hydrogel. The collapsed chains of polymer open the gate/valve for permeation.[176]

In conclusion, these studies indicated that the gel-filled membranes are selective in nature with excellent mechanical strength. Nonselective porous membranes can be made selective by incorporating the hydrogel into pores of the membranes.

1.9 Nanocomposite Hydrogels

Recently, polymer-clay nanocomposite membranes have attracted large attention because of their excellent mechanical and barrier properties. The incorporation of clays into the polymer influences the properties of hydrogels and improves the mechanical and barrier properties. In the foregoing, we give some details on clays, which are used in polymer-clay nanocomposites.

1.9.1 Clays

Clays are hydrous alumino silicates, which are minerals and constitute of soil, sediments and rocks. These clays are also known as layered silicates or phyllosilicates as their structural framework is composed of silica and alumina layers. These layered alumino silicates are classified depending on the condensation of silica sheets with alumina sheets in different ratios. The most commonly used layered silicates belongs to structural family of 2:1 phyllosilicates (trimorphic), where the octahedral alumina sheet is sandwiched between two sheets of tetrahedral silica in such a way that oxygen of octahedral sheet also belongs to tetrahedral sheet. The ability of layered silicates to disperse into individual layer and exchange reactions with organic and inorganic

cations is a vital characteristic for polymer nanocomposite. Since the forces that hold the stacks together are weak, the intercalation of small molecules between layers is easy. The layered silicates generally contain the Na^+ or K^+ ions so they are easily miscible with hydrophilic polymers such as PVA[177] and PEO.[178] In order to improve the compatibility of polymer matrix with layered silicates, hydrophilic silicates are connected to organophilic compound by cation exchange with cationic surfactants such as alkylammonium or alkyl phosphonium (onium). These organoclays lower the surface energy of the silicate surface and improve the compatibility with the polymer matrix.

Montmorillonite is an extensively used dioctahedral 2:1 phyllosilicates, which has ability to show high interlayer expansion or swelling. Nanocomposites based on montmorillonite have been widely studied and reported earlier.[179-181] The structure of montmorillonite has been reported in the literature earlier.[182]

1.9.2 Laponite

Laponite is a synthetic layered silicate belongs to 2:1 family and resembles the natural smectite mineral hectorite in both structure and composition. The major difference in them is significantly smaller size of laponite. Generally natural and other synthetic clays are polydisperse and in micrometer size; on the other hand laponite is nanosize and monodisperse. An aspect ratio of nano clays may be defined as D/t where D is the average platelets diameter and t is the thickness of either the individual platelets or a stack of platelets (**Figure 1.10**). An aspect ratio of laponite is smaller as compared to other clays.

The unit cell of the crystal constitutes of octahedral magnesium ions sandwiched between 2 layers of tetrahedral silicon atoms. These groups are balanced by 20 oxygen and 4 hydroxyl groups (see **Figure 1.11**). Isomorphic substitution of Mg^{2+} by lower valency cations such as Li^+ in the octahedral sites generates the negative charges on the surface of crystal. This negative charge is neutralized (balanced) by adsorption of sodium ions during drying. Empirical formula of unit cell in the crystal is $Na^+_{0.7}[(Si_8Mg_{5.5}Li_{0.3})O_{20}(OH)_4]^{-0.7}$.

Laponite is used in the synthesis of nanocomposite hydrogel where laponite acts as a multifunctional crosslinker and enhances the mechanical properties of the material. In order to facilitate better interactions of clay with polymers, hydrophilic clays are converted into organophilic through ion exchange process with Na^+. We show in **Table 1.8** the different properties of laponite and montmorillonite.

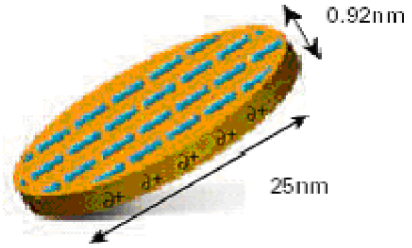

Figure 1.10: A platelet of laponite

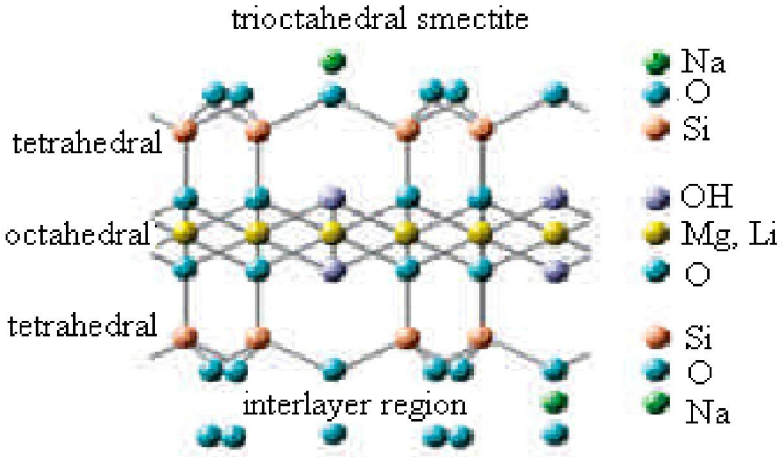

Figure 1.11: Laponite structure

Table 1.8: Properties of Laponite RD and Montmorillonite

	Laponite RD	**Montmorillonite**
Classification	Synthetic	Natural
Type	2:1	2:1
Emprical Formula	$Na^{+}_{0.7}[(Si_8Mg_{5.5}Li_{0.3})O_{20}(OH)_4]^{-0.7}$	$Na_{0.2}Ca_{0.1}Al_2Si_4O_{10}(OH)_2(H_2O)_{10}$
Aspect Ratio(D/t)	25-30 nm/0.95-1 nm	500-1000 nm/0.95-1.3 nm
Surface area	370 m^2/g	700-800 m^2/g

1.9.3 Synthesis of Polymer/Clay Nanocomposites

Different methods for synthesis of polymer nanocomposites have been reported earlier.[183,184]

Mainly, synthesis of polymer and clay nanocomposites involve insitu polymerization of monomer in the presence of layered silicates (clay) by intercalation of suitable monomer followed by polymerization or polymer intercalation from solution. **Figure 1.12** shows the different ways of synthesis of polymer nanocomposites.[185] Suitable solvent system for both polymer and layered silicates limits the above preparation methods. Therefore, polymer melt intercalation is more versatile method, which involves mixing of layered silicates (clay) with the polymer and heating the mixture above the softening point of the polymer.

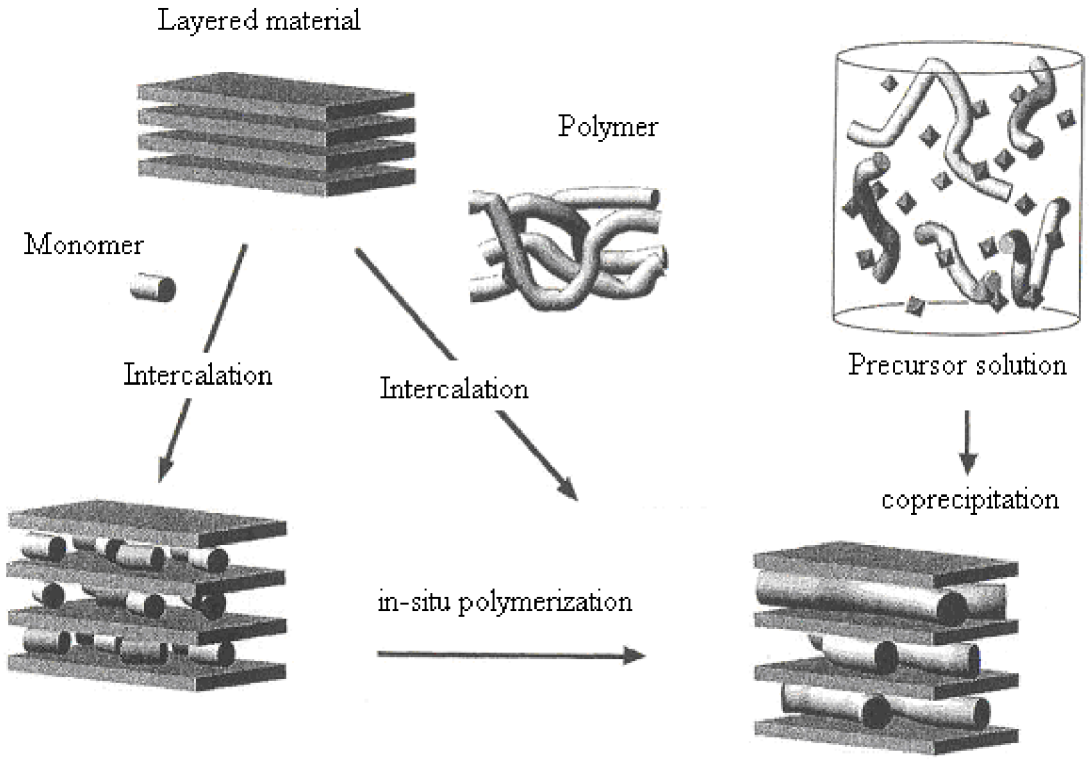

Figure 1.12: Synthesis of Polymer/Clay Nanocomposites

1.9.4 Structure of Polymer/Clay Nanocomposites

Depending on the nature of component used and the method of preparation, mainly two types of structures can be obtained in polymer nanocomposites (see **Figure 1.13)**.

1.9.4.1 Intercalated structure: In this structure, polymer chains penetrate inside the galleries of clays in such a way that the silicate layers expand with well ordered morphology resulting in alternative organic and inorganic layers.

1.9.4.2 Exfoliated structure: When the individual clay layers are separated and uniformly dispersed in the polymer matrix an exfoliated and delaminated structure is obtained. Further, depending on the clay loading two different exfoliated structures can be obtained the one disordered exfoliated structure, in which single clay platelets are randomly suspended in polymer matrix at low silica concentration and other is,

ordered exfoliated structure where they arrange in an ordered fashion, at or above critical clay concentration.

XRD and TEM are important characterization tools to find out the composite structures. In case of intercalated structure, diffraction peaks shift towards the lower angle values. In exfoliated structures, no more diffraction peaks are visible in XRD either due to too large spacing between layers or the absence of ordering.

The polymer nanocomposites showed remarkable improvement in mechanical properties,[186] barrier properties/decreased gas permeability,[187,188] thermal stability,[189] heat resistance and flame retardance,[190,191]

The reduction in the permeability of nanocomposite films is attributed to the additional tortuous path due to the presence of layered silicates with larger aspect ratio in the polymer matrix, which impedes diffusion of gas or solvent molecules. The effective path length for diffusion of solutes is found to increase due to tortuous path (see **Figure 1.14**).[192,193]

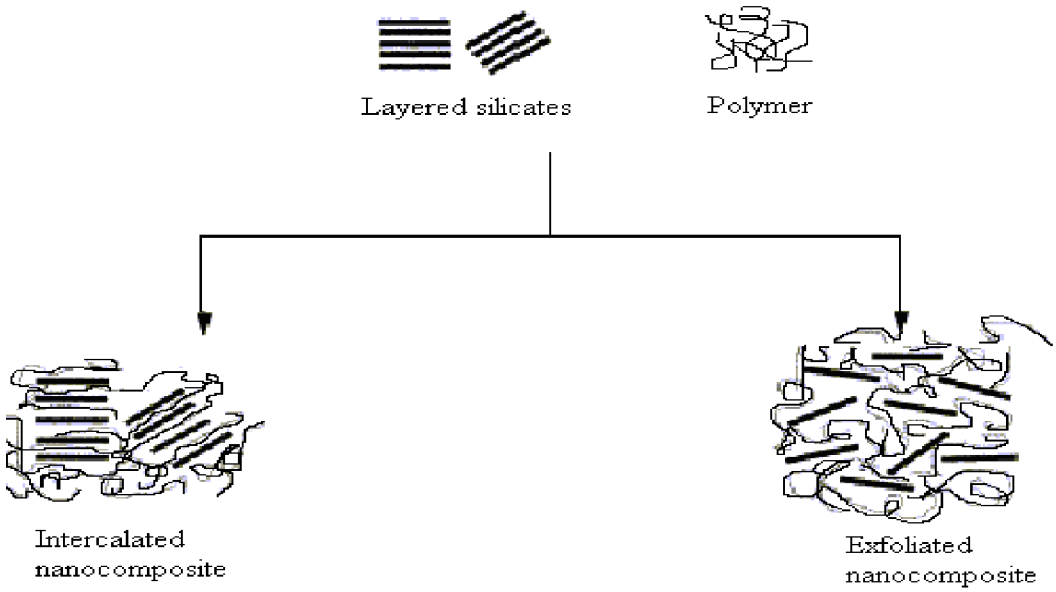

Figure 1.13: Structures of nanocomposites

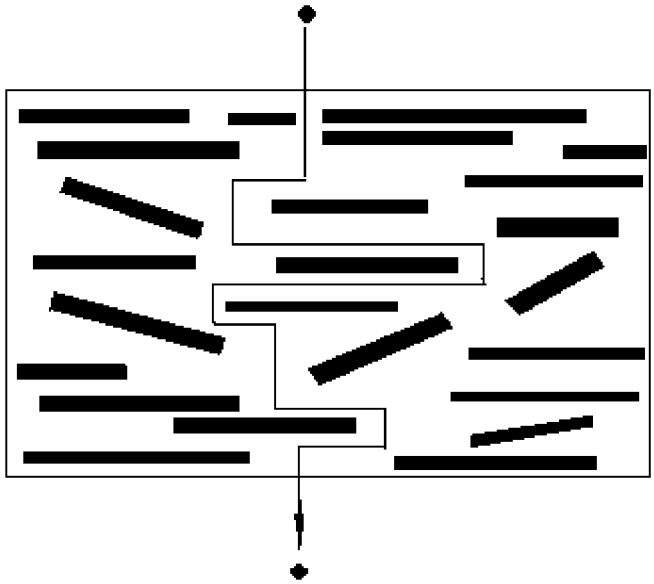

Figure 1.14: Tortuous path to the solute due to presence of clay with larger aspect ratio in the polymer matrix

1.9.5 Nanocomposites Based on Poly (Vinyl Alcohol) (PVA)

PVA is highly hydrophilic, nonionic polymer having –OH functional groups, which can be involved in hydrogen bonding within the molecule or with other electronegative atoms. Due to the hydrophilic nature of polymer and clay, polymer nanocomposite based on PVA can be easily achieved by simple dispersion of clay and polymer in water. Chang et al synthesized PVA nanocomposites with different clays such as Na^+-saponite, Na^+-montmorillonite and organically modified montmorillonite by solution intercalation method and studied the structure and properties of nanocomposite films.[194] The structure and properties of PVA/montmorillonite nanocomposite were investigated by XRD, DSC and TEM and it was found that the new crystalline phase was induced by presence of montmorillonite silicate at low silicate content.[195] This PVA/montmorillonite nanocomposites exhibited superior mechanical, thermal and water vapour transmission properties than respective unmodified polymer.

Xu *et. al.*[196] studied the synthesis and properties of PVA-vermiculite nanocomposites and reported that, acid treated vermiculite was well dispersed in PVA

and the presence of H-bonding between hydroxyl groups of PVA and vermiculite holds the vermiculite layers together more strongly than the van der Waals interactions. In addition to H- bonding, van der Waals forces between uncharged polymer and clay play important role. Grunlan *et. al.*[197] reported n increase in glass transition temperature with increase in clay content, which is attributed to strong interaction between clay and PVA.

1.10 Nanocomposite Hydrogels

In order to improve the mechanical strength of conventional hydrogels, clays are incorporated in the polymer system or in the conventional hydrogel. These hydrogels containing clays are known as nanocomposite hydrogels. These are hydrophilic in nature, insoluble in water with enhanced mechanical and thermal properties than conventional hydrogels

1.10.1 Nanocomposite (NC) Hydrogels Without Organic Crosslinker

NC hydrogels are composed of organic polymer and inorganic clay network without any chemical crosslinker.[198-201] These gels are physical hydrogels, which are insoluble in water where the dissolution is prevented by non-covalent interactions between polymer and clay. For the synthesis of NC gels, clay is in the exfoliated state and uniformly dispersed in aqueous medium followed by in situ free radical polymerization where clay acts as a multifunctional crosslinker. Haraguchi and coworkers[198,200] synthesized and characterized the thermosensitive nanocomposite hydrogels based on poly N-isopropylacrylamide (NIPAm) and water swellable laponite clay. They compared the properties of NC hydrogels with conventional hydrogels and found that NC hydrogels show excellent optical transparency, mechanical properties, swelling behaviour and fast response to deswelling as a function of temperature as compared to conventional PNIPAm gels. The limitations of conventional hydrogels and advantages of nanocomposite hydrogels are shown in **Table 1.9.**

Table 1.9: Comparison between conventional hydrogels and nanocomposite hydrogels

Conventional Hydrogel	Nanocomposite Hydrogel
1. Morphological inhomogeneity due to increasing crosslinking density/pressure/polymerization temperature. 2. Mechanical weakness. 3. Limited swelling at equilibrium and slow response to stimuli. 4. Restricted molecular motions of polymer chains caused by increasing crosslinking density.	1. Structural homogeneity irrespective of preparation conditions. 2. Tough/excellent mechanical properties. 3. Large swelling ratio and rapid response to the stimuli. 4. Random conformation of polymer chains and little restrictions on polymer chains between clay sheets.

The **Figure 1.15** shows the model structure of NC hydrogels proposed by Haraguchi and coworkers. As shown in figure, the neighbouring clay sheets are connected by polymer chains whereas D_{ic} is an intercrosslinking distance, which is equivalent to the clay-clay interparticle distance. Clays act as crosslinker but provide very little restrictions on the flexibility of polymer chains. Improved properties of NC gels are attributed to the flexibility/random conformation of polymer chains between clay sheets. The swelling ratio at equilibrium below LCST and the rate of deswelling above LCST gradually decreased with increasing clay content which is attributed to the increased crosslinking density. As these gels have high mechanical strength and exhibit quick response to external stimuli they have potential applications in biomedical tissue engineering, sensors and as medical devices for artificial muscles and micro-actuators.

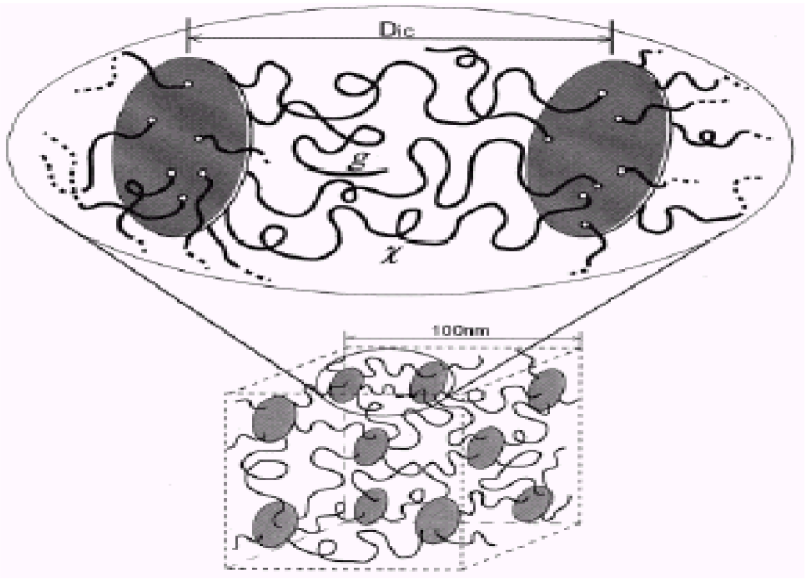

Figure 1.15: Proposed model structure of nanocomposite hydrogels

1.10.2 Nanocomposite Hydrogels in Presence of Organic Crosslinker

These nanocomposite (NC) hydrogels were prepared by in-situ free radical copolymerization of vinyl monomer with organic crosslinker N,N methylene bisacrylamide in presence of layered silicates.[202-207] Liang *et. al.*[204] synthesized thermosensitive poly (N-isopropylacrylamide) [PNIPAm] nanocomposite with organically modified montmorillonite having coupling agent with enhanced thermal transition and increased transition rate. The modification of the interfacial chemistry between the clay minerals and polymer through coupling agent enhanced the thermal transition. The structure of NC gels was investigated by XRD and TEM. The use of NC gels in the controlled released technology has also been demonstrated.[206] The release rates of drugs were profoundly depended on the structure of NC gels.[207]

1.11 Characterization Techniques

We have used in our study the various characterization techniques such as XPS, DMA, XRD, DSC, TGA, and contact angle measurement to elucidate the properties of hydrogel membranes. In the foregoing we will describe briefly about these techniques.

1.11.1 X-ray Photoelectron Spectroscopy (XPS)

XPS is a surface sensitive technique which analyses the electronic structure, atomic compositions in the top (~50Å) surface. Each atom in the surface has core electrons with the distinct binding energy, which helps in the identification of all elements by XPS. Binding energy (BE) is a direct measure of the energy required to remove the electrons concerned from it's initial state to vacuum level. Alternatively, it may be called ionization energy also, which is nothing but the minimum energy required to remove an electron from a given orbital. Since the BE is a characteristic property of atoms and ions, XPS provides the direct information of chemical analysis such as oxidation states and surface concentrations and hence also known as electron spectroscopy for chemical analysis (ESCA).

The principle of this technique is based on the photoelectric effect. When the X- ray beam bombards on the sample, the photon (energy, $h\nu$ where, h = Planck's constant [6.62 X 10^{-34} Js] and ν = frequency [Hz]) is absorbed by an atom in a molecule or solid which leads to emission of electron from any orbital, provided the incident photon energy is higher than the binding energy of electron in that particular orbital. The emitted electrons with some kinetic energy are referred to as photoelectrons. The efficient ionization creates a hole in core shell. The hole near to nucleus is in a very unstable state. So, this hole is filled by the transition of electron from an outer level (L_1) and releases energy in the form of a photon, which is equal to the energy difference between E_K and E_{L1}. The above photon of energy ($h\nu = E_K - E_{L1}$) is known as X-ray fluorescence. Alternatively, this energy can be utilized for the ejection of second electron known as Auger electron and the process is known as

Auger electron emission. In Auger process, the emitted energy is involved in ejecting another electron, whose binding energy is lower than the available energy from the relaxation process. These low energy Auger electrons can escape only from the first few molecular layers and hence more surface sensitive than photoemission. Also since the fluorescence yield of K shell is small, the KLL Auger transitions are used to locate and identify elements on the surface. Auger emission is normally indicated such as KL_1L_2. KLL indicates the photoelectron emission (and hence a hole) from K, electron cascade from L_1-level (to K-level) and the level (L_2) from Auger electron got emitted. Such notations are used for Auger transitions.

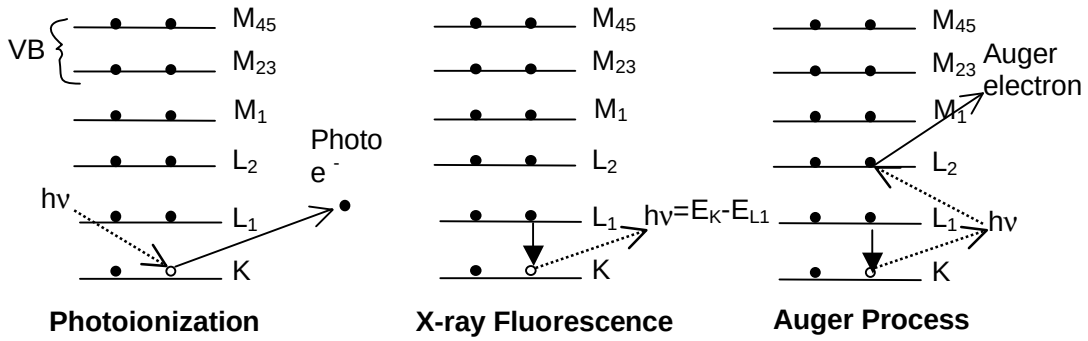

Figure 1.16: Comparison between Photoionization, X-ray Flurosecence and Auger process.

Figure 1.16 shows the comparison between processes such as photoionization, X-ray flurosecence and Auger process.

Although X-rays penetrates to a depth of several micrometers, the ejected electrons generally come from the first few nanometers of any material surface. Electron emitted from the bulk loses its energy in collision and does not reach detector or at the most contribute to background. Thus, the surface sensitivity is not dependent on the X-ray penetration depth but on the photoelectrons escape depth without losing energy.

The binding energy of the photoelectrons can be calculated by Einstein relationship

$$E_b = h\nu - E_k - \Phi \qquad (1.13)$$

Where E_k is the kinetic energy of photoelectron, E_b is a binding energy of the photoelectron, Φ is a work function of the spectrometer.

The peaks observed in the XPS are of three basic types: Peaks due to photoemission from core level, valence level and peaks due to X-ray excited Auger process. In case of polymers, valence band reveal structural information, which is unobtainable from the core level studies. Valence levels are occupied by electrons of low binding energy, which are involved in delocalized, or bonding orbitals.

The peak area with appropriate sensitivity factors can be used to determine the surface composition of the materials.

$$\frac{N_A}{N_B} = \frac{I_A}{I_B}\sqrt{KE_A / KE_B}\,\frac{\sigma_B}{\sigma_A} \qquad (1.14)$$

where, N is number of atom, I is intensity, σ is photo-ionization cross-section and KE is kinetic energy of the photoelectron.

On samples with poor conducting characteristics, like polymers, during photoionization process, a positive charge zone occurs and the intensity of this zone depends on the conducting nature of the material. As a result of the positive potential around the material, the kinetic energy of photoelectrons is reduced. Consequently, this surface charging results in the shift of all XPS peaks to higher binding energies. Therefore, the calibration is necessary and the binding energy has to be calibrated with internal or external reference like adventitious carbon on any sample or depositing a thin layer of metal on the surface. In some cases, surface charging can be neutralized by using a low energy electron flood gun with appropriate energy. BE is very sensitive to the oxidation state and the chemical environment of the electron. Therefore, it shows chemical shift up to 10 eV when atom is linked to different species. Consequently, this can be used to determine the chemical environment of the element. Change in binding energy is normally attributed to change in the oxidation state, effective charge as well as the bonding characteristics between atoms. Same elements with different environment give rise to different measurable binding energy. The chemical shift effect for most of the elements is well-studied and reported in the literature.[208]

Instrumentation:

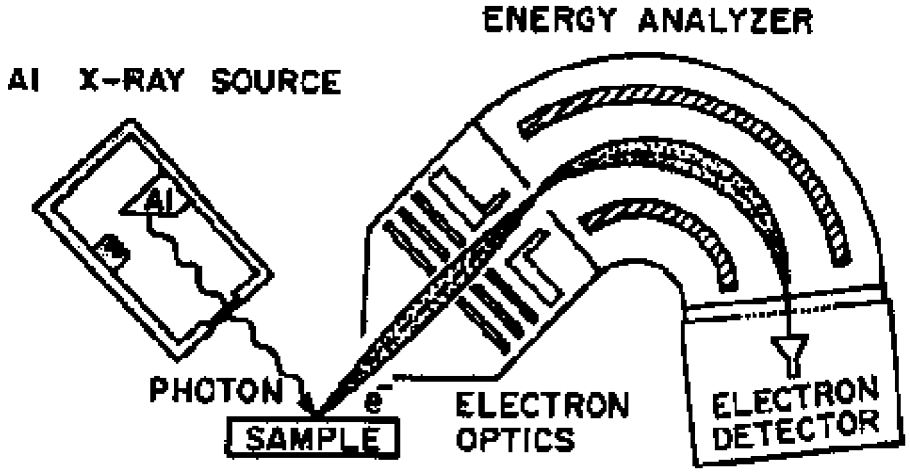

Figure 1.17: Schematic of basic apparatus used in XPS

Figure 1.17 represents the X-ray instruments consist of X-ray source, an energy analyzer for emitted photoelectrons and a detector in a ultra high vacuum chamber. Al Kα (1486.6eV /1 eV width) or Mg Kα (1253.6 ev energy/0.7 eV width) are generally used in soft x-ray sources. High vacuum is normally attained with a combination of several vacuum pumps. Generally, concentric hemispherical analyzer has been explored. Finally the image detector detects the spectra due to photoelectrons.

1.11.2 Dynamic Mechanical Analysis (DMA)

Dynamic mechanical analysis is one of the most important methods to characterize viscoelastic properties of the materials as a function of both the frequency and the temperature.

In dynamic mechanical analysis, a sinusoidal stress (or strain) is applied to the sample and the resulting response of strain or stress is measured as functions of both oscillatory frequency and temperature.[209] In viscoelastic studies, the applied force and resulting deformation both vary sinusoidally with time. Due to the time dependent

properties of viscoelastic materials, resultant response is out of phase with applied stimulus. The strain will also be sinusoidal but will be out of phase with stress as shown in **Figure 1.18**. Viscoelastic materials exhibit phase angle, which lie between the two extremes 0 and 90°.

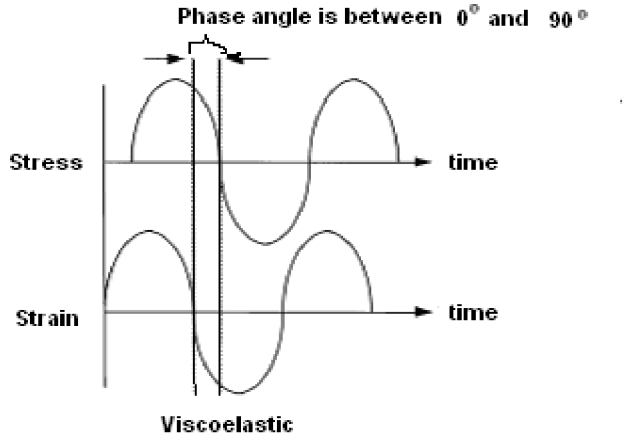

Figure 1.18: Relationship between stress and strain in viscoelastic materials.

This phase lag results from the time necessary for molecular rearrangements and is associated with the relaxation phenomena. The variation of these components as a function of temperature is used to study the molecular motion in the polymers.

The important properties obtained from DMA are

1. storage modulus ($E^{|}$) corresponds to the elastic response to the deformation or stored energy,
2. loss modulus ($E^{||}$) corresponds to the plastic/viscous response to the deformation or dissipated energy,
3. tan δ corresponds to the ratio of loss modulus to storage modulus ($E^{||}/E^{|}$). tan δ is known as loss tangent or damping factor. This is one of the important parameters and seen to increase during transitions between different deformational mechanisms. Therefore, tan δ is useful for the occurrence of molecular mobility transitions such as glass transitions of the polymers.

In the experiments, generally the strain is fixed suitably in the linear region as shown in **Figure 1.19**, by carrying out first the strain sweep test. The parameters $E^{|}$, $E^{||}$ and tan δ give information about the physical and mechanical properties.[210,211]

Furthermore, since these are non-destructive techniques, they enable the study of viscoelastic properties of pharmaceuticals and biomedical systems.[212]

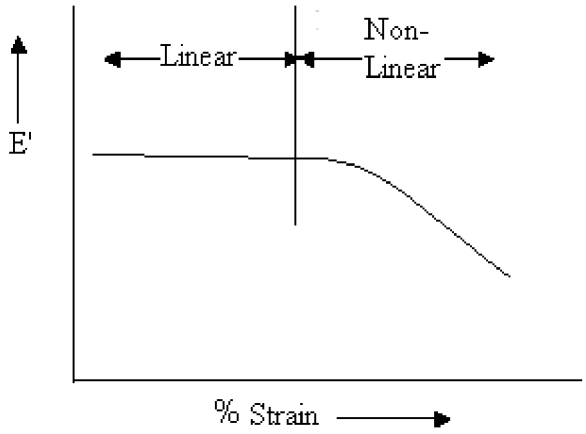

Figure 1.19: Strain sweep test

1.11.3 X-Ray Diffraction (XRD)

X-Ray diffraction (XRD) is one of the most important characterization tools used in solid state chemistry and materials science. It represents a non-destructive analytical technique for identification and quantitative determination of crystalline compounds. The diffraction depends on the crystal structure and on the wavelength. Because the wavelength of X-rays is comparable to the size of atoms, they are ideally suited for probing the structural arrangement of atoms and molecules in a wide range of materials.

X-rays are electromagnetic radiation with typical photon energy. The energy of X-ray photon and its wavelength is related by the equation, which is

$$E = hc/\lambda, \qquad (1.15)$$

where h is Planck's constant [6.62×10^{-34} J-s] and c is speed of light. X-ray used in diffraction has wavelengths lying approximately in the range 0.5-2.5 Å. X-rays are produced by collision of high speed electrons with a metal target. All X-ray tubes contain two electrodes, an anode (the metal target) and a cathode. The common targets

used in X-ray tube include copper (Cu) and molybedenum (Mo) which emit 8 and 14 KeV with corresponding wavelength 1.54 Å and 0.8 Å respectively. Copper makes a good target since it is an excellent heat conductor with a high melting point. X-rays primarily interact with electrons in atoms. If the atoms are arranged in a periodic fashion, as in crystals, the diffracted waves will consist of sharp interference maxima (peaks) with the same symmetry as in the distribution of atoms and hence this diffraction pattern allows to deduce the distribution of atoms in a material. XRD spectrum is usually obtained by measuring the diffracted intensity as a function of diffracted angles 2θ (angle between incident and diffracted beams) and orientation of specimen. The peaks in X-ray diffraction pattern are directly related to the atomic distance by Bragg's law [213,214] (**Figure 1.20**).

$$n\lambda = 2d \sin\theta \qquad (1.16)$$

where, 'λ' is wavelength of X-rays and 'd' is d-spacing between atomic planes (inter-planer distance) in the crystal, 'θ' is the scattering angle and 'n' is an integral representing the order of diffraction peaks.

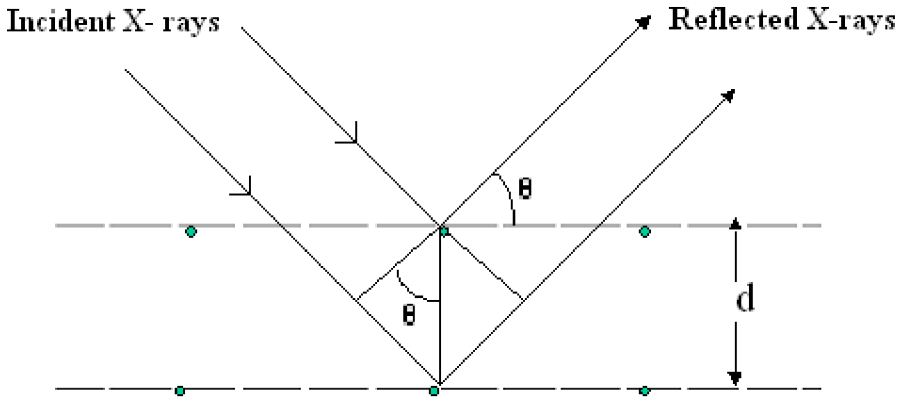

Figure 1.20: Schematic of Bragg's law

Bragg's equation can be utilized for the surface analysis by using X-rays of known wavelength and measuring theta one can determine the d-spacing of various planes in a crystal.

X-Ray diffraction data can be collected by using either transmission or reflection geometry. In reflection mode, X-rays are scattered or reflected from the sample, the reflected X-rays interfere with each other such that in the diffractogram the intense peaks are obtained at corresponding d values according to Bragg's law. In the transmission mode the area detector detects the x-ray transmitted to the sample.

1.11.4 Differential Scanning Calorimetry (DSC)

Differential scanning calorimetry is an important method to determine the thermal properties of the materials. It measures the amount of energy (heat) absorbed or released by a sample when it is heated or cooled at a controlled rate or held at constant temperature.

Typically two types of DSC systems are used; one is *power compensation DSC* where the sample and reference have individual identical heaters and the temperatures of both are controlled independently. The temperature of sample and reference are made identical by varying the power input /output to the two furnaces. The energy required to establish the identical temperature is the measure of enthalpy or heat capacity change in the sample relative to the reference or the difference between the power output of the sample and reference cells corresponds to heat capacity of the sample at that temperature. Second is *heat flux DSC*, where the sample and reference are connected by low resistance heat flow path (a metal disc) which is assembled in a single heater. The temperature difference between sample and reference due to enthalpy or heat capacity changes in the sample is recorded and related to the enthalpy change in the sample using calibration experiment. DSC applications include investigations of glass transition temperature, heat of melting, crystallization studies and identification of phase transformations. This method is used to study processes such as non-isothermal melting and crystallization as a function of temperature and crystallization at constant temperature. Heat of fusion of the sample and it's comparison with the heat of fusion value fully crystalline sample gives the crystallinity of the sample.

In case of instruments Perkin Elmer DSC-2 (power compensation type of DSC) and DSC-7 equipped with Thermal Analysis Data station software, the sample

holder assembly contains two platinum alloy cups and has individual heater and sensor. The differential power required for maintaining the identical conditions is equivalent to the rate of energy absorption or evolution of the sample. The instrument is calibrated for temperature and energy scales using indium and tin as standards. A weighed amount of sample is crimped in an aluminium sample holder with cover and is directly placed in the sample holder.

1.11.5 Thermogravimetric Analysis (TGA)

Thermogravimetric analysis (TGA) is thermal analysis technique used to measure the changes in the weight of samples as a function of temperature and /or time. TGA is commonly used to investigate properties such as thermal stability, oxidation or decomposition temperature, polymer degradation temperatures, residual solvent levels, absorbed moisture content and the amount of inorganic filler in polymer or composite materials. The sample is placed in a small pan attached to a sensitive microbalance and subsequently sample holder portion of the TGA balance assembly is placed into a high temperature furnace. The sample is heated at controlled manner and/ or held isothermally for a specific time. The balance assembly measures the initial sample weight at room temperature and then continuously monitors changes in sample weight (losses or gains) as heat is applied to the sample.

1.11.6 Contact Angle Measurements

Contact angle (θ) determines the nature of the material in terms of its hydrophilicity or wettability. It gives information on the outermost layer of surface within 1nm. Moreover, the contact angle is time dependent phenomenon. Sessile drop, Wilhelmy and Washburn are three different commercially available methods for the determination of contact angle. Uyama and coworkers[215] investigated the contact angle of different polymer films by using telescopic sessile drop, laser beam goniometer and Wilhelmy palte technique and reported the comparison of these methods. However, sessile drop is the most widely used method, which is a direct measurement of a sessile drop of a liquid on the surface. The droplet is in equilibrium with surface by

balancing three forces such as, interfacial tension between solid and liquid (SL), between solid and vapour (SV) and between liquid and vapour as shown in **Figure 1.21**.

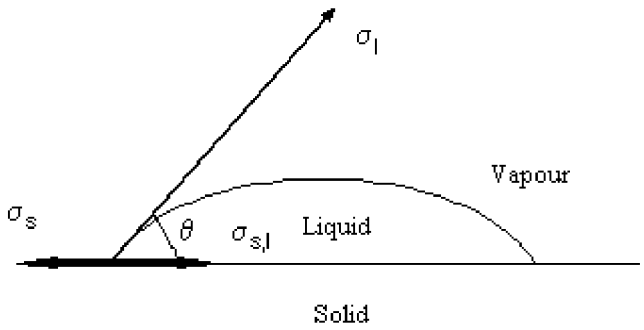

Figure 1.21: Schematic of contact angle

The contact angle can be described using Young's equation.

$$\cos\theta = \frac{\sigma_s - \sigma_{s,1}}{\sigma_1} \qquad (1.17)$$

where, θ is contact angle, σ_s is surface free energy of solid, σ_1 is the surface tension of liquid and $\sigma_{s,1}$ is interfacial tension between solid and liquid. Thus, the surface wettability, which is determined by Young's equation, depends on the surface tension of solid, liquid and solid/liquid interface.[216]

Contact angle is the angle included between the tangent plane to the surface of the liquid and the tangent plane to the surface of the solid, at any point along their line of contact. Drops can be made in advanced edges by addition of liquid and receding edges may be produced by allowing sufficient evaporation or by withdrawing liquid from the drop. **Figure 1.22** shows that the contact angle of nonporous membranes varies as function of hydrophilicity of the material. When the surface is more hydrophilic it can be more easily wetted by water resulting into smaller contact angle. With an increase in hydrophobicity, contact angle increases between surface and the water and it lies between 0 to 90.°

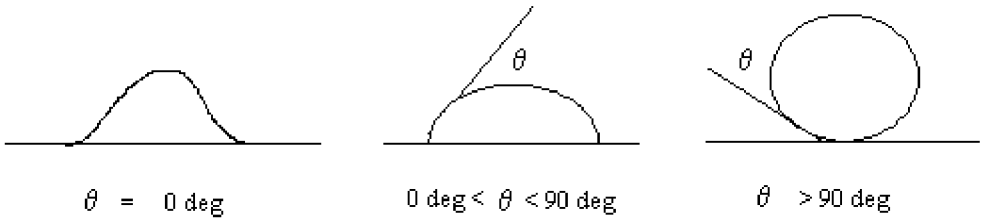

Figure 1.22: Contact angle of nonporous membranes with varying the hydrophilicity of the material.

Many polymers in contact with water show such behaviour. In case of highly hydrophobic polymers such as polyvinylidenedifluoride (PVDF), poly(propylene) (PP), poly(ethylene) (PE), water does not wet the surface and contact angle is more than 90°. However, when θ is lower than 90 °, surface roughness, heterogeneity, and the penetration of the liquid drop due to capillary forces into the porous material may leads to large number of errors in determining the contact angle. Alternative methods have been used to determine the wettability of porous material.[217]

1.12 Applications of Hydrogel Membranes

Hydrogel membranes (including stimuli sensitive hydrogel membranes and gel filled membranes) have applications in bio-separation, controlled drug delivery, bio-hybrid artificial organ and multi-component separations and also in sensors[218,219] and chemical valves.[220] **Figure 1.23** gives a schematics of applications of hydrogel membranes in various fields.

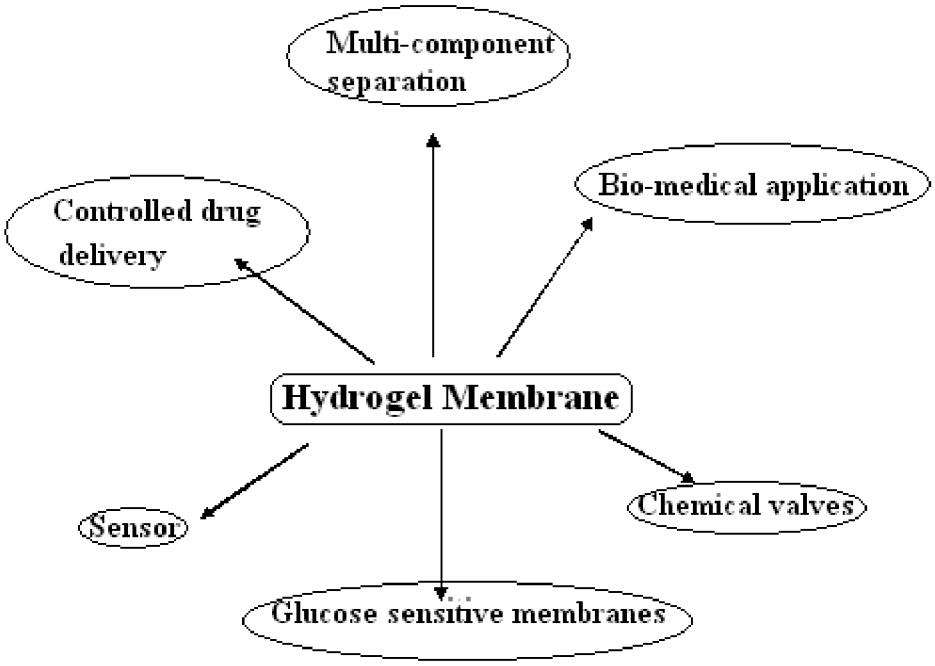

Figure 1.23: Applications of Hydrogel membranes

1.12.1 Multi-Component Separation

Hydrogel membranes, where the pore size of membranes can be controlled by swelling and shrinking property of membranes have been considered to apply in multi-component separations. Liang *et. al.*[176] reported the thermosensitive membrane that exhibits multi-functional separation performance. Liang and coworkers developed temperature sensitive membranes for the rejection of dextrans with different molecular weights from aqueous solution.

1.12.2 Glucose Sensitive Hydrogel Membrane for Insulin Delivery

Diabetes is caused by the inability of pancreas to control the blood glucose concentration. Insulin has to be delivered in an exact amount at exact time. Glucose sensitive hydrogel membranes are intelligent systems that undergo volume changes in response to glucose concentration and can provide a tool for self-regulated insulin

delivery where, a necessary amount of insulin can be administered as a function of glucose concentration. Glucose oxidase is the most widely used enzyme in glucose sensing. In order to develop the glucose sensitive hydrogel membranes glucose oxidase was immobilized in the polymer system, which can then sense the glucose and regulate the insulin delivery. Membranes that have ability to release insulin in response to glucose concentration have been demonstrated.[221,222]

The role of glucose oxidase is to convert glucose into gluconic acid thus, lowering the pH in the hydrogel membrane. Cationic polymer swells at low pH and insulin can then be released. Thus, the pH sensitive hydrogel membranes containing glucose oxidase can control insulin release in response to the glucose concentration. Ishihara and coworkers[223] synthesized a copolymer membrane of N, N-diethylaminoethyl methacrylate and 2-hydroxypropyl methacrylate with a crosslinked poly(acrylamide) membrane in which glucose oxidase was immobilized. **Figure 1.24** shows the schematic of insulin delivery through the glucose sensitive hydrogel membrane. Diffusion of glucose due to concentration gradient in the membrane, which is then catalyzed by glucose oxidase and resulting in conversion of glucose into gluconic acid consequently, the environmental pH becomes lower. Since the membrane is cationic, at the low pH, protonation of amine groups results in the swelling of membrane and insulin delivery is enhanced. This indicates that insulin delivery through hydrogel membrane is strongly dependent on the glucose concentration.

The mechanism of self-regulated insulin release through anionic hydrogel membrane is different from cationic hydrogel. The opening and closing of pores as a result of change in polymer conformation controls the insulin delivery. At basic pH the polymer chains are in the extended conformations due to the electrostatic repulsion between charges. However, when the glucose oxidase converts glucose to gluconic acid, these polymer chains collapse due to the charge neutralization at low pH. Thus, pores open resulting into the enhanced insulin delivery.[225,226]

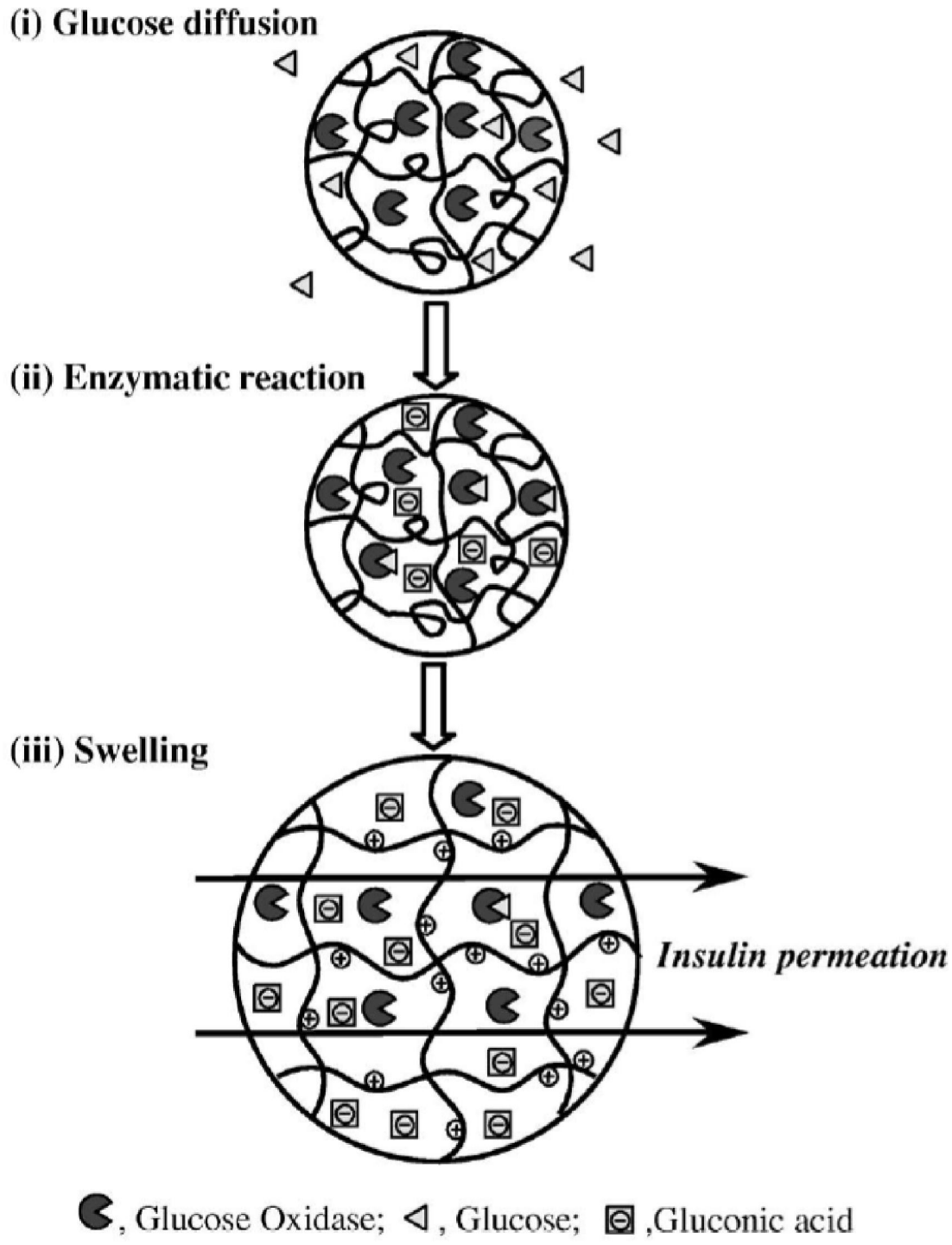

Figure 1.24: Schematic representation of the insulin delivery through glucose sensitive hydrogel membrane [224]

1.12.3 Bio-Medical Applications

Transport properties of membranes are very crucial and these properties make membranes applicable in many bioprocesses. Membranes, which allow facile diffusion of therapeutic proteins secreted by the encapsulated cell and at the same time membrane itself is a barrier to the components of recipient's immune system such as immunoglobulins, have applications in biohybrid organs, immunoisolation, tissue engineering. Hoffman has summarized bio-medical applications of hydrogels particularly the use of hydrogel in tissue engineering.[4] The advantage of hydrogel as a matrix for tissue engineering is, the high water environment of hydrogel which can protect the cells and fragile drugs and allows good transport of nutrients to the cells.

In biohybrid artificial organs, the transplanted cells are macroencapsulated behind the synthetic membrane and in immunoisolation the semipermeable barrier is placed between host and transplanted tissue in order to protect the cells from immune rejection. Colton[227]reviewed the implanted bio-hybrid organs and focused on the implantable immunoisolation devices in which the tissues are protected from immune rejection by enclosure within a semipermeable barrier.

Dai and Barbari[171] have developed PVA gel-impregnated pore membranes with mesh size asymmetry, which have potential applications in biohybrid artifical organs. The gel impregnated pore membranes have transport advantage over ultrafiltration and dialysis membranes and offer a good candidature for biohybrid organs and cell encapsulation. The hydrogel membrane offers promising approach to the immunoisolation of implanted cells.[228]

1.12.4 Controlled Drug Delivery

Hydrogels have been used in controlled drug delivery systems, which exhibit swelling and stimuli dependent drug release. The ideal drug-delivery system should have capacity to sense the changes and alter the drug release accordingly by providing the therapeutics in response to physiological requirements. The controlled drug release as a function of temperature have been evaluated by using thermoresponsive

networks.[57,58] Bae *et. al.*[58] demonstrated the pulsatile drug release pattern through crosslinked P(N-isoproylacrylamide-co-butylmethacrylate) system regulated by temperature changes due to thermosensitive swelling-deswelling behaviour of polymer. pH responsive polymeric networks have been extensively studied due to large variation in physiological pH at various body sites.[229,230]

1.13 Concluding Remarks

The introductory chapter reviews various aspects of hydrogels, membranes and hydrogel membranes. Different types of stimuli-responsive hydrogels have been described. A wide variety of synthetic methodologies available (reported in the literature) to prepare hydrogels and their applications have been discussed. The swelling of hydrogels has been explained on the basis of Flory's theory of swelling. The fundamental interactions which are responsible for the volume transition in hydrogels have been discussed. The important parameters of hydrogel membranes such, swelling ratio (q), degree of crosslinking/molecular weight between crosslinks (M_c), effective mesh size (ξ) which influence the permeability of hydrogel membranes have been explained. Recently, gel filled porous membranes have attracted lot of attention in the separations and the controlled release technology. Various accounts of these have been mentioned. Furthermore, nanocomposite (NC) gels, which have emerged as promising materials in gel based technologies, have been described. Some of the clays such as montmorillonite and laponite, which are used in the NC gels have been elaborated in this chapter.

Finally, a brief description of the various techniques such as XPS, DSC, DMA, XRD, contact angle, etc. which are used in our work have been given in this chapter.

In conclusion, hydrogels and membranes are active areas of research in polymer science and technology as evidenced by large number of publications in the literature. Although there are numerous developments which have taken place in this area, still there is a tremendous scope to design hydrogels in combination with membranes, which can give synergistic properties.

1.14 References

1. Wichterle, O; Lim, D. Nature **1960**, *185*, 117.
2. Ratner, B. D.; Hoffman, A. S. in "Hydrogels for Medical and Related Applications" J. D. Andrade Editor, ACS symposium series, American chemical society, Washington, D. C. **1976**.
3. Ratner, B. D. in "Biocompatibility of clinical implant Materials" volume II, Williams, D. F. Editor, CRC series in Biocompatibility, Chapter 7.
4. Hoffman, A.S. Advanced Drug Delivery Reviews **2002**, *54*, 3.
5. Hoffman, A. S., in "Polymer Gels", DeRossi, D.; Kajiwara, K.; Osada, Y, Yamauchi, A. (Edi), Plenum Press, New York, **1991**, 289.
6. Qiu, Y.; Park, K. Advanced Drug Delivery Reviews **2001**, *53*, 321.
7. Hennink, W.E.; Nostrum, C. F. V. Adv. Drug Delivery Reviews **2002**, *54*, 13.
8. Cicek, H.; Tuncel, A.; J. Polym Sci. Polym. Chem. **1998,** *36*, 543.
9. Bettini, R. Colombo, P.; Peppas, N. A. J. Controlled Release **1995,** *37*, 105.
10. Peppas, N. A.; Berner, R. E. Biomaterials **1980**, *1*, 158.
11. Jameela, S. R.; Jayakrishanan, A. Biomaterials **1995**, *16*, 769.
12. Gehrke, S. H; Uhden, L. H.; McBride, J. F. J. Controlled Release **1998**, *55*, 21.
13. Coviello, T. J. controlled Release **1999**, *60*, 367.
14. Eiselt, P.; Lee, K. Y.; Mooney, D. J. Macromolecules **1999**, *32*, 5561.
15. Stringer, J. L.; Peppas, N. A. J. Controlled Release **1996**, *42*, 195.
16. Peppas, N. A.; Merrill, E. W. J. Appli. Polym. Sci. **1977**, *21*, 1763.
17. Merrill, E. W.; Dennison, K. A.; Sung, C. Biomaterials **1993**, *14*, 1117.
18. Jabbari, E.; Nozari, S. Eur. Polym. J. **2000**, *36*, 2685.
19. Sperinde, J. J.; Griffith, L. G. Macromolecules **1997**, *30*, 5255.
20. Sperinde, J. J.; Griffith, L. G. Macromolecules **2000**, *33*, 5467.
21. Liu, L-S.; Liu, S.-Q.; Ng, S. Y.; Froix, M.; Ohno, T.; Heller, J. J. Controlled Release **1997**, *43*, 65.
22. Gacesa, P. Carbohyd. Polym. **1988**, *8*, 161.

23. Peppas, N. A.; Scott, J. E. J. of Controlled Release **1992**, *18*, 95.
24. Hassan, C. M.; Peppas, N. A. Macromolecules **2000**, *33*, 2472.
25. Lim, D. W.; Choi, S.H.; Park , T.G. Macromol. Rapid Commun. **2000**, *21*, 464.
26. Jeong, B.; Bae, Y.H.; Kim, S.W. Macromolecules **1999**, *32*, 7064.
27. Jeong, B.; Kibbey, M. R.; Birnbaum, J. C.; Won, Y. Y.; Gutowska, A. Macromolecules **2000**, *33*, 8317.
28. Mathur, A. M.; Hammonds, K. F.; Klier, J.; Scanton, A. B. J. Controlled Release **1998**, *54*, 177.
29. Tang, A.; Wang, C.; Stewart, R. J.; Kopecek, J. J. Controlled Release **2001**, *72*, 57.
30. Flory, P. J. in "Principles of Polymer Chemistry", Cornell University Press, Ithaca, New York, **1953**.
31. Chu, Y.; Varanasi, P. P.; McGlade, M. J. Varanasi, S. J. Appli. Polym Sci. **1995**, *58*, 2161.
32. Wang, C.; Li, Y.; Hu, Z. Macromolecules **1997**, *30*, 4727.
33. De, S. K.; Aluru, N. R.; Johnson, B.; Crone, W. C.; Beebe, D. J.; Moore, J. J. of Microelectromechanical Systems, **2002**, *11*, 544.
34. Jeong, B.; Gutowska, A. Trends in Biotechnology **2002**, *20*, 305.
35. Galaev, I. Y.; Mattiasson, B. Trends in Biotechnology **1999**, *17*, 335.
36. Gil, E. S.; Hudson, S. M.; Progress in Polymer Sci. **2004**, *29*, 1173.
37. Hinkley, J. A.; Morgret, L. D.; Gehrke, S. H. Polymer **2004**, *45*, 8837.
38. Harmon, M. E.;Tang, M.; Frank, C. W. Polymer **2003**, *44*, 4547.
39. Osada, Y.; Hasebe, M. Chem. Lett. **1985**, *9*, 1285.
40. Fernández, E.; López, D.; López-Cabarcos, E.; Mijangos, C. Polymer **2005**, *46*, 2211.
41. Suzuki, M. in 'Polymer gels Fundamental and Bio-medical Applications' D. DeRossi (Ed.), Plenum Press, New York, **1991**, 221.
42. Kishi, R.; Ichijo, H.; Hirasa, O. J. Intelligent Mater. Sys. Struct. **1993**, *4*, 533.
43. Brannon-Peppas, L.; Peppas, N. A. Biomaterials **1990**, *11*, 635.

44. Khare, A.R.; Peppas, N. A. J. Biomater. Sci. Poly. Ed. **1993**, *4*, 275.
45. Hoffman, A. S. J. Control. Release **1987**, *6*, 297.
46. Cussler, E. L.; Stokar, M.R.; Varberg, J. E. AIChE J. **1984**, *30*, 578.
47. Freitas, R. F.S.; Cussler, E.L. Chem. Eng. Sci. **1987**, *42*, 97.
48. Tanaka, T. in "Polyelectrolyte Gels:Properties, Preparation and Applications", Harland, R. S.; Prud'homme, R. K. (Edi.) **1992**, ACS Symp. Series 480, Amer. Chem. Soc., Washington, D. C. 1.
49. Heskins, H.; Guillet, J. E. J. Macromole. Sci. Chem. **1969**, *2*, 1441.
50. Schild, H. G.; Prog. Polym. Sci. **1992**, *17*, 163.
51. Hirasa, O.; Ito, S.; Yamauchi, A.; Fujishige, S.; Ichijo, H. in "Polymer Gels", DeRossi, D.; Kajiwara, K.; Osada, Y, Yamauchi, A. Editors, Plenum Press, New York, **1991**, 247.
52. Wei, X.; Hamley, I. W. Polymer **2002**, *43*, 3069.
53. Huglin, M. B.; Liu, Y.; Veleda, J. Polymer **1997**, *38*, 5785.
54. Suzuki, Y.; Tomonaga, K.; Kumazaki, M.; Nishio, I. Polym. Gels Netw. **1996**, *4*, 129.
55. Schild, D. A.; Tirrel, D. A. Macromolecules **1991**, *24*, 948.
56. Park, T. G.; Hoffman, A. S. Macromolecules **1993**, *26*, 5045.
57. Okano, T.; Bae, Y. H.; Jacobs, H.; Kim, S. W. J. Controlled Release **1990**, *11*, 255.
58. Bae, Y. H.; Okano, T.; Hsu, E.; Kim, S. W. Macromol. Chem. Rapid Commun. **1987**, *8*, 481.
59. Hoffman, A. S.; Afrassiabi, A.; Dong, L. C. J. Controlled Release **1986**, *4*, 213.
60. Yamada, N.; Okano, T.; Sakai, H.; Karikusa, F. Sawasaki, Y.; Sakurai, Y. Makromol. Chem. Rapid Commun. **1990**, *11*, 571.
61. Brondsted, H.; Kopecek, J. in "Polyelectrolyte Gels: Properties, Preparation and Applications", Hardland, R. S.; Prudhomme Editors, ACS Symp. Series 480, American Chemical Society, Washington, D.C. **1992**, Chapter 17, 285.

62. Peppas, N. A.; Wright, S. L. Eur. J. of Pharmaceutics and Biophamarmaceutics **1998**, *46*, 15.
63. Ketchalsky, A. Spitnik, P. J. Polymer Sci. **1947**, *2*, 432.
64. Kang, M-S.; Choi, Y-J.; Moon, S-H. J. Membr. Sci. **2002**, *207*, 157.
65. McCormick, C. L.; Elliott, D. L. Macromolecules **1986**, *19*, 542.
66. Butun, V.; Armes, S. P. Macromolecules **1999**, *32*, 4302.
67. Satoh, M.; Yoda, E.; Hayashi, T.; Miyama, J. Macromolecules **1989**, *22*, 1808.
68. Lopez-Leon, T.; Carvelvo,E. L. S.; Seijo, B.; Ortega-Vinuesa, J. L.; Bastos-Gonzalez Journal of Colloid and Interface Science **2005**, 283, 344.
69. Siegel, R. A.; Falamarzian, M.; Firestone; B. A.; Moxley, B. C. J. Controlled Release **1988**, *8*, 179.
70. Patel, V. R.; Amiji,M. M. Pharm. Res. **1996**, 588.
71. Ghandehari, H.; Kopeckova P.; Kopecek, J. Biomaterials **1997**, *18*, 861.
72. Bilia, A.; Carelli, V.; Di Colo G.; Nannipieri, E. Int. J. Pharm. **1996**, *130*, 83.
73. Shiga, T.; Hirose, Y.; Okada, A.; Kurauchi, T. J. Appl. Poly. Sci. **1992**, *46*, 635.
74. Kurauchi, T.; Shiga, T.; Hirose, Y.; Okada, A. in in "Polymer Gels", DeRossi, D.; Kajiwara, K.; Osada, Y, Yamauchi, A. Editors, Plenum Press, New York, **1991**, 237.
75. Kwon, I. C.; Bae,Y. H.;Okano, T.; Kim, S. W. J. Controlled Release **1991**, *17*,149.
76. Mamada, A.; Tanaka, T.; Kungwachakun, D.; Irie, M. Macromolecules **1990**, *23*, 1517.
77. Suzuki, A.; Tanaka, T. Nature **1990**, *346*, 345.
78. Zrinyi, M. Barsi, L.; Buki, A. Polym. Gels Networks **1998**, *5*, 415.
79. Lee, K. K.; Cussler, E. L.; Marchetti, M.; McHugh, M. A. Chem. Eng. Sci. **1990**, *45*, 766.
80. Siegel, R. A.; Firestone, B. A. J. of Controlled Release **1990**, *11*, 181.

81. Davis, R. H. in “Membrane Handbook” edited by Winston, W. S.; Sirkar, K. K. Van Nostrand Reinhold NY, **1992**, chapter 31.
82. Kulkarni, S. S.; Funk, E. W.; Norman, N. L. in “Membrane Handbook” edited by Winston, W. S.; Sirkar, K. K. Van Nostrand Reinhold NY, **1992** a chapter 26.
83. Williams, M. E.; Bhattacharyya, D.; Ray, R. J. McCray, S. B. “Membrane Handbook” edited by Winston, W. S.; Sirkar, K. K. Van Nostrand Reinhold NY, **1992**, chapter 24.
84. Musale, D. A.; Kulkarni, S. S. J. Membr. Sci. Macromole. Chem. Phys. **1998**, *C38*, 615.
85. Nystrom, M. J. Membr. Sci. **1989**, *44*, 183.
86. Nau, F.; Kerherve, F. L.; Leonil, J.; Daufin, G. Biotechnology and Bioengineering **1995**, *46*, 246.
87. Eijndhoven, R. K. C. M. V.; Saksens, S.; Zydney, A. L. Biotechnology and Bioengineering **1995**, *48*, 406.
88. Belfer, S.; Gilron, J. Purinson, Y.; Fainshtain, R.; Daltrophe, N.; Priel, M.; Tenzer, B.; Toma, A. Desalination **2001**, *139*, 169.
89. Ulbricht, M.; Matuschewski, H.; Oechal, A.; Hicke, H-G. J. Membr. Sci. **1996**, *115*, 31.
90. Nabe, A.; Staude, E.; Belfort, G. J. Membr. Sci. **1997**, *133*, 57.
91. Taniguchi, M.; Belfort, G. J. Membr. Sci. **2004**, *231*, 147.
92. Shim, J. K.; Na, H. S.; Lee, Y. M.; Huh, H.; Nho, Y. C. J. Membr. Sci. **2001**, *191*, 215.
93. Gancarz, I.; Pozniak, G.; Bryjak, M. Eur. Polym. J. **1999**, *35*, 1419.
94. Kull, K. R.; Steen, M. L.; Fisher, E. R. J. Membr. Sci. **2005**, *246*, 203.
95. Wavhal, D. S.; Fisher, E. R. Langmuir **2003**, *19*, 79.
96. Kim, K. S.; Lee, K. H; Cho, K.; Park, C. E. J. Membr. Sci. **2002**, *199*, 135.
97. Akhtar, S.; Hawes, C.; Dudley, L.; Reed, I.; Stratford, P. J. Membr. Sci. **1995**, *107*, 209.
98. Li, R. H.; Barbari, T. A. J. Membr. Sci. **1995**, *105*, 71.
99. Osada, Y.; Honda, K.; Ohta, M. J. Membr. Sci. **1986**, *27*, 327.

100. Ito; Park, Y. S.; Imanishi, Y. J. Am. Chem. Soc. **1997**, *119*, 2739.
101. Mika, A. M.; Childs, R. F.; Dickson, J. M. J. Membr. Sci. **1999**, *153*, 45.
102. Mika, A. M.; Childs, R. F.; Dickson, J. M; McCarry, B. E.; Gagnon, D. R. J. Membr. Sci. **1995**, *108*, 37.
103. Iwata, H.; Matsuda, T. J. Membr. Sci. **1988**, *38*, 185.
104. Gholap, S. G.; Musale, D. A.; Kulkarni, S. S.; Karode, S.; Kharul, U. K. J. Membr. Sci.**2001**, *183*, 89.
105. Ito,Y.; Inaba, M.; Chung, D-J.; Imanishi, Y. Macromolecules **1992**, *25*, 7313.
106. Kontturi, K.; Mafe, S.; Manzanares, J. A.; Svarfvar, B. L.; Viinikka, P. Macromolecules **1996**, *29*, 5740.
107. Ito, Y.; Kotera, S.; Inaba, M.; Kono, K.; Imaishi, Y. Polymer **1990**, *31*, 2157.
108. Ito, Y.; Park, Y. S.; Imanishi, Y. Macromol. Rapid Commun. **1997**, *18*, 221-224.
109. Mika, A. M.; Childs, R. F.; West, M.; Lott, J. N. A. J. Membr. Sci. **1997**, *136*, 221.
110. Lee, Y. M.; Ihm, S. Y.; Shim, J. K.; Kim, J. H.; Cho, C. S.; Sung, Y. K. Polymer **1995**, *36*, 81.
111. Liang, L; Shi, M.; Viswanathan, V. V.; Peurrung, L. M.; Young, J. S. J. Membr. Sci. **2000**, *177*, 97.
112. Park, Y. S.; Ito, Y.; Imanishi, Y. Langmuir, **1998**, *14*, 910.
113. Iwata, H.; Oodate, M.; Uyama, Y.; Amemiya, H.; Ikada, Y. J. Membr. Sci. **1991**, *55*, 119.
114. Yokahata, Y.; Noguchi, H.; Seki, T. Macromolecules **1986**, *19*, 493.
115. Peng, T.; Cheng, Y-L. J. Appl. Polym. Sci. **1998**, *70*, 2133.
116. Chung, D-J.; Ito, Y.; Imanishi, Y. J. Appl. Polym. Sci. **1994**, *51*, 2027.
117. Hickey, A. S.; Peppas, N. A. Polymer **1997**, *38*, 5931.
118. Hassan, C. M.; Peppas, N. A. Advances in Polym. Sci. **2000**, *153*, 37.
119. Peppas, N. A.; Merrill, E. W. J. Polym. Sci. Polym Chem **1976**, *14*, 441.
120. Hickey, A. S.; Peppas, N. A. J. Membr. Sci. **1995**, *107*, 229.

121. Gref, R.; Nguyen, Q. T.; Schaetzel, P.; Neel, J. J Appl Polym Sci **1993**, *121*, 49(2), 209.
122. Katz, M. G.; Wydeven, T. J. Appl. Polym. Sci. **1982**, *27*, 79.
123. Toyoshima, K. in "Polyvinyl Alcohol properties and Applications edited by Finch, C. A. John Wiley & Sons **1973**, Chapter 14 , 339.
124. Matsuyama, H.; Teramoto, M.; Urano, H. J. Membr. Sci. **1997**, *126*, 151-160.
125. Gudeman, L. F. Peppas, N. A. J. Membr. Sci. **1995**, *107*, 239.
126. Brannon-Peppas, L.; Peppas, N. A. Chemical Engineering Science **1991**, *46*, 715.
127. Gudeman, L. F. Peppas, N. A. J. Appli. Polym. Sci. **1995**, *55*, 919.
128. Arndt, K. F.; Richter, A.; Ludwig, S.; Zimmermann, J.; Kressler, J.; Kucling, D.; Adler, H. J. Acta Polym. **1999**, 383.
129. Peppas, N. A.; Merrill, E. W. J. Appli. Polym. Sci. **1977**, *21*, 1763.
130. Zentner, G. M.; Cardinal, J. R.; Kim, S. W. J. Pharmaceutical Sciences **1978**, *67*, 1352.
131. Yang, J. M.; Su, W. Y.; Leu, T. L.; Yang, M. C. J. Membr. Sci. **2004**, *236*, 39.
132. Varshosaz, J.; Falamarzian, M. European Journal of Pharmaceutics and Biopharmaceutics **2001**, *51*, 235.
133. Wisniewski, S. J.; Gregonis, D. E.; Kim, S. W.; Andrade, J. D. in "Hydrogels for medical and Related application",edited byAndrade, J. D. **1976**, Chapter 6, 81.
134. Burczak, K.; Fujisata, T.; Hatada, M.; Ikada, Y. Biomaterials **1994**, *15*, 231.
135. Yasuda, H.; Lamaze, C. E.; Ikenberry, L. D. Die Makromolecular Chemie **1968**, *118*, 19.
136. Yasuda, H.; Ikenberry, L. D.; Lamaze, C. E. Die Makromolecular Chemie **1969**, *125*, 108.
137. Wisniewski, S.; Kim, S. W. J. Membr. Sci. **1980**, *6*, 299.
138. Peppas, N. A.; Reinhart, C. T. J. Membr. Sci. **1983**, 15, 275.

139. Schwarte, L. M.; Peppas, N. A. Polymer **1998**, *39*, 6057.
140. Reinhart, C. T; Peppas, N. A. J. Membr. Sci. **1984**, *18*, 227.
141. Lustig, S. R.; Peppas, N. A. J. Appli. Polym. Sci. **1988**, *36*, 735.
142. Ende, M. T. A.; Peppas, N. A. J. Controlled Release **1997**, *48*, 47.
143. Ende, M. T. A.; Hariharan, A.; Peppas, N. A. React. Polym **1995**, *25*, 127.
144. Peppas, N. A.; Wright, S. L. Macromolecules **1996**, *29*, 8798.
145. Bettini, R.; Colombo, P.; Peppas, N. A. J. Controlled Release **1995**, *37*, 105.
146. Bell, C. L.; Peppas, N. A. J. Controlled Release **1996**, *39*, 201.
147. Feil, H.; Bae, Y. H.; Feijien, J.; Kim, S. W. J. Membr. Sci. **1991**, *64*, 283.
148. Yoshida, R.; Okuyama, Y.; Sakai, K.; Okano, T.; Sakurai, Y. J. Membr. Sci. **1994**, *89*, 267.
149. Guilherme, M. R.; Silva, R. d.; Rubira, A. F.; Geuskens, G.; Muniz, E. C. Reactive and Functional Polymers **2004**, *61*, 233.
150. Grassi, M.; Yuk, S. H.; Cho, S. H.; J. Membr. Sci. **1999**, *152*, 241.
151. Nonaka, T.; Ogata, T.; Kurihara, S. J. Appl. Polym Sci. **1994**, *52*, 951.
152. Ogata, T.; Nonaka, T.; Kurihara, S. J. Membr. Sci. **1995**, *103*, 159.
153. Nonaka, T.; Yoda, T.; Kurihara, S. J. Polym. Sci.: Part A: Polym Chem. **1998**, *36*, 3097.
154. Kurihara, S.; Sakamaki, S.; Mogi, S. Ogata, T.; Nonaka, T. Polymer **1996**, *37*, 1123.
155. Ogata, T.; Nonaka, T.; Kurihara, S. J. Membr. Sci. **1995**, *103*, 159.
156. Kurihara, S.; Ueno, Y.; Nonaka, T. J. Appl. Polym. Sci. **1998**, *67*, 1931.
157. Zhang, J.; Peppas, N. A. Macromolecules **2000**, *33*, 102.
158. Kuboto, N.; Matsubara, T.; Eguchi, Y. J. Appl. Polym. Sci. **1998**, *70*, 1027.
159. Muniz, E. C.; Geyskens, G. J. Membr. Sci. **2000**, *172*, 287.
160. Pande, A. K.; Goswami, A.; Mazumder, S. D; Childs, R. F. J. Membr. Sci. **2003**, *217*, 117.
161. Stachera, D. M.; Childs, R. F. J. Membr. Sci. **2001**, *187*, 213.
162. Mika, A. M.; Pandey, A. K.; Childs, R. F. Desalination **2001**, *140*, 265.
163. Mika A. M.; Childs, R. F.; Dickson, J. M. Desalination **1999**, *121*, 149.

164. Jiang, W.; Childs, R. F.; Mika, A. M.; Dickson, J. M. Desalination **2003**, *159*, 253.
165. Stachera, D. M.; Childs, R. F.; Mika, A. M.; Dickson, J. M. J. Membr. Sci. **1998**, *148*, 119.
166. Childs, R. F.; Mika, A. M.; Pandey, A. K.; McCrory, C.; Mouton, S.; Dickson, J. M. Separation and Purification Technology **2001**, *22-23*, 507.
167. Kapur, V.; Charkoudian, J. C.; Kessler, S. B.; Anderson, J. L. Ind. Eng. Chem. Res. **1996**, *35*, 3179.
168. Mika, A. M.; Childs, R. F.; Dickson, J. M. J. Membr. Sci. **2002**, *206*, 19.
169. Mika, A. M.; Childs, R. F.; Dickson, J. M.; McCarry, B. E.; Gagnon, D. R. J. Membr. Sci. **1997**, *135*, 81.
170. Kapur, V.; Charkoudian, J.; Anderson, J. L. J. Membr. Sci. **1997**, *131*, 143.
171. Dai, W. S.; Barbari, T. A. Biomaterials **2000**, *21*, 1363.
172. Dai, W. S.; Barbari, T. A. J. Membr. Sci. **2000**, *171*, 79.
173. Nutt, M.; Crookston, D.; Beitle, R. Separation Science and Technology **2000**, *35*, 785.
174. Chen, J-P.; Chen, H-J. Polymeric Materials: Science and Engineering **2001**, *85*, 591.
175. Chun, S-W.; Kim, J-D. J. Controlled Release **1996**, *38*, 39.
176. Liang, L.; Feng, X.; Peurrung, L.; Viswanathan, V. J. Membr. Sci. **1999**, *162*, 235.
177. Greenland, D. J. J. Colloid Sci. **1963**, *18*, 647.
178. Aranda, P.; RTeiiz-Hitzky, E. Chem. Mater. **1992**, *4*, 1395.
179. Biswas, M.; Sinha Ray, S. Adv. In Polym. Sci. **2001**, *155*, 167.
180. Rodlert, M.; Christopher, J. G. P.; Garamzegi, L.; Leterrier, Y. T.; Grunbauer, H. J. M.; Manson, J-A. E. Polymer **2004**, *45*, 946.
181. Jaing, T.; Wang, Y-H. ; Yeh, J-T. ; Fan, Z-Q. Eur. Polym. J. **2005**, *41*, 459.
182. Giannelis, E. P.; Krishnamoorthi, R.; Manias, E. Adv. Polym. Sci. **1999**, *138*, 107.
183. Alexandre, M.; Dubois, P. Materials Science & Engineering :R :Reports **2000**, *28*, 1.

184. Sinha Ray, S.; Okamoto, M. Progress in Polym Sci. **2003**, *28*, 1539.
185. Komori, Y.; Kuroda, K. in "Polymer-Clay Nanocomposites"edited by Pinnavaia, T. J.; Beall, G. W., John Wiley and Sons,Ltd, **2000**, 3.
186. Liu, X.; Wu, Q. Polymer **2001**, *42*, 10013.
187. LeBaron, P.C.; Wang, Z.; Pinnavaia, T. J. Appli. Clay Sci. **1999**, *15*, 11.
188. Ward, W. J.; Gaines, G. L. J.; Alger, M. M.; Stanley, T. J. J. Membr. Sci. **1991**, *55*, 173.
189. Lepoittevin, B.; Devalckenaere, M.; Pantoustier, N.; Alexandre, M.; Kubies, D.; Calberg, C.; Jerome, R.; Dubois, P. Polymer **2002**, *43*, 4017
190. Gilman, J. W. Applied Clay Science **1999**, *15*, 31.
191. Gilman, J. W.; Jackson, C. C.; Morgan, A. B.; Harris, R. Jr.; Manios, E.; Giannelis, E. P.; Wuthenow, M.; Hilton, D.; Phillips, S. H. Chem. Mater. **2000**, *12*, 1866.
192. Yano, K.; Usuki, A.; Okada, A.; Kurauchi, T.; Kamigaito, O. J. Polym. Sci.: Polym. Chem. **1993**, *31*, 2493.
193. Lan, T.; Kaviratna, P.D.; Pinnavaia, T. J. Chem. Mater. **1994**, *6*, 573.
194. Chang, J-H.; Jang, T.-G.; Ihh, K. J.; Lee, W.-K.; Sur, G. S. J. Appl. Polym. Sci. **2003**, *90*, 3208.
195. Strawhecker, K. E.; Manias, E. Chem. Mater. **2000**, 12, 2943.
196. Xu, J.; Meng, Y. Z.; Li, R. K. Y.; Xu, Y. Rajulu, A. V. J. Polym. Sci. Part B **2003**, *41*, 749.
197. Grunlan, J. C.; Grigorian, A.; Hamilton, C. B.; Mehrabi, A. R. J. Appl. Polym. Sci. **2004**, *93*, 1102.
198. Haraguchi, K.; Takehisa, T.; Fan, S. Macromolecules **2002**, *35*, 10162.
199. Haraguchi, K.; Farnworth, R.; Ohbayashi, A.; Takehisa, T. Macromolecules **2003**, *36*, 5732.
200. Haraguchi, K.; Takehisa, T. Advanced Materials **2002**, *14*, 1120.
201. Shibayama, M.; Suda, J.; Karina, T.; Okabe, S.; Takehisa, T.; Haraguchi, K. Macromolecules **2004**, *37*, 9606.
202. Gao, D.; Heimann, R. B. Polymer Gels and Networks, **1993**, *1*, 225.

203. Churochkina, N. A.; Starodoubtsev, S. G.; Khokhlov, A. R. Polymer Gels and Networks **1998**, *6*, 205.
204. Liang, L.; Liu, J.; Gong, X. Langmuir **2000**, *16*, 9895.
205. Xia, X.; Yih, J.; D'Souza, N. A.; Hu, Z. Polymer **2003**, *44*, 3389.
206. Lee, W-F.; Fu, Y-T. J. Appl. Polym. Sci. **2003**, *89*, 3652.
207. Lee, W-F. Chen, Y-C. J. Appl. Polym. Sci. **2004**, *91*, 2934.
208. Briggs, D.; Seah, M. P. in "Practical Surfgace Anlysis ny Augur and X-ray Photoelectron Spectroscopy", John Whiley and Sons Ltd. NewYork, **1983**.
209. Jones, D. S. International J. of Pharmaceutics **1999**, *179*, 167, 209.
210. Shafee, E. E.; Naguib, H. F. Polymer **2003**, *44*, 1647.
211. Duncan, J. in "Mechanical Properties and Testing of Polymers" edited by Swallowe, G. M. **1999**, Kluwer Academic, 43.
212. Bashaiwoldu, A. B.; Podczeck, F.; Newton J. M. International J. of Pharmaceutics **2004**, *274*, 53.
213. Cullity, B. D. in "Elements of X-ray Diffraction", Addison-Wesley Publishing company Inc., **1956**, Chapter 3.
214. Klugg, H. P.; Alexander, L. E. in "X-ray diffraction procedures", John Wiley & sons: USA, **1974.**
215. Uyama, Y.; Inoue, H.; Ito, K.; Kishida, A.; Ikada, Y. Journal of Colloid and Interface Science **1991**, *141*, 275.
216. Mulder, M. in " Membranes in Bioprocessing Theory and Applications Edited by Howell, J. A.; Sanchez, V.; Field, R. W. Blackie Academic & Professional, **1993**,Chapter 2.
217. Keurentjes, J. T. F.; HArbrecht, J. G.; Brinkman, D.; Hanemaaijer, J. H.; Stuart, M. A. C.; Riet, K. V. J. Membr. Sci. **1989**, *47*, 333.
218. Brinkman, E.; Does, L. vd.; Bantjes, A. Biomaterials **1991**, *12*, 63.
219. Karmis, H. R.; Rao, G.; Barbari, T. A. J. Membr. Sci. **2003**, *212*, 75.
220. Mika, A. M.; Childs, R. F.; Dickson, J. M. J. Membr. Sci. **1999**, *153*, 45.
221. Ishihara, K.; Kobayashi, M; Shionohara, I. Makromol. Chem. Rapid communication **1983**, *4*, 327.
222. Obaidat, A. A.; Park, K. Biomaterials **1997**, *18*, 801.

223. Ishihara, K.; Kohayashi, M.; Ishimaru, N.; Shinohara, I. Polymer J. **1984**, *16*, 625.

224. Miyata, T.; Uragami, T.; Nakamae, K. Advanced Drug Delivery Reviews **2002**, *54*, 79.

225. Ito, I.; Casolaro, M.; Kono, K.; Yukio, I. J. Controlled Release **1989**, *10*, 195.

226. Chu, L-Y.; Li, Y.; Zhu, J-H.; Wang, H-D.; Liang, Y-J. J. of Controlled Release **2004**, *97*, 43.

227. Colton, C. J. Cell Transplant **1995**, *4*, 415.

228. Baker, A. R.; Fournier, R. L.; Sarver, J. G.; Long, J. L.; Goldblatt, P. J.; Horner, J. M.; Selman, S. H. Cell Transplantation **1997**, *6*, 585.

229. Gupta, P.; Varmani, K.; Garg, S. Drug Discovery Today **2002**, *7*, 569.

230. Risbud, M.V.; Hardikar, A. A.; Bhat, S.V.; Bhonde, R. R. J. Controlled Release **2000**, *68*, 23.

CHAPTER 2

Objectives and Scope of the Work

2.1 Objectives and Scope of the Work

The objective of this work is to synthesize and characterize novel hydrogel membranes, which can have potential applications in bio-separations. Recently, major attention has been focused towards developing stimuli-sensitive hydrogels and membranes for selective separations. The combination of hydrogel and membranes provide hydrogel membranes with synergistic properties of both hydrogel and membranes with good mechanical strength. Furthermore, these membranes mimic the biological tissues and exhibit excellent biocompatibility. The swelling and shrinking property of hydrogel can be effectively utilized to adjust the pore size /mesh size of membranes. The permeation through hydrogel membranes not only depends on the molecular structure, but also on the external conditions. Such membranes have applications in bio-separation, controlled drug delivery, bio-hybrid artificial organs, multi-component separations and chemical valves. In this work, we have followed different strategies to develop hydrophilic/hydrophobic stimuli-sensitive hydrogel membranes with good mechanical properties.

The present work is undertaken with the following specific objectives:

1. To synthesize temperature and pH sensitive polyamphoteric hydrogel membranes based on Chitosan [CS]/poly(N-isopropylacrylamide) [PNIPAm]/ poly(2-acrylamido-2-methyl propane sulphonic acid) [PAMPS] terpolymers and to characterize the swelling and permeation behaviour of membranes prepared from these polymers as a function of different external parameters such as temperature, pH etc. Furthermore, chitosan has an excellent film forming property with very good biocompatibility. The appropriate balance between the hydrophilic and hydrophobic components in the membranes can lead to discontinuous volume transitions in the membrane, which can be used to tune the permeation properties of the membrane for selective separations.

2. To design and develop thermosensitive hydrogel membranes based on PVA and N-tertiary butyl acrylamide [NTBA], whose homopolymers do not show lower

critical solution temperature (LCST) at an observable temperature range. To investigate the critical concentration between hydrophilic PVA and hydrophobic NTBA in graft copolymer system, which exhibits a discontinuous transition as a function of temperature. To characterize the swelling and permeation properties as a function of temperature and hydrophobic contents and also, to investigate the physical properties of graft copolymeric membranes by differential scanning colorimetry (DSC), X-ray diffraction (XRD) and dynamic mechanical analysis (DMA).

3. To synthesize novel nanocomposite hydrogel membranes by incorporating water swellable clay such as, laponite into the hydrogel, PVA-g-polyNTBA. To study the influence of clay content on swelling, mechanical and permeation properties of resultant membranes. Nanocomposite membranes are composed of specific polymers and inorganic clays and have attracted increasing attention lately because of their enhanced mechanical properties. Therefore, nanocomposite hydrogels can overcome some of the limitations in the conventional hydrogel membranes such as mechanical weakness, morphological inhomogeneity.

4. To study the phenomenon of wettability in hydrophobic polymers caused by adsorption of hydrophilic polymers. Although most of the synthetic polymers do not adsorb onto hydrophobic surfaces, the PVA spontaneously adsorbs irreversibly onto hydrophobic substrates. However, the underlying mechanism of adsorption is yet to be fully understood. Therefore, in this study, our objective is to get an insight into the mechanism of adsorption. The PVA adsorbed PVDF membranes were subjected to detailed physico-chemical analysis with XPS and EDAX measurements. The adsorption could be an important and simplest method to improve the hydrophilicity of the hydrophobic membranes, which can have implications in reducing the fouling of membranes during bio-separations.

CHAPTER 3

Synthesis and Characterization of Polyamphoteric Hydrogel Membranes based on Chitosan

3.1 Introduction

Polyamphoteric hydrogel membranes are attracting increasing attention lately in the area of biomedical and biochemical separations because of their good biocompatibility and low fouling characteristics. These membranes are having both positive and negative charges and therefore, the permeability of solutes through them can be controlled by pH.[1] In a pH and thermoreversible hydrogel membrane, the mesh size of the membrane can be controlled by both pH and temperature. Transition from the swollen state to the collapsed state or vice versa in the membrane at a certain temperature and a certain pH, influences the permeation characteristics of the membrane.[2] Permeation of solutes through the charged membranes can be by size selection as well as through solute/polymer interactions. However, which one predominates depends on the type of membrane and the solutes to be separated.[3]

Poly(*N*-isopropylacrylamide) [PNIPAm] is a widely studied thermoreversible hydrogel, which exhibits a lower critical solution temperature (LCST) at around 33 °C in an aqueous solution.[4] Below the LCST, the gel is in the swollen state and above LCST it dehydrates into a collapsed state. Therefore, due to their interesting volume transition properties, thermoreversible polymers have shown large number of promising applications in bio-medical fields. Hydrophilic or hydrophobic modifications of thermoreversible polymer disturbs the critical balance of the hydrophilic/hydrophobic interactions and changes the phase transition behaviour.[5,6] In order to retain the temperature induced swelling transition of hydrogel over a broad and useful pH range, the polyelectrolyte complexation phenomenon has been used. For example, Yoo *et. al.*[7]observed the lower critical solution temperature for poly(*N*-isopropyl acrylamide-*co*-acrylic acid) [P(NIPAAm-*co*-AAc)] hydrogel even above the pK_a of poly(acrylic acid) in the presence of poly(allyl amine) which was attributed to the decrease in the binding sites of water due to formation of polyelectrolyte complexation between poly(acrylic acid) and poly(allyl amine). Chitosan [CS] is a poly[β(1→4)-2-amido-2-deoxy-D-glucopyranose], and can be obtained by the N-deacetylation of chitin, poly[β(1→4)-2-acetamido-2-deoxy-D-glucopyranose] which is obtained from the crab and shrimp shells. Generally, chitosan is prepared by

deacetylating chitin with aqueous alkali such as sodium and potassium hydroxides at 120-160°C, which leads to the 70-95% of degree of deacetylation.[8] Further, the complete deacetylation of chitin could be achieved by repeating alkaline treatment.[9] CS is non-toxic and easily bioadsorbable biopolymer with an excellent gel forming properties at low pH values. Below pH 6.5, chitosan in solution, carries a high positive charge density by protonating $–NH_2$ groups. Because of its large number of $–NH_3^+$ groups, it readily interacts with biopolymers such as bone, hair and skin, which are composed of negatively charged mucopolysaccharides and proteins. Chitosan has been used in membrane separations[10-12] and also for removal of metallic impurities as a metal chelating agent since it has ability to bind strongly the heavy and toxic metal ions.[13] Temperature and pH sensitive IPN, semi-IPN hydrogel systems based on chitosan and PNIPAm have already been reported.[14-17] Guan *et. al.*[18] have reported on the semi-IPN hydrogels based on crosslinked chitosan with glutaraldehyde-polyether network. They investigated the pH sensitivity, swelling and release kinetics and the structural changes of the gel in different pH solutions. The graft copolymerisation of vinyl monomers onto chitosan has been reported earlier. **Table 3.1** lists the vinyl monomers grafted onto chitosan. For example, chitosan-g-PNIPAm polymers have been reported with the advantage of their dual sensitivity towards both temperature and pH.[17] However, the effective pH range where the swelling behavior change is very narrow and is only between 4 and 6. Furthermore, under the strong acidic conditions, the graft copolymer tends to become water-soluble which, limits the usage in the wider pH range. Najjar *et. al.* [19] have reported on the grafted copolymer based on chitosan and AMPS. The emphasis was however, given to optimize reaction conditions to get maximum grafting onto chitosan. Although, the system can exhibit amphoteric nature at low pH values, the detailed characterizations have not been reported. PAMPS, bearing sulfonic acid groups, belongs to a class of polyelectrolytes, which have high degree of ionization. Wimonsiri *et. al.*[20] reported on the grafting of monomethoxy ethylene glycol oligomers on the surface of chitosan films. Stoilova *et. al.*[21] investigated the polyelectrolyte complex formation between chitosan and PAMPS. In this chapter, we report on the synthesis and characterization of polyamphoteric membrane based on grafting of NIPAm and AMPS monomers onto

chitosan. The swelling behaviour of these membranes as a function of pH, temperature and ionic strength was studied. Permeability of two ionic drugs (Theophylline and Ciprofloxacin hydrochloride) through these membranes was investigated. The advantages of making terpolymer of chitosan, PNIPAm, PAMPS is that, at low pH the terpolymer will have both positive and negative charges on the polymer chain and can exhibit interesting swelling behaviour and permeating characteristics. Furthermore, since PAMPS is hydrophilic in nature, it can reduce the tendency of fouling of membranes during the separation process.

Table 3.1 Details of grafting various vinyl monomers onto chitosan

Monomer	Initiator	Solvent	Reference
Vinyl Pyrrolidone	KPS	Aqueous acetic acid	22
AAc	KPS/FAS	Acrylic acid solution	23
AN	CAN	Aqueous acetic acid	24
MMA	H_2O_2/FAS	Aqueous	25
NIPAm	CAN	Aqueous acetic acid	17
AN, MMA, MAA, VA	AIBN	Aqueous acetic acid	26
AMPS	KPS	Aqueous acetic acid	19
AAm	KPS /BisAm	Aqueous acetic acid	27
AAc, AAm	KPS/ BisAm	Aqueous acetic acid	28
4-Vinyl pyridine	CAN	Aqueous acetic acid	29
DMMESA	CAN	Aqueous acetic acid	30
HEMA	CAN	Acetone	31
HEMA	UV irradiation	Acetone/water	31
HEMA	γ-irradiation	Methanol	31
HEMA (CS film)	γ-irradiation	Methanol/water	32
NIPAm	γ-irradiation/ Ammonium ferrous sulfate	Aqueous acetic acid	33
Styrene	γ-irradiation	Styrene/methanol	34
AN, MMA	KPS	Aqueous acetic acid	35

AAm: Acrylamide
AMPS: 2-acrylamido-2-methylpropane-sulfonic acid
AAc: Acrylic acid
AN: Acrylonitrile
AIBN: Azobisisobutyronitrile
CAN: Ceric ammonium nitrate
DMMAESA: N, N, dimethyl-N-methacryloxy ethyl-N-3-sulfopropyl ammonium
HEMA: 2-hydroxyethylmethacrylate
FAS: Ferrous ammonium sulfate
NIPAm: N-isopropyl acrylamide
MMA: Methyl methacrylate
MAA: Methacrylic acid
KPS: Potassium persulfate
VA: Vinyl acetate

3.2 Experimental

3.2.1 Materials

Chitosan (85% deacetylated) was procured from Sigma-Aldrich. N-Isopropylacrylamide (NIPAm) and 2-acrylamido-2-methyl propane sulfonic acid (AMPS) monomers were procured from Aldrich Chemicals, USA and Lubrizol respectively. Potassium persulfate (KPS) and N, N'-methylene bis acrylamide (Bis-Am) were purchased from Loba chemicals and SD Fine Chemicals Ltd., India respectively. N, N, N', N'-Tetramethylethylene diamine (TEMED) was purchased from Aldrich chemicals, USA. Theophylline and Ciprofloxacin hydrochloride were obtained from Aldrich chemicals, USA and Iotras Pharma, India respectively. The structures of chitosan, NIPAm, AMPS, Bis-Am and TEMED are shown in **Figure 3.1**.

The molecular weight of chitosan was determined from intrinsic viscosity, [η] measurements in a buffer solvent system (0.3 M acetic acid and 0.2 M sodium acetate) at 25^{o}C using Mark-Houwink-Sakurada equation (with Mark-Houwink constants, K= 7.4 x 10^{-4} dlg^{-1}, α = 0.76).[36] The viscosity average molecular weight was found to be 260,000 g/mole.

3.2.2 Synthesis of Chitosan Hydrogel Membrane

Chitosan hydrogel membranes were prepared by graft copolymerization of NIPAm and AMPS monomers simultaneously onto chitosan at 30 ^{o}C using potassium persulfate, [KPS] as an initiator and TEMED as an accelerator. Chitosan solution was prepared in 1.0% acetic acid solution and the monomers, initiator, accelerator and cross linker (Bis-A) were dissolved in the reaction mixture. The stoichiometry of the reactions is given in **Table 3.2**. In two terpolymer hydrogel membranes, the concentration of AMPS was 5.0 and 10.0 wt (%) on the basis of the weight of the NIPAm monomer. Nitrogen was purged through this solution to remove the oxygen, which can act as a free radical scavenger. This solution was poured into petridish to polymerize and cast membranes. The gelation took place in 5-10 minutes depending

on the concentration of the accelerator. These hydrogel membranes were kept for air-drying for 8 days at room temperature to fecilitate the easy removal of membranes from the petri dish. Further, these hydrogel membranes were soaked in acetone, water and acidic buffers to remove the unreacted monomers if any. The thicknesses of dry membranes were found to be in the range of 40-50 μm.

A. Cationic nature of chitosan

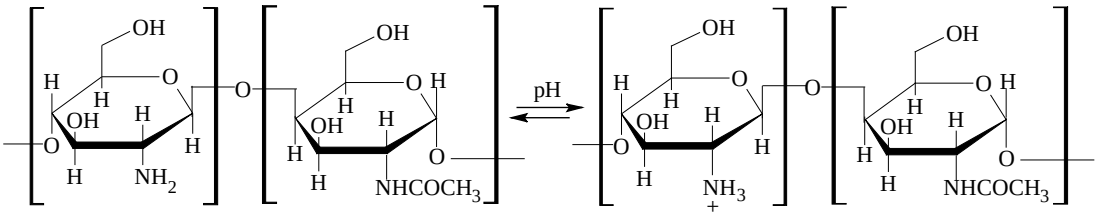

pH > 6.3 pH < 6.3

B. Anionic nature of AMPS

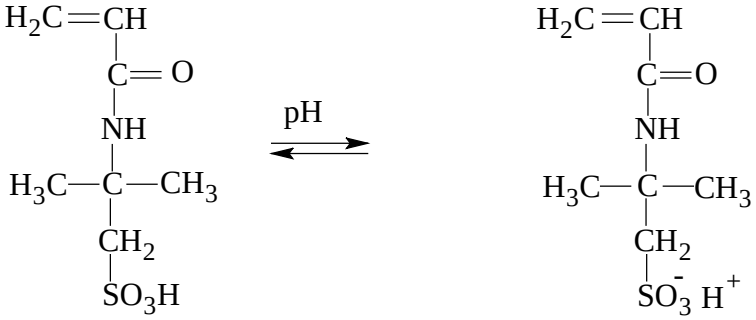

pH < 2.6 pH > 2.6

C. N-isopropyl acrylamide (NIPAm)

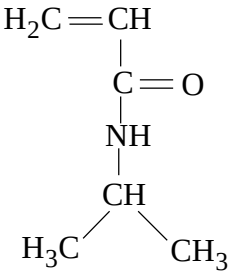

D. N, N’-Methylene bisacrylamide (Bis-Am)

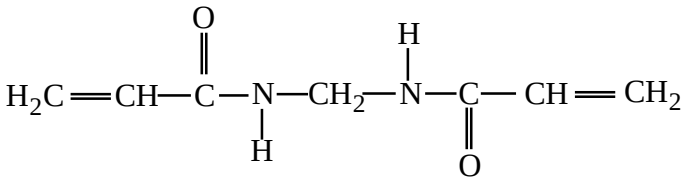

E. N, N, N’, N’-Tetramethylethylene diamine (TEMED)

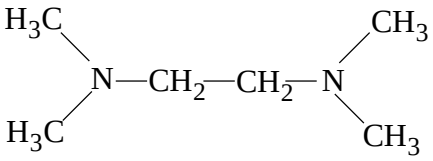

Figure 3.1 The chemical structures of Chitosan, NIPAm, AMPS, Bis-Am and TEMED

Table 3.2. Stoichiometry for the preparation of hydrogel membranes

Membrane	Chitosan soln. (1% in acetic acid) (ml)	NIPAm (g)	AMPS (g)	KPS (g)	Bis-Am (g)	TEMED (μL)
CS-PNIPAm	8.0	0.3125	0.0	0.04	0.0468	40
CS-PNIPAm-PAMPS-5	8.0	0.3125	0.015	0.04	0.0468	40
CS-PNIPAm-PAMPS-10	8.0	0.3125	0.0312	0.04	0.0468	40

NIPAm: N-Isopropyl acrylamide
AMPS: 2-Acrylamido-2-methyl propane sulfonic acid
Bis-Am: N, N'-Methylene bis acrylamide
KPS: Potassium persulfate
TEMED: N, N, N', N'–Tetramethylethylene diamine

3.3 Characterization

3.3.1 FT-IR Spectroscopy

FT-IR spectra were recorded using a Perkin Elmer FT-IR spectrometer of model (16 PC) at resolution of 4 cm^{-1}. The analysis was carried out using thin films. Chitosan film was made in acetic acid solution by solvent evaporation method.

3.3.2 Swelling Ratios at Different pH, Ionic strength and Temperature

Buffers were made from McIlvain buffer (0.1M citric acid and 0.2 M Na_2HPO_4) from 2.6 to 7.0 pH. The buffers were made at ionic strength (*I*) corresponding 0.5 M and 0.02 M by diluting with distilled water. *I* was calculated from the equation,

$$I = \frac{1}{2}\sum C_i Z_i^{\,2} \qquad (3.1)$$

Where,

C_i is the molar concentration and Z_i is the valency of various ionic species.

The dried pre-weighed membranes were kept in corresponding pH, salt solutions in a constant temperature bath. The temperature was varied from 20 to 50 ^oC and the equilibration time was 24 hours. The swollen samples were reweighed after wiping the surface gently.

The swelling ratio (q) of membranes was calculated using the following equation,

$$q = \frac{W_2}{W_1} \qquad (3.2)$$

where, W_2 and W_1 are wet and dry weights of the membrane, respectively.

3.3.3 Permeation Studies

Permeation experiments were carried out at different temperatures and pH using a two chamber (donor and receptor) diffusion cell with a chamber volume of 70 cm^3 (**Figure 3.2**). Pre-conditioned membranes were mounted between two halves of the donor and receptor cell, which were further clamped together and sealed tightly with the rubber packing. The effective membrane area in the cell was 1.76 cm^2. The solution was at the donor side of the cell and the receptor was having only the buffer. A fixed volume (1.0 ml) of the sample was taken out at various time intervals from the

receptor cell and the solute concentration was measured using an UV spectrophotometer at appropriate wavelengths. After taking out samples from the receptor cell each time, the same amount of fresh buffer solution was added to the receptor cell to maintain the constant volume at the receptor cell. Two drugs chosen for the permeation studies were, theophylline (MW= 180) and ciprofloxacin hydrochloride (MW= 365). The concentrations of these solutes were determined by UV spectrophotometer at wavelengths of 271 nm and 277 nm, respectively. The initial concentration of theophylline and ciprofloxacin hydrochloride in the donar cell was 0.02 mg/ml.

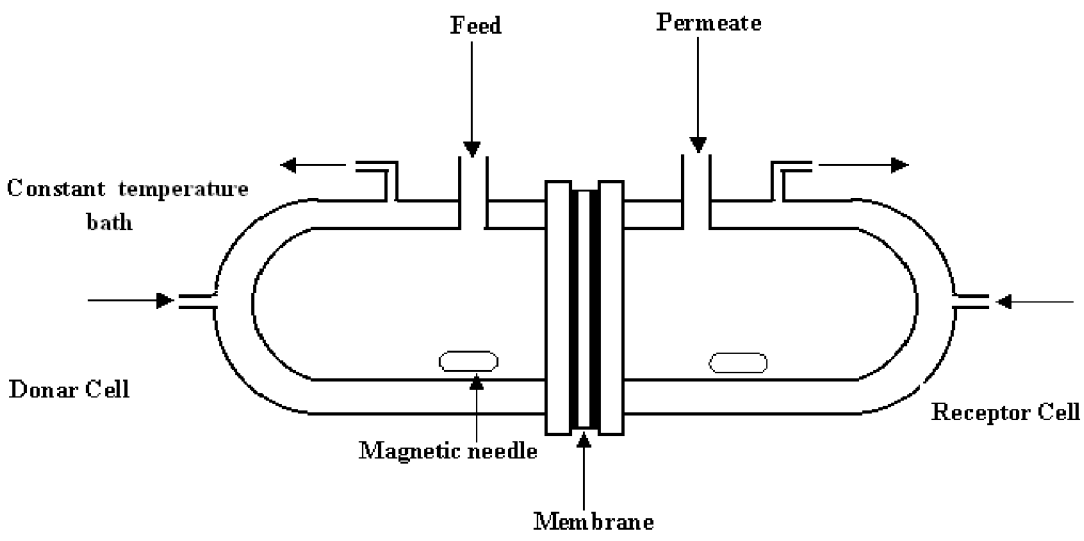

Figure 3.2: Schematics of the two-chamber (donor and receptor) diffusion cell for the permeation study.

3.4 Results and Discussion

3.4.1 Graft copolymerization

Chitosan has both reactive amino and hydroxyl groups that can be used to chemically alter its properties under mild reaction conditions. Chitosan and its derivatives have become useful polysaccharides in the biomedical area because of their numerous and interesting biological properties such as biocompatibility, biodegradability and non-toxic properties. Chitosan in particular, exhibits pH responsive behavior as a weak polybase due to the large number of amino groups in its chain. The modification of chitosan through grafting has become increasingly important. Large number of vinyl monomers has been grafted using initiators such as ceric ammonium nitrate (CAN), persulfates and Fenton's reagent. In our system, the grafting of NIPAm and AMPS monomers onto chitosan was done by using KPS as a redox initiator. The redox initiator generates a free radical on the chitosan backbone and the vinyl monomers polymerize on the backbone. The copolymerization of these monomers onto chitosan can lead to the grafted pendant PNIPAm and PAMPS chains. This could be attributed to the fact that, the reactivity ratios r_1 and r_2 of NIPAm and AMPS monomers are reported to be 2.4 ± 0.8 and 0.03 ± 0.02 respectively [37] and since $r_1 >> r_2$, the NIPAm monomer has a strong affinity to enter into the growing PNIPAm chain. Therefore, the grafted chain will have large number of NIPAm units. Furthermore, we observed that the LCST of the grafted copolymer did not change significantly which clearly indicated that the AMPS units were not incorporated in the PNIPAm growing chain. We have used the crosslinking agent, Bis-Am in the polymerization in order to enhance the stability of the membranes in the aqueous medium. The reaction mechanism is given in **Figure 3.3**. This can lead to some formation of semi-IPNs in the terpolymer. However, the structural evidence of these IPNs is beyond the scope of this work.

1. Role of TEMED as an accelerator in generation of free radical [38]

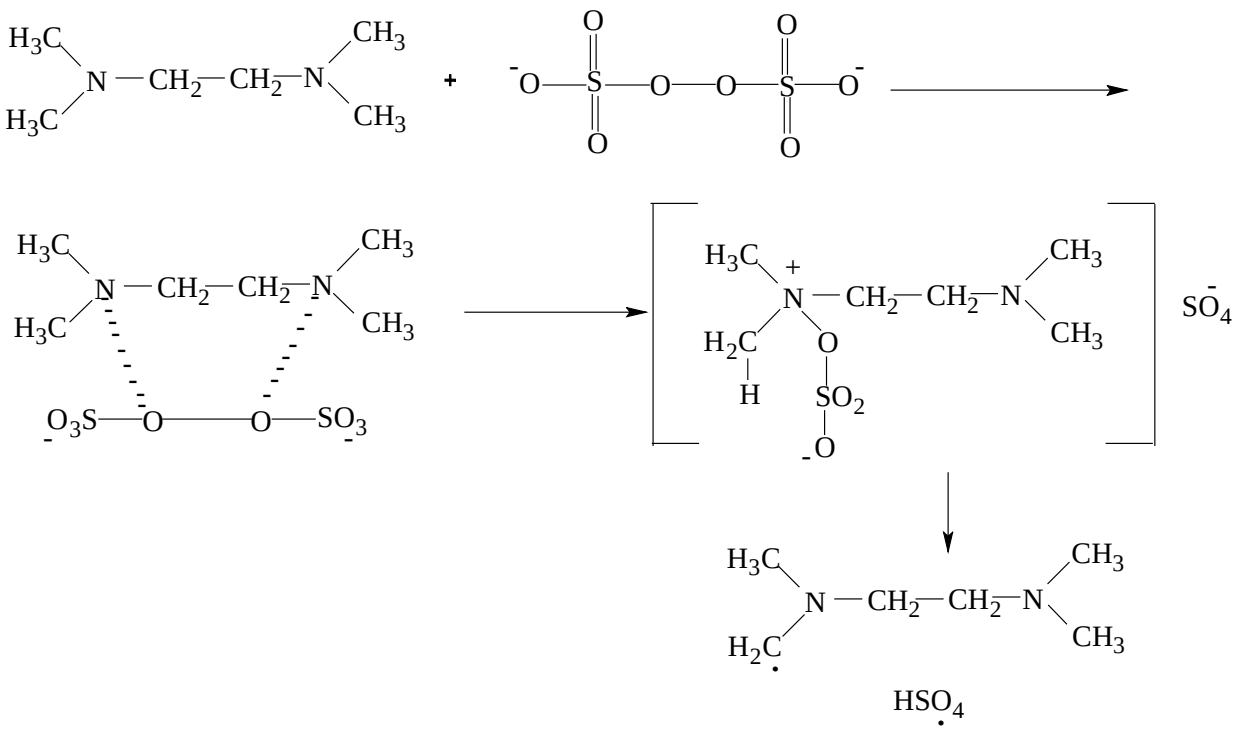

2. Radical sites generated by persulfate initiator on chitosan ($R^{\cdot}$)[19,28]

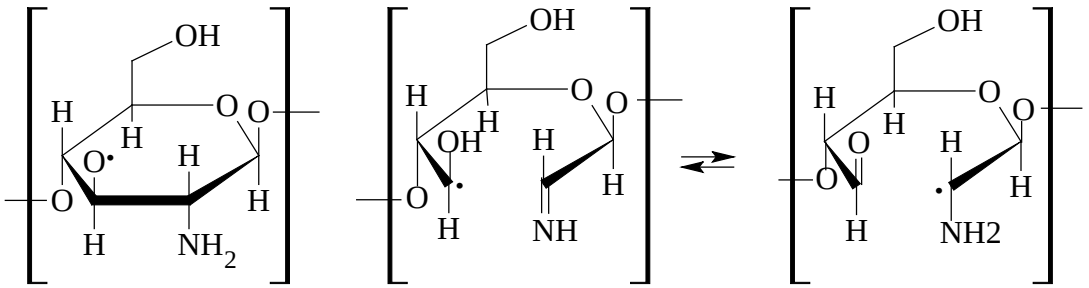

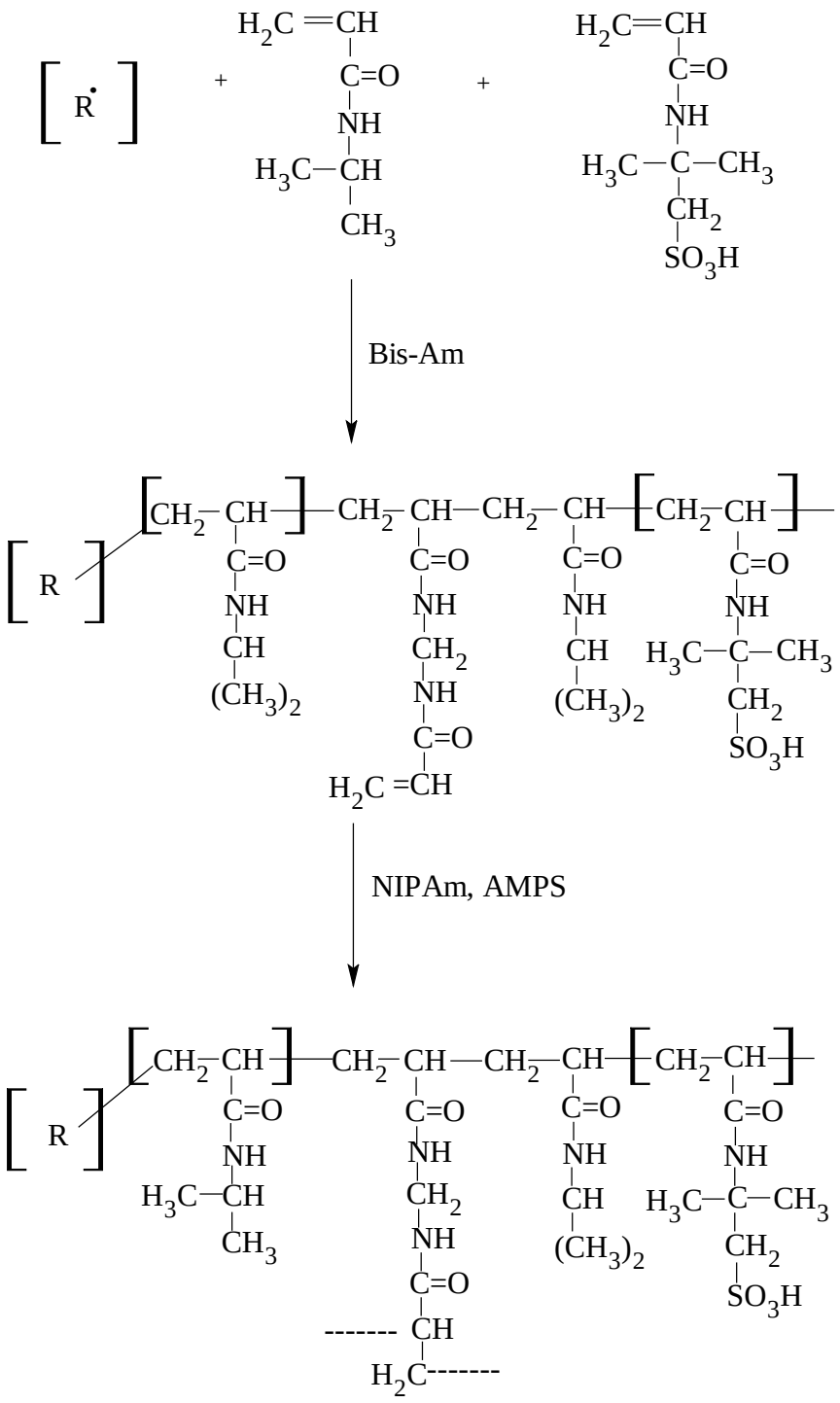

Figure 3.3: Reaction mechanism of chitosan with NIPAm and AMPS by using KPS as an initiator and TEMED as an accelerator.

3.4.2. Proof of Grafting by FT-IR Spectroscopy

Incorporation of NIPAm and AMPS onto chitosan was confirmed by FT-IR spectroscopy. Chitosan membrane shows characteristic broad –OH peak at 3450 cm^{-1}, peak at 900 cm^{-1}, 1154cm^{-1} for anti symmetric stretching of C-O-C bridge, 1653 cm^{-1} and 1580 cm^{-1} for amide I (carbonyl stretching) and amide II (-N-H bending vibration), respectively as shown in **Figure 3.4 (a)**. In the CS-PNIPAm membrane, apart from the chitosan bands, there are new bands at 1368 cm^{-1} and broad band at 1653 cm^{-1}, which are attributed to the isopropyl groups and –CONH of PNIPAm. While in the case of terpolymer CS-PNIPAm-PAMPS membrane, there exists an additional peak at 1040 cm^{-1}, which corresponds to S=O stretching frequency of PAMPS as shown in **Figure 3.4 (b)**. Modified chitosan membranes also show 2 broad peaks between 1600-1700 cm^{-1} and 1500-1600 cm^{-1} which are due to the inter, intra, non-bonded carbonyl and -NH groups respectively. The chitosan (85% deacetylation) has $–NHCOCH_3$ groups, which show peaks between 1600-1700 cm^{-1} and 1500-1600 cm^{-1}. With addition of NIPAm and AMPS to chitosan, number of amide groups increases which results in inter/intra molecular H-bonding hence resulting in broadening of the peaks.

(a)

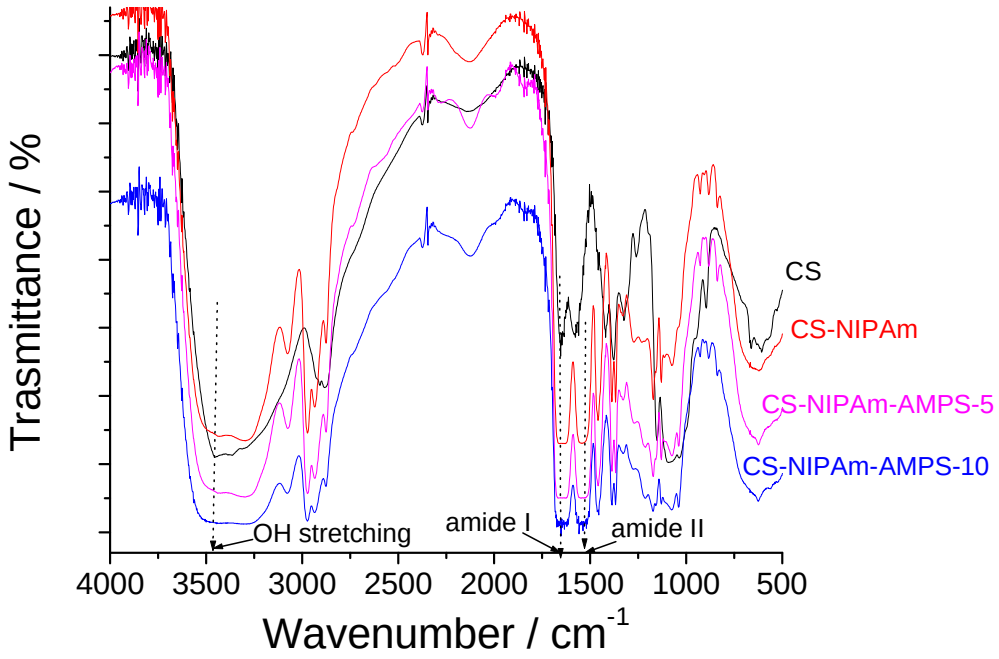

Figure 3.4 (a): FT-IR spectra of chitosan, CS-PNIPAm, CS-PNIPAm-PAMPS-5 and CS-PNIPAm-PAMPS-10 films in the range of 4000-500 cm^{-1}.

(b)

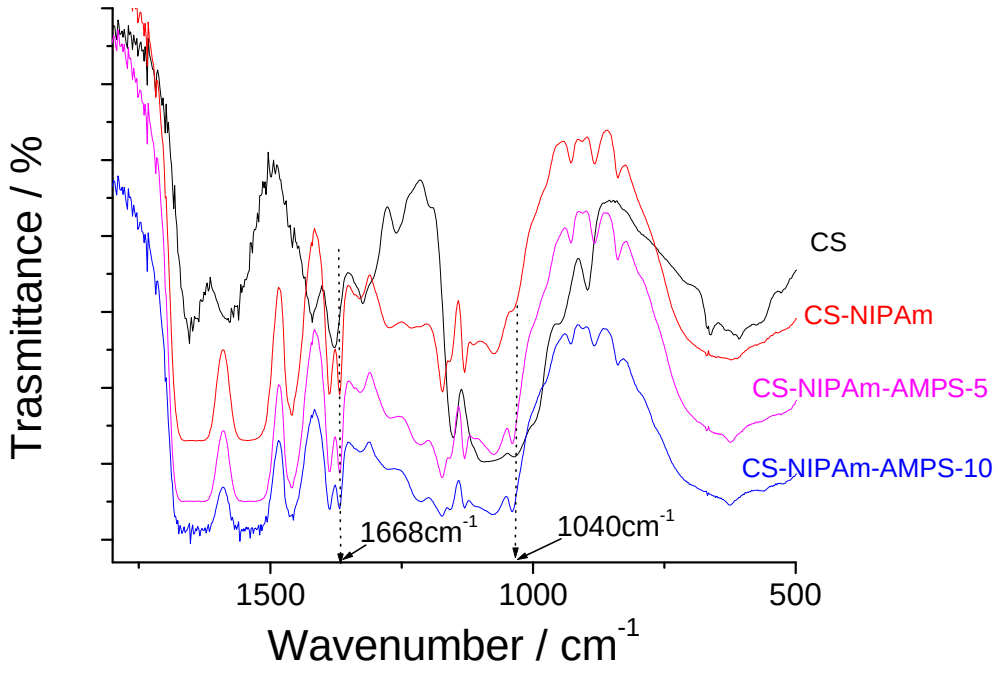

Figure 3.4 (b): FT-IR spectra of chitosan, CS-PNIPAm, CS-PNIPAm-PAMPS-5 and CS-PNIPAm-PAMPS-10 films in the range of 1800-500 cm^{-1}.

3.4.3. pH Dependent Swelling Ratios

We show in **Figure 3.5** the pH dependent equilibrium swelling ratios of three hydrogel membranes with the different contents of PAMPS at 30 ^{o}C. The addition of PAMPS onto CS-PNIPAm polymer introduces a negative charge on the chain and makes the polymer system an amphoteric in nature.

Chitosan is a cationic polyelectrolyte with pK_a value of 6.3 and below this pH, it is positively charged. Whereas, PAMPS is an anionic polyelectrolyte with pK_a value of 2.86.[39] Therefore, above the pH 2.86, PAMPS is in the ionized form. The presence of both the ions on the polymer chain makes the swelling properties interesting in this system. It can be seen from the figure that, for CS-PNIPAm polymer (with no AMPS) the swelling ratios are higher at lower pH due to the electrostatic repulsion between the positive charges as a result of ionization of chitosan at lower acidic pH. Upon increasing the pH, there is a decrease in the electrostatic repulsion due to the reversal of NH_3^+ to NH_2, which causes the decrease in swelling.

It can also be readily seen from the figure that, addition of PAMPS to CS-PNIPAm polymer increases the hydrophilicity of the system and increases the swelling ratios in the entire pH range studied. It is interesting to note that as the pH increases from 1 to 2.8, the swelling ratio of CS-PNIPAm-PAMPS-5 and CS-PNIPAm-PAMPS-10 increase, show a maximum at pH 3 and start to decrease thereafter. This decrease in swelling ratio is due to the electrostatic attraction between the positive and negative charges present in the chains. The electrostatic attraction reduces the coil dimensions and subsequently decreases the swelling ratios. Furthermore, at higher pH, the ionic strength effects start to establish the shielding of electrostatic repulsions and hence reduce the swelling ratios further.

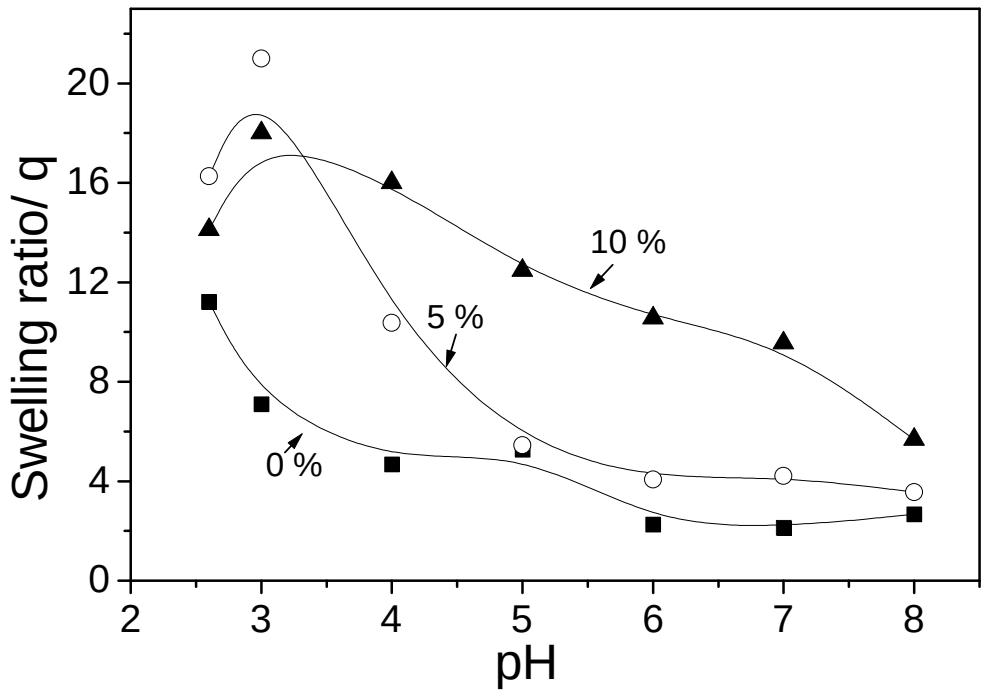

Figure 3.5: Influence of pH on the swelling ratio of CS-PNIPAm-PAMPS hydrogel membranes with the different contents of PAMPS at 30 ^{o}C and Ionic strength of I = 0.5M.

3.4.4 Temperature Dependent Swelling Ratios

Temperature dependent swelling of all the membranes were performed at three different pH values (pH = 3, 4, 7). We show in **Figure 3.6** the equilibrium swelling ratios of CS-PNIPAm membrane as a function of temperature at three different pH values 3, 4, 7. As expected, the swelling ratios are high at low pH, which is due to the electrostatic charge repulsion of the protonated amine groups in the chitosan. Furthermore, swelling ratios decrease as the temperature is increased. This is due to the presence of PNIPAm chains in the membrane, which are strongly thermosensitive in nature. It is well established that below the LCST (32 ^{o}C), the PNIPAm chains are hydrophilic in nature and are in the expanded state of conformation. There is extensive hydrogen bonding (H-bonding) between the polymer and water, which contributes to the high swelling ratios. However, upon increasing the temperature, the H-bonding between the polymer and water decrease significantly and there is a large increase in the intermolecular hydrophobic interactions. As a result, the PNIPAm chains undergo coil-to-globule transition, which reduces the swelling ratios.[40]

It is important to note here that, at all the pH values, the swelling ratios decrease continuously without showing any discontinuous volume transitions. The incorporation of PAMPS into CS-PNIPAm system however, increases the hydrophilicity of the membrane and in turn increases the swelling ratios. We show in **Figure 3.7**, the temperature dependent equilibrium swelling ratios of the above mentioned membranes at pH 3.0. It can be seen that, the swelling ratios are high at temperatures below 35 °C and especially, still higher in the presence of higher incorporation of PAMPS (CS-PNIPAm-PAMPS 10). Furthermore, there is a distinct discontinuous volume transition close to the LCST of PNIPAm. The discontinuous volume transition becomes more predominant at higher content of PAMPS in the system. This discontinuous volume transition is very important in designing hydrogel membranes for the controlled drug delivery systems and offers an “on-off” switch mechanism to facilitate the release of active drugs from membranes.

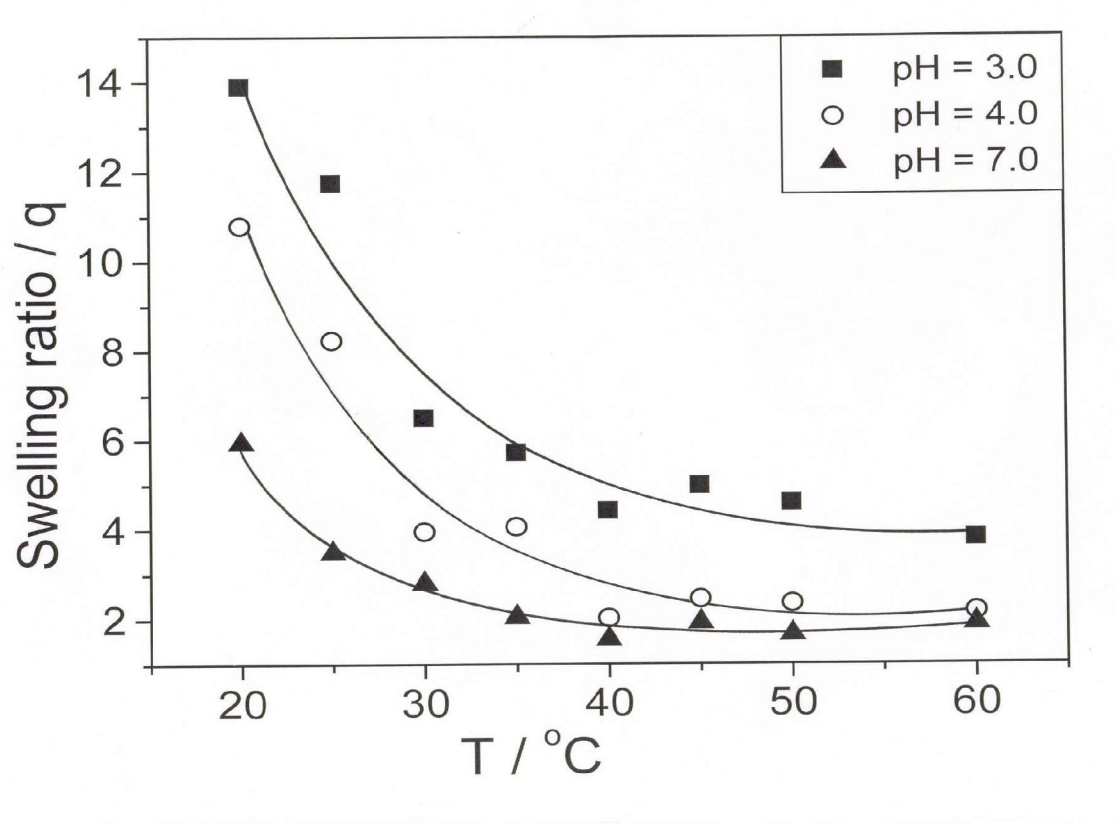

Figure 3.6: Temperature dependent swelling ratios of CS-PNIPAm membrane at three different pH values.

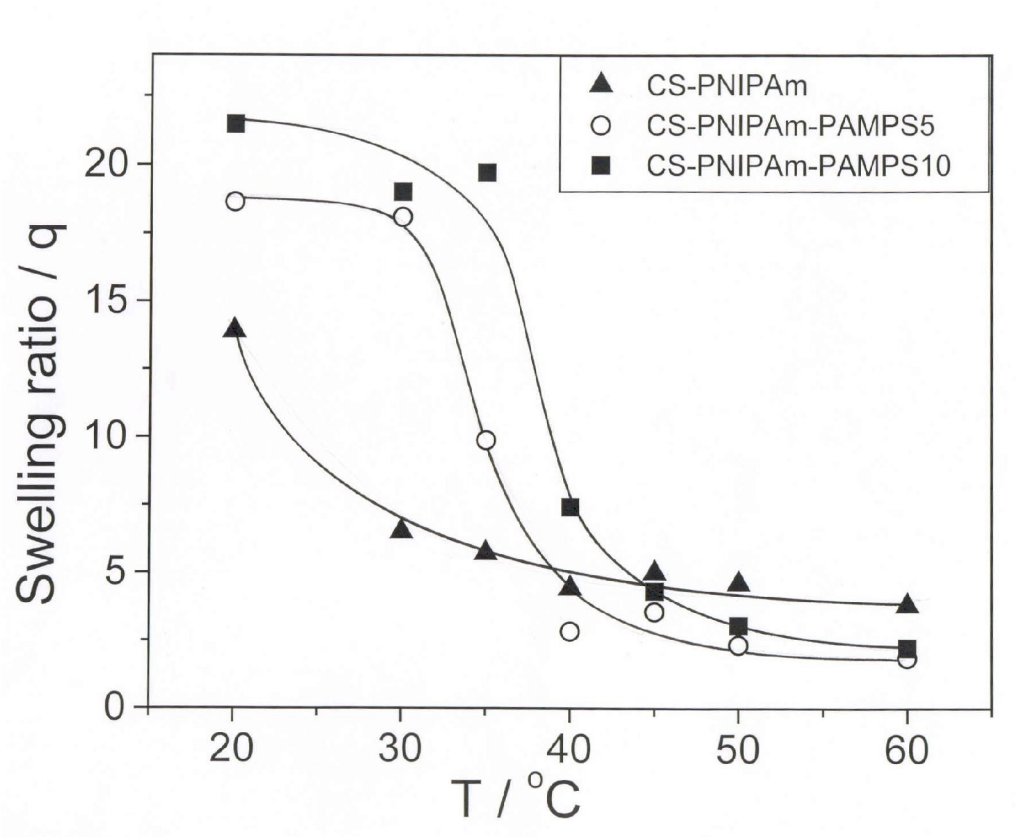

Figure 3.7: Temperature dependent swelling ratios of CS-PNIPAm-PAMPS membranes at pH = 3.0 and at two different PAMPS contents.

The observed discontinuous volume transition can be recoursed to the fact that, it has been shown in the past that polyacrylamide [PAAm] gels in acetone/H_2O mixtures, do not show discontinuous transition.[41] However, upon hydrolysis of the –$CONH_2$ groups in the PAAm into PAA-salt begin to show distinct discontinuous transition. This is due to the increase in hydrophilicity of the gel by incorporating ionic charges into the gel. The mode of volume transition depends very much on the presence of charge on the polymer chain. Therefore, our observation of discontinuous transition is in line with the earlier finding that, the incorporation of PAMPS into CS-PNIPAm gel increases the hydrophilicity of the whole system by addition of charges on the polymer chain which in turn, gives rise to discontinuous volume transition. The incorporation of PAMPS into CS-PNIPAm gel, causes addition of opposite charges to CS-PNIPAm membrane at a lower pH of 3.0. So, at this pH, CS-PNIPAm-PAMPS membrane forms polyelectrolyte complex between positive and negative charges which results in a discontinuous volume transition. Therefore, we show that by addition of PAMPS into CS-PNIPAm system one can get discontinuous transition as a function of temperature. Furthermore, we show in **Figure 3.8** the data of swelling ratios verses temperature for CS-PNIPAm-PAMPS-5 at pH 3 and 7. It can be readily seen that the discontinuous transition is more pronounced at pH 3 and becomes continuous at pH 7. The continuous transition at pH 7 is due to the chitosan becoming neutral at this pH. In addition to this there is a possibility of intra chain H-bonding between chitosan and PNIPAm, which would lead to increase in hydrophobicity of the membrane and decrease the interactions with water. Similar observation was made by Huglin *et. al.*[42] in the case of poly (NIPAm-co-AA) hydrogels at low pH.

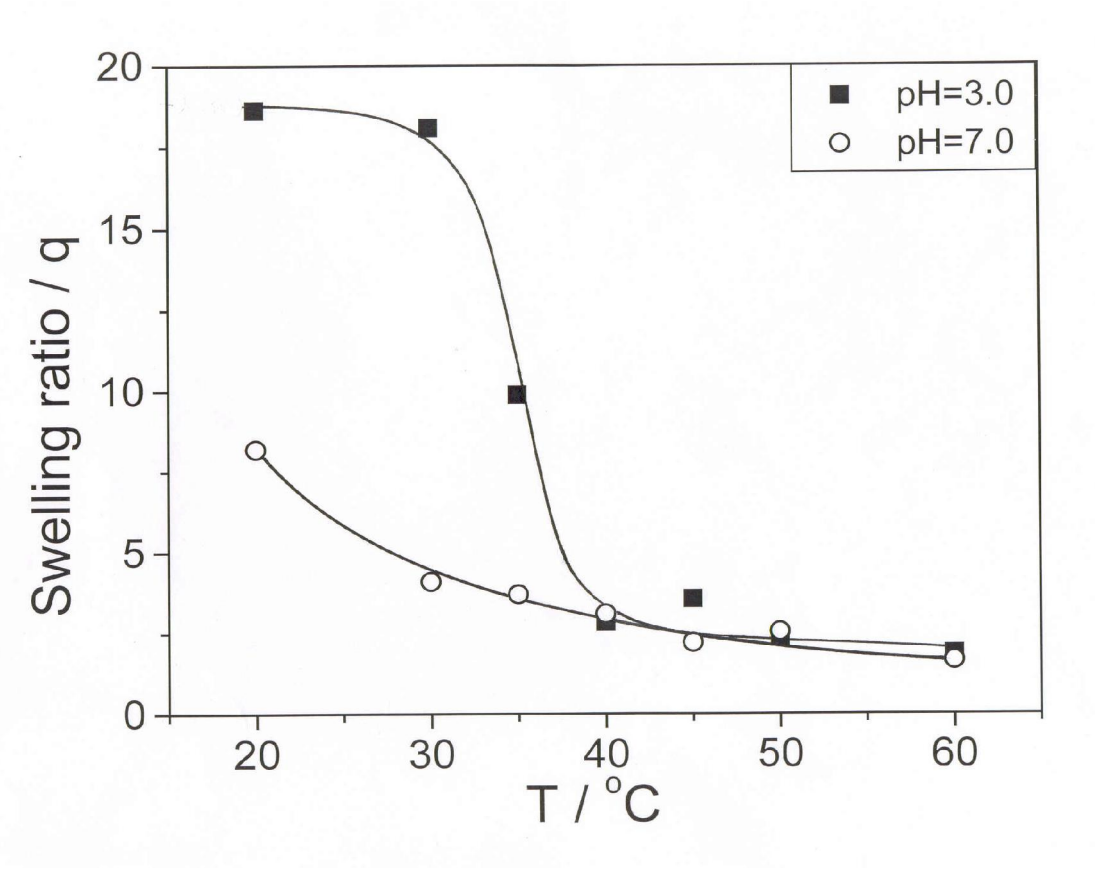

Figure 3.8: Effect of temperature on the swelling behaviour of CS-PNIPAM-PAMPS-5 membrane at two pH values.

3.4.5 Influence of pH and Ionic strength on the Swelling

As mentioned earlier, CS-PNIPAm-PAMPS is an interesting system which exhibits both +ve and –ve charges on the polymeric chains at certain pH conditions. The amphoteric nature of the system can give rise to interchain complexations, which can lead to coiled conformation of the chains. This conformation in turn decreases the swelling ratios. We show in **Figure 3.9** the swelling ratios of CS-PNIPAm-PAMPS-10 as a function of pH at two different ionic strengths. At low ionic strength, the swelling ratio keeps on increasing with pH. At low pH, both chitosan and PAMPS are in the ionized state. The polyelectrolyte complexation between the opposite charges can create an -inter or -intra chain crosslinking (physical) thus reducing the swelling ratios. However, at high pH, the positive charge on the chitosan is neutralized and the complexation breaks resulting into the reduction of physical crosslinking. This leads to the enhanced swelling ratios.

On the contrary, at high ionic strength and low pH, the ionic groups screen the charges on the membrane and prevent the formation of interchain complexation. Thus, the physical crosslinking is reduced resulting in the high swelling ratios. However, upon increasing the pH, the charge neutralization of chitosan reduces the electrostatic repulsions in the chains and it is further reduced by the excess ionic groups, which screens the electrostatic interactions. Consequently, the swelling ratios decrease.

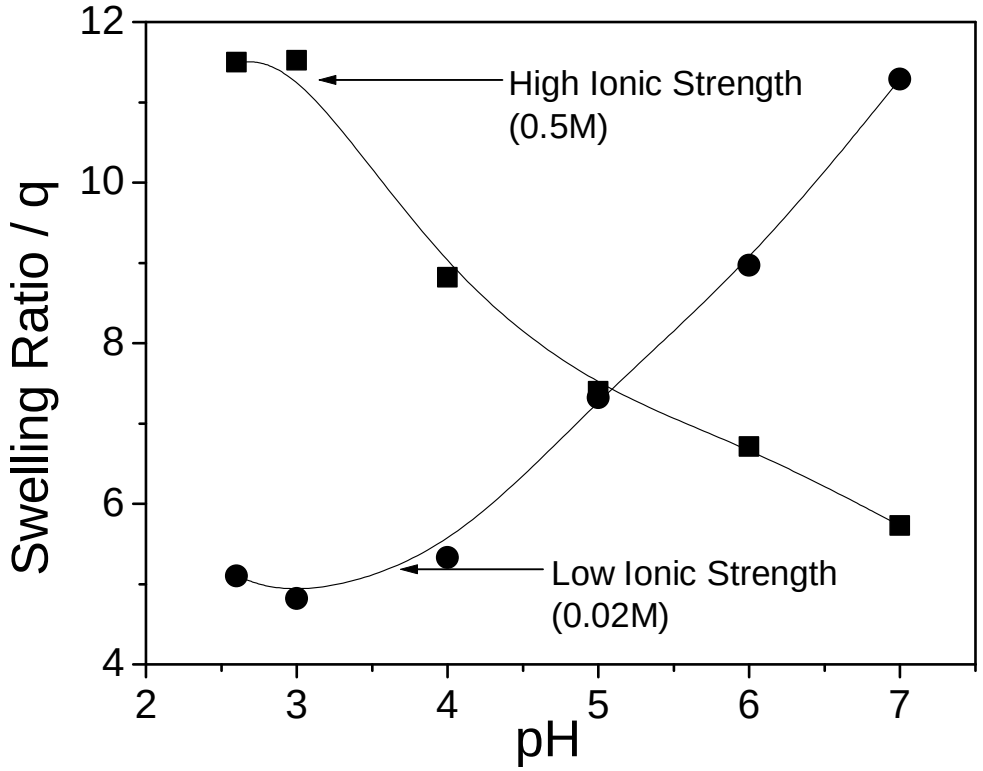

Figure 3.9: Influence of Ionic strength (*I*) on the pH dependent swelling ratios of CS-PNIPAm-PAMPS-10 membrane.

3.4.6 Permeation of Solutes

The permeation of solutes through hydrogel membranes depends on properties such as hydrophilic-hydrophobic balance, degree of crosslinking and effective mesh-size, nature of functional groups and charges on the membrane. As per the Fick's law of diffusion, the permeability of the solute can be given by the equation,

$$\frac{\mathrm{P}}{\delta} = \frac{-V}{2At} \ln \frac{\Delta C_t}{C_0} \qquad (3.3)$$

Where,

C_t = Solute concentration in the receptor cell (mg/ml)

C_0 = Initial solute concentration in the donor cell (mg/ml)

V = Volume of each half cell (ml)

A = Effective permeation area (cm^2)

P = Permeability coefficient (cm/s)

t = Time (h or s)

δ = Thickness of the membrane (mm)

The above equation can be rewritten as,

$$\ln(1-2\frac{C_t}{C_0}) = \frac{-2A}{V} Pt \qquad (3.4)$$

To determine the permeability coefficient, P, a plot of $-V/2A\ln(1-2C_t/C_0)$ against t was constructed and a linear fitting was performed. The slope of the linear portion of the graph yields the permeability coefficient.

We show in **Figure 3.10** the permeabilities of theophylline in CS-PNIPAm-PAMPS-5 membrane at two different temperatures, one below (30 ^{o}C) and one above (40 ^{o}C) the LCST of PNIPAm. It can be readily seen that, the slope is larger at higher temperature (40 ^{o}C), which indicates the higher permeability for theophylline at higher temperature compared to the one at lower temperature. This observation is in line with the report made by Kubota *et. al.*[43] where, they have reported the theophylline release from PAA-g-oligo (*N*-isopropyl acrylamide) gel at higher temperature. This can be attributed to the fact that the PNIPAm chains in the hydrogel membrane undergo coil-

globule transition at higher temperature and are present in the collapsed state. As a result, the hydrogel network opens up the channels for enhanced permeation of solutes. At lower temperature however, the PNIPAm chains are in the expanded state, which fills the channels and subsequently reduce the permeation rates. This phenomenon can be effectively used to design hydrogel membranes for specific end applications.

In **Figure 3.11**, we show the results of theophylline permeability in two membranes with different hydrophilic polymer content. The membranes CS-PNIPAm-PAMPS-5 and CS-PNIPAm-PAMPS-10 contain 5.0 and 10.0% hydrophilic polymer (PAMPS) respectively. As can be seen from the figure that, the permeability of theophylline is more in the CS-PNIPAm-PAMPS-10 membrane. This is due to the increase in the hydrophilicity of the membrane, which enhances the solubility of theophylline in the membrane resulting in the enhanced permeation.

The influence of the size of solutes on the permeation characteristics of the membrane CS-PNIPAm-PAMPS-5 is shown in **Figure 3.12**. Two solutes, theophylline and ciprofloxacin of different molecular weights have been used for the permeation studies. The results clearly show that as the size of the solute increases the rate of permeation decreases.

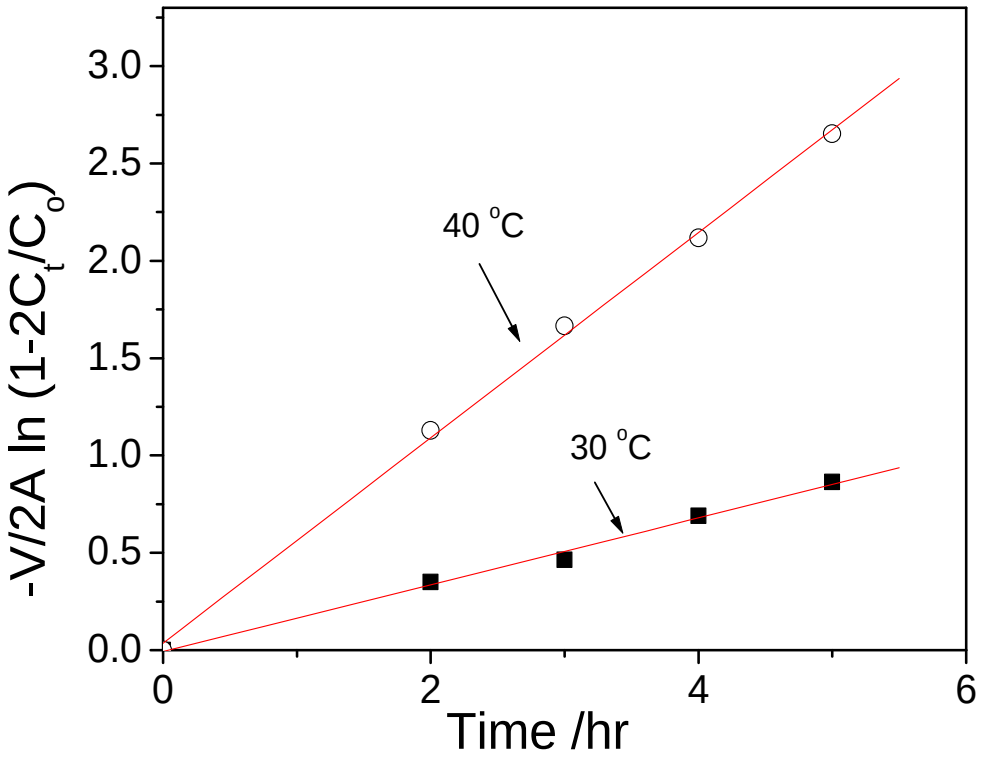

Figure 3.10: Permeation of Theophylline through CS-PNIPAm-PAMPS-5 membrane at two temperatures and at constant pH = 4.0.

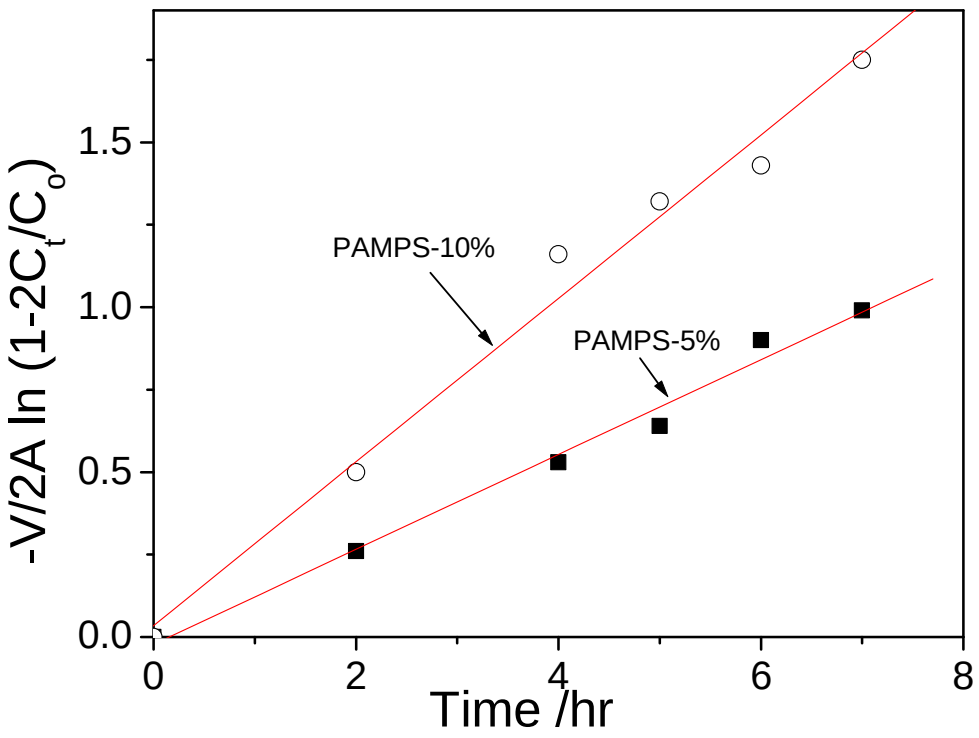

Figure 3.11: The influence of hydrophilicity (PAMPS content) membrane on the permeation of Theophylline at constant pH (4.0) and temperature (30 ^{o}C).

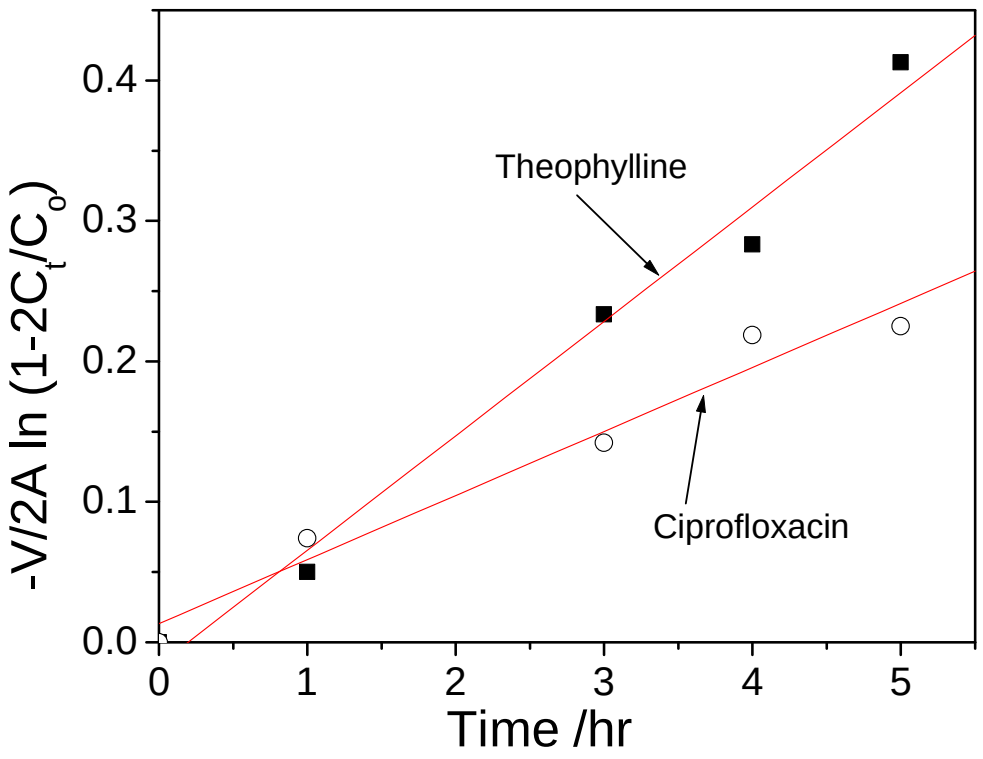

Figure 3.12: Effect of solute size on the permeation of CS-PNIPAm-PAMPS membrane at constant pH (4.0) and temperature (30 ^{o}C).

3.5 Conclusions

In conclusion, we have demonstrated that the combination of Chitosan, PNIPAm and PAMPS gives polyamphoteric hydrogel membranes with good mechanical strength and good handling characteristics. The swelling behaviour of membranes was very much influenced by pH, temperature and ionic strengths of the external medium. The addition of PAMPS to CS-PNIPAm polymer increased the hydrophilicity of the system and the swelling ratios. Furthermore, PAMPS induced a discontinuous swelling transition to the hydrogel membrane which can have potential in stimuli sensitive separations using membranes. Permeability of solutes through these membranes has been investigated at different temperatures. The results showed the dual sensitivity of membranes towards pH and temperature. The formation of polyelectrolyte complex between chitosan and PAMPS showed influence on the lower critical solution temperature of PNIPAm. The permeabilties of solutes through these membranes were strongly dependent on the size of solutes, solution temperature and hydrophilicity of the membranes.

In summary,

1. CS-PNIPAm-PAMPS membranes exhibit polyamphoteric nature having both positive and negative charges with dual sensitivity towards pH and temperature.
2. The addition of PAMPS to CS-PNIPAm enhanced the hydrophilicity of the system and also induced the discontinuous volume transition as a function of temperature.
3. The membrane exhibited higher permeability of theophylline at higher temperature compared to lower temperature. Further, permeability through membrane also increased with an increased in hydrophilicity of membrane. These membranes also exhibited size exclusion phenomenon i.e. when the size of solute increases, rate of permeation decreases.

3.6 References

1. Matsuyama, H.; Tamura, T.; Kitamura, Y. Separation and Purification Technology **1999**, *16*, 181.
2. Zhang, J.; Peppas, N. A. Macromolecules **2000**, *33*, 102.
3. Peppas, N. A.; Wright, S. L. Eur. J. Pharmaceutics and Biopharmaceutics **1998**, *46*, 15.
4. Heskins, M.; Guillet, J. E. J. Macromol. Sci. Chem. A **1968**, *8*, 1441.
5. Lee, W-F.; Yuan, W-Y. J. Appl. Polym. Sci. **2000**, *77*, 1760.
6. Feil, H.; Bae, Y. H.; Feijen, J.; Kim, S. W. Macromolecules **1993**, *26*, 2496.
7. Yoo, M. K.; Sung, Y. K.; Lee, Y. M.; Cho, C. S. Polymer **2000**, *41*, 5713.
8. Kurita, K. in "Desk References of Functional Polymers: Synthesis and Applications" Edited by Arshaday, R. American Chemical Society, Washington **1996**, Chapter 1.15.
9. Mima, S.; Miya, M.; Iwamoto, R.; Yoshikawa, SD. J. Appl. Polym. Sci. **1983**, *28*, 1909.
10. Ge, J.; Cui, Y.; Yan, Y.; Jiang, W. J. Membr. Sci. **2000**, *165*, 75.
11. Modrzejewska, Z.; Korus; I.; Owczarz, P. J. Membr. Sci. **2001**, *181*, 229.
12. Ruckenstein, E.; Xianfang, Z. J. Membr. Sci. **1998**, *142*, 13.
13. Varma, A. J.; Deshpande, S. V.; Kennedy, J. F. Carbohydrate Polymers **2004**, *55*, 77.
14. Wang, M.; Qiang, J.; Fang, Y.; Hu, D.; Cui, Y.; Fu, X. J. Polym. Sci. Part A: Polym. Chem. **2000**, *38*, 474.
15. Wang, M.; Fang, Y.; Hu, D. Reactive & Functional Polymers **2001**, *48*, 215.
16. Lee, W-F.; Chen, Y-J. J. Appl. Polym. Sci. **2001**, *82*, 2487.
17. Kim, S. Y.; Cho, S. M.; Lee, Y. M., Kim, S. J. J. Appl. Polym. Sci. **2000**, *78*, 1381.
18. Guan, Y. L.; Shao, L.; Liu, J.; Yao, K.D. J. Appl. Polym. Sci. **1996**, *62*, 1253.
19. Najjar, A. M. K.; Yunus, W. M. Z. W.; Ahmad, M. B.; Rahman, M. Z. A. J. Appl. Polym. Sci. **2000**, *77*, 2314.

20. Amornchai, W.; Hoven, V. P.; Tangpasuthadol, V. Macromol. Symp. **2004**, *216*, 99.
21. Stoilova, O.; Koseva, N.; Manolova, N.; Rashkov, I. Polym. Bulletin **1999**, *43*, 67.
22. Yazdani-Pedram, M.; Retuert, J. J. Appl. Polym. Sci. **1997**, *63*, 1321.
23. Yazdani-Pedram, M.; Retuert, J.; Quijiada, R. Macromol. Chem. Phys. **2000**, *201*, 923.
24. Pourjavadi, A.; Mahdavinia, G. R.; Zohuriaan-Mehr, M. J.; Omidian, H. J. Appl. Polym. Sci. **2003**, *88*, 2048.
25. Lagos, A.; Reyes, J. J. Polym. Sci. Part A: Polym. Chem. **1988**, *26*, 985.
26. Blair, H. S.; Guthrie, J. Law, T-K.; Turkington, P. J. Appl. Polym. Sci. **1987**, *33*, 641.
27. Yazdani-Pedram, M.; Lagoes, A.; Retuert, J. Polymer Bull. **2002**, *48*, 93.
28. Mahdavinia, G. R.; Pourjavadi, A.; Hosseinzadeh, H.; Zohuriaan, M. J. Eur. Polym. J. **2004**, *40*, 1399.
29. Yilmaz, E.; Caner, H.; Hasipoglu, H.; Yilmaz, O. Eur. Polym. J. **1998**, *34*, 493.
30. Zhang, J.; Yuan, Y.; Shen, J.; Lin, S. Eur. Polym. J. **2003**, *39*, 847.
31. Casimiro, M. H.; Botelho, J. P.; Leal, J. P.; Gil, M. H. Radiation Phy. And Chem. **2005**, *72*, 731.
32. Singh D. K.; Ray, A. R. J. Appl. Polym. Sci. 1994, 53, 1115.
33. Cai, H.; Zhang, Z. P.; Sun, P. C.; He, B. L.; Zhu, X. X. Radiation Phy. And Chem. **2004**
34. Pengfei, L.; Maolin, Z.; Jilan, W. Radiation Phy. And Chem. **2001**, *61* 149.
35. Prashanth, K.V. H.; Tharanathan, R. N. Carbohydrate Polymers **2003**, *54*, 343
36. Rinaudo, M.; Milas, M.; Dung, P. L. International J. Biological Macromolecules **1993**, *15*, 281.
37. Xue, W.; Champ, S.; Huglin, M. B. Polymer **2000**, *41*, 7575.
38. Guilherme, M. R.; Silva, R. da.; Rubira, A. F.; Geuskens, G.; Muniz, E.C. Reactive and Functional Polymers **2004**, *61*, 233.
39. McCormick, C. L.; Elliott, D. L. Macromolecules **1986**, *19*, 542.
40. Schild, H.; G. Prog. Polym. Sci. **1992**, *17*, 163.

41. Tanaka, T. Sci. Am. **1981**, *244*, 110.
42. Velada, J. L.; Liu, Y.; Huglin, M. B. Macromol. Chem. Phys. **1998**, *199*, 1127.
43. Kubota, N.; Matsubara, T.; Eguchi, Y. J. Appl. Polym. Sci. **1998**, *70*, 1027.

CHAPTER 4

Synthesis and Characterization of Hydrophobically Modified Poly(Vinyl Alcohol) Hydrogel Membrane

4.1 Introduction

Poly(vinyl alcohol) [PVA] is obtained from the partial hydrolysis of poly(vinyl acetate). The degree of hydrolysis determines its solubility and phase separation in water. It also dictates the extent of intra/inter H-bonding between the polar hydroxyl groups and water. PVA is highly hydrophilic, non-toxic and biocompatible polymer with excellent film forming property. PVA films have good mechanical strength, low fouling potential and long-term temperature and pH stability. These properties of PVA have led their use in bio-separations. In order to be useful in areas of medical and pharmaceutical applications, PVA must be crosslinked either chemically or physically. PVA membranes have been chemically crosslinked with difunctional glutaraldehyde in the presence of sulfuric acid, acetic acid or methanol.[1,2] But leaching of harmful residues can limit its use in medical or pharmaceutical applications therefore, other methods of chemical crosslinking of PVA have been investigated which include the use of electron beam or gamma irradiation.[3] Heat-treatment or annealing of membranes at elevated temperatures can form crystallites, which serve as physical crosslinks.

It has been reported that the properties of environmentally sensitive PVA membranes can be controlled by external conditions such as pH, temperature etc and hence they have applications in controlled drug delivery, protein separations etc. The pH sensitive PVA membranes were synthesized by making interpenetrating networks of PVA with crosslinked chitosan[4] or polyacrylic acid.[5-7] The temperature sensitive membranes were prepared by graft copolymerization of N-isopropyl acrylamide [NIPAm] onto PVA.[8-12] In PVA-g-polyNIPAm copolymer membranes, PVA provides the mechanical strength to the membranes and the NIPAm determines the temperature dependent swelling properties of the membranes. However, the unannealed membranes of PVA-g-polyNIPAm polymer are very soft and weak and require crosslinking or annealing in order to make them mechanically strong. In the past it has been shown that most of the thermosensitive membranes were based on homopolymer of poly (N-isopropylacrylamide) or in combination with other polymer. [13-16]

In this chapter, we propose to design a thermosensitive membrane based on PVA and N-Tertiary butyl acrylamide [NTBA]. Although the homopolymers of PVA and polyNTBA do not show any LCST behaviour in the observable temperature range, the copolymer at a critical composition show a distinct discontinuous volume transition. N-tertiary butyl acrylamide [NTBA] is a hydrophobic monomer, which upon grafting onto PVA gives interesting properties.

The glass transition temperature and the crystallization of the copolymer membranes were studied using DSC, DMA and XRD. Permeation of different solutes through these membranes was investigated as a function of solute size and hydrophobicity of the membranes.

4.2 Experimental

4.2.1 Materials

PVA was procured from S.D. fine Chemicals Ltd., India. NTBA was purchased from Aldrich Chemicals, USA. Potassium persulfate [KPS] was purchased from Loba chemicals, India. Glutaraldehyde was procured from S.D. fine Chemicals Ltd., India. Theophylline, lysozyme and bovine serum albumin [BSA] were obtained from Aldrich chemicals, USA; while vitamin B_{12} was purchased from S. D. fine chemicals, India. The structures of PVA and NTBA are shown in the **Figure 4.1**.

Molecular weight of PVA was determined by measuring intrinsic viscosity of PVA in dimethyl sulfoxide [DMSO]. Mark-Houwink's equation ($[\eta] = KM_n^{\alpha}$ where, $K = 1.58 \times 10^{-4}$ dlg^{-1}, $\alpha = 0.84$)[17] was used to determine the molecular weight at 30 °C. The viscosity average molecular weight was found to be 60,000 g/mole.

a) Poly (Vinyl Alcohol) [PVA] with 87-89% degree of hydrolysis

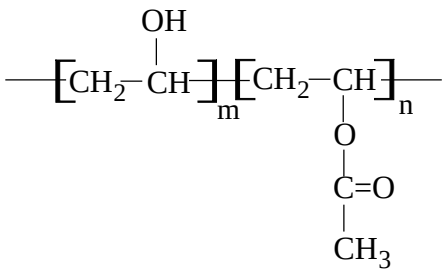

b) N-Tertiary Butyl Acrylamide [NTBA]

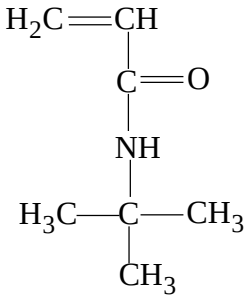

Figure 4.1 Chemical Structures of PVA and NTBA

4.2.2. Synthesis of PVA-g-polyNTBA copolymers

PVA-g-polyNTBA copolymers were synthesized by grafting NTBA onto PVA at 42 °C using potassium persulfate as an initiator. PVA solution was prepared in DMSO and NTBA and initiator were dissolved in the reaction mixture. Nitrogen was purged to remove the dissolved oxygen. The graft polymerization was carried out at 42 °C for 22 hours. Acetone was used to precipitate the graft copolymer after polymerization. The obtained copolymers were washed with acetone to remove unreacted monomers. Series of PVA-g-polyNTBA copolymers were prepared by incorporating varying concentrations of NTBA. The stoichiometry of the reactions is given in **Table 4.1**. The copolymers were abbreviated as PVAN2 to PVAN18 in the text. For example, PVAN2 means Poly(vinyl alcohol)-g-poly(*N*-tertiary butyl acrylamide) with 2 mol % of NTBA.

Table 4.1: The stoichiometry of the reaction [Potassium persulfate (KPS) = 2-wt %]

Sr. No.	Sample Code	PVA mol %	NTBA mol %
1	PVAN2	98	2
2	PVAN3	97	3
3	PVAN4	96	4
4	PVAN7	93	7
5	PVAN12	88	12
6	PVAN18	82	18

4.2.3. Synthesis of poly(N-tertiary butyl acrylamide) homopolymer [polyNTBA]

PolyNTBA homopolymer was synthesized in order to understand the difference in properties of graft copolymer and homopolymer membranes.

KPS (0.1 wt%) initiator was dissolved in NTBA monomer solution in DMSO. Nitrogen was purged to remove the dissolved oxygen. The polymerization was carried out at 42 °C for 22 hours. The white precipitate collected in the solution. Homopolymer of NTBA [poly(NTBA)] obtained was insoluble in DMSO. The precipitated polymer was filtered and re-dissolved in acetone and reprecipitated in water.

4.2.4. Preparation of Membranes

The dried PVA-g-polyNTBA copolymers were dissolved in DMSO. The membranes were made by pouring 20 cm^3 of 4 % (wt/vol) PVA-g-polyNTBA/DMSO solution into a petri dish (4.8 cm diameter), and the solvent was allowed to evaporate at 60 °C for 7 days. The obtained membranes were too soft in water especially, with low content of NTBA. Therefore, the membranes were annealed at different temperatures for different times to increase the mechanical strength of membranes for permeation experiments.

The polyNTBA membrane for DMA analysis were made by pouring 4 % (wt/vol) polymer/acetone solution into flat petri dish and acetone was allowed to evaporate at 30 °C.

The PVA and graft copolymer membranes were annealed by heating dried membranes at high temperature in oven.

4.2.5. Preparation of Chemically Crosslinked PVA Hydrogel Membrane

PVA hydrogel membranes were synthesized by in situ crosslinking of PVA with glutaraldehyde followed by solvent evaporation. (5ml, 4%) PVA aqueous solution was mixed with 1 ml of different concentrations of glutaraldehyde solution and 0.25 ml, 2-wt% H_2SO_4 as a catalyst. The solution was stirred properly and was poured into flat petri dish. The crosslinking of PVA was followed by solvent evaporation at 60 °C. This chemically crosslinked membrane was used to study the swelling behaviour of PVA hydrogel membrane as a function of temperature.

The reaction pathway for crosslinking of PVA using glutaraldehyde in the presence of acid is shown in **Figure 4.2**

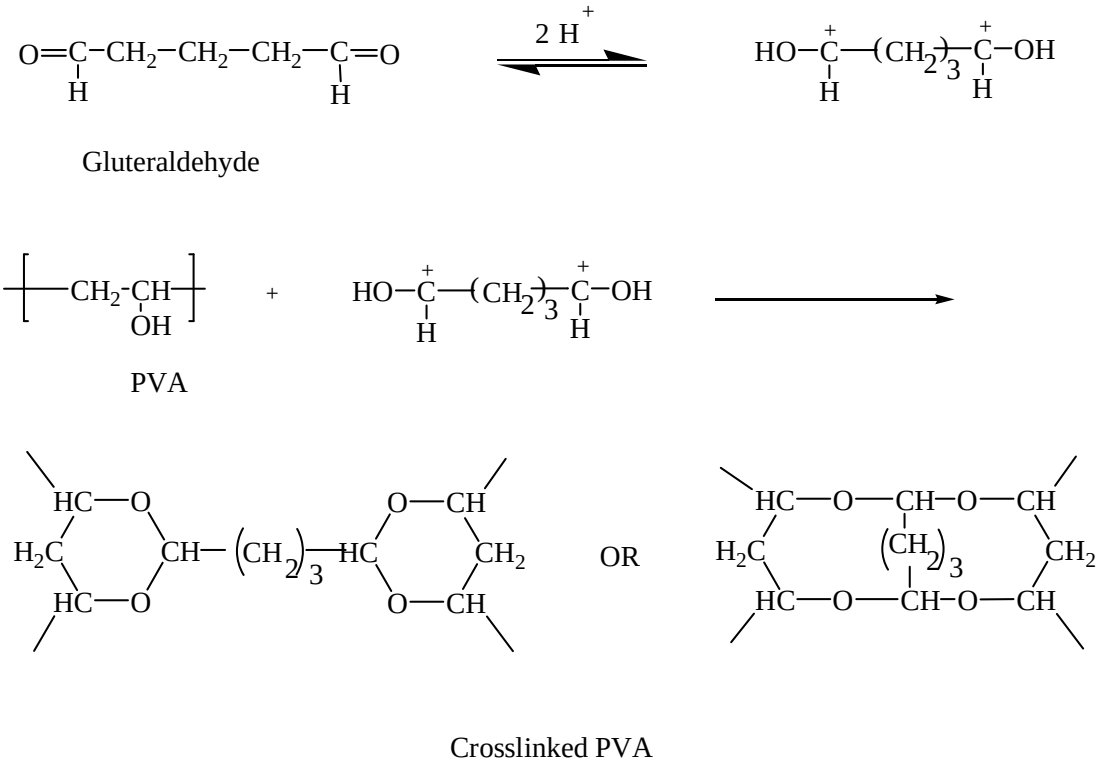

Figure 4.2: Crosslinking of PVA with glutaraldehyde

4.3 Characterization

4.3.1 FT-IR Spectroscopy

For FT-IR analysis, thin films of grafted copolymers were casted by solvent evaporation method by pouring 5 cm^3 of 4 % (wt/vol) PVA-g-polyNTBA/DMSO solution into a flat petri dish (4.8 cm diameter), and evaporating the solvent at 60 °C for 2 days. Fourier transform infrared analysis was carried out using a Shimadzu's FT-IR-8300 spectrometer at resolution of 4 cm^{-1}.

4.3.2 NMR Spectroscopy

The NMR spectra were recorded using Bruker DRX –500 spectrometer operating at a proton and carbon frequency of 500.13 and 125.4 MHz respectively. The samples were made by dissolving PVA and graft copolymers in DMSO-d6 and poly NTBA in Acetone-d6.

4.3.3 Contact angle Measurements

Contact angles of PVA and PVA-g-polyNTBA membranes were measured by using Rame-Hart telescopic goniometer and Gilmont syringe. Contact angle is the angle included between the tangent plane to the surface of the liquid and the tangent plane to the surface of the solid, at any point along their line of contact. The contact angle measurements were carried out by sessile drop method. The drop of deionized water was placed on the membranes by using syringe and the angle was measured by using goniometer.

4.3.4 Swelling Ratio of Membranes

The dried, pre-weighed membranes were kept in water in a constant temperature bath for different temperatures in the range of 10–60 °C for 24 hours and re-weighed after wiping the surface gently. Since the membrane thickness was very small, 24 hours equilibrium time was found to be sufficient.

The swelling ratio (q) of membranes was calculated using the following equation,

$$q = \frac{W_2}{W_1} \qquad (4.1)$$

where, W_2 and W_1 are wet and dry weights of the membrane respectively.

4.3.5 Differential Scanning Calorimetry (DSC)

A Perkin Elmer DSC-2 was used for studying the melting and crystallization behaviour of the polymeric membranes. The temperature and energy scales were calibrated with the standard procedures. The melting studies were performed in the temperature range of 50-240 °C at the heating rate of 10 °C/min in the N_2 atmosphere.

4.3.6 X-ray Diffraction (XRD)

X-ray diffraction studies of polymeric membranes were done with a Rigaku D_{max} 2500 X-ray diffractometer with Cu K_α radiation (wavelength = 0.1514 nm)

4.3.7 Dynamic Mechanical Analysis (DMA)

The dynamic mechanical properties of the samples were studied with a Rheometrics DMTA IIIE dynamic mechanical analyzer. The samples were analyzed in the tensile mode. The temperature sweep was carried out from 30 to 180 °C and the sample was heated at the rate of 5 °C/min. The frequency was 10 rad/s and the strain was 0.1%.

4.3.8 Permeation studies

Permeation experiments were carried out using a two-chamber (donor and receptor) diffusion cell with a chamber volume of 70 cm^3. Pre-conditioned membranes were mounted between two halves of the donor and receptor cell, which were further clamped together and sealed tightly with the rubber packing. The effective membrane area in the cell was 1.76 cm^2. The solution was at the donor side of the cell and the receptor was having only the buffer. A fixed volume (1.0 ml) of the sample was taken out at various time intervals from the receptor cell and the solute concentration was measured using an UV spectrophotometer at appropriate wavelengths. After taking out samples from the receptor cell each time, the same amount of fresh buffer solution was

added to the receptor cell to maintain the constant volume at the receptor cell. The solutes chosen for the permeation studies were, theophylline (MW = 180), vitamin B_{12} (MW = 1355), lysozyme (MW = 14,600) and bovine serum albumin [BSA] (MW = 66,000). The concentrations of these solutes were determined by UV spectrophotometer at wavelengths of 271 nm for theophylline, 280 nm for lysozyme and BSA, 361nm for vitamin B_{12}. Membranes, which were annealed at 120 °C for 6 hours, were chosen for the permeation studies.

4.4 Results and Discussion

4.4.1 Synthesis of Graft Copolymers

Graft copolymerizations of vinyl monomers onto PVA have been done by γ-irradiation,[18] or using redox initiators such as ceric ammonium nitrate [CAN],[19,20] potassium persulfate [KPS].[21] KPS is a widely used initiator for polymerization in aqueous medium. It generates sulfate ion radicals by its thermal or photochemical decomposition. The mechanism of free radical grafting is shown in **Figure 4.3**. Persulfate ion induces a radical on the PVA backbone chain and then the vinyl monomer, NTBA polymerizes on to PVA. The persulfate ion is a strong oxidizing agent and it is possible that it can oxidize some of the generated radicals (secondary alcohol) into carbonyl groups. However, KPS has been well established for initiating graft copolymerization onto PVA. In our work, we have used KPS as a redox initiator to graft copolymerises NTBA onto PVA using DMSO as a solvent medium. KPS readily decomposes in the DMSO medium as compared to the aqueous medium. The reaction was carried out at 42 °C for 22 hours. In the reaction mechanism, we propose that the termination of the grafting pendant chain in the graft copolymerisation occurs via disproportionation, which does not lead to inter-chain crosslinking. This is very well evidenced by the solubility of the obtained graft copolymers.

Initiation

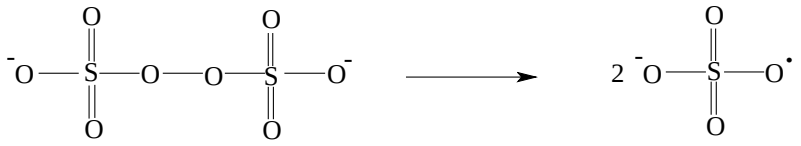

Propogation

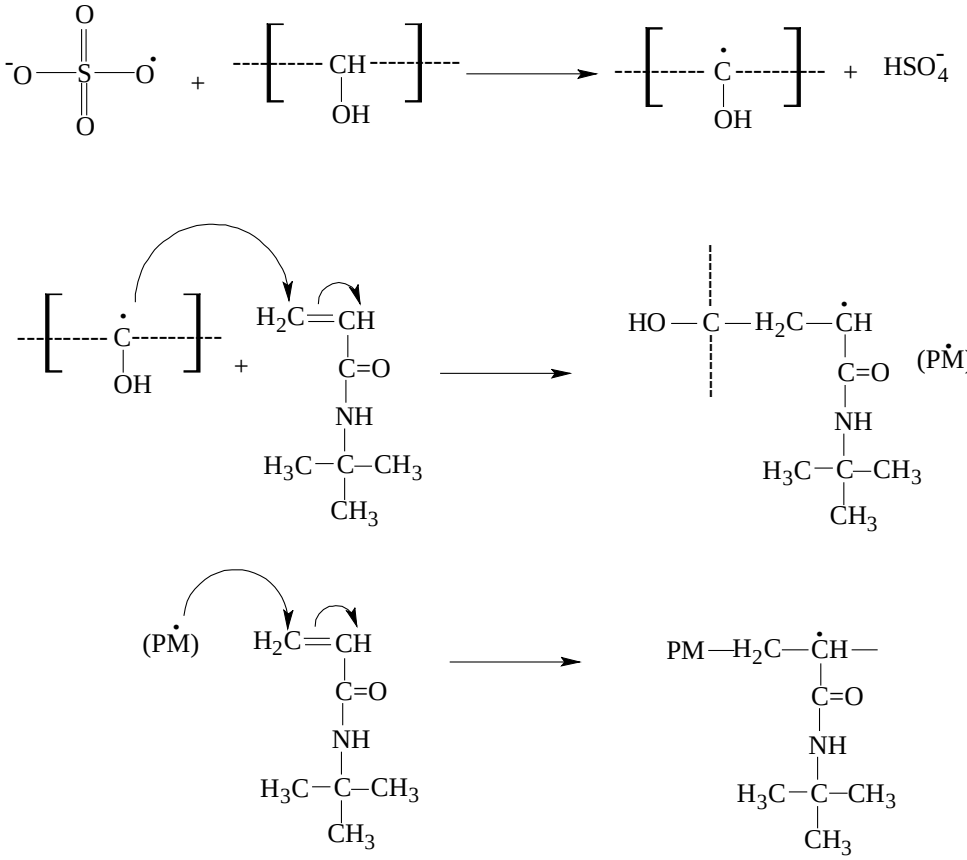

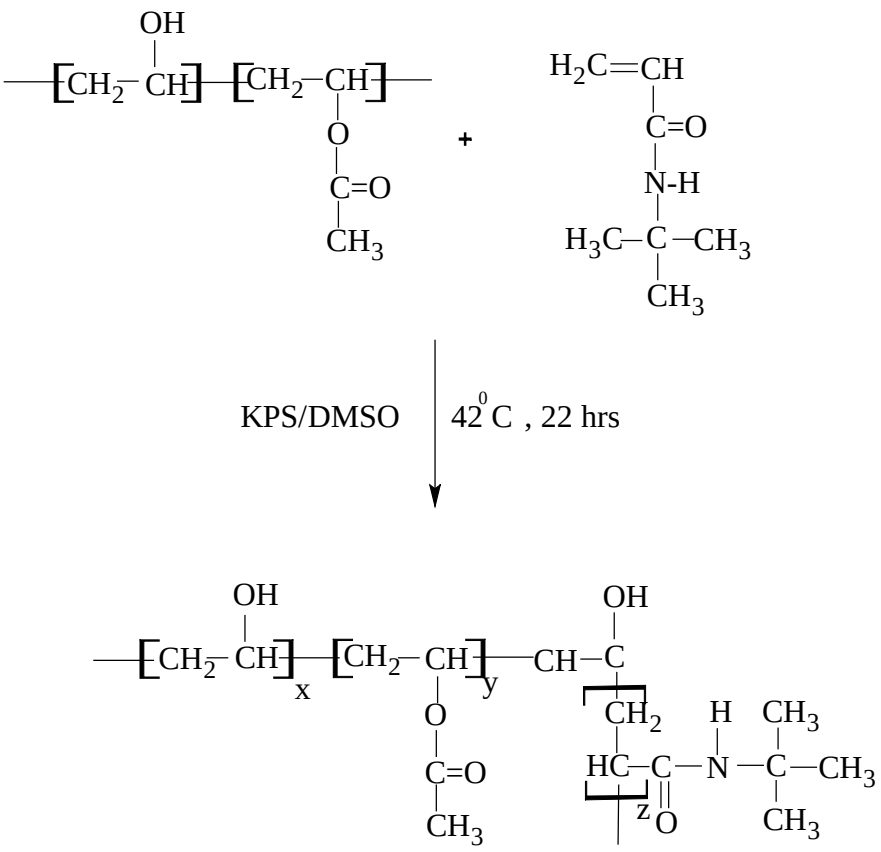

Figure 4.3: Reaction mechanism of grafting of NTBA onto PVA by using KPS as an initiator. (degree of hydrolysis of PVA = 87-89%)

Elemental analysis, FT-IR spectra and contact angle measurements confirmed and supported the fact that by increasing the amount of NTBA in the reaction mixture, the amount of incorporated NTBA in the graft copolymers increases. Elemental analysis results (**Table 4.2**) showed the increased percentage of nitrogen in graft copolymer membranes with increase in NTBA concentration in the reaction mixture. However, there is a difference in the theoretical and experimental values which can be attributed to the reduction in the diffusion of bulky NTBA monomer towards the reactive site of polymer chains.

Table 4.2: Percentage of Nitrogen content in PVA-g-polyNTBA polymer films by elemental analysis

Polymer Film	Nitrogen content (%)	
	Theoretical	Experimental
PVAN2	0.52	0.40
PVAN3	0.76	0.57
PVAN4	1.00	0.67
PVAN7	1.84	1.17
PVAN12	3.15	1.67
PVAN17	4.14	1.95

4.4.2 FT-IR spectra

We show in **Figure 4.4**, the FT-IR spectra of PVA and PVA-g-polyNTBA copolymer membranes. The PVA spectrum show characteristic broad band at 3340 cm^{-1} corresponding to the O-H stretching vibration of the hydroxyl group of the PVA. The sharp band at 1735 cm^{-1} corresponds to the C=O stretching of the acetate group of PVA. The backbone aliphatic C-H stretching vibrations give sharp bands at 2940 cm^{-1} and 2910 cm^{-1}. The PVA-g-polyNTBA membranes show a distinct new band at 1654 cm^{-1} which can be attributed to the C=O stretching of the amide groups of NTBA. The

N-H stretching vibrations of the amide group can not be distinguished since they overlap with the O-H stretching vibrations. However, the N-H bending can be seen at 1510 cm^{-1}. Since the number of acetate groups in our PVA remains same and not affected by the grafting reaction, the ratio of the intensities of the amide C=O to ester C=O can be used qualitatively to know the extent of incorporation of polyNTBA in the polymer. We show in **Table 4.3**, this ratio as a function of increase in NTBA content. It can be readily seen that, the ratio increases with respect to increase in the NTBA content in the graft copolymer, which clearly indicates the increase in the percentage of the grafting. **Figure 4.5** shows the absence of amide carbonyl stretching at 1654cm^{-1} in PVA while these increased in intensity of amide carbonyl stretching with increase in NTBA content in graft copolymer membranes.

Table 4.3: The ratio of intensities of carbonyl (C=O) peaks of $-OCOCH_3$ and -CONH groups of PVA and PVA-g-polyNTBA polymer films.

Polymer Film	Intensity Ratio I_{1654}/I_{1735}
PVA	0
PVAN2	0.245
PVAN3	0.292
PVAN4	0.376
PVAN7	0.541
PVAN12	0.756
PVAN18	1.084

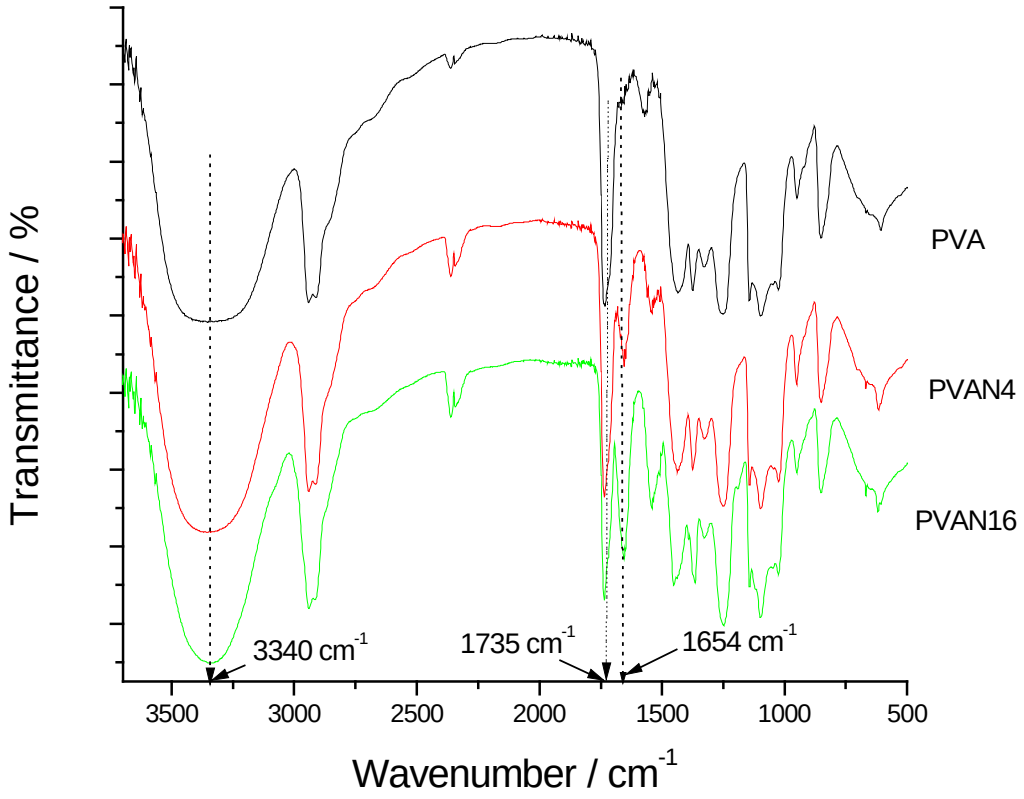

Figure 4.4: FTIR spectra of PVA, PVAN4 and PVAN12 films in the range of 3700-500 cm^{-1}.

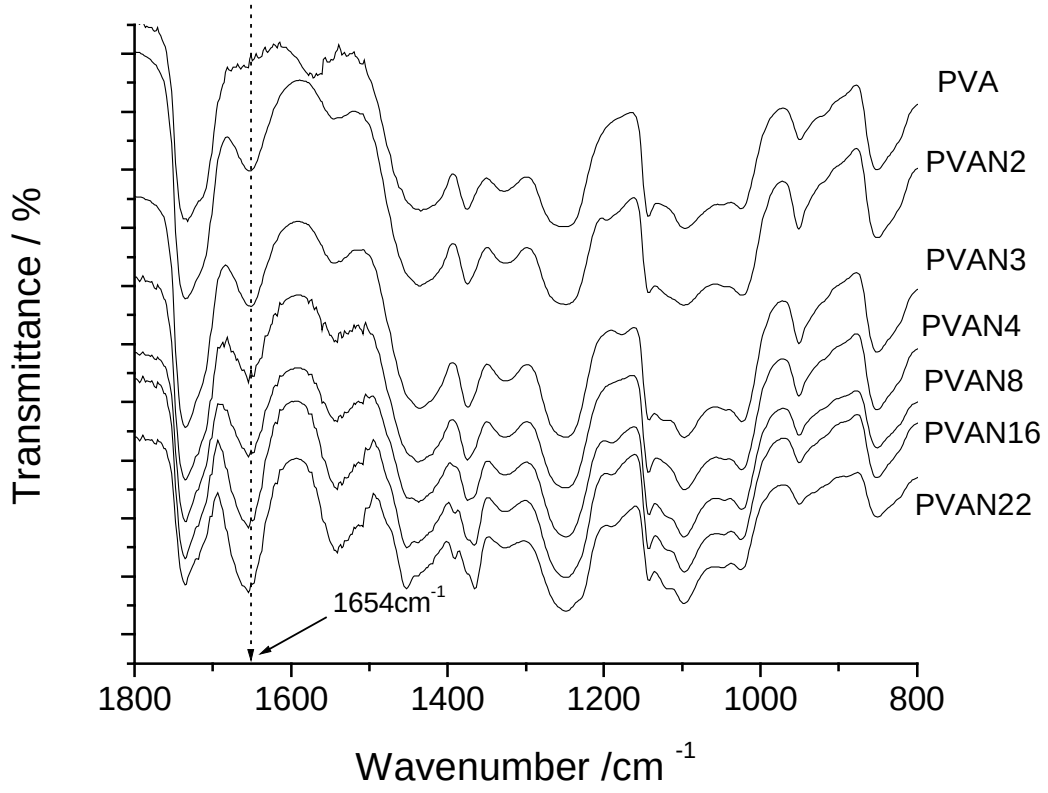

Figure 4.5: FTIR spectra of PVA and PVA-g-polyNTBA films in the range of 1800-800 cm^{-1}.

4.4.3 Contact Angle Measurements

Hydrophilicity or wettability of the membranes can be determined by contact angle (θ) between the membrane and water. When surface is more hydrophilic it can be more easily wetted by water resulting into smaller contact angles. The results are summarized in **Table 4.4**. It can be readily seen that, as the NTBA content in the membrane increases the hydrophobicity increases and the contact angle increases. This clearly indicates the increase in overall hydrophobicity of the membranes with the enhanced grafting of hydrophobic NTBA onto PVA.

Table 4.4: Contact angle (θ) of PVA and PVA-g-polyNTBA polymer films.

Polymer Film	Contact Angle (θ, degree)
PVA	28
PVAN2	54
PVAN3	60
PVAN4	64
PVAN7	70
PVAN12	73
PVAN18	74

4.4.4 ^{1}H and ^{13}C NMR spectroscopy

We show in **Figure 4.6(A)**, the ^{1}H spectrum of PVA in DMSO. It can be seen from the ^{1}H NMR spectrum of PVA that, methylene protons of the backbone appear at 1.3-1.5 ppm and the methine protons attached to –OH and $–OCOCH_3$ appear at 3.8 and 3.9 ppm, respectively. The $–CH_3$ protons of the acetate group give a characteristic peak at 1.95 ppm. The hydroxyl proton (-OH) of the PVA are separated into triads at

4.25/4.49/4.68 ppm due to the hydrogen bonding between –OH groups of the polymer and DMSO.

We show in **Figure 4.6(B)** the ^{1}H spectrum of PVA-g-polyNTBA taken in DMSO. All the peaks, which appeared in the PVA, were also present in the PVA-g-polyNTBA polymer with a very little change in the chemical shift values. However, an extra peak at 1.2 ppm appears which corresponds to methyl protons of tert-butyl groups. This clearly confirms the grafting of NTBA onto PVA.

The ^{13}C spectra of PVA and PVA-g-polyNTBA are shown in **Figure 4.7(A)** and **4.7(B),** respectively, which give the characteristic chemical shifts of carbon in the polymer. In the PVA spectrum, the methyl carbons of the acetate group give peak at 21 ppm and methylene carbons of the polymer backbone appeared at 45 ppm. The backbone methine carbons attached to –OH and $–OCOCH_3$ groups give peaks at 65 ppm and 79.3 ppm respectively. The carbonyl carbon of the acetate groups shows peak at 170.3 ppm. Besides these peaks, the PVA-g-polyNTBA [**Figure4.7(B)**] gives peaks at 28.7 ppm and 50.3 ppm corresponding to methyl carbon and tertiary carbon of the tertiary butyl group of the polymer respectively. This confirms unequivocally the grafting of NTBA onto PVA.

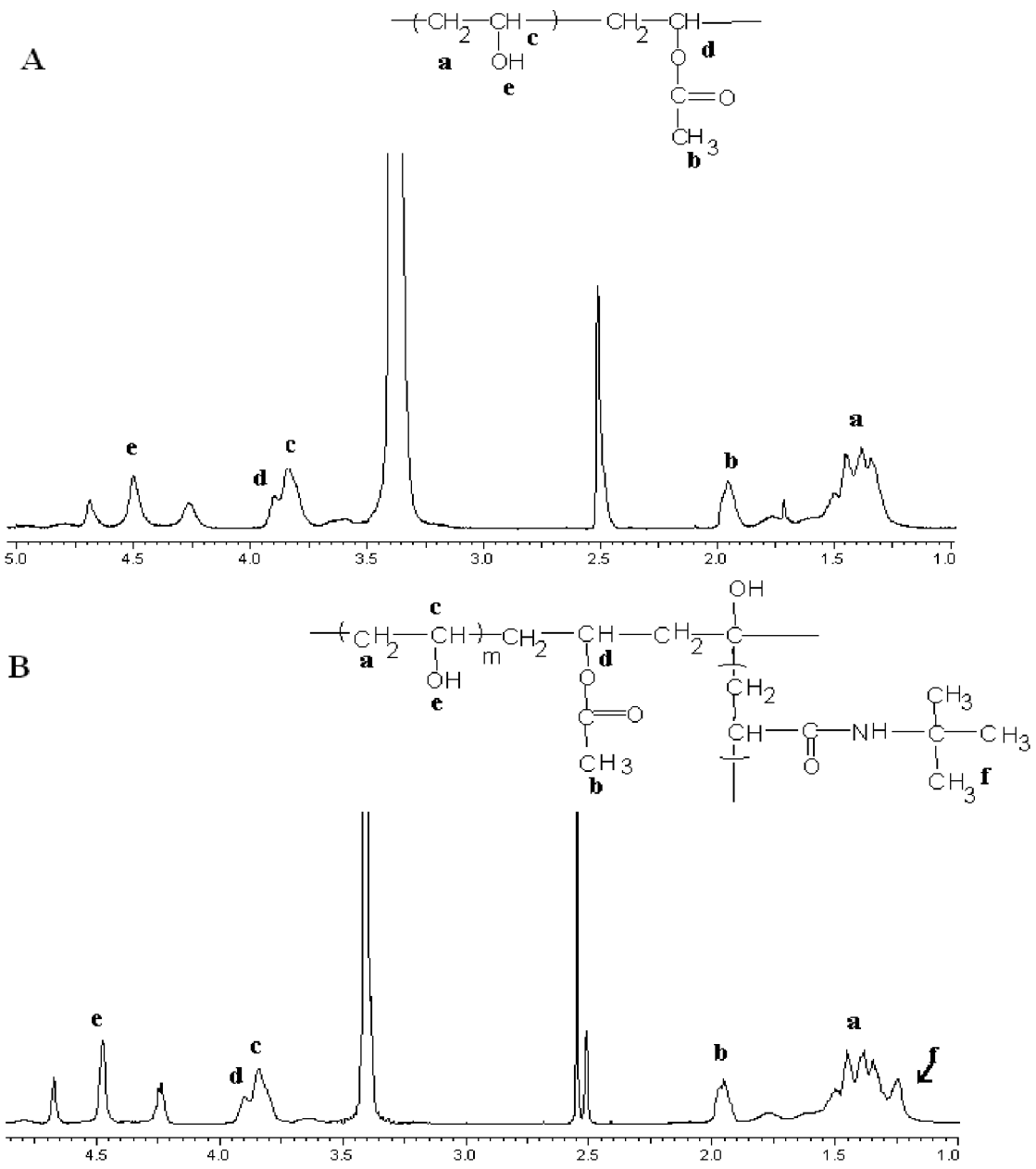

Figure 4.6: ^{1}H NMR spectra of (A) PVA ; (B) PVA-g-polyNTBA copolymer in DMSO.

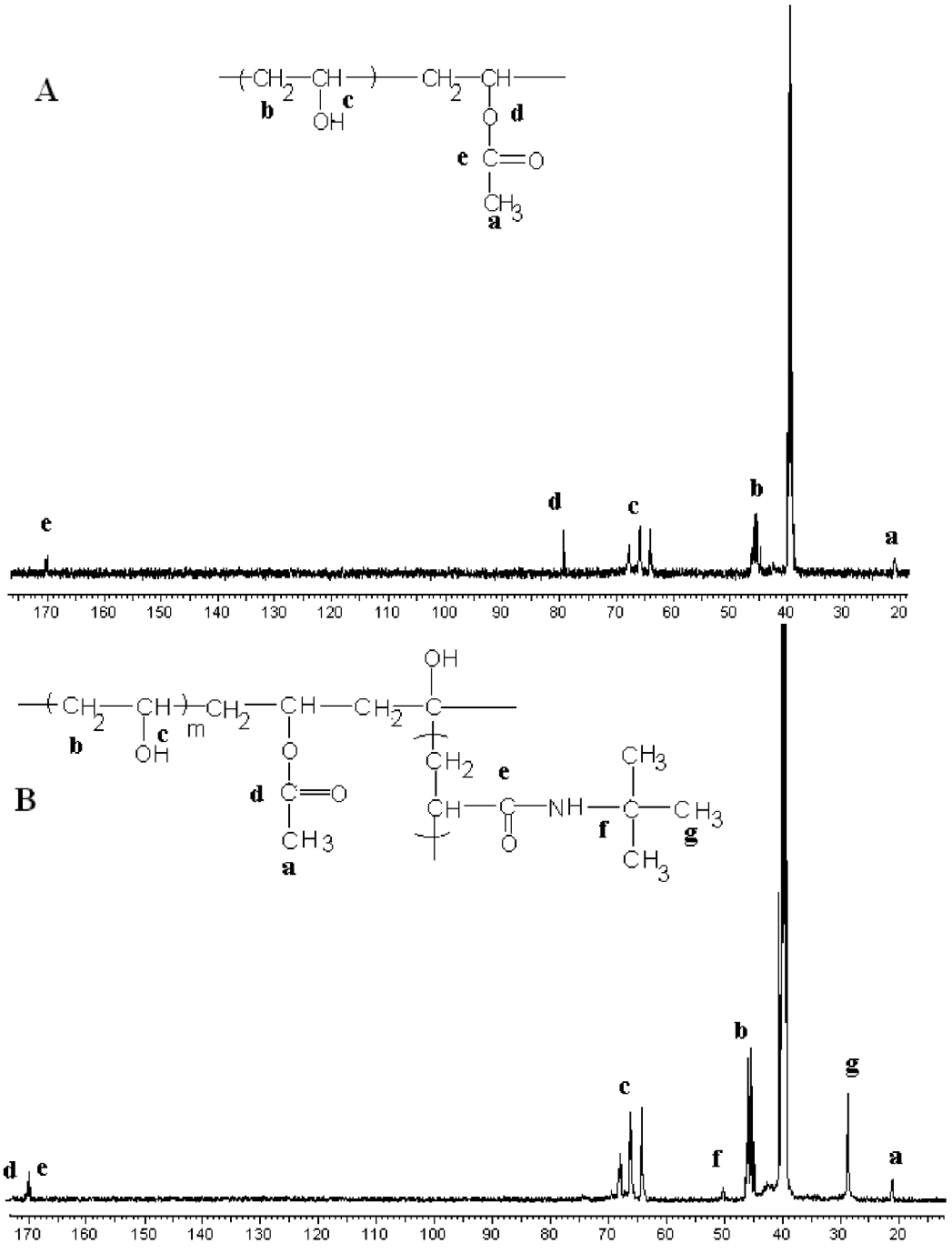

Figure 4.7: ^{13}C NMR spectra of (A) PVA ; (B) PVA-g-polyNTBA copolymer in DMSO

4.4.5 Swelling Ratios of the Membranes

All the PVA-g-polyNTBA copolymer membranes used for swelling studies were annealed at 120 °C for six hours. The annealing treatment gives good mechanical strength to the membranes. In order to ensure the same history, similar preconditioning parameters were used for all the membranes.

We show in the **Figure 4.8**, the temperature dependent (10-60 °C) swelling ratios (q) of copolymer membranes in water with different contents of NTBA in the membranes. Over a temperature range of 10-60 °C, it can be readily seen from the figure that, membranes with low NTBA (PVAN3, PVAN4) content show higher swelling ratios in the temperature range of 10-30 °C and undergo discontinuous swelling-collapse transition between 30 and 40 °C. It is intriguing at once that, although the homopolymer of PVA hydrogel membrane prepared by chemical crosslinking of PVA with glutaraldehyde showed a increase in the swelling ratio with respect to temperature as shown in **Figure 4.9**, the incorporation of small amount of NTBA resulted into a discontinuous swelling transition and showed decrease in swelling ratios. This can be attributed to the increased hydrophobicity of the membrane due to the presence of NTBA. This property of discontinuous transition with respect to temperature will be very useful in the controlled release of active ingredients from the PVA membranes. The discontinuous transition mainly arises due to two factors, namely, H-bonding interactions and hydrophobic interactions. The higher swelling ratios of the membranes with low concentrations of NTBA at low temperature can be attributed to the strong H-bonding interactions between the polymer and water. It is well established that the hydroxyl groups of PVA form strong H-bonding with water thus enhancing the hydrophilicity of the system. However, upon increasing the temperature, the H-bonding between polymer and water breaks and the inter/intramolecular hydrophobic associations dominate resulting in the collapse of polymer chains which gives rise to low swelling ratios.

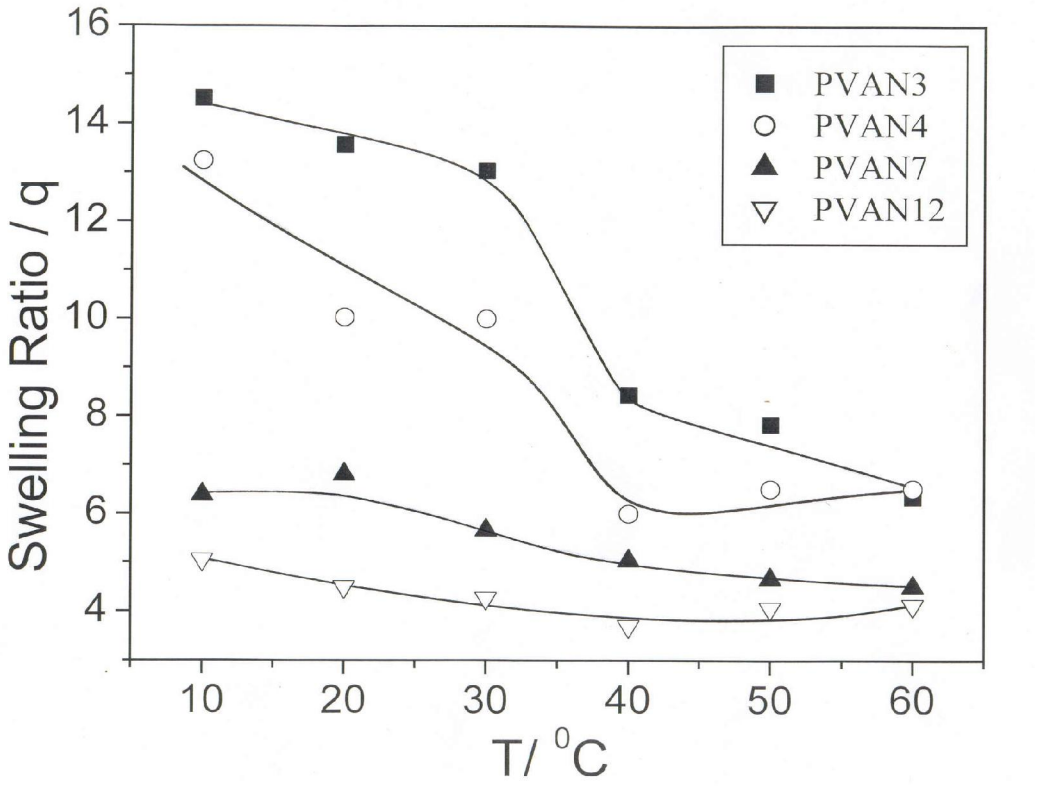

Figure 4.8: Temperature dependent swelling ratios of PVA-g-polyNTBA copolymer membranes with different concentrations of NTBA.

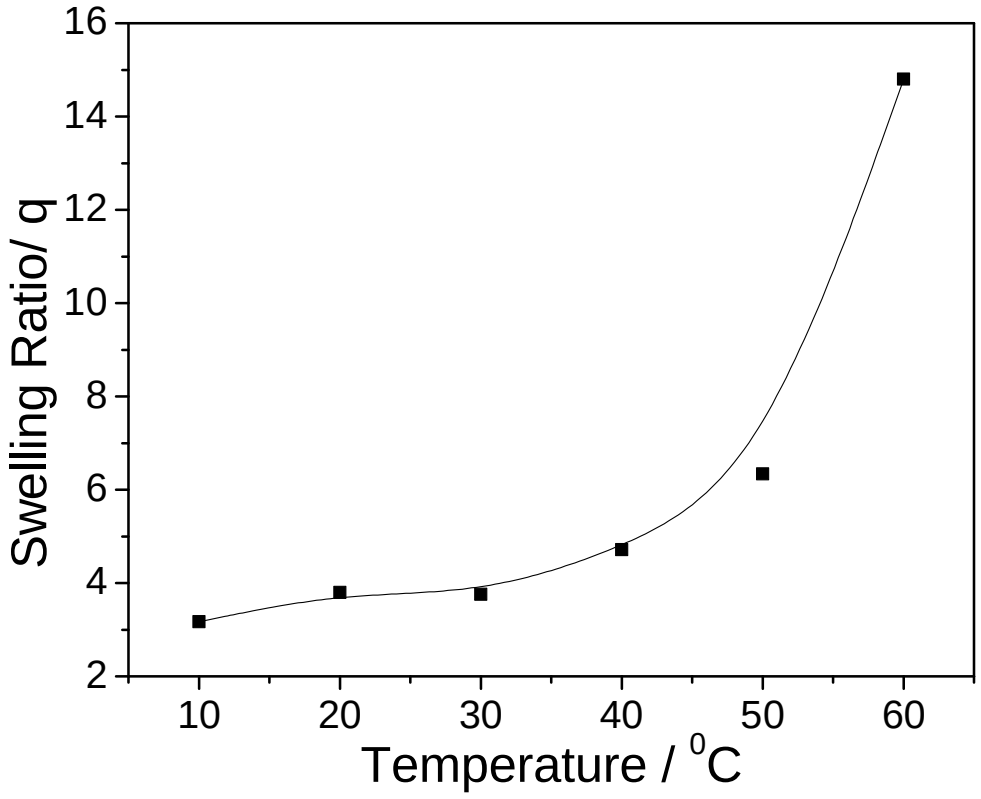

Figure 4.9: Effect of temperature on the swelling of chemically crosslinked PVA hydrogel membrane, Glutaraldehyde = 0.1%

At high NTBA content, the hydrophobicity of the membrane increases strongly and there is a formation of inter/intra molecular association via the hydrophobic groups. The tendency of hydrophobic groups to cluster can lead to three-dimensional network which can be viewed as pseudo-crosslinks. Therefore, the formation of crosslinks reduces swelling ratios in water significantly. One can see from the figure that at very high concentration of NTBA, the swelling ratios are very low and almost become temperature independent. It is also interesting to note that, these membranes are completely transparent in the dry and swollen state in spite of the large quantities of hydrophobic NTBA content.

4.4.6 Thermal Analysis of membranes

The melting transition temperature and the heat of fusion determined from DSC for the homopolymer and graft copolymer samples are presented in **Table 4.5**. As can be seen from the table, the melting transition temperature, T_m, of graft copolymers are lower than that of virgin polymer, PVA. Thus, melting transition temperature of PVA decreases as a result of grafting of NTBA, however, it seems that it does not depend on the percentage of grafting of NTBA. The decrease in T_m with addition of NTBA indicates that incorporation of pendent polyNTBA chains hinders the crystallization process and results in crystallites with lower thermal stability.

It is also observed that the samples with lower NTBA content (3 mol % and 4 mol %) show recrystallization during heating. The recrystallization observed above T_g implies that, the segmental motions of the chain favour the crystallization. This crystallization of the solid observed on heating above T_g leads to crystallites with lower thermal stability. The values of heat of fusion however, do not show any trend as such with respect to % of grafting.

Table 4.5: Melting parameters of PVA and PVA-g-polyNTBA polymer films as determined by DSC.

Polymer Films	T_m /°C	Δ H, cal/g
PVA	189.74	5.51
PVAN3	183.59	5.64
PVAN4	188.15	5.37
PVAN7	172.35	5.64
PVAN12	182.53	5.79
PVAN18	182.80	4.77

4.4.7 Dynamic Mechanical Analysis (DMA)

The dynamic mechanical analysis of the membranes was carried out to find out the variation of the tan delta peak (glass transition temperature at experimental frequency of 10 rads/sec). tan delta (δ) is known as loss tangent or damping factor which corresponds to the ratio of loss modulus (energy dissipated per cycle) to the storage modulus (maximum potential energy stored during the cycle) ($E^{||}/E^{|}$). This is one of the important parameters and seen to increase during transitions between different deformational mechanisms. Storage modulus ($E^{|}$) corresponds to the elastic response to the deformation and in this study, $E^{|}$ confirmed the increase in crystallinity in annealed membranes.

Figure 4.10 shows the tan delta peaks for the PVA and graft copolymer membranes with different contents of NTBA. The tan delta peak for pure PVA is observed at 73 °C where as for polyNTBA membrane, it is observed at about 169 °C. It is also observed that the tan δ peak temperature is lower than that of PVA for the lower NTBA content i.e. for 2 mol % and 3 mol % of NTBA. However, an increase in

NTBA content results in an increase in the tan delta peak temperature and the peak also becomes broader as compared to PVA. The broadening of the tan delta peak and the shift of the peak may be ascribed to the random distribution of polyNTBA chains on the PVA membrane. The broad peak could be due to super positioning of two transitions each corresponding to the PVA and polyNTBA.

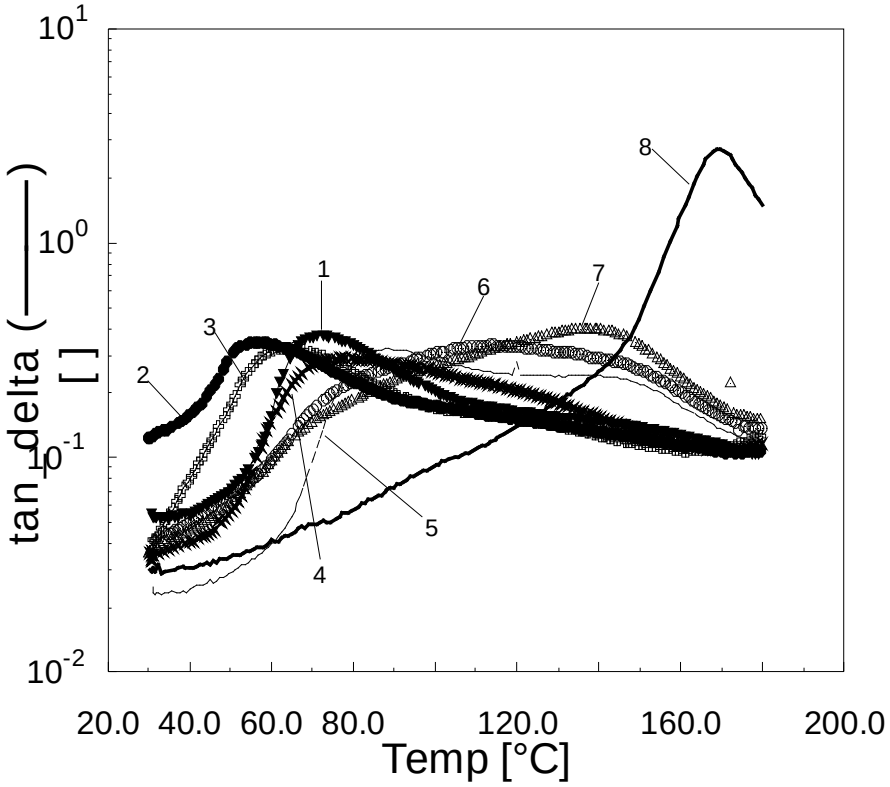

Figure 4.10: tan delta peaks for membranes of pure polymers and graft copolymers with different content of NTBA. PVA(1), PVAN2(2), PVAN3(3), PVAN4(4), PVAN7(5), PVAN12(6), PVAN18(7), polyNTBA(8).

4.4.8 Annealing of PVA-g-polyNTBA membranes

It is known that PVA membranes become insoluble upon annealing. The mechanical properties, degree of crystallinity and the permeability of PVA membranes strongly depend upon the temperature and the time of annealing. Extensive heat treatment at temperatures above 180 °C induces chemical changes such as unsaturation, chain scission and crosslinking.[22] The atactic PVA is usually 20-35% crystalline[23] and upon annealing above T_g, its crystallinity can increase upto 55%,[24-26] especially in the presence of diluents such as water, ethylene glycol etc.

The similarities in transport properties of two PVA membranes, one radiation crosslinked and the other annealed at 120 °C have suggested a similar structural characterization.[27] The properties of PVA hydrogel membranes thus, strongly depend on the annealing conditions.

We show in **Figure 4.11**, the swelling ratio of PVAN4 membrane which is annealed at different temperatures for 6 hours. The temperature and the time of equilibrium swelling measurements were kept constant at 20 °C and 24 h respectively. It can be seen from the figure that, membranes annealed at temperatures below 120 °C exhibited almost the same swelling ratios suggesting no significant change in the structure. However, annealing above 120 °C decreased the swelling ratio drastically indicating increased crystallinity in the membranes. The crystalline regions act as giant crosslinking points and decrease the swelling ratios significantly. The crystalline regions are impermeable to penetrating molecules. It becomes apparent that, the bulky tert-butyl groups hinder the crystallizability at lower temperature but upon increasing the annealing temperature to more than 140 °C, the chain mobility increases and facilitates the crystallization. It can be seen from the figure that, the swelling ratio of a membrane annealed at 170 °C decreased from 11.4 to 2.2.

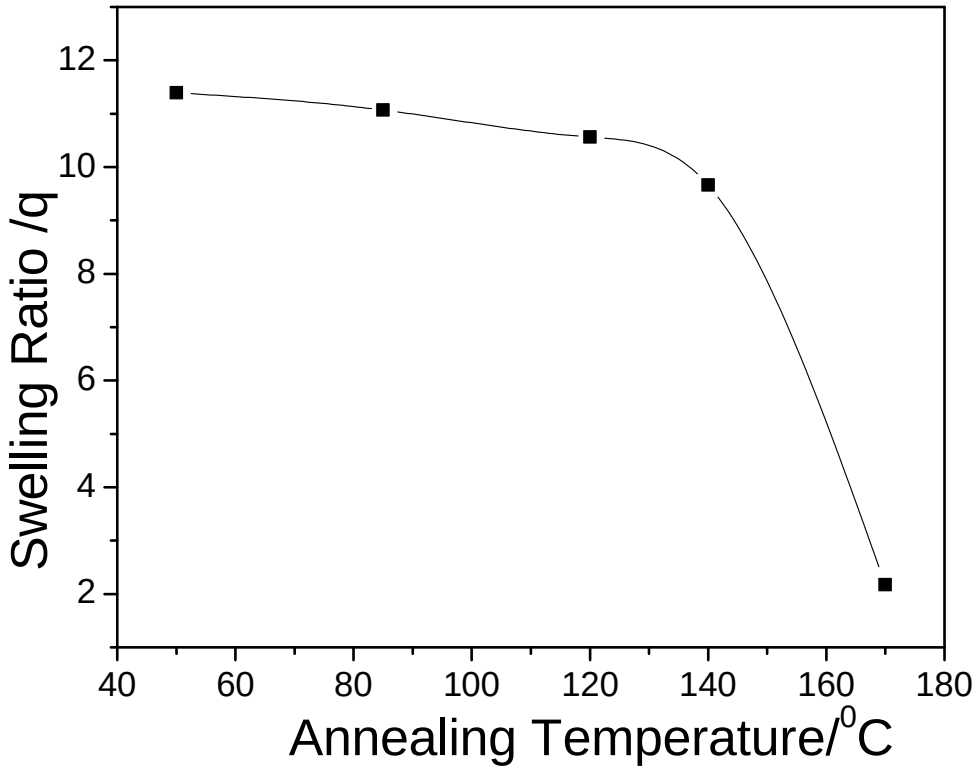

Figure 4.11: Effect of annealing temperatures at constant period of 6 hours on the swelling ratios of PVAN4 membrane at 20 °C.

We show in **Figure 4.12**, the swelling ratios of PVAN4 membrane annealed at 170 °C for different time intervals. It can be seen that, the annealing effects are more predominant after an annealing time of 1 hour. The swelling ratio decreases drastically after 1 hour annealing. The swelling studies of these annealed membranes showed lower swelling ratios as compared to the virgin samples. This observation can be attributed to the increased crystallinity of annealed samples. The crystalline zones act like crosslink points which decrease the swelling ratio.

The thermal analysis of the annealed samples show increase in the heat of fusion indicating increased crystallinity. The degree of crystallinity for PVA membrane was determined by comparison of heat of fusion of polymer (ΔH_f) with the heat of fusion of the 100% crystalline polymer (ΔH_c) as

$$\text{Degree of crystallinity } X = \frac{\Delta H_f}{\Delta H_C} \qquad (4.2)$$

Where, the reported value of heat of fusion (ΔH_c) of 100 % crystalline PVA is 1.05 kcal/mol[24] and the % of crystallinity was found to increase from 23 to 41 % as a result of annealing. It was also found that the crystalline region retained in the swollen state. The swollen annealed PVA membrane showed 16% crystallinity as obtained from DSC. PVA membrane dissolved in water but after annealing of the membrane at 170 ºC for 3 hours, it showed 2.4 swelling ratio at 30 ºC and 16% crystallinity. This increase in crystallinity as a result of annealing prevents the solubility of PVA membrane in water.

Similar increase in the heat of fusion was observed for graft copolymers also. The value of heat of fusion (ΔH_f) for PVAN4 membrane increases from 4-6 to 10 cal/gram when annealed from 1 min to 3 hrs at 170 °C and this clearly suggests that the annealing results in increased crystallinity. XRD results also support the results of thermal analysis.

We have also performed XRD studies on the membranes annealed for different times and the results are discussed in the foregoing. XRD of neat PVA sample exhibit peaks at 19.8° and 24.5° corresponding to 101 and 200 planes.[28] In the graft copolymer these

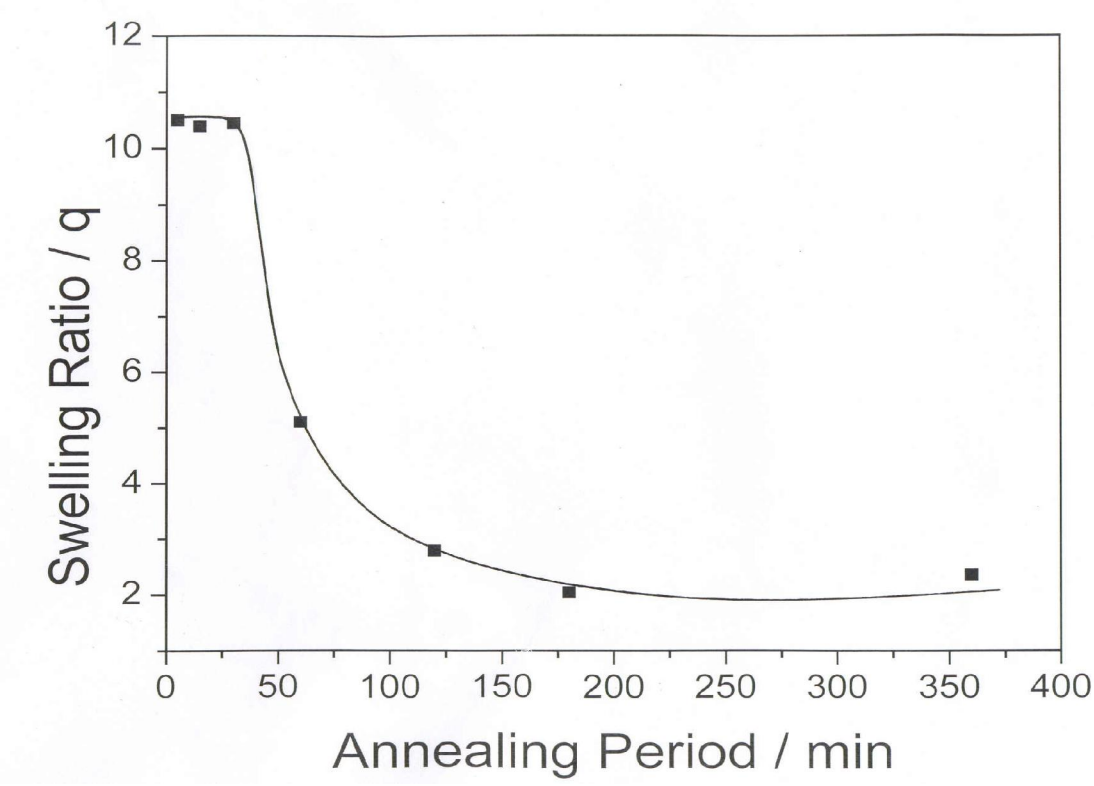

Figure 4.12: Influence of the annealing period at constant temperature of 170 °C on the swelling ratios of PVAN4 membrane at 20 °C.

two peaks are observed at the same 2θ values. However, when the graft copolymer membrane was annealed, the XRD pattern changes as shown in **Figure 4.13**.

Table 4.6 shows the XRD data of the samples annealed at 170 °C for different times. It is observed that the samples exhibit two peaks at 19.8° (corresponding to 101 plane) and at 24.5° (corresponding to 200 plane). It is interesting to note that with increase in annealing time the relative ratio of intensities of these two peaks changes. The peak at 24.5° becomes predominant than that at 19.8°. This observation may be ascribed to the increase in crystalline order of PVA in PVA-g-polyNTBA membranes. This result is in accordance with the DSC results discussed earlier.

The DMA results of annealed PVA membrane are shown in **Figure 4.14**. It can be seen that the annealed sample exhibits higher storage modulus than that of the virgin membrane over the entire temperature range. This increase in the modulus can be attributed to the increased crystallinity of the membrane as a result of annealing.

Table 4.6: XRD of PVAN4 membrane annealed at 170 °C for different periods.

Annealing period, min	2θ	d -value	Intensity	I/I_0
1	19.8	4.4802	3046	100
	24.45	3.6377	1594	52
	30.55	2.9238	738	24
	31.65	2.8246	978	32
	37.00	2.4276	814	27
30	19.50	4.5485	4585	74
	24.15	3.6822	6230	100
	30.45	2.9332	931	15
	31.45	2.8422	1153	19
	36.65	2.4500	4300	69
180	19.70	4.5027	3908	21
	24.50	3.6304	18417	100
	37.00	2.4276	12309	67

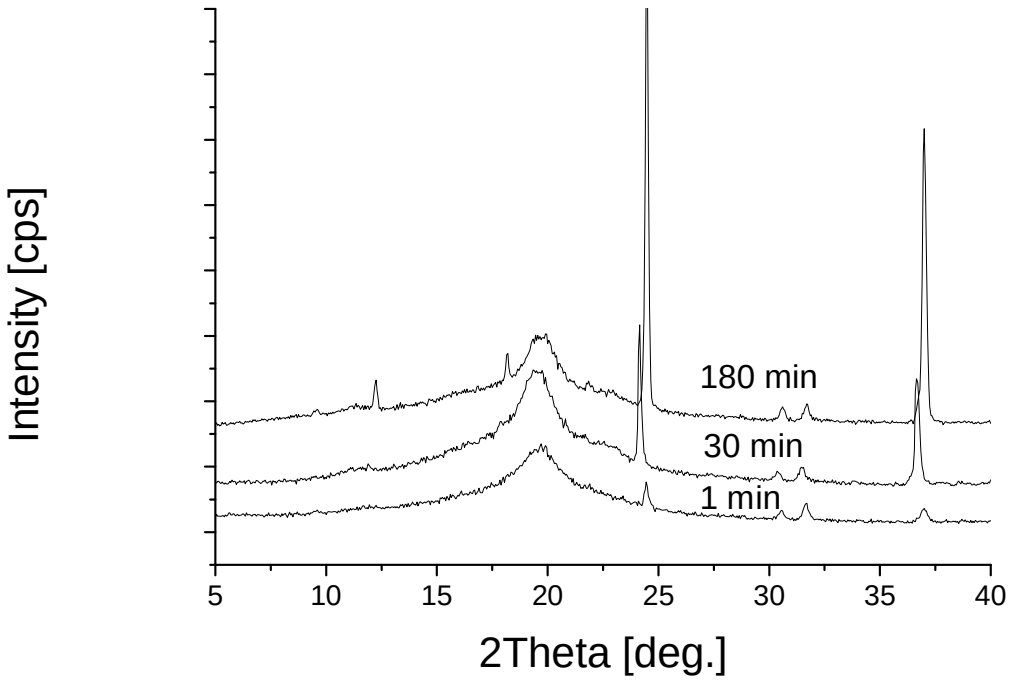

Figure 4.13: X-Ray Diffractograms of the PVAN4 membrane annealed at 170 °C for different periods.

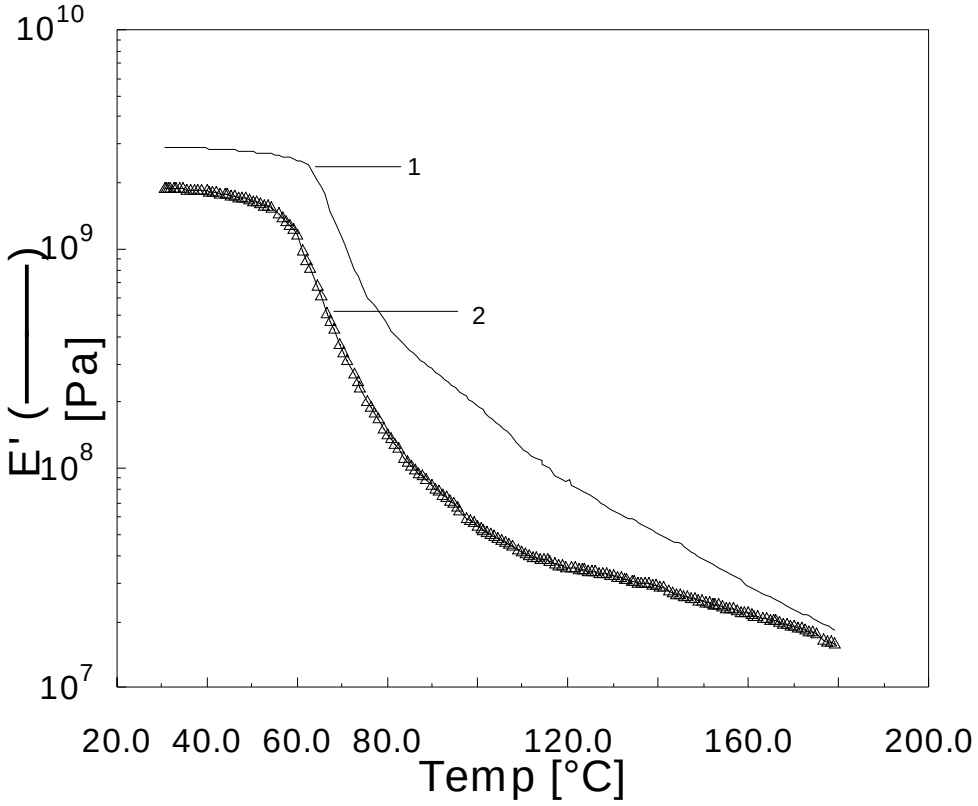

Figure 4.14: Effect of annealing at 170 °C for 3 hours on the storage modulus (E$^{|}$) of annealed PVA membrane(1) and virgin PVA membrane(2).

4.4.9 Permeation studies

The permeation of solutes through hydrogel membranes depends on properties such as hydrophilic-hydrophobic balance, degree of crosslinking and effective mesh-size, nature of functional groups and charges on the membrane. As per the Fick's law of diffusion, the permeability of the solute can be given by the equation,

$$\frac{\mathrm{P}}{\delta} = \frac{-V}{2At} \ln \frac{\Delta C_t}{C_0} \tag{4.3}$$

Where,

C_t = Solute concentration in the receptor cell (mg/ml)

C_0 = Initial solute concentration in the donor cell (mg/ml)

V = Volume of each half cell (ml)

A = Effective permeation area (cm^2)

P = Permeability coefficient (cm/s)

t = Time (h or s)

δ = Thickness of the membrane (mm)

The above equation can be rewritten as,

$$\ln(1-2\frac{C_t}{C_0}) = \frac{-2A}{V} Pt \tag{4.4}$$

To determine the permeability coefficient, P a plot of $-V/2A\ln(1-2C_t/C_0)$ against t was constructed and a linear fitting was performed. The slope of the linear portion of the graph yields a permeability coefficient, P.

Solute permeation experiments were performed using three representative solutes with different molecular weights and hydrodynamic sizes. We show in **Figure 4.15**, the permeation of theophylline, lysozyme and BSA through PVAN4 membrane at 30 °C. The membrane was annealed at 120 °C for 6 hours before taking it for permeation studies. It can be seen from the figure that as the size of solute increases the permeability decreases. Although the membranes are not chemically crosslinked, the heat treatment/annealing induces crystallinity in the membrane and the organized regions with parallel chains form the crystallites. For example, the average

crystallinity of PVA film increases from 25-27 % to 56 % upon annealing at 150 °C for 3 h.[26] The crystalline zones act as a giant crosslinking region in the membrane and obstacle to the penetrant molecules during the permeation. Therefore, the crystalline structure of the membrane will have notable influence on the transport properties. It can be noted that theophylline with a hydrodynamic radius of 3.7 Å diffuses faster as compared to BSA with a hydrodynamic radius of 22.5 Å. Whereas lysozyme, having the hydrodynamic radius of 14.6 Å shows the intermediate permeation.

In the past, the permeability of solutes with different sizes has been correlated to the effective mesh sizes of the PVA membranes, which have been chemically crosslinked using glutaraldehyde. The swelling ratios of these membranes with different degrees of crosslinking were determined and the mesh sizes were calculated using Flory-Rehner's theory of swelling.[29] The other parameters such as interaction parameter [$\chi_{PVA\text{-}H2O}$], characteristic ratio [C_n], molecular weight of the repeat unit [M_r] were obtained from the literature. However, in our system the membranes were not chemically crosslinked but the swelling property mainly arises due to the hydrophobicity and the thermally induced crystallization in the membrane. As mentioned earlier, the crystalline zones act like a crosslink points and the membranes show swelling rather than dissolving in the solvent medium. Under this circumstances it is rather difficult to draw correspondence between the chemically crosslinked structure and the physical interaction of the crystallites. Therefore, determination of mesh size is not possible in our systems. However, in order to study the influence of the hydrophobicity of the membrane on the permeation, we show in **Figure 4.16**, the permeability of BSA protein through two PVA-g-polyNTBA graft copolymer membranes with 4 and 12 mole % NTBA content. It can been readily seen that, the PVAN12 membrane is highly hydrophobic in nature and exhibit very low swelling ratios and the BSA diffusion is negligible. Whereas, PVAN4 membrane showed significant diffusion of BSA. These studies clearly indicated that the selective permeation of solutes can be effected with changing the hydrophobicity of the membranes. As discussed earlier, PVAN3 and PVAN4 membranes exhibit discontinuous volume transitions with respect to temperature. We performed permeability measurements of vitamin B_{12} through PVAN4 membrane at two different

temperatures 30 °C and 40 °C in which the membrane is in the swollen and collapsed state, respectively. **Figure 4.17** shows the temperature dependent permeability of vitamin B_{12} through PVAN4 membrane. The solute diffusion is higher in the swollen state (30 °C) as compared to the collapsed state (40 °C). The collapse state of the membrane still has significant quantity of water and shows some swelling ratio which gives a slight permeability to Vitamin B_{12}.

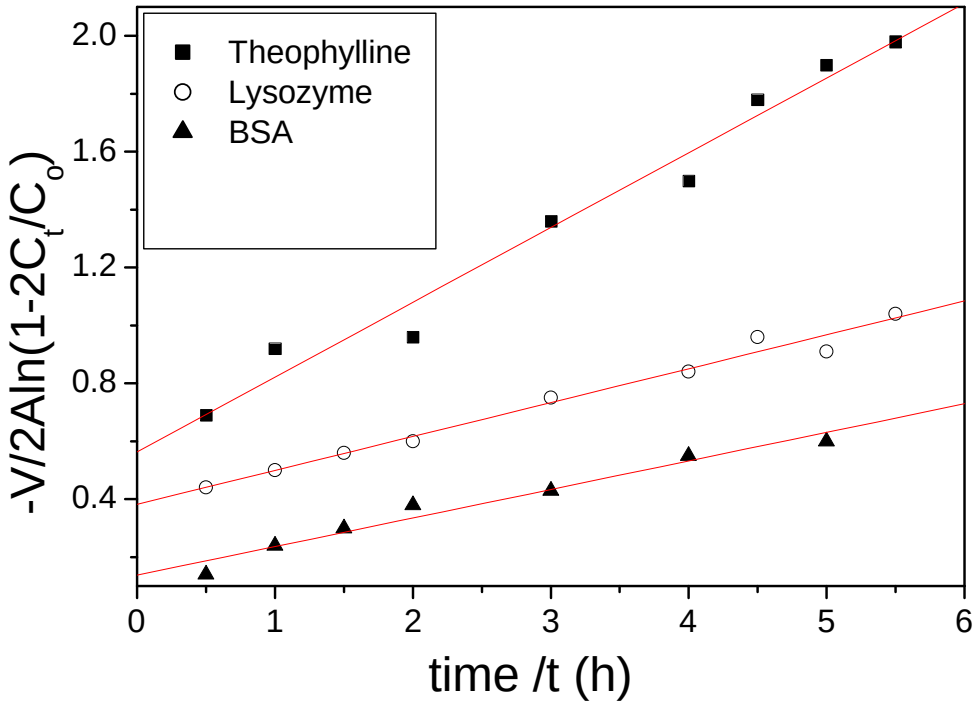

Figure 4.15: Effect of solute size on the permeation of PVAN4 membrane at 30 °C.

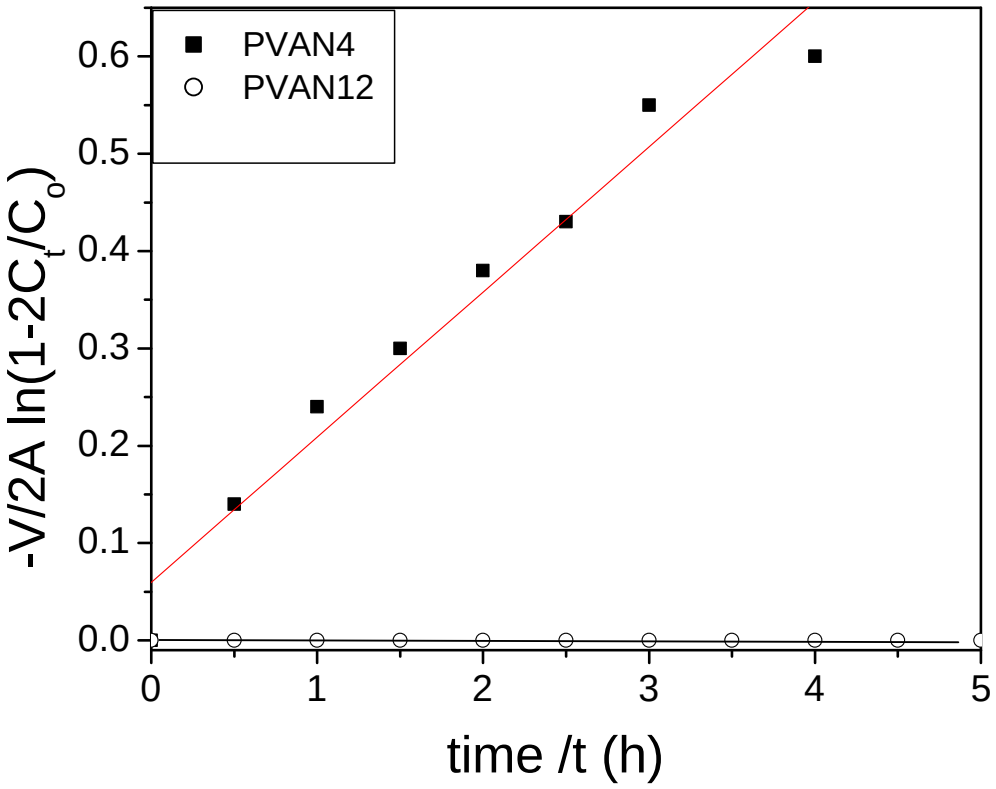

Figure 4.16: Influence of membrane hydrophobicity on the permeation of BSA through PVAN4 and PVAN12 membranes at 30 °C.

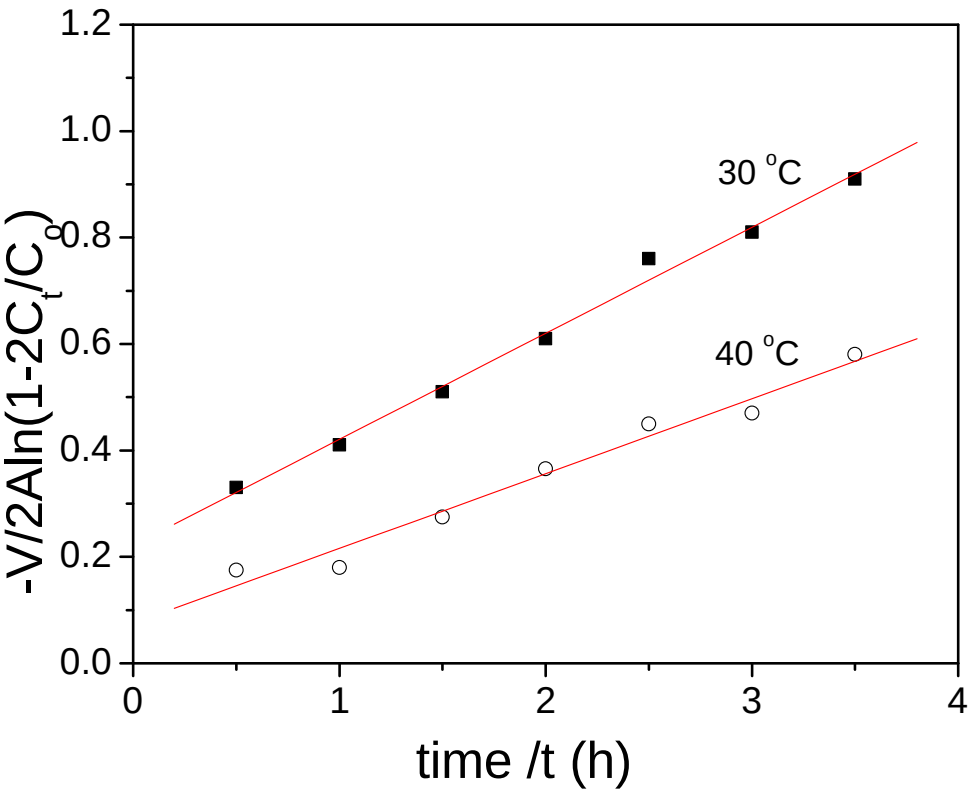

Figure 4.17: Permeation of Vitamin B_{12} through PVAN4 membrane at two temperatures.

4.5 Conclusions

Hydrophobically modified membranes of PVA-g-polyNTBA were synthesized by graft copolymerization of NTBA onto PVA by free radical polymerization. Elemental analysis, FT-IR and NMR spectroscopy confirmed the incorporation of NTBA onto PVA. The swelling behaviour of graft copolymer membranes was very much influenced by temperature of the external medium, hydrophobic content, annealing temperature and period. DSC, XRD and DMA results showed the increased crystallinity of membranes as a function of annealing. The permeabilities of solutes through these membranes were strongly dependent on the size of the solute, solution temperature and hydrophobicity of the membrane.

In summary,

1. Contact angle measurements and swelling studies revealed the decrease in hydrophilicity with an increase in NTBA content in graft copolymer.
2. The swelling behaviour studies of these membranes showed that the lower content of NTBA in graft copolymers exhibits the discontinuous volume transition as a function of temperature whereas, high content of NTBA showed decrease in swelling ratio with very little influence of temperature on the swelling.
3. The decrease in swelling ratio, increase in heat of fusion as well as storage modulus after annealing of membranes, confirmed the increase in crystallinity as a result of annealing.
4. DMA showed broadening of tan δ peak with increase in NTBA concentration which can be attributed to the random distribution of poly NTBA on the PVA membranes.
5. Permeability study of PVAN4 membranes exhibited size exclusion phenomenon. Permeability also influenced by the hydrophilicity of membranes and the external temperature. It was found that BSA diffusion through PVAN12 membrane was negligible compared to PVAN4 membrane and further diffusion of Vitamin B12 through

PVAN4 was higher at lower temperature when the membrane is in swollen state.

4.6 References

1. Dai, W. S.; Barbari, T. A. J. Membr. Sci. **1999**, *156*, 67.
2. Kim, K. J.; Lee, S-B; Han, N-W. Polymer J. **1993**, *25*, 1295.
3. Benlian, W.; Makoto, K.; Sukekuni, M.; Etsuo, K. Polym Gels Network **1998**, *6*, 71.
4. Kim, S. J.; Park, S. J.; Kim, S. I. Reactive and Functional Polymers **2003**, *55*, 53.
5. Gudeman, L. F.; Peppas, N. A. J. Appl. Polym. Sci. **1995**, *55*, 919.
6. Shin, H. S.; Kim, S. Y.; Lee, Y. M.; Lee, K. H.; Kim, S. J.; Rogers, C. E. J. Appl. Polym. Sci. **1998**, *69*, 479.
7. Peppas, N. A.; Wright, S. L. Eur. J. Pharmaceutics and Biopharmaceutics **1998**, *46*, 15.
8. Nonaka, T.; Ogata, T.; Kurihara, S. J. Appl. Polym. Sci. **1994**, *52*, 951.
9. Sun, Y-M.; Huang, T-L. J. Membr. Sci. **1996**, *110*, 211.
10. Ogata, T.; Nonaka, T.; Kurihara, S. J. Membr. Sci. **1995**, *103*, 159.
11. Kurihara, S.; Ueno, Y.; Nonaka, T. J. Appl. Polym. Sci. **1998**, *67*, 1931.
12. Nonaka, T.; Yoda, T.; Kurihara, S. J Polym Sci Part A, Polym Chem **1998**, *36*, 3097.
13. Muniz, E. C.; Geusken, G. J. Membr. Sci. **2000**, *172*, 287.
14. Yoshida, R.; Okuyama, Y.; Sakai, K.; Okano, T.; Sakurai, Y. J. Membr. Sci. **1994**, *89*, 267.
15. Lee, W-F.; Chen, Y-J. J. Appl. Polym. Sci. **2001**, *82*, 2487.
16. Zhang, J.; Peppas, N. A. Macromolecules **2000**, *33*, 102.
17. Pritchard, J. G. Poly(Vinyl Alcohol):Basic Properties and Uses, Polymer Monographs, Gordon and Breach, New York **1970**.
18. Maolin, Z.; Ning, L.; Jun, L.; Min, Y.; Jiugiang, L.; Hongfei, H. Radiation Physics and Chemistry **2000**, *57*, 481.

19. Aminabhavi, T. M., Naik, H,G. J. Appl. Polym. Sci. **2002**, *83*, 244.
20. Aminabhavi, T. M., Naik, H,G. J. Appl. Polym. Sci. **2002**, *83*, 273.
21. Ikada, Y.; Nishizaki, Y.; Sakurada, I. J. Polym. Sci. A, Polym. Chem. **1974**, *12*, 1829.
22. Ellison, T. M.; Spencer, H. G. J. Polym. Sci. B **1963**, *1*, 707.
23. Finch , C. A. Polyvinyl Alcohol, New York:Wiley, **1973**.
24. Peppas, N. A.; Merrill, E. W. J. Appl. Polym. Sci. **1976**, *20*, 1457.
25. Peppas, N.A.; Merrill, E. W. J. Polym. Sci. A, Polym. Chem. **1976**, *14*, 441.
26. Gref, R.; Nguyen, Q. T.; Schaetzel, P.; Neel, J. J. Appl. Polym. Sci. **1993**, *49*, 209.
27. Katz, M. G.; Wydeven, T. J. Appl. Polym. Sci. **1982**, *27*, 79.
28. Nishio, Y.; Manley, RStJ. Macromolecules **1988**, *21*, 1270.
29. Matsuyama, H.; Teramoto, M.; Urano, H. J. Membr. Sci. **1997**, *126*, 151.

CHAPTER 5

Nanocomposite Hydrogel Membranes Based on PVA: Synthesis and Characterization

5.1 Introduction

Hydrogels are hydrophilic three dimensional polymeric networks which are insoluble in water due to the presence of chemical or physical crosslinks. Because of their crosslinked structures, which are random in nature, the conventional hydrogels have morphological inhomogeneity and inferior mechanical properties. Therefore, recently nanocomposite (NC) hydrogels have gained importance due to their enhanced mechanical property. These hydrogels contain clays and are known as nanocomposite (NC) gels. It is well established that the mechanical and barrier properties of hydrogel membranes can be significantly increased by incorporation of clays.[1] The influence of inorganic clay on the properties of chemically crosslinked hydrogels have been studied earlier.[2-5] The first report on the stimuli-responsive polymer-hydrogel-clay nanocomposite based on PNIPAm and montmorillonite was made by Messesmith and Znidarsich.[6] Churochkina et al found that incorporating clay into polyacrylamide gel enhanced the mechanical properties of gel with little influence on swelling.[2] Stimuli-sensitive nanocomposite hydrogels based on N-isopropyl acrylamide (NIPAm) and acrylic acid (AA) have also been demonstrated. Recently, organoclay-polymer nanocomposites have come into existence, wherein the clay has been organically modified. Liang et al reported the thermosensitive nanocomposite hydrogel based on organically modified montmorillonite and poly(N-isopropylacrylamide) with enhanced thermal response.[3] Xia et al investigated nanocomposite gels based on poly(N-isopropylacrylamide)/Na-montmorillonite.[4] Lee and Fu studied the influence of organically modified montmorillonite content on poly (N-isopropylacrylamide) nanocomposite hydrogel.[5] Haraguchi and coworkers[7-9] reported novel nanocomposite hydrogels without an organic crosslinker where well-dispersed clay acts as multifunctional crosslinker. They investigated the effect of laponite content on the characteristics properties of thermosensitive nanocomposite PNIPAm/laponite gels, in comparison with conventional PNIPAm gel crosslinked with organic crosslinker. These nanocomposite gels exhibited enhanced swelling/deswelling behaviour and mechanical properties.[7] They proposed the applications of these nanocomposite gels in biomedical tissue-engineering, sensors, drug delivery systems and mechanical devices

such as artificial muscles and micro-actuators. Although there are many reports on the NC gels based on PNIPAm, there are a few reports on the NC gels based on PVA. Poly (vinyl alcohol) is a nontoxic, biocompatible, highly hydrophilic polymer with an excellent film forming property. It has been reported that hydrophilic nonionic polymers such as PVA and PEO easily adsorb onto clay surfaces.[10,11] PEO adsorption onto surface of laponite was investigated by light scattering measurements.[11] The adsorption of PVA onto clay surface occurs through strong hydrogen bonding between the hydroxyl groups of PVA and the oxygen atoms of silicate layers.[12-14] Previously, we have reported hydrophobically modified PVA hydrogel membrane with N-tertiary butyl acrylamide (NTBA), which exhibits discontinuous volume transition at low NTBA content. Unlike the PNIPAm, the hydrophobically modified PVA has an excellent film forming property and this property prompted us to study the NC hydrogel membranes based on modified PVA.

This work was undertaken with a view to improve the mechanical strength of PVA-g-polyNTBA membranes by incorporating clay (laponite) and to study the influence of clay on the swelling and permeation properties of the resulting nanocomposite membranes. Nanocomposite hydrogel membranes were synthesized by varying laponite content and the incorporation of laponite in the membranes was evaluated by FT-IR studies and thermogravimetric analysis (TGA). The swelling properties of membranes were studied as a function of temperature and laponite content.

5.2 Experimental

5.2.1 Materials

PVA and NTBA were purchased from the S.D. Fine chemicals, India and Aldrich chemicals, USA respectively. Potassium persulfate [KPS] was procured from Loba chemicals, India. Laponite RD was purchased from Laporte Ind. Ltd.

Theophylline and hemoglobin [Hb] were obtained from Aldrich chemicals, USA; while vitamin B_{12} was purchased from S. D. fine chemicals, India.

5.2.2 Synthesis of PVA-g-polyNTBA2 graft copolymer

PVA-g-polyNTBA2, henceforth abbreviated as PVAN2, where 2 mole% of NTBA was used for synthesis of graft copolymer. Synthesis of graft copolymer was carried out using KPS as an initiator. Procedure of synthesis of graft copolymer was reported earlier in Chapter 4. Briefly, NTBA monomer, initiator and PVA were dissolved in DMSO. Nitrogen was purged in the solution in order to remove the dissolved oxygen. The graft polymerization reaction was carried out at 42 ºC for 22 hours. The graft copolymer was precipitated in acetone.

5.2.3 Synthesis of Nanocomposite hydrogel membranes

PVAN2/DMSO 4 % (wt/vol), 20 cm^3 of solution was mixed with aqueous suspension of laponite and stirred properly. The composition of laponite and polymer is given in **Table 5.1**. The NC hydrogel membranes were made by pouring the solution into a flat petri dish (4.8 cm diameter), and the solvent was allowed to evaporate at 60 °C for 7 days.

The membranes were annealed at 120 °C/140 °C for 6 hours before they were used for swelling studies.

Table 5.1: Stiochiometry of nanocomposite membranes

Wt % of laponite	PVAN2 (g)	Laponite (g)	Water (ml)
2.5	0.8	0.02	2.0
5.0	0.8	0.04	2.0
10.0	0.8	0.08	4.0
20.0	0.8	0.16	4.0

5.3 Characterization

5.3.1 Fourier transform infrared analysis (FT-IR)

FT-IR analysis was done using a Shimadzu FT-IR-8300 spectrometer at a resolution of 4 cm^{-1}. Thin films of PVAN2 polymer and nanocomposites were made by evaporating solvent at 60 °C and used for FT-IR analysis. FT- IR spectrum of laponite (as a reference) was also recorded using nujol as a medium.

5.3.2 Swelling ratio of membranes

The dried, pre-weighed membranes were kept in water in a constant temperature bath for different temperatures in the range of 10–60 °C for 24 hours and re-weighed after wiping the surface gently. Since membrane thickness is very small, 24 hours equilibrium time was found to be sufficient.

The swelling ratio (q) of membrane was calculated using the following equation,

$$q = \frac{W_2}{W_1} \tag{5.1}$$

where, W_2 and W_1 are wet and dry weights of the membrane, respectively.

5.3.3 Differential Scanning Calorimetry (DSC)

Perkin Elmer DSC-7 was used for studying the melting and crystallization behaviour of the polymeric membranes. The temperature and energy scales were calibrated with the standard procedures. The melting studies were performed in the temperature range of 50-240 °C at the heating rate of 10 °C/min in N_2 atmosphere.

5.3.4 Dynamic Mechanical Analysis (DMA)

The dynamic mechanical properties of PVAN2 and nanocomposite membranes were studied with a Rheometrics DMTA IIIE dynamic mechanical analyzer. The

samples were analyzed in the tensile mode. The temperature sweep was carried out from 30 to 180 °C and the sample was heated at the rate of 5 °C/min. The frequency was 10 rad/s and the strain was 0.1%.

5.3.5 Thermogravimetric Analysis (TGA)

TGA of PVAN2 and nanocomposite membranes was carried out by using Perkin Elmer TGA-7. The samples were heated from 50-700 ºC at the heating rate of 10 ºC/min under nitrogen atmosphere.

5.3.6 Permeation Studies

Permeation experiments were carried out using a two-chamber (donor and receptor) diffusion cell with a chamber volume of 70 cm^3 as shown in chapter 3. Pre-swollen membranes were mounted between two halves of the donor and receptor cell, which were further clamped together and sealed tightly with the rubber packing. The effective membrane area in the cell was 1.76 cm^2. The solute solution was at the donor side of the cell and the receptor was having only water. A fixed volume (1.0 ml) of the sample was taken out at various time intervals from the receptor cell and the solute concentration was measured using an UV spectrophotometer at appropriate wavelengths. The solutes chosen for the permeation studies were, theophylline (MW = 180), vitamin B_{12} (MW = 1355), Hb (MW = 64-67,000). The concentrations of these solutes were determined by UV spectrophotometer at wavelengths of 271 nm for theophylline, 405 nm for Hb and 361nm for vitamin B_{12}. Membranes, which were annealed at 150 °C and 160°C for 6 hours have been chosen for the permeation studies.

5.4 Results and Discussion

5.4.1 Synthesis of nanocomposite membranes

Laponite is a synthetic clay which belongs to a family of phyllosilicates (trimorphic) 2:1 with an empirical formula of $Na^{+}_{0.7}[(Si_8Mg_{5.5}Li_{0.3})O_{20}(OH)_4]^{-0.7}$

having diameter of 300Å and height about 10Å.[15] The details of Laponite are explained in chapter 1. Laponite exhibits broad XRD pattern indicating that laponite has low crystallinity.

In this study, we have used laponite without any organic modification. Although, PVAN2 is made partially hydrophobic, the clay can still be homogenized with PVAN2 without the need for organic modifications. We have varied the clay content from 2 to 20% and membranes were casted. These nanocomposite membranes showed superior mechanical properties due to the fine scales of clay dispersed in the polymer matrix. PVA has a strong tendency to form hydrogen bonding within itself as well as with other species containing highly electronegative groups. Laponite has electronegative oxygen and hydroxyl groups, which can assist the adsorption of PVA onto laponite surface. The adsorption of PVAN2 onto surfaces of laponite is presumed to occur through hydrogen bonding. Apart from hydrogen bonding, van der Waals forces between polymer segments and clay surface would also play an important role in the overall adsorption process. The interactions between PVAN2 and laponite and the influence of these on swelling and mechanical properties were investigated and discussed in the foregoing.

FT-IR analysis and TGA supports the increase in laponite content in nanocomposite membranes with increasing laponite concentration in the feed, as discussed in the following.

5.4.2 FT-IR Analysis

We show in **Figure 5.1** FT-IR spectra of PVAN2 copolymer membrane, laponite and nanocomposite membranes with varying laponite concentrations. The broad band observed at 3350 cm^{-1} in the IR spectra is due to the OH stretching of PVA and laponite. as well as N-H stretching vibration of NTBA in the graft copolymer. The sharp band at 1735 cm^{-1} and 1654 cm^{-1} corresponds to the C=O stretching of the acetate and amide groups of PVAN2 respectively. Laponite spectrum shows characteristic bands at 1013 cm^{-1} and 654 cm^{-1} which corresponds to Si-O-Si stretching frequencies. It can be readily seen from **Figure 5.2** that the intensity of the

Si-O-Si stretching band increases with respect to increase in laponite content in nanocomposite gels, which qualitatively indicates the increase in laponite concentration from 2.5% to 20% in the nanocomposite membranes. Furthermore, the nanocomposite membranes show slight shift in Si-O-Si stretching frequency to lower value as compared to laponite. This shift can be attributed to the interactions between PVAN2 polymer and the clay through Si-OH groups.

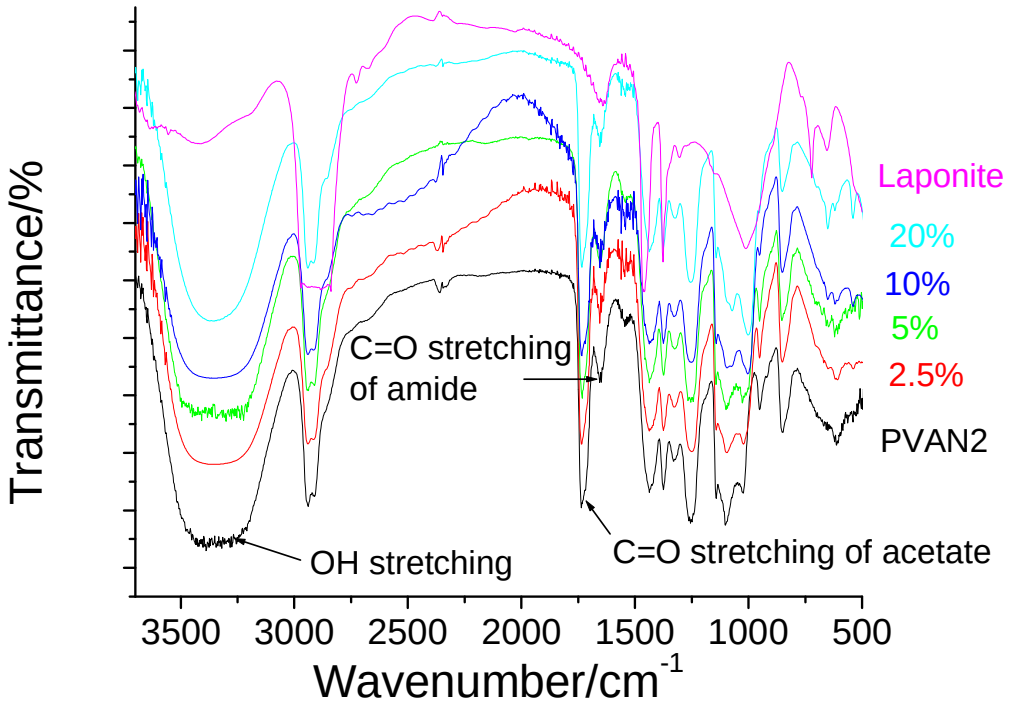

Figure 5.1: FT-IR spectrum of the PVAN2 copolymer membrane and nanocomposite membranes with different loadings of laponite (scale range: 3700-500 cm^{-1}).

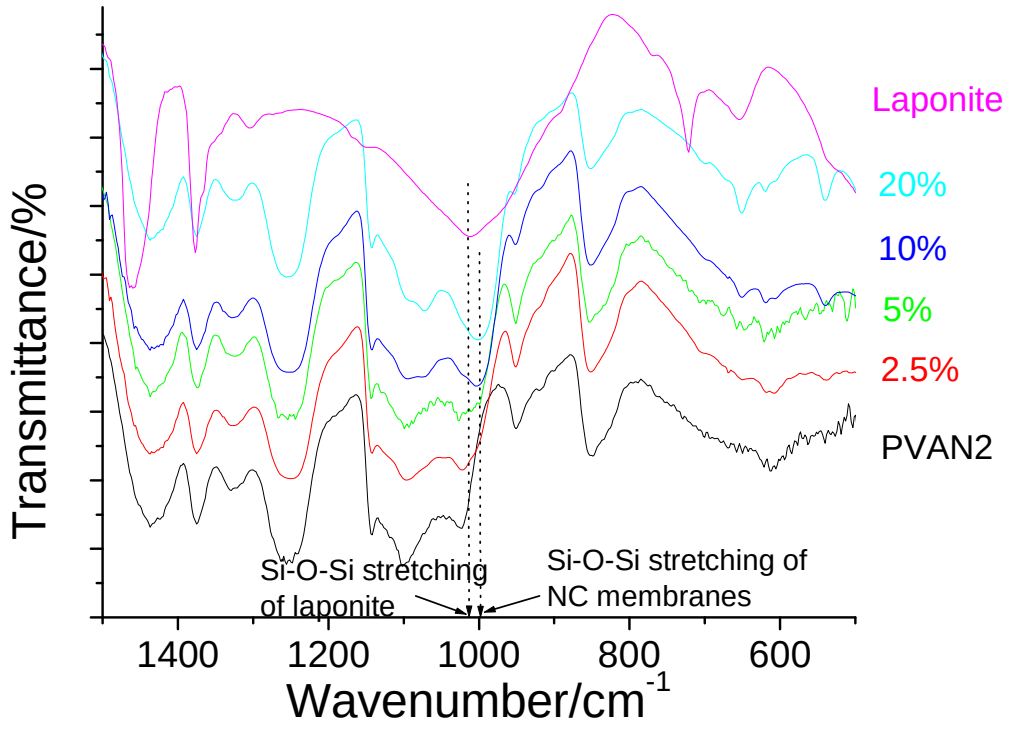

Figure 5.2: FT-IR spectra of PVAN2 and nanocomposite membranes with different loading of laponite (scale range: 1500-500 cm^{-1}).

5.4.3 Thermogravimetric Analysis (TGA)

We show in **Figure 5.3** TG curves of PVAN2, laponite and nanocomposite membranes with laponite content of 2.5%, 5%, 10% and 20%. Laponite shows loss of weight near 100 °C, which is mainly from the evaporation of water in the intercalated layer. It can be seen from the figure that the degradation temperature decreases in nanocomposite membranes and such decrease was also observed for polystyrene/organically modified montmorillonite nanocomposites.[16] The decrease in degradation temperature suggests that the presence of laponite may facilitate the degradation of PVAN2 copolymer membrane. The weight ratio of clay incorporated in the nanocomposite membranes were evaluated by TGA measurements. The nanocomposite membranes exhibit plateau after 500 °C due to presence of an inorganic residue. Therefore, the inorganic contents in the nanocomposite membranes could be obtained from the weight percentage of the residue at 600 °C. It was found that the weight ratio of laponite in the nanocomposite membranes obtained from the plateau correspond to the initial feed composition. Virgin PVAN2 membrane shows 5.13% weight retained at 600 °C. This could be due to the presence of some infusible residue. Therefore, the amount of clay in nanocomposite membranes was calculated by subtracting this value from the observed weight % of nanocomposite membranes at the same temperature.

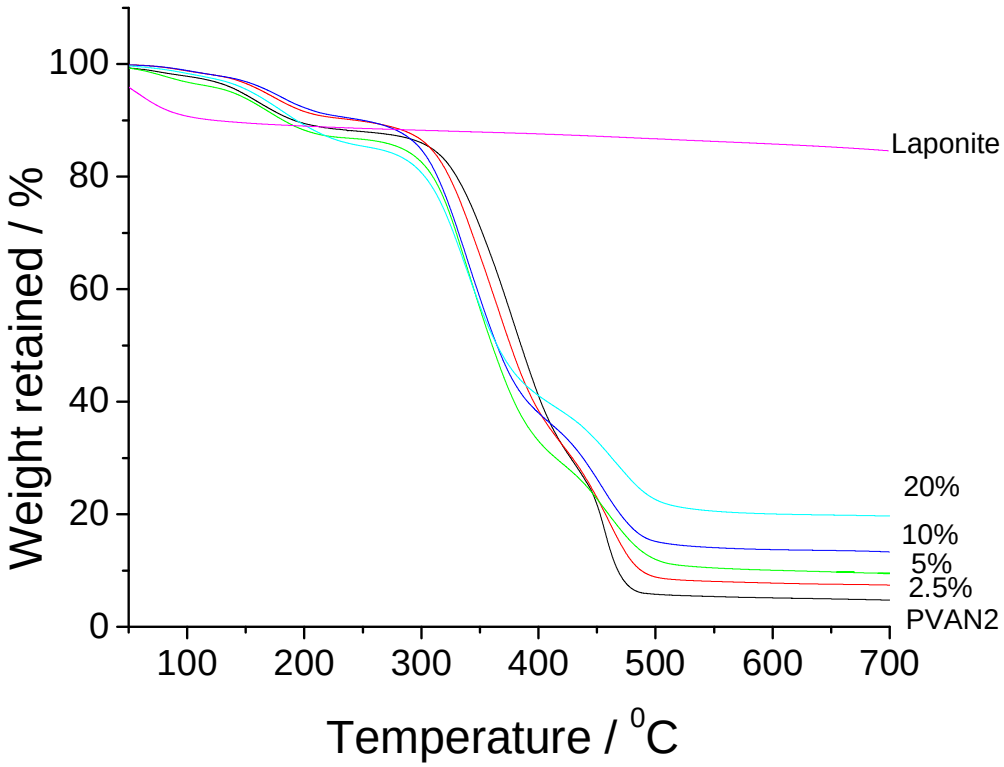

Figure 5.3: TG curves of PVAN2, laponite and nanocomposite membranes

5.4.4 Differential Scanning Calorimetry (DSC)

DSC curves of PVAN2 copolymer membrane and the nanocomposite membranes are shown in **Table 5.2**. The data revealed that with an increase in laponite content in the nanocomposite membranes, the value of heat of fusion (ΔH_f) as well as melting transition of the membranes decreased. The decreased value of T_m is due to the formation of crystals with lower thermal stability. Since the degree of crystallinity is the measure of ratio of heat of fusion of polymer to the heat of fusion of 100% crystalline polymer, the decrease in ΔH_f value indicates the decreased degree of crystallinity of the nanocomposite membranes. Our results are in line with Ogata *et.al.*[17] who reported that the well dispersed montmorillonite in PVA-montmorillonite composites showed reduction in heat of fusion and crystallinity with increase in montmorillonite content. Yu *et. al.*[18] also indicated the suppression in crystalline behaviour of PVA in polymer nanocomposites by introduction of organophilic montmorillonite.

Table 5.2: Thermal analysis of PVAN2 and nanocomposite membranes with 5%. and 20% laponite

Membrane	**T_m/°C**	**T_c/°C**	**ΔH_f (J/g)**
PVAN2	174	122	95.647
5%	173	135	94.37
20%	168	-	79.88

5.4.5 Swelling Behaviour

PVAN2 graft copolymer membrane with 2-mole % of NTBA is partially hydrophobic and partly dissolves in water. Therefore all the membranes were annealed to prevent the dissolution of membranes and to improve the mechanical properties.

The influence of laponite content on the swelling behaviour of the membranes at 30 °C is shown in the **Figure 5.4**. It can be seen from the figure that the swelling ratios of the nanocomposite membranes gradually decrease with an increase in the laponite content in the membranes. The decrease in swelling ratio with increasing laponite content can be attributed to the increase in physical crosslinking in which the clay may act as a physical crosslinker. Similar observation was made by Haraguchi *et. al.*[7] in both nanocomposites and conventional hydrogels. Xia *et. al.*[4] reported the decrease in swelling with increase in clay content in poly(N-isopropylacrylamide)/Na-MLS nanocomposite gels. Laing *et. al.*[3] have reported a thermoresponsive polymer-clay nanocomposite with enhanced temperature response based on organically modified clay-PNIPAm. Surprisingly, in their study, the swelling ratios of NC gels increased with an increase in the clay content and the kinetics of swelling was faster as compared to the normal clay-PNIPAm NC gels. The most efficient thermal transition and the increase in swelling ratios in their studies were attributed to the presence of coupling agent, which interfaces the clay and polymer. However, we find that their explanation on the above effect is not convincing. We believe that, since the clay acts as a physical crosslinker, the swelling ratio is expected to decrease with an increase in clay content.

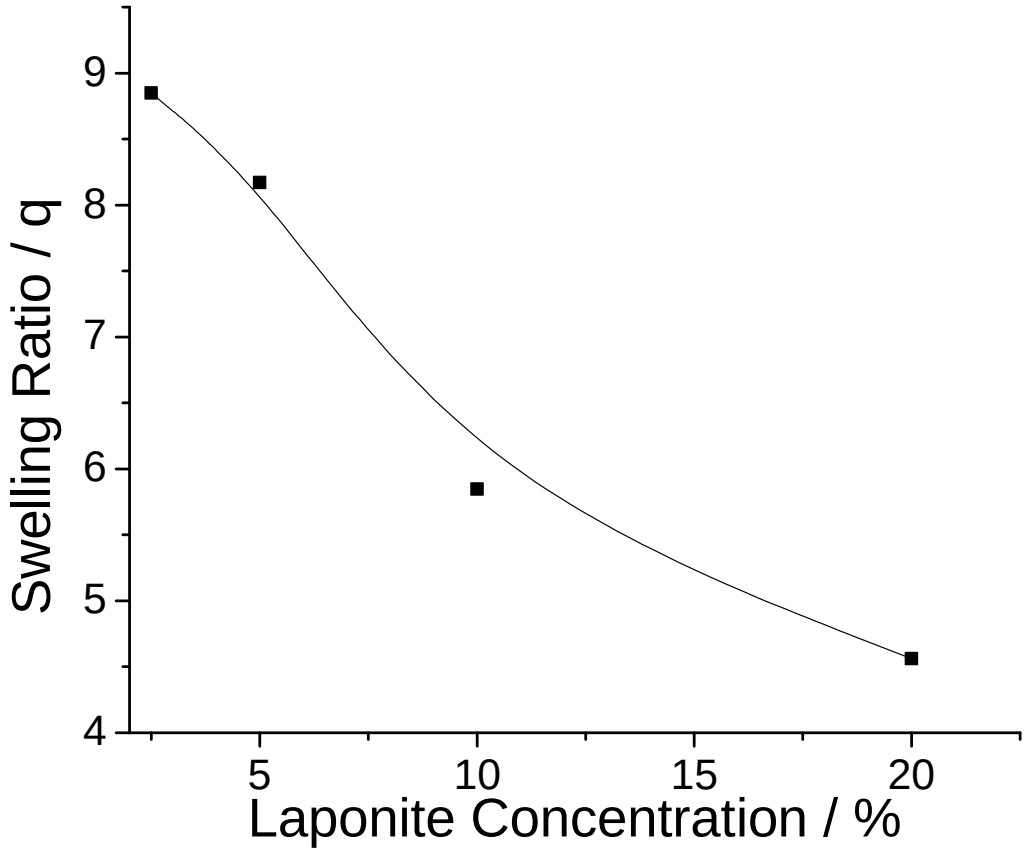

Figure 5.4: Influence of laponite concentration on the swelling ratio of membranes at 30 °C (membranes, annealed at 140 °C for 6 hours prior to swelling)

We show in **Figure 5.5** the temperature dependent (10-60 °C) swelling ratios (q) of PVAN2 membrane and nanocomposite membrane with 20% laponite content, annealed at 120 °C for 6 hours. The swelling ratios were measured in water. It can be readily seen from the figure that, PVAN2 membrane exhibits higher swelling ratios in the lower temperature range of 10-30 °C and decrease in swelling ratio with increasing temperature. The higher swelling ratios of the membranes at low temperature can be attributed to the strong H-bonding interactions between the polymer and water. The hydroxyl groups of PVA form strong H-bonds with water molecules, which enhance the interaction between PVA and water. However, upon increasing the temperature, the H-bonding between polymer and water breaks and inter/intramolecular hydrophobic associations due to the presence of hydrophobic, N-tertiary butyl groups dominate resulting into the collapse of polymer chains. The collapse of the polymer chains lead to decrease in the swelling ratio. However, the swelling behaviour of 20% nanocomposite membrane with respect to temperature is totally different. The swelling ratios of NC hydrogels are lower compared to PVAN2 at all the measured temperatures. This can be due to presence of laponite, which acts as a crosslinker. However, it is intriguing to note that, at the constant laponite loading of 20% the swelling ratio in the NC gels slightly increase with temperature. This could be attributed to the fact that, the laponite being hydrophilic in nature inhibits the hydrophobic associations of PVAN2 chains resulting into slight increase in swelling ratios. Therefore, the temperature dependent swelling of NC gels is a complex phenomenon, which involves the interactions between polymer-clay-water and interplay between these dictates the swelling ratios.

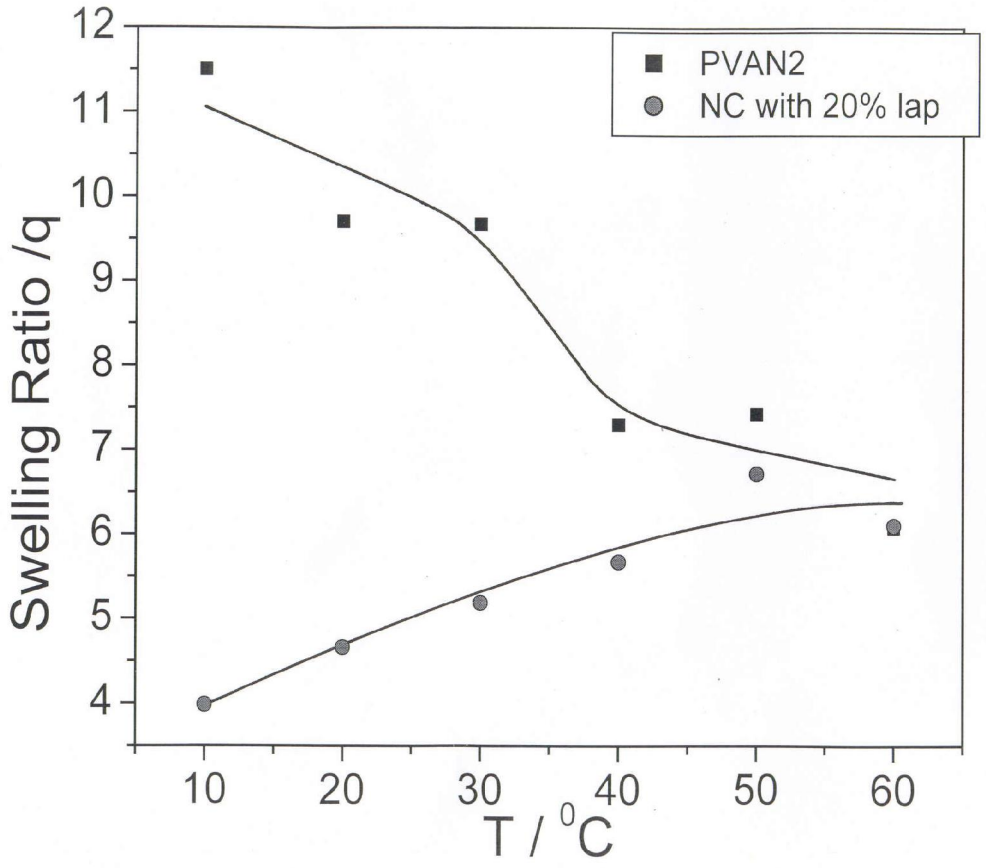

Figure 5.5: Temperature dependent swelling of PVAN2 and 20% nanocomposite membrane annealed at 120 °C for 6 hours.

5.4.5 Dynamic Mechanical analysis

The dynamic mechanical analysis (DMA) gives information about the variation of storage modulus ($E^{|}$), loss modulus ($E^{||}$) and tan delta (tan δ) with temperature at a fixed frequency. The DMA of PVAN2 and all the nanocomposite hydrogel membranes were carried out in the temperature range of 30 to 180 °C. We show in **Figure 5.6** the variation of storage modulus ($E^{|}$) with temperature for annealed and unannealed PVAN2 composite membranes. It can be seen that annealing results in a significant increase in the storage modulus over the entire temperature range. The observed increased in $E^{|}$ could be attributed to the presence of secondary interactions such as van der Waals forces that favour further adsorption of PVAN2 onto laponite by bridging clay surface and polymer into close contact.

We show in **Figure 5.7**, the tan δ curves for PVAN2 and membranes with different laponite contents. The tan δ peak temperature for the polymer PVAN2 and the nanocomposite membranes remains almost constant irrespective of laponite content. However, tan δ peak values of nanocomposite membranes decrease upon increase in laponite content. Since tan δ value is directly proportional to the amorphous content of the membrane, its decrease indicates the decrease in the amorphous content of the nanocomposite membrane. In an ideal case this decrease should be balanced by an increase in crystallinity. However, we find that our DSC results indicate the decrease in crystallinity. Therefore, the decrease in tan δ peak values with respect to increase in laponite content can be ascribed to the formation of rigid amorphous phase (RAP) resulting from the constrained volume of amorphous phase. The constrained volume of amorphous phase can arise from the surface interactions of clay and polymer through functional groups. **Table 5.3** shows the tan δ peak values at and their normalized values with respect to 100% PVAN2 content. The significant decrease in tan δ values with increase in laponite content indicates the existence of the RAP. Similar observations were made by Ogata et al[17] on the PVA/montmorillonite blend system.

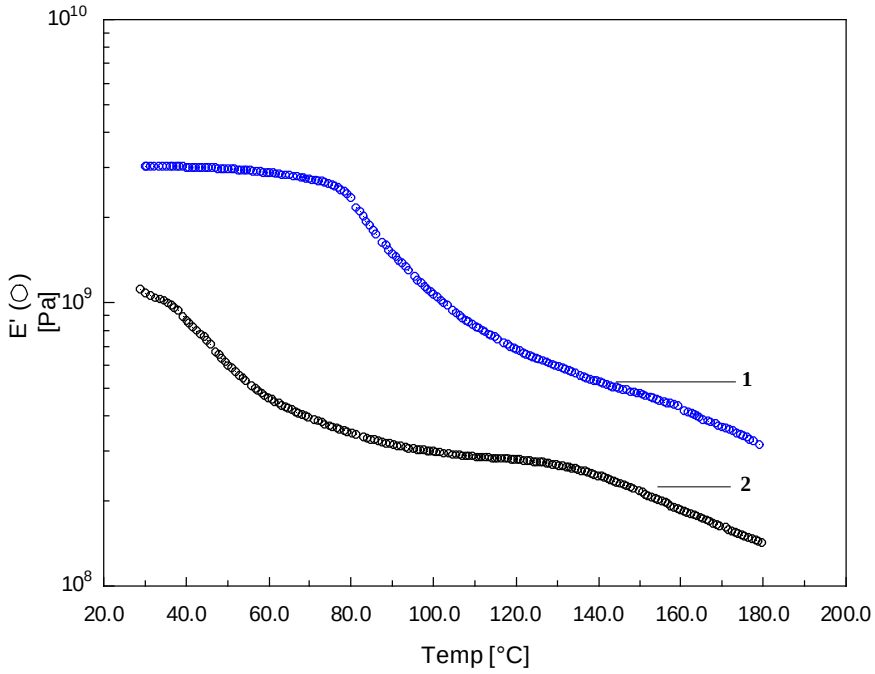

Figure 5.6: Effect of annealing on the storage modulus, E| as a function of temperature for the sample PVAN2 with 20% laponite; annealed [170 °C] (1) and without annealing (2)

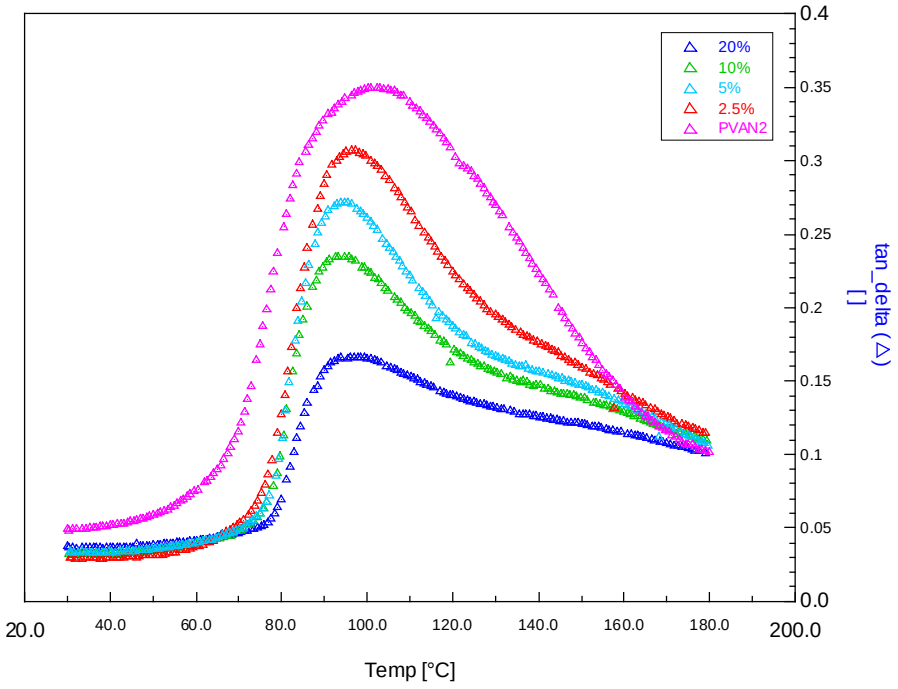

Figure 5.7: Effect of laponite on the tan δ peak as a function of temperature for annealed membranes [annealed 170 °C].

We show in **Figure 5.8** shows temperature dependent storage modulus ($E^{|}$) of PVAN2 and all nanocomposite membranes, which were annealed at 170 °C for 6 hours. It can be readily seen from figure that, the modulus of the membranes increases systematically with increase in the laponite content. The data from **Table 5.4** also shows that, below the glass transition temperature (T_g), the increase in storage modulus is about 37% whereas increase in the modulus above the T_g is about 90%. This result clearly shows that the addition of laponite has a strong effect on the elastic properties of the membranes. The increase in modulus can be attributed to the nanoscale dispersion of laponite leading to efficient interactions between polymer and clay or creation of three dimensional network or physical crosslinks in the structure.

Table 5.3: Tan δ and normalized Tan δ values at peak temperature for membranes

Membranes	**Tan δ at peak value After annealing**	**Normalized value of Tan δ**
PVAN2	0.3499	-
2.5%	0.3075	0.3411
5%	0.2717	0.3324
10%	0.2346	0.3054
20%	0.1668	0.2799

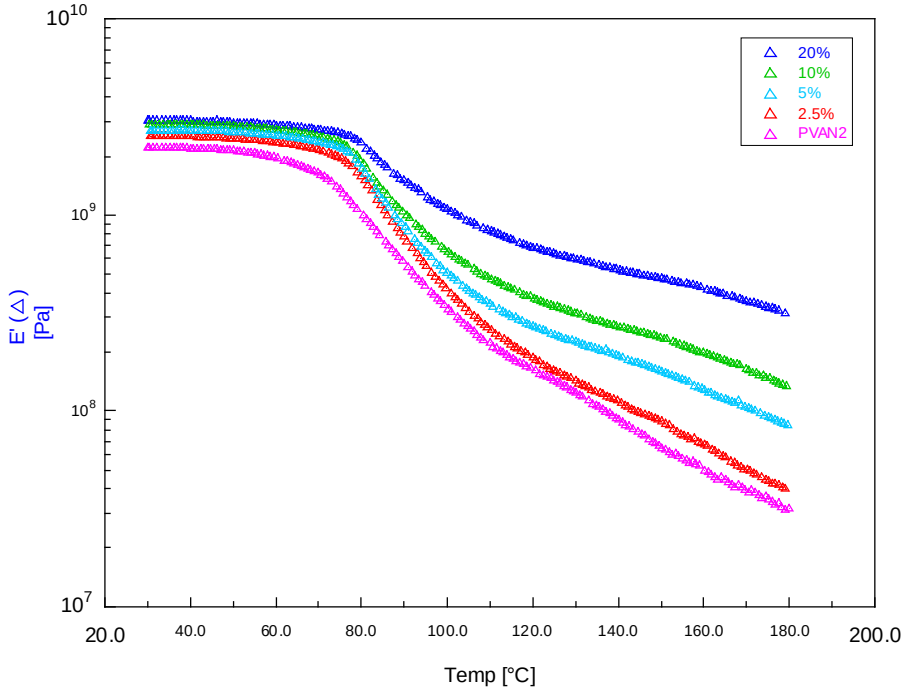

Figure 5.8: Influence of laponite content on the storage modulus ($E^{|}$) of annealed PVAN2 and nanocomposite membranes.

Table 5.4: Storage modulus ($E^{|}$) of annealed membranes at 30 °C and 170 °C.

Membranes	$E^{|}$ (Pa) at 30 °C	$E^{|}$ (Pa) at 170 °C
PVAN2	2.2036×10^{9}	3.8423×10^{7}
2.5%	2.5441×10^{9}	5.0251×10^{7}
5%	2.7133×10^{9}	1.0367×10^{8}
10%	2.8920×10^{9}	1.6112×10^{8}
20%	3.0294×10^{9}	3.6555×10^{8}

5.4.7 Permeation Studies

The permeation of solutes through nanocomposite membranes depends on the aspect ratio of clay[19], clay content and tortuosity path[20,21,22] and electrostatic interactions between membrane and solutes when both are charged.[5] Permeability of the membranes is determined by using the following equation,

$$\ln(1-2\frac{C_t}{C_0}) = \frac{-2A}{V}Pt \qquad (5.2)$$

Where,

C_t = Solute concentration in the receptor cell (mg/ml)

C_0 = Initial solute concentration in the donor cell (mg/ml)

V = Volume of each half cell (ml)

A = Effective permeation area (cm^2)

P = Permeability coefficient (cm/s)

t = Time (h or s)

To determine the permeability coefficient, P, a plot of $-V/2A\ln(1-2C_t/C_0)$ against t was constructed and a linear fitting was performed. The slope of the linear portion of the graph yields a permeability coefficient, P.

Solute permeation experiments were performed using three representative solutes with different molecular weights and hydrodynamic sizes in order to understand the effect of solute size on the permeation through nanocomposite membrane. We show in **Figure 5.9**, the permeation of theophylline, vitamin B_{12} and hemoglobin (Hb) through a membrane with 20% laponite at 30 °C. In order to enhance the mechanical strength of membrane in water, the membrane was annealed at 150 °C for 6 hours before taking it for permeation studies. It can be seen from the figure that as the size of solute increases the permeability decreases.

In order to study the influence of laponite content on the permeation properties of the nanocomposite membranes, we studied the permeation of Hb through the PVAN2 membrane and nanocomposite membranes with varying laponite

concentration. The relative permeability of Hb through the PVAN2 membrane and nanocomposite membranes with 10% and 20% laponite is shown in **Figure 5.10**. It can be readily seen from the figure that the permeability of solute through nanocomposite membranes reduced compared to the PVAN2 membrane. This reduction in permeability can be attributed to the well-dispersed laponite in the polymer matrix, which are impermeable to the solute. Solute has to follow a tortuous path in the nanocomposite membranes due to the presence of clay, which results into increase in effective path of diffusion and consequently, permeability through nanocomposite membranes decreases.

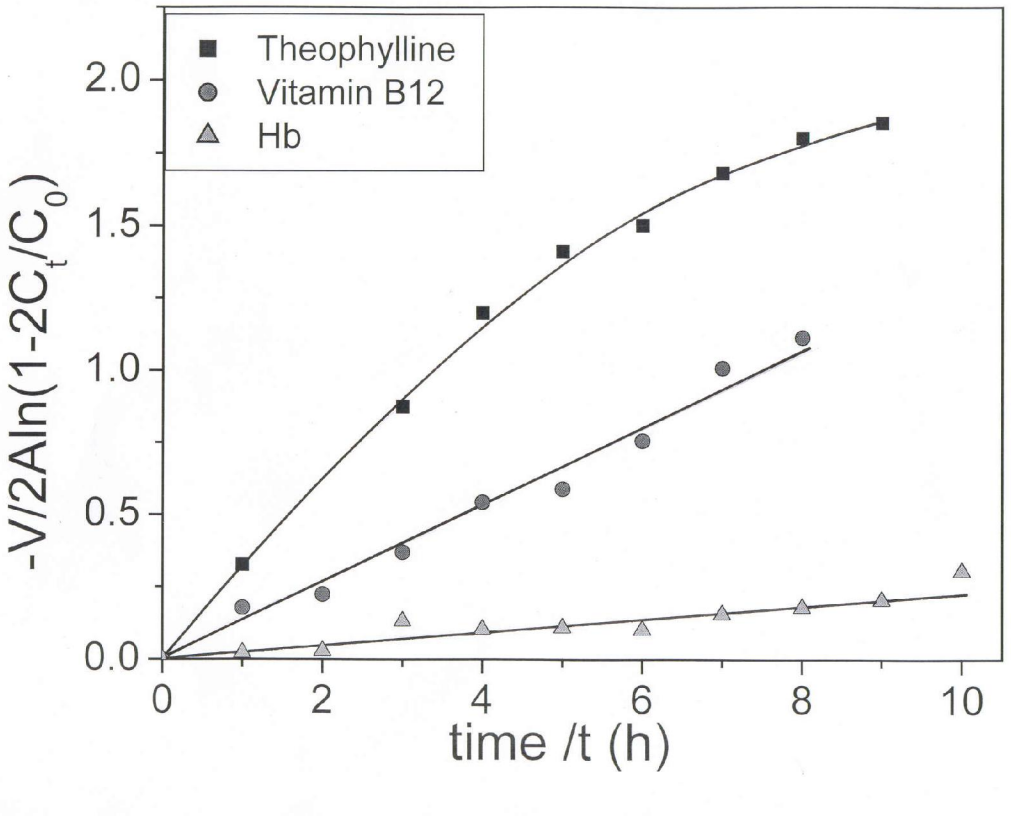

Figure 5.9: Size exclusion phenomenon of 20% nanocomposite membrane at 30°C.

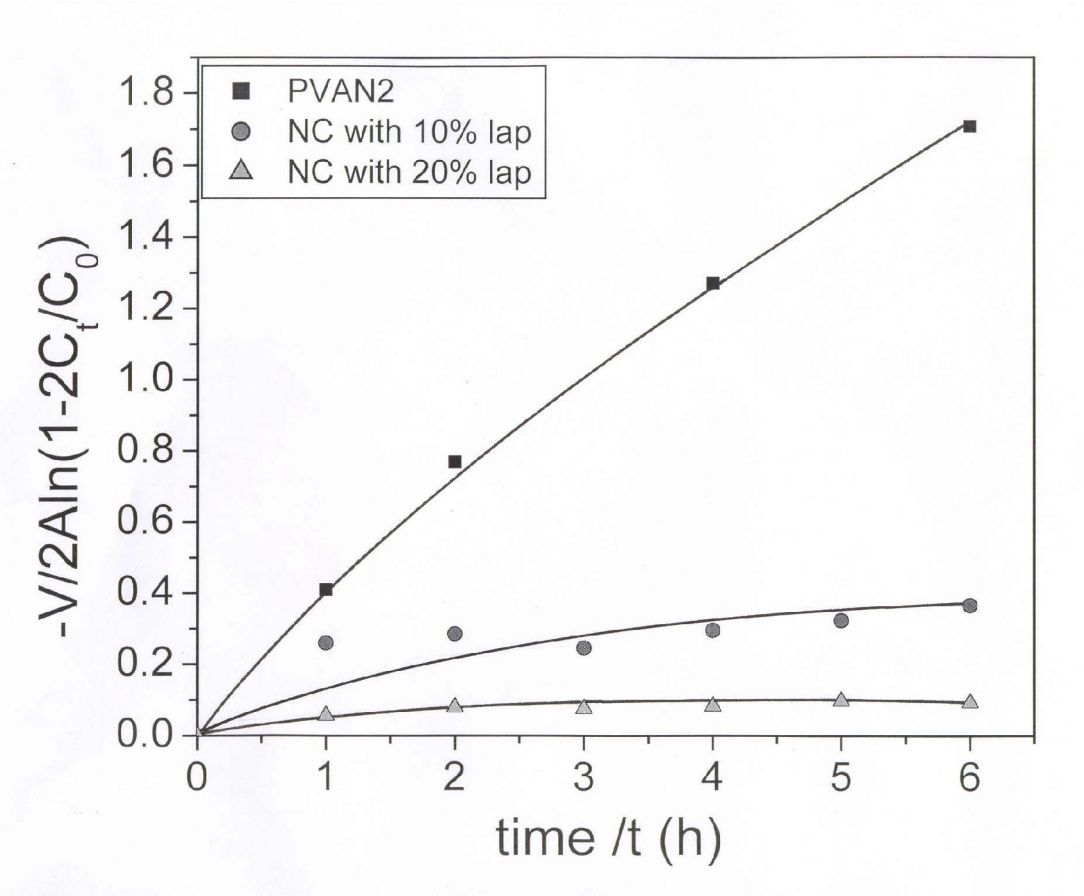

Figure 5.10: Relative permeability of hemoglobin (Hb) through membranes as a function of laponite content at 30 °C (membranes annealed at 160°C for 6 hours).

5.5 Conclusions

Thermosensitive nanocomposite hydrogel membranes based on PVAN2 and water swellable laponite were synthesized by varying laponite concentration. The incorporation of laponite in nanocomposite membranes was demonstrated by FT-IR spectroscopy and thermogravimetric analysis. The swelling of nanocomposite membranes was very much dependent on the laponite content and the solution temperature. Dynamic mechanical analysis indicated the enhanced mechanical property with an increase in laponite concentration in nanocomposites. The permeabilities of the membranes were strongly dependent on the solute size as well as the laponite concentration in membrane.

In summary, nanocomposite membranes exhibited following characteristics,

1. The swelling of nanocomposite membranes in water decreased with an increase in the laponite content. PVAN2 membrane exhibited decrease in swelling ratio with increasing temperature. On the contrary, the swelling ratio of nanocomposite membrane with 20% laponite slightly increased with increasing temperature.
2. Dynamic mechanical analysis showed the systematic increase in storage modulus with laponite content, which indicates the enhancement of mechanical property after laponite addition. It also showed the decrease in tan delta peak values of nanocomposite membranes with an increase in laponite concentration in nanocomposites. The decrease in tan delta peak values can be attributed to the formation of rigid amorphous phase.
3. The permeabilities of the nanocomposite membranes were strongly dependent on the solute size i.e. exhibiting the size exclusion phenomenon.

   The presence of well-dispersed laponite in nanocomposite membranes reduced the permeability of hemoglobin solute due to an increased effective path for diffusion (tortuosity effect).

5.6 References

1. Alexandre, M.; Dubois, P Materials Science and Engineering **2000**, *28*, 1.
2. Churochkina, N. A.; Starodoubtsev, S. G.; Khokhlov, A. R. Polymer Gels and Networks **1998**, *6*, 205.
3. Liang, L.; Liu, J.; Gong, X. Langmuir **2000**, *16*, 9895.
4. Xia, X.; Yih, J.; D'Souza, N. A.; Hu, Z. Polymer **2003**, *44*, 3389.
5. Lee, W-F.; Fu, Y-T. J. Appli. Polym. Sci. **2003**, *89*, 3652.
6. Messersmith, P. B.; Znidarsich, F. in "Nanophase and Nanocomposite Materials II", MRS Symposium Proceedings **1997**, 457.
7. Haraguchi, K.; Takehisa, T.; Fan, S. Macromolecules **2002**, *35*, 10162.
8. Haraguchi, K.; Farnworth, R.; Ohbayashi, A.; Takehisa, T. Macromolecules **2003**, *36*, 5732.
9. Haraguchi, K.; Takehisa, T. Advanced Materials **2002**, **14**, 1120.
10. Greenland, D. J. J. Colloid Sci. **1963**, *18*, 647.
11. Zebrowski, J.; Prasad, V.; Zhang, W.; Walker, L. M.; Weitz, D. A. Colloids and Surface A : Physicochem. Eng. Aspects **2003**, *213*, 189.
12. Emerson, W. W.; Raupach, M. Australian J. of Soil Research **1964**, *2*, 46.
13. Toyoshima, K. in "Polyvinyl Alcohol, Properties and Applications", Finch, C. A.(Edi) A Wiley-Interscience Publication, **1973**, Chapter13.
14. Xu, J.; Meng, Y. Z.; Li, R. K. Y.; Xu, Y. Rajulu, A. V. J. Polym. Sci. Part B **2003**, *41*, 749.
15. Bonn, D.; Kellay, H.; Tanaka, H.; Wegdam, G.; Meunier, J. Langmuir **1999**, *15*, 7534.
16. Wang, D.; Zhu, J.; Yao, Q.; Wilkie, C. A. Chem. Mater. **2002**, *14*, 3837.
17. Ogata, N.; Kawakage, S.; Ogihara, T. J. Appl. Polym. Sci. **1997**, *66*, 573.
18. Yu,Y-H.; Lin, C-Y.; Yeh, J.-M.; Lin, W-H. Polymer **2003**, *44*, 3553.
19. Cypes, S. H.; Saltzman, W. M.; Giannelis, E. P. J. Controlled Release **2003**, *90*, 163.
20. Messersmith, P. B.; Giannelis, E. P. J. Polym. Sci. A Polym. Chem. **1995**, *33*, 1047.

21. Yeh, J-M.; Yu, M-Y.; Liou, S-J. J. Appli. Polym. Sci. **2003**, *89*, 3632.

22. Xu, R.; Manias, E.; Snyder, A. J.; Runt, J. Macromolecules **2001**, *34*, 337.

CHAPTER 6

Molecular Origins of Wettability of Hydrophobic Poly(Vinylidene Fluoride) Microporous Membranes upon Poly(Vinyl Alcohol) Adsorption: Surface and Interface Analysis by XPS

6.1 Introduction

Applications of hydrophobic membranes in bio-separation are limited since they are susceptible for irreversible protein adsorption and fouling. There are several approaches, which have been reported to render membranes hydrophilic in nature such as chemical modification,[1,2] plasma treatment[3-7] and coating.[8-11] The modification involves the introduction of polar functional groups onto the polymer surface by surface grafting, coupling reactions etc.[12,13] However, the modification of fluoropolymers by chemical methods in particular, is rather difficult due to their very good chemical resistance. Therefore, alternative approaches have been explored.

Recently, the adsorption of hydrophilic polymers onto hydrophobic surfaces has attracted major attention although the concept of protein adsorption onto hydrophobic biological membranes was known much earlier. For example, in order to improve the wettability, adhesion and chemical reactivity, the hydrophobic surface of a fluoropolymer, poly(tetrafluoroethylene-*co*-hexafluoropropylene) [FEP] film was modified by poly(L-lysine) [PLL] by simple adsorption technique.[14] The adsorption characteristics were studied by X-ray photoelectron spectroscopy [XPS] and contact angle measurements. It was observed that, PLL adsorbs only under certain conditions such as at pH 11, when it exists in the hydrogen bonded ∝–helix conformation.

Although, most of the synthetic water soluble polymers do not adsorb onto hydrophobic surfaces, it has been shown that poly (vinyl alcohol) [PVA] spontaneously adsorbs onto hydrophobic substrates.[15-20] PVA is highly hydrophilic, non-toxic and biocompatible polymer with an excellent film forming property. The films have high mechanical strength, low fouling potential and long-term temperature and pH stability. PVA was found to be unique such that it is atactic and yet semicrystalline. These properties of PVA have led its use in bioseparations. Kozlov *et al* [15] have studied the adsorption of PVA onto different hydrophobic substrates, which include fluoropolymers, hydrophobic polyolefins, silicon wafers and polyester films. They generalized the phenomenon of adsorption of PVA from the aqueous solution onto hydrophobic surfaces and hypothesized that the hydrophobic interactions or the displacement of water molecules from the hydrophobic solid water interfaces and

crystallization drives the adsorption. Serizawa *et. al.*[16] have reported on the formation of multiple thin layers on the gold surface by repetitive PVA adsorption and drying process.

Coupe and Chen[17] have examined the effect of PVA concentration on the kinetics of adsorption by XPS. They have also reported that PVA adsorption onto FEP showed greater adsorbed amount and improved wettability. It was thought that the cause of adsorption is low solubility of PVA in conjunction with crystallization at FEP/water interface, which is an additional driving force of adsorption and stabilization of the film by inter/intramolecular hydrogen bonding. The driving force for the multilayer assembly could be due to the intermolecular H-bonding between the initially adsorbed PVA in the dry state and PVA chain in aqueous solution. The average thickness of PVA in the multilayer adsorption can be calculated by the following equation,

$$\ln\left(\frac{N}{N_0}\right)\sin\theta = \frac{nZ}{\lambda} \qquad (6.1)$$

where, N and N_0 are the fluorine content in the adsorbed (FEP-PVA) and un-adsorbed FEP films. n is the number of layers, Z is the average layer thickness, λ is the mean path of the electron and θ is the take off angle.

Nash *et al*[18] have reported on the adsorption of PVA onto poly(styrene-divinyl benzene) beads for use in affinity chromatography. Despite the fact that PVA adsorption onto various hydrophobic surfaces has been studied extensively for a variety of applications, the exact mechanism of irreversible adsorption of PVA onto hydrophobic porous substrates is not understood. In the present work, we have studied the adsorption of PVA onto highly porous, hydrophobic poly(vinylidene fluoride) (PVDF) membranes and give more insight into the mechanisms of adsorption. The improved wettability of the hydrophobic PVDF membranes was investigated by water flux and contact angle measurements. The incorporation of PVA onto PVDF membranes was confirmed by XPS and EDAX studies. The influence of concentrations and molecular weights of PVA on the adsorption was also investigated by using XPS. XPS studies clearly showed a surface domination of PVA with the

formation of interface between PVA and PVDF. Further, the energy of the highest occupied molecular orbital (HOMO) of PVDF changes to lower binding energy and the nature of HOMO changes from fluorine to oxygen derived upon PVA adsorption, which could be the origin of wettability.

6.2 Experimental

6.2.1 Materials

Poly (vinyl alcohol) of MW 31000 ,67000 and 205000 were purchased from Fluka and PVA with MW 186000 was obtained from Aldrich, USA. The degree of hydrolysis was in the range of 86.7-88.7 mol%. The hydrophobic porous PVDF membranes with pore size of 0.45μm were purchased from Millipore.

6.2.2 Adsorption of PVA onto PVDF Membranes

PVA solutions with different concentrations 0.5-20% were prepared by heating respective weights of PVA in water at 80°C and allowed them to cool to room temperature. The heating helps in breaking of self H-bonded PVA chains and enhances the solubility. Adsorption and water flux experiments were carried out by using stirred cell (**Figure 6.1**). The pressure applied was controlled by nitrogen gas. Hydrophobic PVDF membrane was fitted in a magnetically stirred cell and 10 ml PVA aqueous solutions with different concentrations was added to the cell and stirred for 15 min. A 0.2 bar pressure was applied to pass PVA solution through the membrane. The concentration of PVA was changed and different membranes with varying concentration of PVA were prepared. These adsorbed membranes were washed with deionized water and hot water to remove any unadsorbed polymer on the surface until the permeate showed negligible UV absorbance for PVA in the washed liquid.

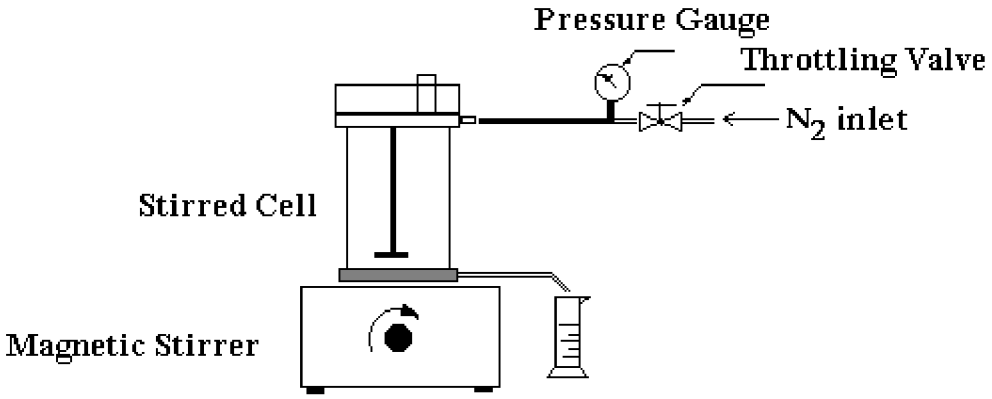

Figure 6.1: Schematic of the stirred cell

6.3 Characterization

6.3.1 Water Flux (Permeation Study)

Permeate fluxes of pure water were measured on adsorbed membranes in stirred cell at 0.6 bar and at room temperature. Dry membrane samples for characterization were treated with iso-propanol and then hexane followed by vacuum drying for 24 hours.

6.3.2 X-ray Photoelectron Spectroscopy (XPS)

XPS was studied using a VG Microtech Multilab ESCA 3000 spectrometer[21,22] with a non-monochromatized Al Kα X-ray (hν = 1486.6 eV) on virgin PVDF membrane and after adsorption of PVA on PVDF membranes. Base pressure in the analysis chamber was maintained at 3-6 x 10^{-10} mbar range. The energy resolution of the spectrometer was set at 1 eV at a pass energy of 20 eV. Binding energy (BE) was calibrated with respect to Au $4f_{7/2}$ core level at 83.9 eV. The error in all the BE values reported is ±0.1 eV.

6.3.3 Energy Dispersive X-ray Analysis (EDAX)

Bulk composition of both virgin PVDF and PVA adsorbed PVDF membranes were carried out by using EDAX (Phoenix, EDAX international, USA) at an accelerating voltage of 20 KV.

6.3.4 Mercury Intrusion Porosimetry

Porous properties of the membranes were studied by using mercury intrusion porosimetry (Autoscan-33 mercury porosimeter from Quantachrome, USA) in the pressure range of 0-33000 PSIG.

6.3.5 Contact Angle Measurement

Contact angle measurements were carried out with Rame Hart telescopic goniometer equipped with a Gilmont syringe. Demineralized water was used for contact angle measurements.

6.3.6 Thermal Gravimetric Analysis (TGA)

TGA measurements were performed on a Perkin Elmer TGA-7. The membrane samples were heated from 50-700°C temperature range at a heating rate 10°C/ min under nitrogen atmosphere.

6.3.7 FT-IR Analysis

Fourier transform infrared (FT-IR) spectra were recorded using Thermo Nicolet Nexus 870 FTIR with continuμm microscope in reflectance mode using 32 X magnification (MCT-A Detector was used).

6.4 Results and Discussion

6.4.1 FT-IR Spectroscopy

Adsorption of 4% PVA with different molecular weights of PVA on PVDF membranes was confirmed qualitatively by using FT-IR spectroscopy. The FT-IR spectra of virgin PVDF and PVA adsorbed PVDF membranes are shown in **Figure 6.2**. A PVA spectrum is not shown in this figure since it is recorded in transmittance mode. However, FT-IR spectra of PVDF and absorbed membranes are recorded in reflectance mode. All the spectra presented here are the difference spectra of PVA adsorbed PVDF films and blank PVDF film. Virgin PVDF shows the absorption bands at 815, 844, 890, 1141, 1205, 1273, 1345, 1422 cm^{-1}. The absorption bands in the region of 1120-1280cm^{-1} are characteristics of C-F stretching of PVDF. The C-H

stretching of alkane groups of PVDF appears at 2986 and 3027 cm^{-1}. In addition to the PVDF peaks, the adsorbed membranes show characteristic new broad band near 3372 cm^{-1} (dotted line as shown in figure) which can be attributed to the -OH stretching frequency of PVA. The presence of OH stretching band in adsorbed membranes confirmed the adsorption of PVA on PVDF membranes.

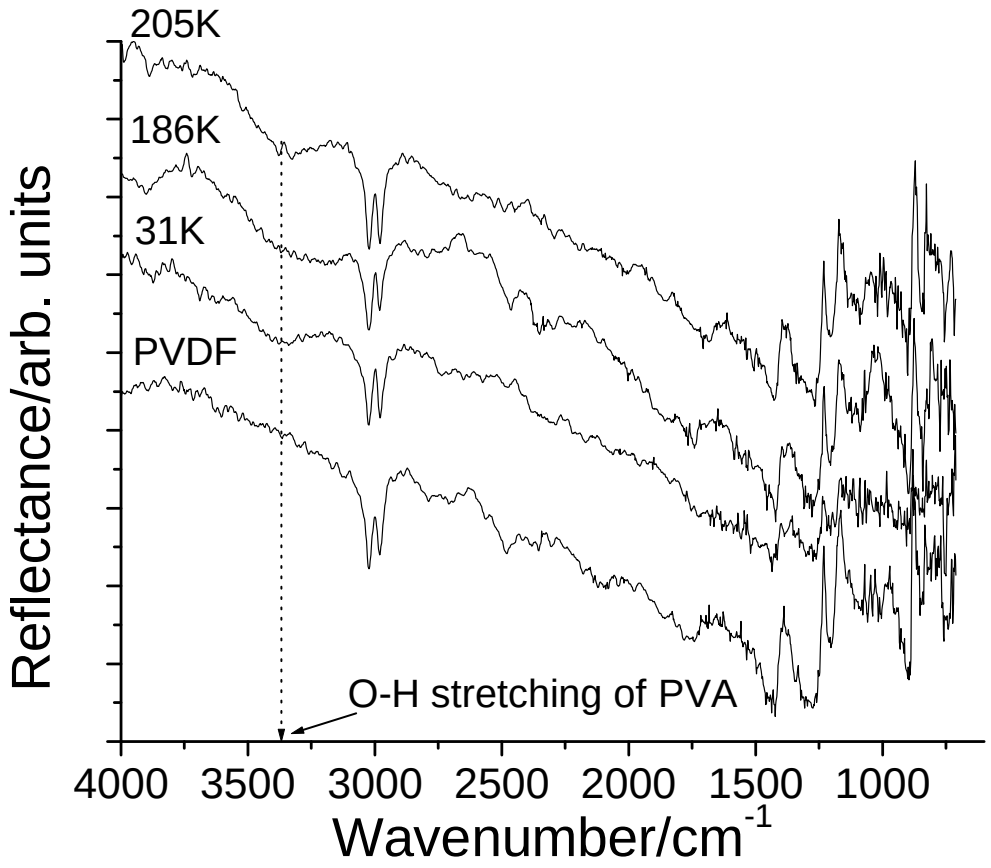

Figure 6.2: FT-IR spectra of PVDF and PVA adsorbed PVDF membranes

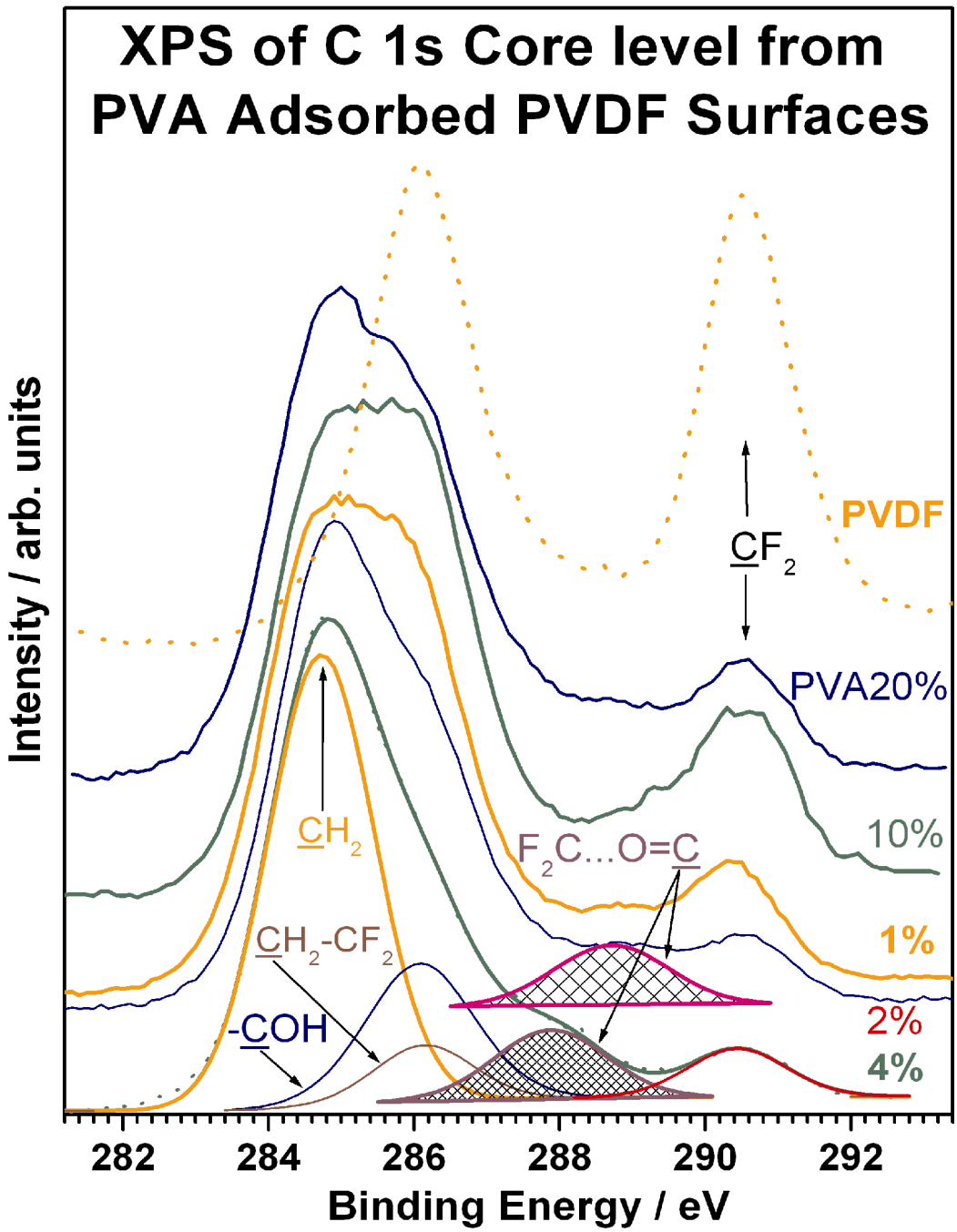

Figure 6.3: Carbon 1s core level spectra from virgin PVDF and PVA adsorbed PVDF surfaces. C 1s from 4% PVA treated surface is deconvoluted to show the individual peaks and note the shift in binding energy of carbonyl carbon in it

6.4.2 XPS of Carbon 1s core level

XPS is an important tool, which gives invaluable information on the atomic compositions of the surfaces. We show in **Figure 6.3** a comparison of carbon 1s (C1s) core level spectra from untreated PVDF membrane and PVA adsorbed PVDF membranes with different PVA concentrations. It is to be noted that the PVDF membranes treated with high (≥10%) and low (≤1%) PVA concentrations do not show uniform PVA adsorption and patchy surfaces are observed by naked eyes. Further, a change in molecular weight of PVA from 31 K to 67 K also does not have significant influence in the binding energy (BE) of any of the elements, except for surface composition (*vide infra*).

PVDF membranes show two carbon features at 286 and 290.6 eV due to CH_2 and CF_2 group carbons, respectively. However upon treatment with 1% PVA solution for 15 minutes a dramatic decrease in CF_2 intensity and a broadening in the CH_2 carbon peak indicated the adsorption of PVA on PVDF. The carbon species at lowest BE (284.7 eV) and at 286 eV is attributed to the all backbone methylene group carbons and carbons attached to oxygen in PVA, respectively. A small peak is discernible at around 288.5 eV. On increasing the PVA concentration to 2%, a further decrease in CF_2 group intensity and a corresponding decrease in the intensity of associated CH_2 group were observed. In the case of 2% PVA adsorption, a peak at 288.5 eV is clear and it is comparable in intensity to that of CF_2 group at 290.6 eV. On further enhancement in the PVA concentration upto 4% shows an additional changes of lowest CF_2 group intensity and a comparatively higher intensity of the peak at 287.9 eV. Deconvolution was performed to show the individual components for all C 1s peaks. It is assumed for deconvolution that, CF_2 and the associated CH_2 groups from the PVDF should have the same intensity ratio as observed on pure PVDF. The carbons associated with hydroxyl groups in PVA are attributed to the peak at 286.1 eV. The carbonyl carbon from PVA (since it is 87% hydrolyzed it has acetate groups) is attributed to the peak between 287.9 to 288.7 eV and this particular group is suspected to be at the interface between the PVA and PVDF. A considerable decrease in the BE of the above interface on 4% PVA adsorbed membrane clearly indicates that

there could be some charge transfer from carbonyl oxygen to PVDF chain, likely through the carbons of CF_2 group, which are electron deficient **(see Figure 6.4).**

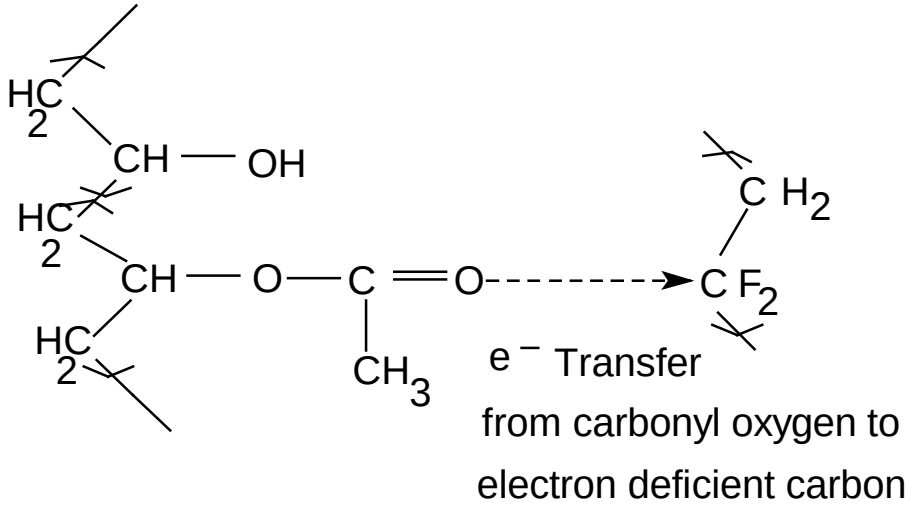

Figure 6.4: Charge transfer from carbonyl oxygen to electron deficient carbon of PVDF

Higher percentage of PVA adsorbed samples (≥10%) show an increase in CF_2 and the corresponding CH_2 group intensity. The interface carbonyl carbon also shifts to higher BE to 288.7 eV. However, the patchy non-uniform surfaces observed on higher PVA adsorption makes the comparison difficult to the results from low percentage PVA treated (<10%) surfaces. Nonetheless, the qualitative trend observed in our results clearly shows that, the higher PVA percentage treatment does not necessarily increase the PVA content on the PVDF surfaces. Apparently, 4% PVA concentration treatment on PVDF displays the maximum PVA adsorption and indicates that there is a threshold PVA coverage on PVDF. This is further confirmed from the above observation of increasing CF_2 intensity ≥5% PVA adsorbed surfaces (*vide infra* **Figure 6.6**). This observation reiterates that it is not just a physical multiple deposition of PVA on PVDF, but a limited PVA adsorption and a fairly strong interaction between PVA and PVDF. Other core level and valence band studies substantiate our above conclusions.

6.4.3 XPS of Oxygen 1s core level

Figure 6.5a shows the oxygen 1s core level spectra from PVA adsorbed PVDF membrane surfaces after normalization to 4% PVA adsorbed surfaces. As expected, the virgin PVDF surface does not show any significant oxygen 1s intensity and is not shown in **Figure 6.5**a. On PVA adsorption with 1, 2 and 10% solution shows oxygen 1s peak at 532.4 eV (dotted line) with a marginal change in full width at half-maximum (FWHM) of 2.3±0.1 eV. However oxygen 1s from 4% PVA adsorbed surface shows a shift in BE to 531.9 eV and an additional broadening to lower BE with a FWHM = 2.8 eV. This indicates that there is an additional oxygen component, which plays a significant role on 4% PVA adsorbed membranes. Deconvolution of oxygen 1s core level from PVA (1, 2 and 10%) adsorbed PVDF surfaces also shows two peaks with a BE difference of 0.7 eV and the low BE feature appearing at 532 eV. However, 4% PVA surface shows two components at 531.5 and 532.8 eV. Further the intensity ratio of low to high BE feature is 3:2 for 4% and higher PVA concentration, and it is 3:5 for 1 and 2% PVA adsorbed surfaces. Hence, it is suggested that the oxygen at low BE might be playing a crucial role in the interface formation with PVDF backbone.

6.4.4 XPS of Fluorine 1s core level

Figure 6.5b shows the fluorine 1s core level spectra from PVDF and PVA adsorbed PVDF membrane surfaces. Virgin PVDF surfaces shows intense F 1s peak at 688.2 eV. However, all PVA adsorbed PVDF membranes show the F 1s peak at 687.8 eV, with different intensities. This clearly indicates that there is a significant increase in the electron density of fluorine due to PVA adsorption, irrespective of the concentration of PVA. F 1s peak intensity decreases, exactly the same manner as with CF_2 group intensity in C 1s results **(Figure 6.3)**; an intensity decrease from 1% PVA to 4% PVA and then interestingly it increases above 4% PVA concentration. This result also clearly suggests that there exist a threshold coverage of PVA on PVDF and it is about 4%.

6.4.5 Valence Band XPS Studies

Figure 6.5c shows the valence band (VB) spectra obtained from PVDF and PVA adsorbed PVDF membrane surfaces. Virgin PVDF membrane shows a small peak around 6 eV and a number of other bands at 7.3, 8.8, 9.5, 12.9 and 15.2 eV are attributed to F 2p, C 2p and C 2s derived features.[23] Our VB results on PVDF is in excellent agreement with the earlier ultraviolet photoemission spectral results.[23] The HOMO around 6 eV is from the bonding orbitals of the carbon atoms in the main chain and the antibonding orbitals of the C-F bonds.[23] Upon PVA adsorption on PVDF membranes, there is a development of a new filled band at BE ≤ 5 eV and it shifts with the increasing percentage of PVA. The shift in the BE of the top most band is indicated by solid arrows in **Figure 6.5c**. Furthermore, the photoemission onset also shifts to lower BE in resonance with the BE of the top most band and the lowest onset energy observed at 4% PVA adsorbed surface is at 2 eV (broken arrow). Additionally an increase in PVA concentration increases the BE of the HOMO to higher BE. There is an overall agreement between the VB features from PVDF and PVA adsorbed PVDF membranes in terms of BE; however, the sharpness and the intensity of the bands decreases and starts broadening with increase in PVA concentration and a maximum broadened VB features were observed at 4% PVA adsorbed surfaces. Additional increase in PVA concentration again starts showing sharper PVDF features at the same BE as on virgin PVDF. It is to be noted that the insulating character of PVDF changes upon PVA adsorption and a resistance value in the range of 60-100 GΩ is observed for any PVA adsorbed PVDF membranes. The positive static charging observed in XPS on PVDF, also decreases very significantly upon PVA adsorption. This is in agreement with a decrease in the HOMO energy of PVA adsorbed PVDF membranes.

It is to be noted from the literature that the oxygen 2p derived orbital as well as unsaturated carbon-carbon bonds here brings in the high density of states of HOMO.[24] From this viewpoint it is likely that the development of the new filled band below 5 eV, which is also HOMO for PVA adsorbed PVDF surfaces (**Figure 6.5c)** should be derived from oxygen 2p features. An increase in the intensity of HOMO of PVDF at 6

eV and a decrease in F 1s core level BE on PVA adsorbed surfaces indicates some electron filling of C-F antibonding band. This suggests, a decrease in C-F bonding character at least on the surface and interface of PVDF and might be a reason for the enhanced and irreversible bonding between PVA and PVDF. Furthermore, certain specific orientation between PVA and PVDF might enhance the extent of adsorption and/or interaction among them and especially at 4% PVA adsorbed surface the interaction may be the highest. Such geometric alignments between PVA and PVDF cannot be ruled out for the maximum water permeability (discussed in the foregoing) and also the special features observed in XPS results. Molecular modeling studies might throw more light on such orientations and their effects on properties.

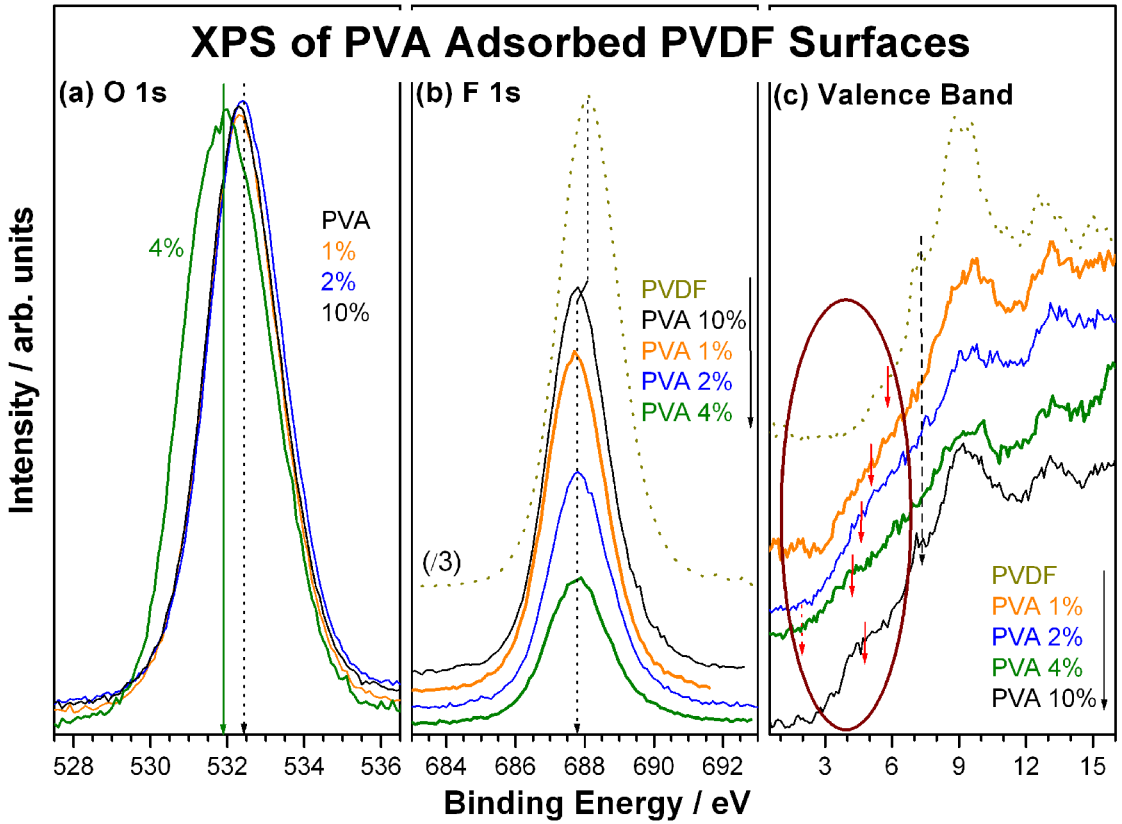

Figure 6.5: XPS recorded from (a) O 1s core level, (b) F 1s core level, and (c) valence band on virgin PVDF and PVA adsorbed PVDF membrane surfaces.

6.4.6 Surface Concentration of Constituent Elements

Figure 6.6 shows the surface atom percentage of all the elements analyzed on virgin PVDF and 31 K PVA adsorbed PVDF membranes. Further, the top and bottom surfaces of the membranes are also analyzed at normal emission angle as well as at grazing angle to probe any enhancement of PVA on the surface. **Figure 6.6a** shows the carbon atom percentage from CF_2 group carbons and all other carbon atoms clubbed together. This is mainly to show how the PVDF contribution to surface changes with PVA adsorption. Although PVDF should show 1:1 ratio of CF_2:CH_2, a reasonably high CH_2 percentage indicates that the C-F bonds are projected in such a way that fluorine towards surface and carbon towards the subsurface, and it may be likely due to minimize the surface energy. Total fluorine atom percentage (51%) is slightly higher than carbon atom percentage (49%). Nonetheless, this indicates the surface is somewhat rich in fluorine and the carbon and fluorine atom percentage ratio is close to 1:1 on PVDF. 1-2% PVA adsorbed PVDF membrane surface shows a drastic reduction in the F-content to less than 20% on the surface and a simultaneous increase in the oxygen content of more than 20%. A corresponding decrease in CF_2 group carbon atom percentage also is observed. These observations reiterate that an increase in oxygen atom percentage is exclusively due to PVA adsorption. Independent of PVA concentration, a very significant fluorine atom percentage (8-20%) on PVA adsorbed PVDF surfaces hints that the PVA adsorption is exclusively limited to surface, likely less than the probing depth of XPS, which is about 5 nm. A simple comparison of virgin and 4% PVA adsorbed PVDF surfaces displays a change in surface atomic character from predominant fluorine to carbon and oxygen derived, respectively. This is further confirmed from the EDAX analysis of PVA adsorbed onto PVDF membranes. Irrespective of concentration and molecular weight (31K or 67 K) of PVA, the weight percentage of oxygen (varies between 4.5±0.6%), carbon (58±1%) and the fluorine (38±0.8%) does not change significantly.

The total carbon atom percentage from all other carbons also increases, mainly due to contributions from adsorbed PVA. The 4% PVA adsorbed PVDF membrane shows a further increase in non-fluoro carbon atom percentage and a minimum

amount of fluorine content of 8%. Notably, oxygen atom percentage also decreases to a low level of 16%; however it is significantly higher than the fluorine content. A careful comparison of all atom percentages reveal that the non-fluoro carbon content is highest and other atom percentages are at their lowest on 4% PVA adsorbed surfaces and this might be due to rearrangement of methylene backbones of PVA to an optimal configuration. A further increase in PVA percentage decreases the non-fluoro carbon percentage and it shows around 60% for all higher PVA levels. However, the fluoro-carbon percentage and fluorine content remains between 4-7% and 15-20%, respectively, at high PVA levels. Oxygen percentage was remained around 22-24% for all high PVA adsorbed PVDF membranes and that also indicates that the excess PVA was not adsorbed on the PVDF surfaces and PVA adsorption was limited to surface.

The above measurements made at grazing emission angle revealed some changes in the atom percentage on the surfaces compared to normal emission, especially with F and O atoms at low PVA levels. About 3% decrease in oxygen at grazing angle compared to normal and to the same extent but an increase in fluorine at grazing angle compared to normal on 1% PVA adsorbed PVDF membranes reveals that PVA amount is not sufficient to fully cover the PVDF surfaces and it is likely that there may be some portions of PVDF membrane without any PVA adsorbed on it. The difference between normal and grazing angle decreases with increasing PVA% up to 4%. Oxygen content does not show any difference between normal and grazing emission angle on 4% PVA adsorbed membranes with lowest F-content indicates that all PVDF pores are likely adsorbed with PVA for few monolayers, within the probing depth of about 5 nm in XPS. It is needless to state that the top surface layers are highly crucial in determining the wettability of any surfaces. Further an increase in PVA% reverses the trend that is observed below 4%. This behavior is attributed to the viscous nature of PVA at higher percentage, which might prevent efficient PVA adsorption on PVDF membrane surfaces.

Selected PVA adsorbed PVDF membrane surfaces were analyzed on the bottom surfaces also to see the change in atomic content. About 10-17% oxygen content and 20-30% fluorine content definitely indicates that PVA got adsorbed throughout the bulk surfaces of the PVDF membrane. However, the higher percentage

and hence viscous PVA hinders its diffusion and adsorption on PVDF. However some amount of PVA adsorption throughout the bulk surfaces is obtained even with viscous PVA solutions. Our EDAX analysis also confirms the same.

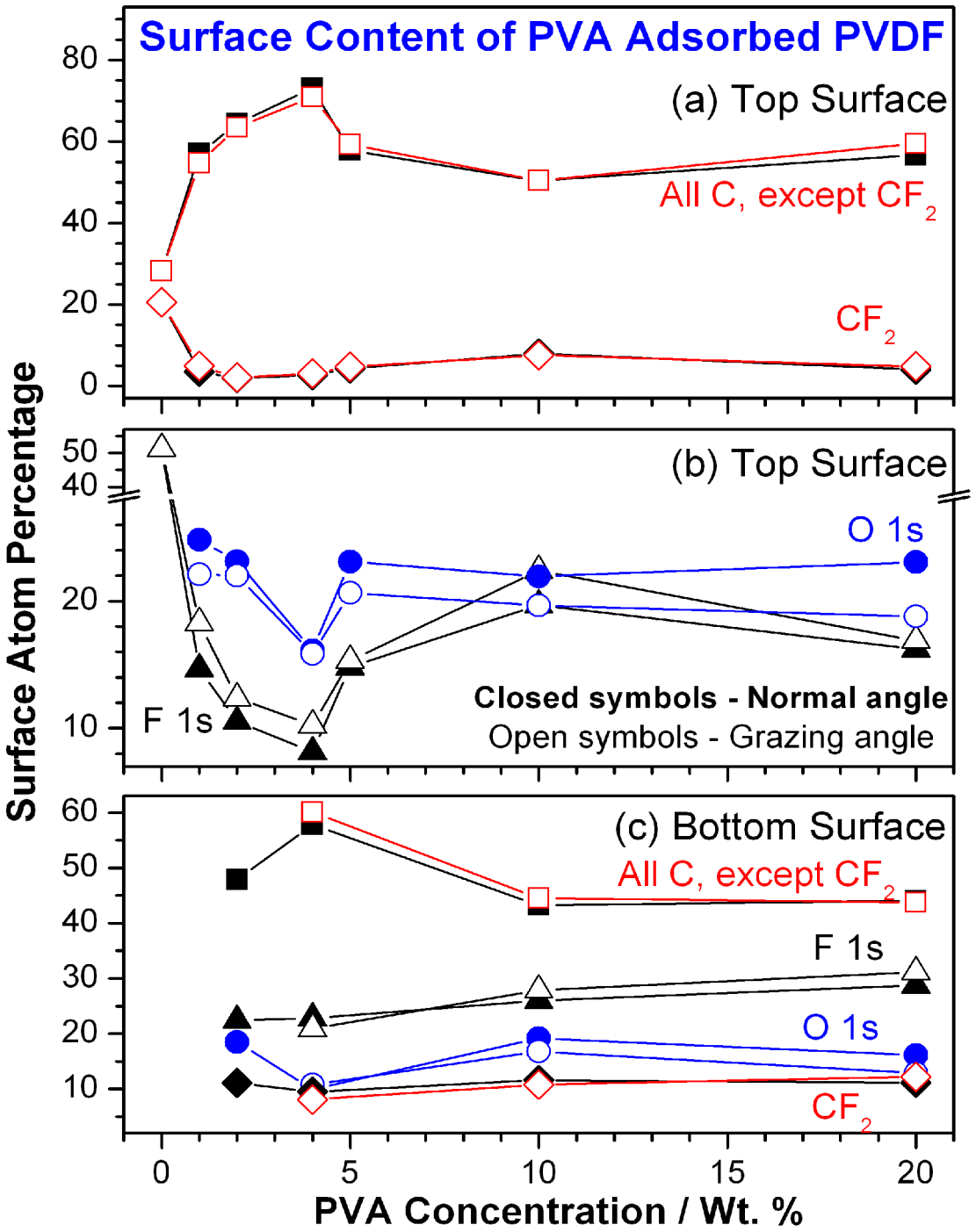

Figure 6.6: Plots of Surface atom percentage measured on top (a and b) and bottom (c) surfaces of PVDF and 31 K PVA adsorbed PVDF membranes from XPS results.

6.4.7 Membrane Texture Properties

Some of the representative membranes were subjected to mercury porosimetry analysis and the results are shown in **Figure 6.7**. Differential pore volume to pressure (dV/dP), cumulative surface area and pore number fraction is plotted against the pore size distribution in **Figures 6.7a, b and c,** respectively for PVDF (blue dotted), 31 K PVA 4% (orange) and 67 K PVA 4% (green) adsorbed on PVDF membranes. Differential pore volume to pressure indicates that the micro pore size decreases to a significant extent but not dramatically upon PVA adsorption. However, it is to be noted that the two intermediate size pores of 0.015 and 0.03 μm on PVDF membrane disappears completely after PVA adsorption. Besides, it creates a range of nano pores in the membrane (dotted box in **Figure 6.7a**). Some of the above points affirmed from the observation of same extent of cumulative surface area found from micro pores before and after PVA adsorption. However the main reason for high surface area on virgin PVDF membrane is due to intermediate pores and PVA adsorption should have been really effective on these pores and hence the size of these pores shrinks greatly to nanopore sizes **(Figure 6.7b).** However, the nanopores created after PVA adsorption contributes in a major way to an increase in surface area. Originally, there are no nanopores available on the virgin PVDF membranes.

Pore number fraction measured also indicates that the micro pore size reduced significantly with both 31 K and 67 K PVA adsorption. A definite decrease in pore size, from 0.22 μm on PVDF to 0.13 μm, is evident after PVA adsorption compared to virgin PVDF (see dotted box in **Figure 6.7c**). Creation of nanopores too is evident and that contributes to the maximum for pore number fraction. Furthermore, nanopores with certain sizes (5.5, 8 and 13 nm) are completely absent on 67 K PVA adsorbed surface indicates that there could be some preferred alignments of backbone chains and molecular modeling studies might throw light which is beyond the scope of the present work. The above textural properties before and after PVA adsorption on PVDF, mainly suggest that the PVA adsorption preferentially takes place on intermediate pores on PVDF and then on micro pores. It is also to be noted that the different backbone chain lengths in 31K and 67K PVA have some effect on textural properties.

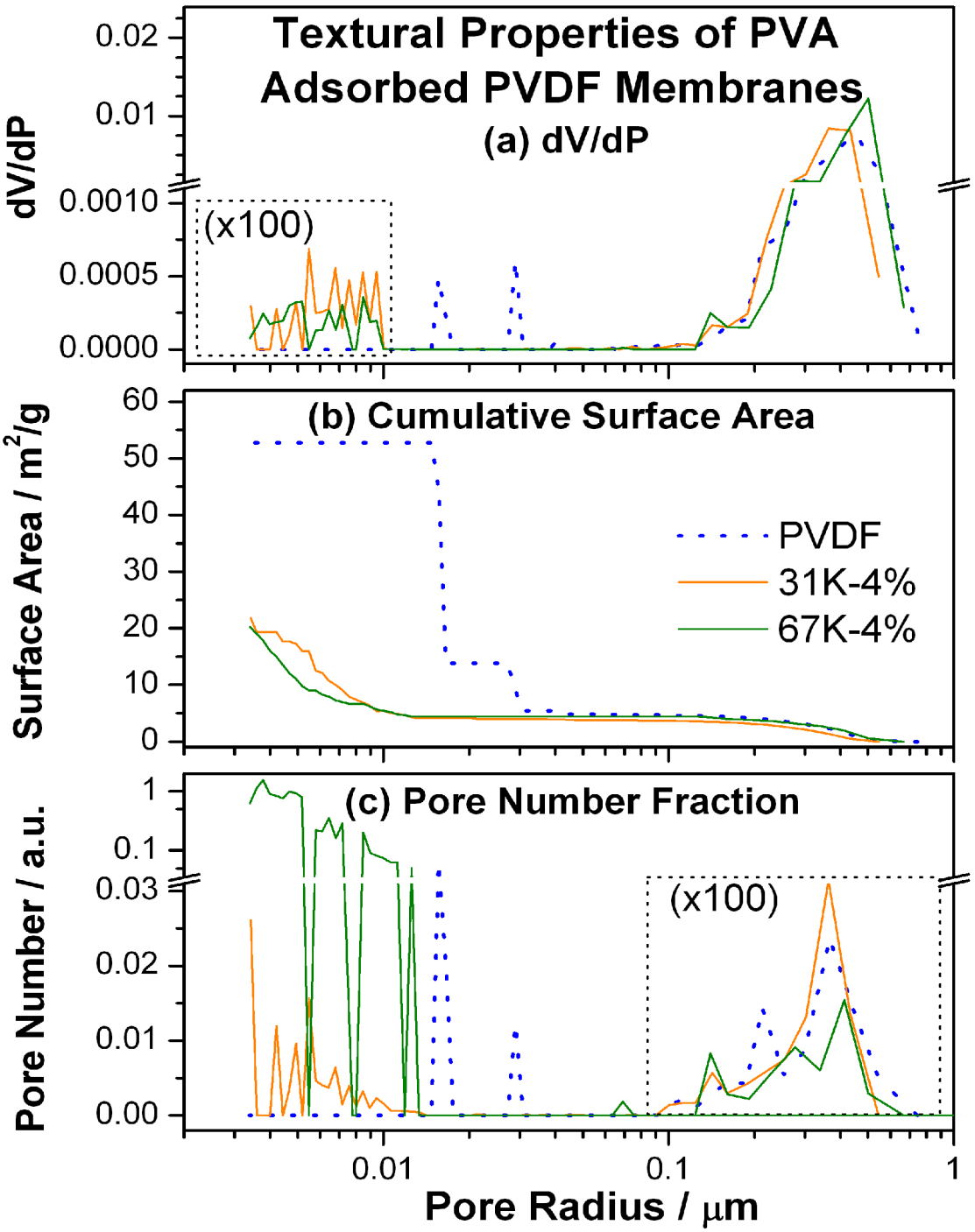

Figure 6.7: Textural properties measured from mercury porosimeter are plotted against pore radius of PVDF and PVA on PVDF membranes. (a) Differential pressure to differential volume change, (b) surface area and (c) pore number fraction.

6.4.8 Water Permeation Studies

The untreated PVDF membranes are microporous and highly hydrophobic in nature. Therefore, they did not show any water permeation at 0.6 bar. However, upon hydrophilizing them with PVA, they showed high water permeation. We show in **Figure 6.8**, the water permeation of PVDF membranes treated with PVA (31 K) of different concentrations. It can be readily seen that, the water flux increases and is maximum for PVDF membranes treated with 4% PVA and then it remains almost constant. This also supports the existence of a threshold coverage of PVA on PVDF at 4% concentration. The increase in water flux is attributed to the increase in hydrophilicity of the PVDF membranes. The increase in hydrophilicity was further confirmed by contact angle measurements. We have not given any data on contact angle measurements. The quantitative measurement of the contact angle was limited by the porous nature of the PVDF membrane. The irreversible adsorption of PVA on PVDF is intriguing and perhaps can be considered as the simplest method of converting hydrophobic membranes into hydrophilic membranes. The membrane textural properties indicated the change in size of intermediate pores after adsorption of PVA. The critical balance of PVA concentration on the PVDF membranes and the pore size can influence the permeability of membranes.

A comparison of **Figures 6.6** and **6.8** reveals that the water permeability increases somewhat linearly with increase in carbon content (except fluoro carbons) **(Figure 6.6a).** Similarly, the water permeability and fluorine content on the surface displays an inverse but linear trend. However such a relation is not obvious between oxygen content and water permeability, due to very small amount of oxygen in PVA molecule. This also indicates that the diminishing fluorine content and an optimally adsorbed PVA content on the surface might be equally important for water permeability in the present case.

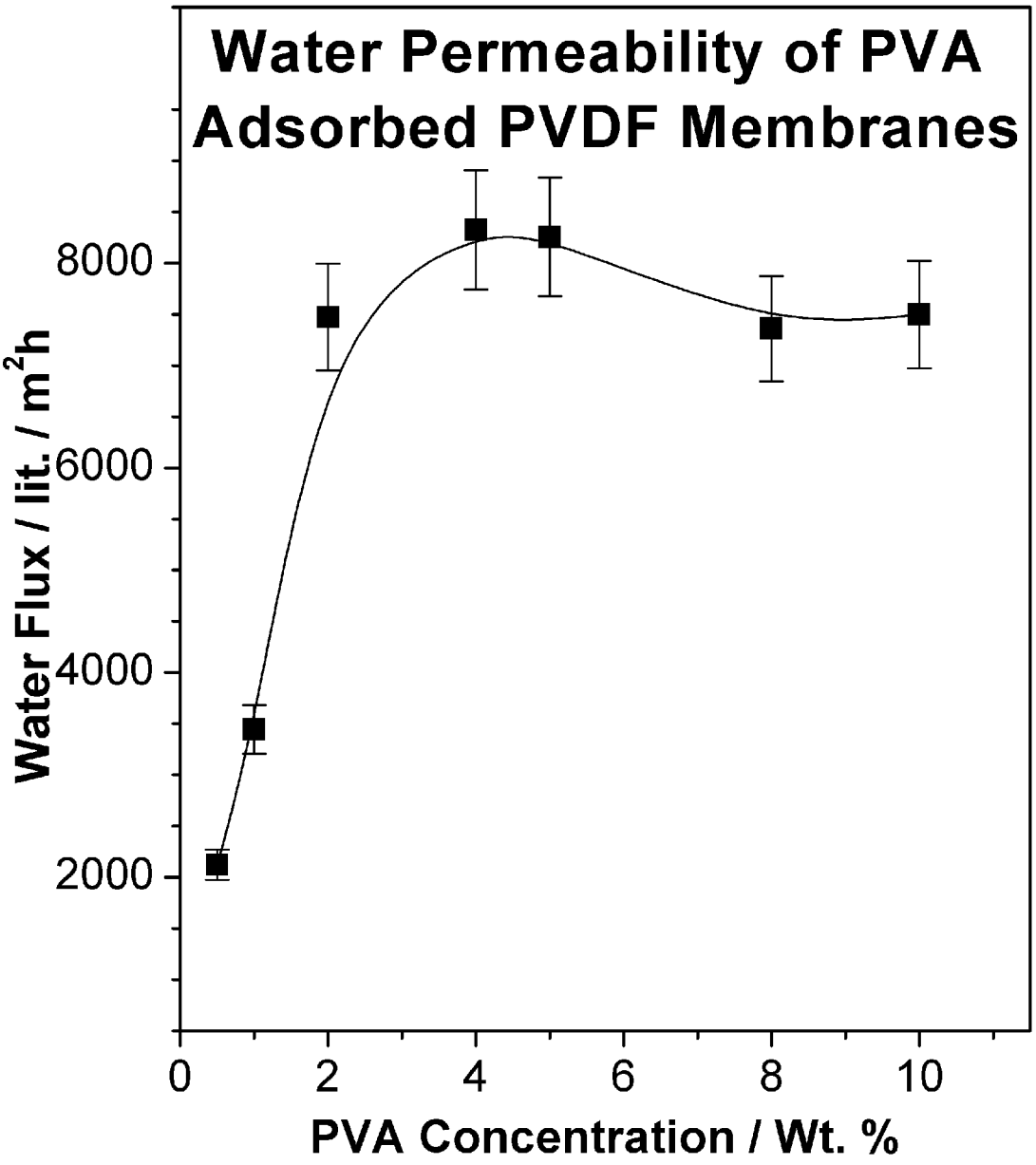

Figure 6.8: Rate of water permeability on PVA (31 K) adsorbed PVDF membranes at 0.6 bar.

6.4.9 TGA analysis

Thermal properties of PVDF and PVA adsorbed PVDF membranes were studied by thermo gravimetric analysis. PVDF homopolymer shows thermal stability upto temperature 470 ºC and above this temperature it shows loss of weight with elimination of HF.[25] PVA generally shows two regions of thermal degradation near 300ºC and 400ºC.[26] **Figure 6.9** shows the TGA curves of PVA, PVDF, 2%, 4%, 10% PVA adsorbed PVDF membranes. It was observed from the figure that the onset of thermal decomposition of PVA adsorbed membranes shifted to higher temperature than PVDF membrane. [PVDF membrane shows thermal degradation (onset temperature) at 470 ºC while PVA adsorbed PVDF membranes shifts slightly higher temperature in the range of 477-483 ºC.] Similarly PVA adsorbed PVDF membranes exhibited 11-15 ºC increase in decomposition temperature for 20% weight loss than virgin PVDF membrane. This result indicates that the adsorption of PVA on the PVDF membrane marginally enhanced the thermal stability of membrane. The increase in thermal decomposition temperature can be attributed to the strong interaction between PVA and PVDF.

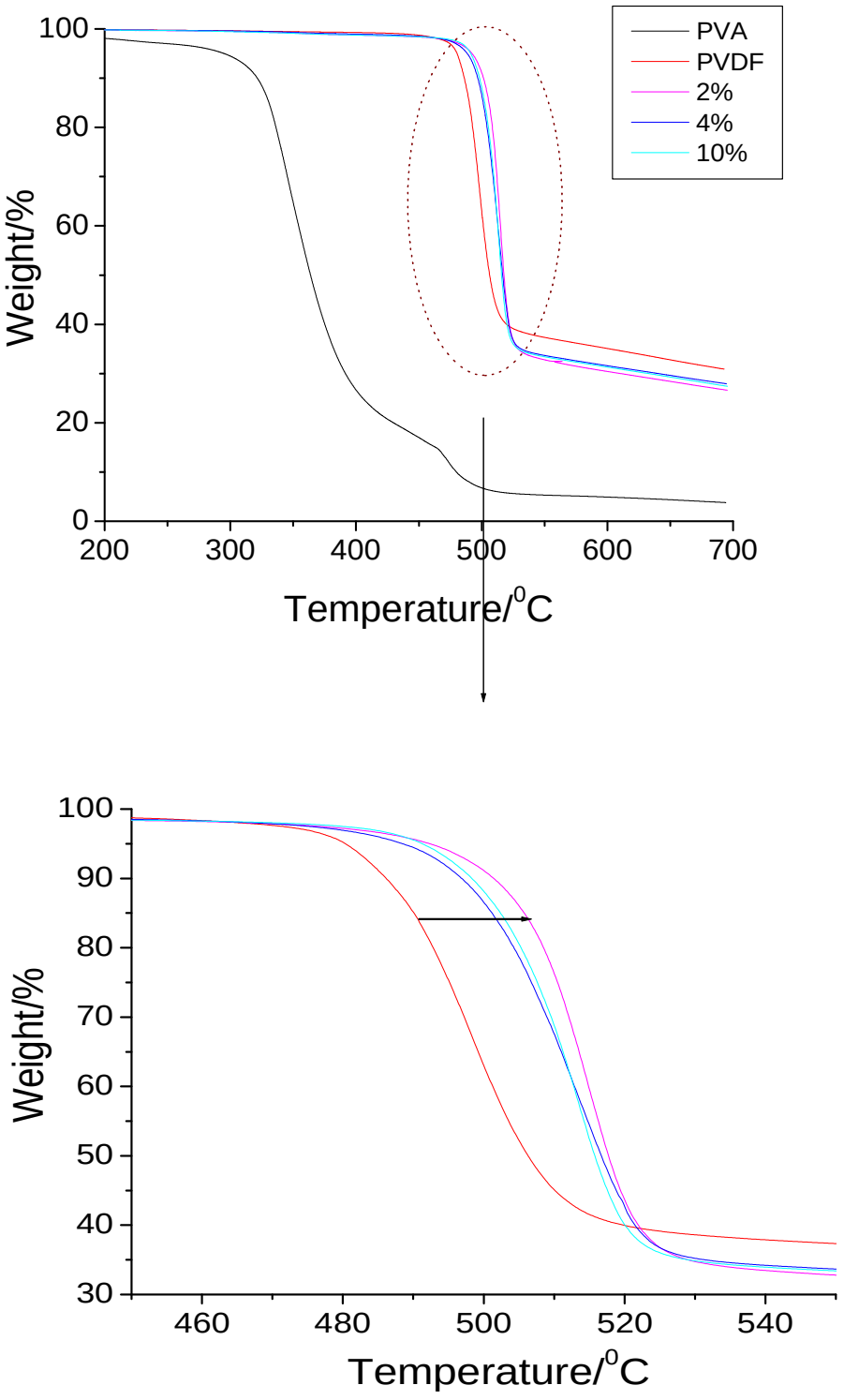

Figure 6.9: Thermogravemetric analysis of PVA, PVDF and PVA adsorbed onto PVDF membranes.

6.5 Conclusions

Molecular origins of wettability of irreversibly adsorbed PVA on PVDF membranes have been explained mainly through surface and interface analysis by XPS. An interface formation between PVA and PVDF was demonstrated and it is likely due to the interaction between carbonyl group of PVA and the CF_2 group of PVDF backbone. Likely there is some charge transfer from PVA to PVDF and a decrease in F 1s BE suggests a reduction in C-F bonding character upon PVA adsorption. A new highest occupied valence band observed on PVA adsorbed PVDF membranes clearly indicate that the nature of top most orbitals/bands changes from mostly F and C on PVDF to oxygen derived on PVA adsorbed membranes and hence a change in hydrophobic to hydrophilic character. This is further supported from the surface atomic content of PVDF and PVA adsorbed PVDF membranes. Water permeability studies on the membranes show a maximum permeability with 4% PVA concentration adsorbed PVDF membrane. XPS studies and water permeability experiments indicate that the threshold value is 4%. There is also a considerable change in textural properties of the adsorbed membranes, which support our conclusions.

In summary, PVA adsorbed PVDF membranes exhibit the following characteristics

1. A dramatic decrease in CF_2 intensity and broadening of CH_2 carbon peak as compared to pristine PVDF upon adsorption of PVA onto PVDF membrane.
2. XPS studies indicate the charge transfer from carbonyl carbon to electron deficient carbons of CF_2 groups and a decrease in F 1s binding energy.
3. XPS and water permeability experiments indicate that there is a threshold PVA (i.e. 4%) coverage onto PVDF.
4. PVA adsorbed PVDF membranes exhibit high thermal decomposition temperature than the pristine PVDF membrane.

5. Adsorption of PVA onto PVDF membranes results into increase in hydrophilicity of the PVDF membrane and consequently an increase in water permeability of membranes.

6.6 References

1. Nabe, A.; Staude, E.; Belfort, G. J. Membr. Sci. **1997**, *133*, 57.
2. Belfer, S.; Gilron, J.; Purinson, Y.; Fainshtain, R.; Daltrophe, N.; Priel, M.; Tenzer, B.; Toma, A. Desalination **2001**, *139*, 169.
3. Gancarz, I.; Pozniak, G.; Bryjak, M. Eur. Polym. J. **2000**, *36*, 1563.
4. Kim, K. S.; Lee, K. H.; Cho, K.; Park, C. E. J. Membr. Sci. **2002**, *199*, 135.
5. Wavhal, D. S.; Fisher, E. R. Langmuir **2003**, *19*, 79.
6. Wang, P.; Tan, K. L.; Kang, E. T.; Neoh, K. G. J. Membr. Sci. **2002**, *195*, 103.
7. Ulbricht, M.; Belfort, G. J. Membr. Sci. **1996**, *111*, 193.
8. Akhtar, S.; Hawes, C.; Dudley, L.; Reed, I.; Stratford, P. J. Membr. Sci. **1995**, *107*, 209.
9. Stengaard, F. F. Desalination **1988**, *70*, 207.
10. Hvid, K. B.; Nielsen, P. S.; Stengaard, F. F. J. Membr. Sci. **1990**, *53*, 189.
11. Na, L.; Zhongzhou, L.; Shuguang, X. J. Membr. Sci. **2000**, *169*, 17.
12. Uyama, Y.; Kato, K.; Ikada, Y. Advances in Polymer Science **1998**, *137*, 1.
13. Kato, K.; Uchida, E.; Kang, E-T.; Uyama, Y.; Ikada, Y. Prog. Polym. Sci. **2003**, *28*, 209.
14. Shoichek, M. S.; McCarthy, T. J. Macromolecules **1991**, *24*, 1441.
15. Kozlov, M.; Quarmyne, M.; Chen, W.; McCarthy T. J. Macromolecules **2003**, *36*, 6054.
16. Serizawa, T.; Hashiguchi, S.; Akashi, M. Langmuir **1999**, *15*, 5363.
17. Coupe, B.; Chen, W. Macromolecules **2001**, *34*, 1533.
18. Nash, D. C.; McCreath, G. E.; Chase, H. A. J. Chromatography A **1997**, *758*, 53.
19. Witt, J. A. De; Ven, T. G. M van de Langmuir **1992**, *8*, 788.
20. Barette, D. A.; Hartshorne, M. S.; Hussain, M. A.; Shaw, P. N.; Davies, M. C. Anal. Chem. **2001**, *73*, 5232.

21. Velu, S.; Suzuki, K.; Gopinath, C. S. J. Phys. Chem. B **2002**, *106*, 12737.
22. Velu, S.; Suzuki, K.; Yoshida, H.; Hattori, T.; Gopinath, C. S. Phys. Chem. Chem. Phys. **2002**, *4*, 1990.
23. Morikawa, E.; Choi, J.; Manohara, H. M.; Ishii, H.; Seki, K.; Okudaira, K. K.; Ueno, N. J. Appl. Phys. **2000**, *87*, 4010.
24. Maehl, S.; Neumann, B.; Schneider, B.; Schlett, V.; Baalmann, A. J. Polym. Sci. A **1999**, *37*, 95.
25. Zulfigar, S.; Zulfigar, M.; Rizvi, M.; Munir, A.; McNeill, I. C. Polym. Degrad. Stability **1994**, *43*, 423.
26. Gilman, J. W.; VandeerHart, D. L.; Kashiwagi, T. Fire and Polymer II : Materials and Tests for Hazard Prevention, American Chemical Society, ACS symposium series 599, **1994**, Chapter 11.

CHAPTER 7

Conclusions and Direction for Future Work

7.1 Conclusions

The present work was focused on the synthesis and characterization of hydrogel membranes for bio-separations. These membranes exhibit stimuli sensitive nature and therefore, the swelling and permeation properties of membranes were dependent on the external stimuli. The attempt was also made to synthesize nanocomposite hydrogel membranes with enhanced mechanical properties. Furthermore, XPS was used to investigate the molecular origin of wettability of porous membranes (PVDF) upon adsorption of hydrophilic polymer, poly(vinyl alcohol).

The conclusions of each chapter are summarized below

1. The polyamphoteric hydrogel membranes based on chitosan, poly(N-isopropylacrylamide) [PNIPAm] and poly(2-acrylamido-2-methyl propane sulphonic acid) [PAMPS] were synthesized and characterized. The swelling behaviour of membranes was very much influenced by pH, temperature and ionic strength of the external medium. The addition of PAMPS to CS-PNIPAm polymer increased the hydrophilicity of the system and the swelling ratios. Furthermore, PAMPS induced a discontinuous swelling transition to the hydrogel membrane, which can have potential in stimuli sensitive separations using membranes. The permeabilties of solutes such as theophylline and ciprofloxacin hydrochloride through these membranes were strongly dependent on the size of solutes which decreased with an increase in size of solute. The permeability of theophylline increased at temperature above LCST of PNIPAm and it also enhanced with an increase in hydrophilicity of the membranes.
2. Hydrophobically modified poly(vinyl alcohol) [PVA] membranes were synthesized by graft copolymerization of N-tertiary butyl acrylamide [NTBA] onto PVA by free radical polymerization. Elemental analysis, FT-IR and NMR spectroscopy confirmed the incorporation of NTBA onto PVA. The swelling behaviour of graft copolymer membranes was very much influenced by

temperature of the external medium, hydrophobic content, annealing temperature and period. Particularly the hydrogel membrane with low content of NTBA gave discontinuous volume transitions, which has application in separation process. Annealing of these membranes improved the crystallinity of membranes, which was demonstrated by DSC, XRD and DMA. The permeability of these membranes was dependent on the size of solutes where the solute with smaller hydrodynamic radius diffuses faster than the solute with larger hydrodynamic radius. The permeability increased with an increase in the hydrophilicity of membranes and the decrease in solution temperature indicating that the permeability increases with an increase in swelling ratio of membranes and vice-versa.

3. The thermosensitive nanocomposite hydrogel membranes based on PVA-g-polyNTBA and water swellable clay, laponite were synthesized by varying laponite concentration. FT-IR spectroscopy and thermal gravimetric analysis confirmed the incorporation of laponite in nanocomposite membranes. The swelling of nanocomposite membranes in water was very much influenced by the laponite concentration and it decreased with an increase in laponite content. Also nanocomposite membrane with 20% laponite content exhibited slight increased in swelling ratio with increasing temperature. The mechanical properties of the nanocomposite membranes were found to increase with an increase in the laponite concentration in the feed. The permeabilities of the membranes were strongly influenced by the solute size as well as laponite concentration in membrane. The incorporation of laponite enhanced the tortusity in nanocomposite membranes and consequently, permeability through NC membranes reduced as compared to PVAN2 membrane.

4. The adsorption of PVA onto porous hydrophobic PVDF membranes was carried out and found that the adsorption is reversible and results in increase in hydrophilicity and water permeability of PVDF membrane. Molecular origin of wettability of irreversibly adsorbed PVA onto PVDF membrane was explained mainly through surface and interface analysis by XPS. The charge transfer from carbonyl carbon of PVA to electron deficient carbons of CF_2

groups of PVDF and the decrease in F 1s binding energy suggests a reduction in C-F bonding character upon PVA adsorption. There was also a considerable change in textural properties of the adsorbed membranes. Further, XPS and water permeability experiments indicated that there is a threshold PVA (i.e. 4%) coverage onto PVDF.

7.2 Directions for the Future Work

This work could be further extended as follows,

1. We have studied the polyamphoteric thermosensitive hydrogel membranes based on chitosan and poly N-isopropylacrylamide (NIPAm) exhibiting discontinuous volume transition as a function of temperature. Clinical applications of thermoresponsive hydrogels based on PNIPAm have limitations since they are not biocompatible. Further, the copolymers of PNIPAm and their derivatives are not biodegradable and require extensive toxicity studies before clinical/pharmaceuticals applications. So we would like to synthesize thermo and pH sensitive hydrogel membranes based on chitosan and biodegradable hydrophobic polymers by achieving hydrophilic and hydrophobic balance between them. We would like to explore the applications of such membranes in the bio-medical field.
2. We have demonstrated in our work that, incorporation of laponite clay into PVA gives hydrogel membranes with enhanced mechanical properties. Permeation experiments exhibited longer tortuosity path for diffusing molecules. The pervaporation studies using these membranes can be very interesting and can give excellent selectivity for the separation of some of the industrially important chemicals. Furthermore, the transmission electron microscopy (TEM) can give more insight on the morphology of these membranes and the tortuosity can be related to the amount of clay content in the membrane. This can be an important aspect for future investigation.

3. Recently, gel filled porous membranes are attracting increasing attention because of the possibility of making them as size selective in nature. The swelling and shrinking property of hydrogel can be utilized to adjust the pore size of the membrane. However, incorporation of hydrogel in the pores of membranes is a challenging task. Novel strategies have to be adopted put the gel efficiently in the pores and structural characterization of these gel-filled membranes has to be performed. We propose to take up work in this direction in future.